Comparative Study of Chelating Agents in the Treatment of Heavy Metal Poisoning on Early Zebrafish Embryo Development followed by Quantitative PCR Studies

Inaugural dissertation

of the Faculty of Science,

University of Bern

presented by

Dib, Chakif

Supervisor of the doctoral thesis:

Prof. Dr. Julien Furrer

Department of Chemistry, Biochemistry and Pharmaceutical Sciences

Bern, **28th of Feb 2025**

Acknowledgments

First, I would like to acknowledge Prof. Dr. Julien Furrer for allowing me to be part of his research group (Nuclear Magnetic Resonance Group) and for his continuous support throughout a variety of interdisciplinary projects, where I have become able to carry scientific questions in international environments. I would also like to thank Dr. Martial Piotto for evaluating my thesis and Prof. Dr. Christoph von Ballmoos for chairing my PhD defense.

I am grateful to the Group members, Dr. Martina Vermathen, Dr. Ilche Gjuroski, and Dr. Camilo Melendez, for their contributions to the research projects and for helping me tackle scientific questions and challenges. I would also like to thank the Bachelor Student Janosch Imhof and the Master Student Celal Bahtiyar for their invaluable contributions.

I would also like to thank all the members of the Department of Chemistry, Biochemistry, and Pharmaceutical Sciences, especially the Group of Leidel, especially Dr. Ahmed Elhelbawi for the quantitative-PCR experiments, the Group of Krämer, particularly Beatrice Frey for the Scanning Electron Microscopy (SEM) and X-ray diffraction analytics, the Group of Prof. Dr. Stefan Schürch for the High-Resolution Mass Spectrometry (HRMS) experiments, and the Group of Luciani for allowing us to use their Dynamic Light Scattering (DLS) device.

I would like to show my sincere to all the scientists who have come along the way during the period time of my studies, the Group of Prof. Dr. Peter Vermathen from the sitem insel AG, Bern, for numerous High-Resolution Magic Angle Spin (HR-MAS) experiments, the Group of Prof. Dr. Christoph Kempf from the Department of BioMedical Research, University of Bern, especially to Dr. Nico Ruprecht that generously conducted Inductively Coupled Plasma-Mass Spectrometry (ICP-MS) measurements of several compounds.

Finally, I would like to thank my family and friends for all their support. The years I spent at the University of Bern and the City of Bern were among my most incredible experiences. I had the chance to improve my scientific research skills and my personality on a professional level.

Abstract of the Doctoral Thesis

The following dissertation comprises two research projects in which I have participated across various disciplines to tackle scientific questions with a solution-oriented goal, aiming for global well-being.

The first project was related to people experiencing high levels of metal intoxication within their body, where we had the chance to evaluate five chelation medications used to determine the optimal treatment option, highlighting the effectiveness of the chelating agents depending on the heavy metal involved and provide valuable insights into optimizing treatments for heavy metal toxicity. To address this, we used zebrafish—a rapidly developing and experimentally traceable model widely recognized for toxicological studies. Zebrafish are commonly identified in toxicological studies due to their rapid development, genetic tractability, and transparent physiology, allowing precise experimental tracking and assessment. This model enabled detailed observation of chelation therapies' physiological and biochemical impacts on heavy metal detoxification. The findings from this project have significant implications for improving clinical outcomes in patients with heavy metal intoxication and contribute to the ongoing refinement of chelation-based treatment protocols.

The second project was aligned with pharmaceutical sciences, where we were able to explore formulation and design methodologies within the pharmaceutical domain. This involved studying and investigating the structural properties and interactions of the novel liposomes and ruthenium(II)--based metal complexes and ultimately advancing the project towards developing a formulation for human administration to target cancer cells efficiently. NMR spectroscopy provided critical insights into the structural interactions between ruthenium complexes and liposomes, including multilamellar vesicles (MLVs). These investigations enabled a deeper understanding of how these complexes integrate within lipid-based delivery systems. Following the structural analysis, strategies were developed to optimize the formulation for effective cancer cell targeting. This work advances metal-based therapeutic agents and liposomal drug delivery systems, offering a promising avenue for targeted cancer therapies and enhancing the precision of pharmaceutical applications.

Table of Contents

PART ONE: TOXIC METAL COMPLEXES AND CHELATING AGENTS

Chapter One: Background and Knowledge

1.0. Introduction to Mercury (Hg), Lead (Pb), and Cadmium (Cd)

1.1. Natural and Anthropogenic Sources of Hg, Pb and Cd

Mercury (Hg), lead (Pb), and cadmium (Cd) are naturally occurring heavy metals distributed widely in the earth's crust and have been classified as one of the most toxic elements approved by the World Health Organization (WHO) [1, 2]. These metals derive mainly from natural sources, including volcanic activity, erosion, weathering of mineral deposits, and the biological cycling through ecosystems (see **Table 1.1.1** and **1.1.2**) [3-5]. During volcanic eruptions, a variety of metals are released into the atmosphere, including lead, mercury, and cadmium, which can remain in the atmosphere for extended periods, depending on the type and scale of the eruption [6].

Mercury, lead, and cadmium can also be naturally bound to other mineral compounds (see **Table 1.1.1**). For instance, Hg can bind to sulfur (e.g., cinnabar) and selenium (e.g., tiemannite), and other metals such as gold (Au) and silver (Ag) [7]. Pb can also bind to sulfur (e.g., galena) and others such as sulfates (e.g., anglesite) and carbonates (e.g., cerussite), often associated in ores with zinc (Zn) (e.g., sphalerite), and other ore deposits such as Ag, and Cu. The primary source of cadmium is sphalerite (ZnS), and it is commonly found in association with Pb, Iron (Fe), and Copper (Cu) ores [8, 9].

Table 1.1.1: Natural sources of Hg, Pb, and Cd and their metal- mineral-binding.[9]

Metal compound	Natural sources	Metal-binding	Mineral-binding
Mercury	Earth's Crust	Au and Ag	Cinnabar (HgS), tiemannite (HgSe)
Lead		Zn, Ag, Cu	Galena (PbS), anglesite ($PbSO_4$), and cerussite ($PbCO_3$)
Cadmium		Pb, Cu and Fe	sphalerite (ZnS)

The emission of mercury into the atmosphere exceeds 2,200 metric tons per year. One-third of these discharges originate from the decay of Hg-containing sediment and volcanic eruptions, and two-thirds mainly from human activities [10]. Nearly 80% of the contribution from human activities is disposed into the environment as mercury vapor that derives from coal power plants. Around 15% are from fertilizers and soil waste where contamination takes place in the soil, and the remaining 5% is derived from industrial wastewater entering natural waters [11, 12]. Several environmental sources of different forms of Hg exist, including elemental (metallic) Hg, organic Hg, and inorganic Hg.

Elemental mercury (Hg^0) has been widely used in thermostats, added to latex paint, and dental amalgams, to some extent entering the atmosphere in a vaporized form [10]. The zero-oxidation state of Hg^0 represents the only metal in liquid form at room temperature. Organic mercury (CH_3Hg^+) is found in fish, whereas ethyl mercury ($CH_3CH_2Hg^+$) is mainly found in vaccine preservatives [13]. In some cases, Hg is bound to airborne particles, which can be transported long before settling on the earth's surface. The interest in mercury toxicity has increased in modern science. However, it has been known as a neurotoxic substance for centuries, yet there remains controversy on the mechanism of interaction with biochemical processes. Once elemental Hg is released into the air, it is transported over a wide-range distance by wind patterns, in which it then undergoes complex chemical reactions and transformations in the atmosphere, such as oxidation, photo-oxidation, and particulate binding [10]. Oxidation of Hg occurs by atmospheric compounds such as ozone (O_3) and halogens (e.g., Cl). The process leads to the formation of oxidized Hg (Hg^{2+}), which is easily removed from the atmosphere due to its solubility in water. The photo-oxidation of Hg can be promoted by ultraviolet light, increasing its potential to be deposited in aquatic ecosystems [14].

Moreover, some oxidized Hg can bind to particulate matter, which can be later removed by gravity or precipitation [15]. Once Hg is transformed, its removal from the atmosphere occurs through various deposition mechanisms, including wet and dry deposition. Wet deposition promotes Hg to enter ecosystems via surface waters or onto the land through rain, snow, fog, etc [16]. Dry deposition promotes Hg to settle onto surfaces such as soil, water bodies, and vegetation without precipitation. However, Hg does not remain stationary in the environment because of the re-emission processes of Hg. Hg deposited on soil and water can be re-emitted into the atmosphere under certain conditions, such as high temperatures or changes in the chemical environment. When Hg is present in the water bodies or soil, microbial activity or changes in temperature can cause Hg to be volatilized back into the air in the form of elemental Hg through evaporation [17]. Mercury deposited on plants can also be re-emitted in the atmosphere through foliar uptake and evapotranspiration [18]. However, anthropogenic activities have significantly altered the presence and concentration of these metals in the environment [6].

Lead (Pb) is known for its unique physiochemical properties, such as malleability, poor conductivity, softness, and slow dissolution in water, and has been used for centuries in many applications such as the manufacturing of pipes for drinking water, as well as additives to gasoline [19]. Leaded petrol was one of the most significant sources of atmospheric lead in the 20th century. Lead compounds were added to gasoline as an anti-knock agent and paint [20]. In developed countries, the use of lead is limited but is still used in gas and other lead-containing products, i.e., pigments, ceramics, and batteries. Despite its beneficial contribution in many applications, lead is

highly toxic and is one of the most widespread environmental health hazards. Because of its usage in many applications, it can enter the environment mainly from anthropogenic activities such as land application, mining, and smelting through the recycling of waste materials and the combustion of fossil fuels [21]. Lead is also found in small quantities in cigarette smoke. The tobacco plant can accumulate lead from the soil, and when burned, small amounts of lead are released into the atmosphere.

Pb is introduced into the atmosphere during the weathering of rocks and minerals, where the natural breakdown of rocks and minerals takes place through physical and chemical weathering processes. Over time, trace amounts of lead are released into the atmosphere and become airborne [22]. Nowadays, the emission of Pb exceeds 100,000 metric tons per year from both natural and human activities. Though this is a relatively minor source compared to industrial activities, it contributes to local lead contamination, particularly in areas with high smoking rates [23]. In countries where lead-based paints are still in use, the sanding, scraping, or burning of these paints can release lead particles into the air. This is particularly common in older buildings and homes. Recycling lead-containing materials, such as lead-acid batteries or old lead-based products, can also contribute to atmospheric lead. Improper handling or processing in certain recycling facilities can release lead particles [25-27].

Coal contains trace amounts of cadmium, and when coal is burned for energy production, cadmium is released into the atmosphere as part of the emissions. Power plants that rely on coal for electricity generation are significant sources of atmospheric cadmium [18]. Cadmium is also commonly found in ores that contain zinc, lead, and copper. Smelting and refining these metals often release cadmium as a byproduct. Smelters are significant sources of cadmium emissions, especially in regions with prevalent zinc production. Historically, cadmium was used in pigments for paints, particularly in yellow, red, and orange paints. Although its use has declined significantly due to health concerns, cadmium can still be found in older paints. Sanding or scraping old painted surfaces can release cadmium into the air, contributing to its presence in indoor and outdoor environments [27]. The extraction of metals such as zinc, lead, and copper often release cadmium into the environment as a byproduct. During mining and ore processing, cadmium can be emitted into the atmosphere, water, and soil. Mining operations in regions with high cadmium concentrations in ores are a significant source of environmental cadmium pollution [28]. Cadmium is used in the production of rechargeable batteries, particularly batteries. The production and disposal of these batteries can result in cadmium emissions, mainly when they are improperly disposed of or recycled. Cement manufacturing can release trace amounts of cadmium into the atmosphere, primarily when raw materials containing cadmium are used in production. This source is considered minor compared to others, but it can still contribute to localized cadmium pollution,

particularly in areas with high cement production [29]. These activities release cadmium into the air, water, and soil. The primary industrial sources include coal combustion, smelting and refining of metal, pigments for paints, and mining operations [19, 31]. Anthropogenic activities are the most significant contributors to cadmium pollution in the environment, exceeding 3000 metric tons annually [28].

1.2. Their Impact on Humans' Health Conditions

For human well-being, only zinc (Zn), iron (Fe), copper (Cu), cobalt (Co), selenium (Se), manganese (Mn), molybdenum (Mo) are the only trace metals considered to be essential, at specific doses for each metal. [31]. Human exposure to Hg, Pb, and Cd derives from their advanced chemistry and complex interactions with other elements, as described previously. Each of these metals exhibits distinct coordination chemistry and redox properties that lead to a variety of compounds that impact human health (see **Table 1.1.3**) [28].

Table 1.1.2: Mercury, lead, and cadmium species, deriving from human activities and their existence in biological systems through several consumptions.

Metal compound	Sources
Elemental Mercury (Hg^0)	dental amalgams, fossil fuels
Organic mercury (CH_3Hg^+)	fish, poultry, pesticides
Inorganic mercury ($HgCl_2$)	demethylation of organic mercury, oxidation of elemental mercury
Lead	mining, smelting, battery manufacturing, food, drinking water
Cadmium	production of nickel-Cd batteries, Cd-containing paint production, food (rice, potato)

The primary source of mercury exposure for most people is consuming contaminated seafood, which is present in the form of CH_3Hg^+, the most toxic form, and found at high concentrations in large fish (e.g., shark, swordfish, tuna) [32]. Other pathways include air, water, and occupational settings due to their environmental persistence and bioaccumulation ability. Certain occupations involve a higher risk of mercury exposure due to the handling of mercury-containing products or exposure to mercury vapors, including miners, mercury manufacturing and processing plants, and dental professionals. In the 1830s, the Western world introduced Hg as dental amalgam, consisting of 50% Hg, 22-32% silver (Ag), 14% tin (Sn), 8% copper (Cu), and other trace metals [33]. A few countries, including Sweden and Norway, have banned dental amalgams due to health and environmental concerns, but they remain used as dental fillings worldwide. Dental amalgams are the primary source of Hg in the central nervous system (CNS), which is initially released from amalgams, existing as elemental Hg (Hg^0), and metabolized to inorganic Hg ($HgCl_2$) in the human body [34]. Various studies have described molecular and cellular effects of organic Hg in the nervous system, which found that Hg^{2+} may play a crucial role

after exposure to CH_3Hg^+ and $CH_3CH_2Hg^+$ and have suggested that the existence of Hg^{2+} in neurons results from the breakdown of organic Hg in glial cells, and that the levels of Hg^{2+} were higher after the exposure to $CH_3CH_2Hg^+$ [33]. The health effects of mercury exposure depend on several factors, including the type of mercury, the level of exposure, the route, and the duration of exposure. The most common forms of mercury that cause health problems in humans are elemental mercury ($Hg^{0)}$, inorganic mercury (Hg^{2+}), and methylmercury (CH_3Hg) [15].

Methylmercury exposure, particularly during pregnancy, infancy, and childhood, is associated with developmental and neurological effects [35]. These effects include cognitive deficits, motor and coordination deficits, memory loss, and cognitive dysfunction in adults. In addition, inorganic mercury (Hg^{2+}) can accumulate in the kidneys, causing kidney damage and potentially leading to renal failure. This is mainly a risk for workers in industries that use or produce inorganic mercury, such as mining and chemical manufacturing [36]. Previous studies suggest that exposure to low levels of mercury may cause an increase in the risk of cardiovascular diseases, including hypertension and heart disease [37, 38]. The exposure may also affect the immune system, leading to autoimmunity and increased susceptibility to infections by altering immune responses and causing inflammatory reactions [39]. All forms of mercury are one of the leading causes of adverse effects, including respiratory, immune, dermatologic, renal, reproductive, and developmental sequelae. Researchers have also suspected that Hg is involved in the etiology of neurodegenerative diseases such as Alzheimer's disease (AD), Amyotrophic Lateral Sclerosis (ALS), Multiple Sclerosis (MS), Parkinson's Disease (PD), or Autism Spectrum Disorder (ASD). Previous studies have indicated that toxic metals may accumulate in the fetus, resulting in preterm birth and reduced birth size [40]. The interaction between Hg(II) and selenium (Se) compounds can reduce the bioavailability and inhibit the functions of selenium by binding to the active sites of seleno-enzymes. Another way metals exhibit toxic behavior in the body is by blocking calcium (Ca)-binding proteins, including calmodulin. Therefore, metals can interfere with cellular processes by substituting Ca on essential constituents and inducing neuroinflammatory change. The interaction of CH_3Hg with the synthesis of Deoxyribonucleic Acid (DNA), Ribonucleic Acid (RNA), and protein, especially the attachment of Hg to SH-groups has a significant role in the changes of secondary DNA and RNA and structural modifications in ribosomal proteins. This impact may also be associated with epigenetic changes such as DNA methylation.

Lead is a potent neurotoxin that poses significant risks to the nervous system, with even minimal exposure having detrimental effects [41]. Although less common than ingestion or inhalation, dermal exposure to lead can occur in specific occupational settings where workers handle lead-containing materials. Despite the widely recognized health hazards, lead exposure

remains a significant issue, especially for high-risk groups like children, pregnant women, and individuals employed in specific industries. The effects of lead exposure are well-established, and even low levels of exposure can cause a range of adverse health outcomes, including developmental delays, cognitive impairments, and neurological damage. As lead-based paint deteriorates, it produces lead dust, which can settle on surfaces and become a source of exposure when children play on floors, touch contaminated surfaces, or put their hands in their mouths [25, 41]. Children are particularly at risk, as low levels of lead exposure can lead to cognitive deficits, learning challenges, and behavioural disorders, including symptoms commonly associated with Attention Deficit Hyperactivity Disorder (ADHD) and other conduct-related conditions. For adults, chronic exposure to lead has been linked to memory impairments, diminished cognitive abilities, and a heightened likelihood of developing neurodegenerative disorders such as Alzheimer's disease [42]. Lead has been shown to induce vascular damage and promote the development of atherosclerosis, a pathological condition characterized by arterial hardening, thereby elevating the risk of cardiovascular events such as myocardial infarction and cerebrovascular accidents [43].

Cadmium is classified as a human carcinogen and is harmful to various organs, particularly the kidneys, bones, and lungs [44]. Cadmium exposure can occur through various environmental and occupational routes, with sources including contaminated food, water, air, and tobacco smoke, as well as certain industrial activities [34, 51]. Cadmium is absorbed by plants, mainly through contaminated soil, and accumulates in certain crops such as rice, leafy vegetables, and root vegetables as well as seafood, especially shellfish and certain fish like tuna, due to contamination in aquatic environments [46].

Tobacco smoke is another significant source of cadmium exposure. Cadmium is present in tobacco plants because the metal accumulates in the plants' soil. Smoking results in direct inhalation of cadmium, which can lead to significant exposure, particularly in long-term smokers [27]. It is estimated that smokers have a higher body burden of cadmium compared to non-smokers [47]. Chronic exposure to cadmium primarily affects the kidneys, leading to kidney dysfunction and, in severe cases, kidney failure. Prolonged exposure to cadmium can cause bones to become weakened, increasing the risk of fractures. This condition is known as Itai-Itai disease, which was first reported in Japan and is characterized by severe pain, bone fractures, and kidney dysfunction due to chronic cadmium exposure [46, 48]. Chronic exposure to cadmium has been associated with increased blood pressure, which may contribute to the development of cardiovascular disease over time. Cadmium exposure has also been shown to affect reproductive health, particularly in men, where it can lead to reduced sperm quality and fertility and may also affect fetal development in pregnant women [49-51].

Table 1.1.3: Mercury, lead, and cadmium species and their routes of absorption, distribution, metabolism, cause of toxicity, and excretion.

	Elemental Mercury	**Organic Mercury**	**Inorganic Mercury**	**Lead**	**Cadmium**
Absorption	75-85% of vapor absorbed	95-100% in the intestinal tract; 100% of inhaled vapor	7-15% of ingested dose absorbed	Gastrointestinal ingestion, inhalation	Gastrointestinal ingestion, inhalation
Distribution	BBB, kidney	BBB, kidney,	kidney	CNS, kidney	Kidney, liver, skeleton
Metabolism	Oxidized intracellularly to inorganic mercury by catalase and H_2O_2	Slowly demethylated to inorganic mercury	Methylated by intestinal microflora	No metabolic transformation	No metabolic transformation
Cause of Toxicity	Oxidation to inorganic mercury	Demethylation to inorganic mercury; binding to proteins	Binding to proteins	Binding to proteins	Protein-binding
Excretion	Urine, feces, sweat, and saliva	10% urine, 90% in bile, feces	Urine, sweat, saliva, bile, feces	Urine, small portion in feces	Urine, feces

When humans experience high levels of metal concentration within their bodies, the so-called chelation therapy is recommended. Chelation is only recommended when toxicity symptoms are present, and lab tests confirm toxic levels. There are specific concentrations of heavy metals for recommended chelation therapy (see **Table 1.1.4**) [52, 53]**.**

Table 1.1.4: Recommended reference levels for initiating chelation therapy in mercury, lead, and cadmium exposure**.**

Metal	Blood level	Urine level (24h)	Note
Mercury	**> 50 µg/L**	**> 100 µg/g creatinine**	**Chelation used with symptoms present**
Lead	**> 70 µg/dL (adults)** **> 45 µg/dL (children)**	**N/A**	**Emergency chelation for high lead levels**
Cadmium	**> 5 µg/L**	**> 10 µg/g creatinine**	**Chelation is rarely used for cadmium**

Chapter Two: Chelation Therapy in Metal Detoxification – Chelating Agents

2.0. Chelation Therapy – State of the Art

Chelation therapy, or chelet, deriving from Greek philosophy, is a medical treatment used to remove heavy metals or other toxic substances from the body by binding them to chelating agents. This treatment is primarily employed to treat poisoning caused by metals such as mercury, lead, mercury, and cadmium and to manage metal overload disorders such as excess copper or iron. Chelation therapy works through the chemical properties of chelating agents, which contain specific functional groups like amines, thiols, or carboxyl groups that can bind to metal ions. These interactions result in the formation of stable, water-soluble complexes, neutralizing the toxic effects of the metal. The process consists of three key stages: the chelating agents bind to metal ions in the bloodstream or tissues, a stable complex is created between the agent and the metal, and the resulting complex is eliminated from the body through urine or feces. This process effectively decreases the toxic metal load and alleviates its harmful impact on the body [52].

The living body is made up of chelates, including alpha-lipoic acid (ALA), cysteine (Cys), and glutathione (GSH) (see **Figures 1.2.1** and **1.2.5**), which are naturally occurring compounds in the human body and are not FDA-approved. However, all kinds of ALA are widely available as nutritional supplements, especially in the US, in the form of tablets, capsules, and aqueous liquids, and have been used as an antioxidant to cellular glucose utilization for metabolic disorders and type-2 diabetes [54]. In 1966, Germany approved LA as a drug for the treatment of diabetic neuropathy, and it is available as a non-prescription pharmaceutical [54, 55]. Among the clinically approved chelating agents are the derivatives of the British Antidot-Lewisite (BAL) known as dimercaptosuccinic acid (DMSA), approved in Germany, and dimercaptopropansulfonic acid (DMPS), approved in the US (see **Figures 1.2.3** and **1.2.4**) [56, 57].

2.1. Alpha-Lipoic Acid (ALA) and Dihydrolipoic Acid (DHLA)

Lipoic acid, also known as alpha-lipoic (ALA) acid and thioctic acid, is an organosulfur compound derived from octanoic acid [59]. ALA contains functional groups such as thiols and carboxylic acids, enabling it to coordinate with metal ions, participate in redox reactions, and chelate toxic metals like mercury and cadmium [60]. ALA contains two sulfur atoms connected by a disulfide bond in the 1,2-dithiolane ring. It is the oxidized form of its relative dihydrolipoic acid (DHLA), where sulfur atoms exist as a thiol.

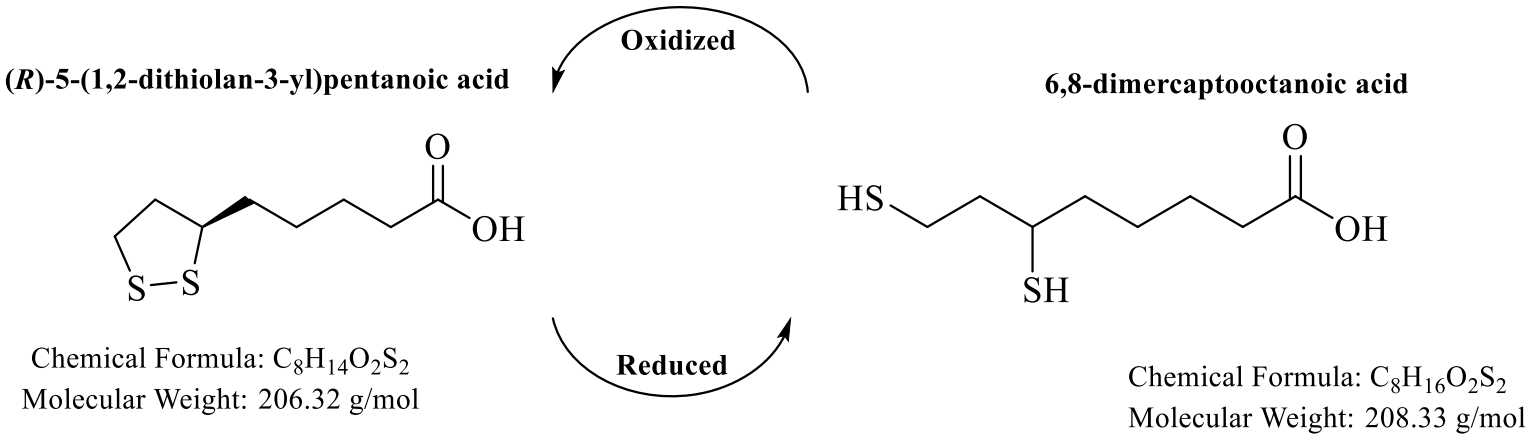

Figure 1.2.1: Chemical structures and properties of ALA (right) and DHLA (left). Intracellular activity of ALA and its conversion to DHLA after cellular penetration.

The pK_a of alpha-lipoic acid is 4.7, with deprotonated COO^-, where the dissociation constant of the carboxylic acid group is ionized chiefly at physiological pH (~7.4), which is essential for its absorption, bioavailability, and antioxidant activity [61]. DHLA has a slightly higher pK_a, around 6.3, making it more likely to be deprotonated at physiological pH (~7.4).

(*R*)-(+)-lipoic acid (RLA) occurs naturally, but (*S*)-(-)-lipoic acid (SLA) is being synthesized and used in dietary supplement materials and compounding pharmacies [62].

Figure 1.2.2: The two enantiomers of ALA (R- and S-lipoic acid).

However, ALA has limitations, including poor water solubility, low bioavailability, and susceptibility to degradation under improper conditions. Despite these challenges, its therapeutic potential in conditions like diabetes, neurodegenerative diseases, and oxidative stress-related disorders remains significant, driven by its ability to chelate metals, modulate inflammatory pathways, and neutralize reactive oxygen species. Efforts to enhance its stability and delivery, such as encapsulation techniques, continue to improve its clinical efficacy and pharmacological applications [63].

2.2. Dimercaptosuccinic (DMSA) and Dimercatpopropansulfonic acid (DMPS)

Dimercaptosuccinic acid, also known as DMSA ((2S,3S)-2,3-Bis(sulfanyl)butanedioic acid, contains two thiols (-SH) groups and two carboxylic acids (-COOH) groups. DMSA exists in two forms, meso- and racemic-DMSA, and the difference between both relies on their stereochemistry [64]. The meso-form is a biologically active compound with a symmetric structure, containing one chiral center in the R-configuration and the other in the S-configuration. Rac-DMSA is asymmetric is the biologically active compound and is a 50>50 mixture of two enantiomers, R, R- and S, S-DMSA; both chiral centers are either in the R-configuration or S-configuration [65].

Both forms are slightly soluble in water, where the pK_{a_1} values of the carboxylic acid are ~3.7, and pK_{a_2} ~4.9, pK_{a_3} and pK_{a_4} for the thiol groups with ~9.5 and ~10.5, respectively. The thiol groups are very reactive and bind to heavy metals, forming stable complexes [66].

meso-2,3-Dimercaptosuccinic acid

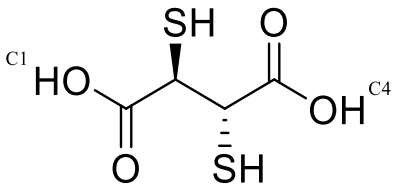

rac-2,3-Dimercaptosuccinic acid

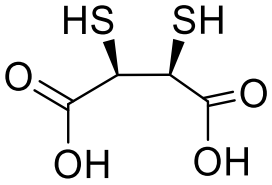

Chemical Formula: $C_4H_6O_4S_2$
Molecular Weight: 182.21 g/mol

Figure 1.2.3: The chemical structures and properties of meso- and rac- DMSA.

Dimercaptopropanesulfonic acid, also known as DMPS (2,3-Dimercapto-1-propane-1-sulfonic acid), contains two thiols (-SH) groups responsible for metal chelation and a sulfonic acid (-SO_3H) group that enhances high solubility in water and is sparingly soluble in organic solvents. The first and second thiol groups, with pK_a ~8.5 and 9.5, bind to heavy metals like mercury, arsenic, and lead, forming water-soluble complexes (see **Table 1.2.1**) [67].

2,3-Dimercapto-1-propanesulfonic acid

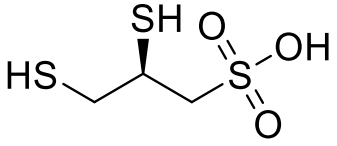

Chemical Formula: $C_3H_8O_3S_3$
Molecular Weight: 188.27

Figure 1.2.4: The chemical structure and properties of DMPS.

Table 1.2.1: DMSA and DMPS as metal chelators.

Chelating agents	Activation metabolism	Coordination (binding) groups	Elements chelated
DMSA	Excretion via urine >90% as DMSA – cysteine disulfide conjugates	Oxygen and sulfhydryl	Lead, arsenic, mercury, cadmium, silver, tin, copper
DMPS	84% of IV dose excreted through urine	Oxygen and sulfhydryl	Mercury, arsenic, lead, cadmium tin, silver, copper, selenium, zinc, magnesium

2.3. Cystein (L-Cys) and Glutathione (L-GSH)

L-Cystein and L-Glutathione are sulfur-containing amino acid compounds with critical roles in biochemistry due to their -SH groups. The carboxyl group (-COOH) of L-Cys has a pK_a value of 1.7, amino group 10.78, and thiol group 8.33, where each group deprotonates at basic or acidic conditions [68]. The pK_a values of L-GSH) are also primarily associated with its three functional groups, the carboxyl group 2.12, the amino group 9.62, and the key thiol group 8.75 [69].

2-amino-3-sulfhydrylpropanoic acid

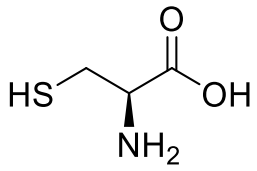

Chemical Formula: $C_3H_7NO_2S$
Molecular Weight: 121.15 g/mol

γ-Glutamylcysteinylglycine

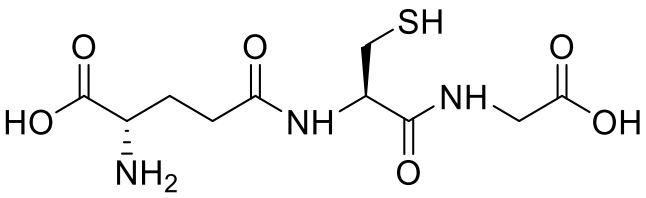

Chemical Formula: $C_{10}H_{17}N_3O_6S$
Molecular Weight: 307.32 g/mol

Figure 1.2.5: L-Cys (right) and L-GSH (left) chemical structures and properties.

The thiol group in L-cysteine enables it to engage in redox reactions, forming disulfide bonds essential for protein structure and neutralizing reactive oxygen species (ROS), thereby protecting cells from oxidative damage [70]. It also exhibits metal-chelating properties, binding to toxic metals such as mercury, lead, and cadmium to reduce their toxicity and aid in their removal from the body [71]. Furthermore, L-cysteine is a precursor to hydrogen sulfide (H_2S), a signaling molecule involved in regulating vascular health and providing cytoprotection [72]. However, L-cysteine is sensitive to environmental conditions and can oxidize to form cystine, a dimer linked by a disulfide bond. [73].

Glutathione (GSH) is a tripeptide composed of glutamate, cysteine, and glycine, renowned for its critical role in maintaining cellular redox balance and protecting against oxidative stress. The presence of a reactive thiol (-SH) group on the cysteine residue enables glutathione to act as a potent antioxidant, neutralizing reactive oxygen species (ROS) [74]. Additionally, it is involved in regenerating other antioxidants, such as vitamins C and E, and in maintaining the reduced state of thiol groups in proteins, which is essential for their structural and functional integrity. As a key player in the cellular defense system, glutathione contributes to immune function, DNA synthesis, and repair, as well as apoptosis regulation [75]. Its concentration is tightly regulated, and a decline in GSH levels is associated with various pathological conditions, including neurodegenerative diseases, cancer, and aging. While its hydrophilic nature allows it to act effectively in aqueous environments, glutathione's stability can be compromised by oxidative conditions [76].

2.4. Chemical Principles for Interaction

The chelation therapy aims to remove toxic metals from the human body. This requires that the metal chelators' chemical affinity be higher than the affinity of the metal ions [77]. To form a 1-to-1 complex between the metal chelator and the metal ion, the interaction is described by the equilibrium, *Eq. 1*:

$$K_1 = \frac{[ML]}{[M][L]} \tag{1}$$

K_1 is the stoichiometric stability constant, M is the solvated metal ion, and L is the chelator. At the same time, the brackets denote the concentrations of interacting species at equilibrium.

Hence, if the chelating agent contains several coordinating groups, the calculations for the equilibrium would be more complicated. In addition, when complexation occurs in the body, the total concentrations of the free L and M are much lower than the total $[L_t]$ and $[M_t]$ in the body; this can be described as the conditional stability constant or effective stability constant, K_{eff}. In theory, the chelatable metal fraction, $[ML]$, is determined by conditional stability constant K_{eff} and the tissue concentration $[L_t]$ of the metal chelator; this can be described by arranging *Eq 1*:

$$\frac{[ML]}{[M_t]} = k_{eff}[L_t] \tag{2}$$

However, previous studies have indicated that a high tissue concentration $[L_t]$ and a significant ML concentration can only be achieved with chelators with relatively low toxicity. Furthermore, to achieve efficient chelation treatment, the reaction should never reach equilibrium, and the chelate formed should be removed continuously from the equilibrium, i.e., via urine [77, 78].

Regarding the chemical stability of a therapeutic chelate, it is worth noting that the initial assessment of a ligand's (*L*) affinity for a toxic metal can be inferred using the Hard-Soft Acid-Base (HSAB) (see **Table 1.2.2**). Lewis defined an acid as an electron pair acceptor and a base as an electron pair donor. Based on this definition, positively charged metal ions are classified as acids because they function as electron acceptors. Forming a solvated (hydrated) metal ion creates a complex where water molecules act as electron donors, making H_2O a Lewis base. Similarly, many oxygen-containing compounds also serve as Lewis bases.

In aqueous solutions, metal ions exist in solvated forms, and during chelation or complexation, water molecules in the solvation shell are replaced by another ligand (another Lewis base), forming a metal complex [80]. Lewis's acids and bases can be categorized as "hard" or "soft." Complex metal ions are characterized by small size, high charge, and strong retention of their valence electrons. Examples include Li^+, Mg^{2+}, and Fe^{3+}. Conversely, soft metal ions, such as Cu^+, Hg^{2+}, As, Po^{2+}, and Pt^{2+}, are relatively larger and do not hold their valence electrons as tightly [80].

The stability of metal complexes and chelates depends on the hardness or softness of the metal ion and the ligand, as explained by Pearson in his Hard-Soft Acid-Base (HSAB) theory. Stable complexes generally result from interactions between hard and hard bases or soft acids and soft bases. For instance, complex bases, typically containing oxygen as a donor atom, form stable complexes with hard acids like Fe(II) and Fe(III).

In contrast, soft ligands, such as those containing sulfur or selenium, form stable complexes with soft metals like mercury, polonium, arsenic (As), copper(I), and lead. Hard-hard complexes are predominantly electrostatic, as exemplified by the iron-oxygen bond, whereas soft-soft complexes exhibit more covalent bonding, such as the mercury-thiol bond.

Metals like mercury and arsenic have notably high electronegativity (approximately 2.0 on the Pauling scale), predisposing them to covalent bonding with carbon and sulfur. This property accounts for the abundance of organomercurial and organoarsenic compounds [81].

Table 1.2.2: Hard-Soft Acid-Base Theory.

Coordinating groups			**Metal ions**		
Hard	*Intermediate*	*Soft*	*Hard*	*Intermediate*	*Soft*
H_2O, OH^-, $RCOO^-$ NH_3, RNH_2, Cl^-, F^-, RO^-,	$C_6H_5NH_2$	RS^-, RSH, R2S	Ca^{2+}, Li^+, Na^+, K^+, Mg^{2+}, $Al3^+$, Fe^{3+}, Mn^{2+}, Be^{2+}, Sr2+ Ga^{3+}, Cr^{3+}, Sn^{4+}, UO_2^{2+}, VO^{2+}, $(CH3)_2Sn^{2+}$	Fe^{2+}, Zn^{2+}, Pb^{2+}, Co^{2+}, Ni^{2+}, Cu^{2+}, Bi^{3+}. Sn^{2+}, Sb^{2+}	Ag^+, Au^+, Cu^+, Pd^{2+}, Pt^{2+}, Pt^{4+}, CH_3Hg^+, Hg^+, Hg^{2+}, Cd^{2+}

Chapter Three: Zebrafish as a Model Organism

3.0. Background in Zebrafish Embryo

3.1. Importance of Zebrafish in Research

The zebrafish (Danio rerio) is a small freshwater species that has become one of the most popular model organisms in biological research, especially in developmental biology, genetics, and disease modeling. The zebrafish embryo offers several advantages, such as transparency, rapid development, and the ability to manipulate genes, making it a valuable tool for studying early development, organogenesis, and disease processes. In the 20th century, zebrafish were first used as a model organism. Still, they were only used in the 1990s after significant advances in genetics and genomics were made and widely adopted for developmental and disease research [82].

Compared to humans, over 70% of genes associated with human diseases are functional homologs in zebrafish, which makes them an excellent model for studying the genetic bases of diseases [83]. Zebrafish embryos develop externally, making them accessible for experimental manipulation and observation from the earliest stages of development. Their small size, rapid embryonic development (with major structures forming within the first 24 hours), and high reproductive output (a female can lay hundreds of eggs per week) make zebrafish a cost-effective and robust model for genetic screens, drug discovery and disease modeling [84].

3.2. Developmental Stages and Embryology

Zebrafish embryos develop exceptionally rapidly, completing major morphological and physiological events in the first 24-48 hours post-fertilization. These stages are highly conserved, and the well-characterized timeline of zebrafish development makes them an ideal system for studying embryogenesis and organogenesis (see **Figure 1.3.1**).

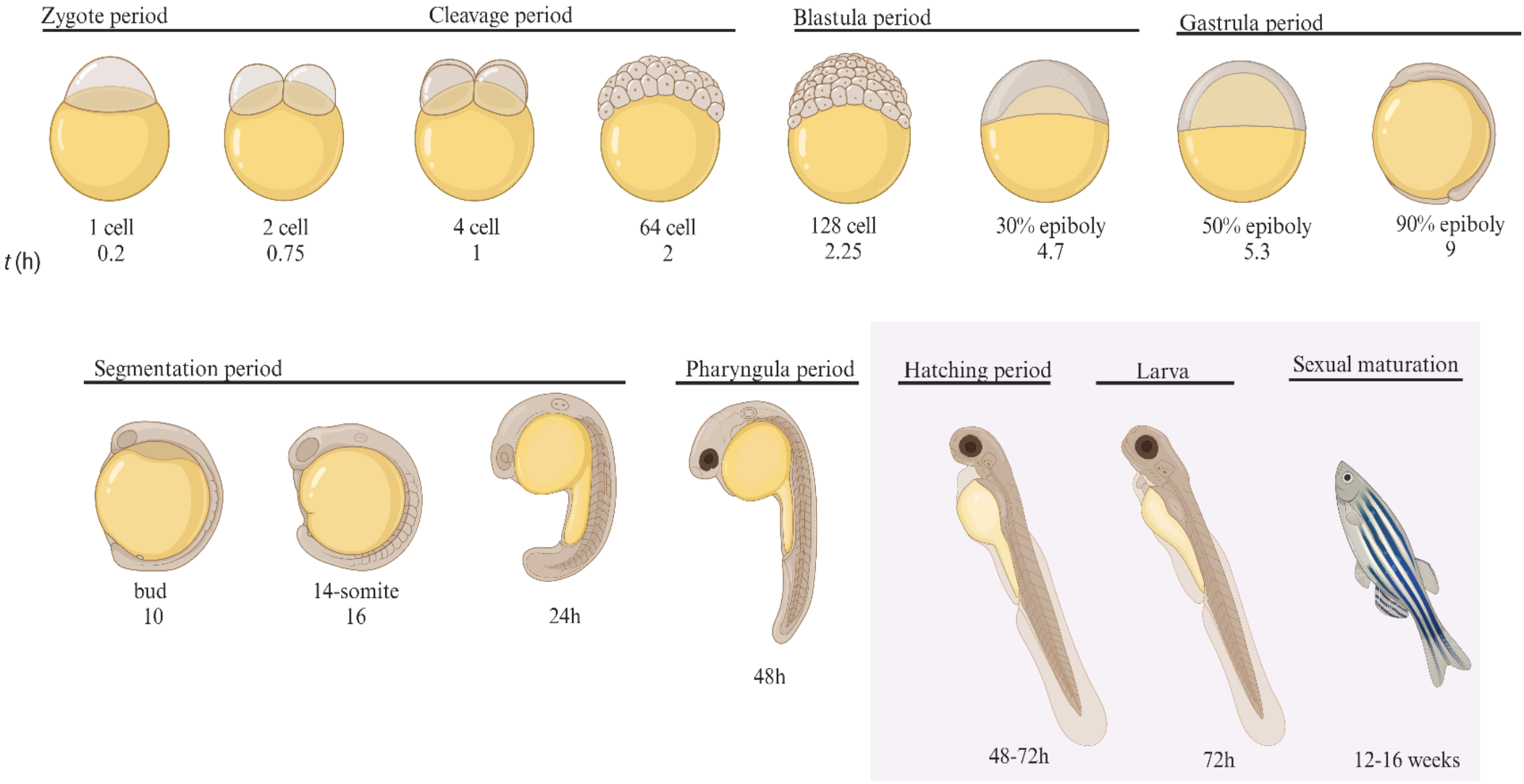

Figure 1.3.1: Representation scheme for the developmental stages of a Zebrafish embryo. Figure created by Author using biorender.com.

Fertilization (fertilization to cleavage 0-3 hours) occurs externally, with the sperm and egg meeting in the water. After fertilization, the zygote undergoes rapid cleavage, which results in the formation of a blastula, a ball cell with a hollow interior (0-3 hours post-fertilization). This early cellular division is notable because it involves minimal cell growth, with cells simply dividing into smaller blastomers. The cleavage process is crucial for determining the basic architecture of the embryo [85]. Within the first few hours, the cells of the blastula become organized, and the first cellular divisions set the stage for the formation of the primary germ layers (ectoderm, mesoderm, and endoderm) that will give rise to all the tissues and organs of the zebrafish [86].

Gastrulation (3-6 hours post-fertilization) is a critical process that defines the body plan of the developing embryo and results in the formation of the three primary germ layers. This process begins around 3 hours post-fertilization and involves extensive cell migration and rearrangement. The mesodermal layer will form tissues such as muscles, blood vessels, and the heart, while the ectoderm will give rise to the skin and nervous system, and the endoderm will form the gut and associated organs. During gastrulation, epiboly, the spreading of the ectodermal cells, is particularly noteworthy. The ectodermal cells spread outwards, covering the yolk cell and extending to form a continuous layer. At the same time, invagination occurs, where cells from the mesoderm and endoderm migrate inward to form the inner layers of the embryo.

Neurulation and organogenesis (6-24 hours post-fertilization), where the neural tube formation begins at approximately 6 hours post-fertilization. The ectodermal cells at the embryo's midline differentiate into the neural plate, which folds to form the neural tube. This process is crucial for the formation of the central nervous system. The zebrafish neural tube develops rapidly and begins to differentiate into the brain and spinal cord.

By 24 hours post-fertilization (24-72 hours post-fertilization), the first significant organs—such as the heart, blood vessels, and brain—begin to form. The zebrafish heart starts beating around 24 hours, and circulation begins soon after, facilitating oxygen delivery to tissues. The kidneys, liver, and other organs also shape during this time. At approximately 24 hours post-fertilization, the embryo hatches and becomes a free-swimming larva. The zebrafish larva is fully transparent, allowing real-time observation of organ function and behavior. This transparency is a key feature that makes zebrafish larvae popular for live imaging. During this stage, the larval heart beats at a high rate, the blood circulates through vessels, and the brain shows electrical activity, all of which can be visualized using advanced imaging techniques.

At 48 hours post-fertilization, the larvae begin to exhibit simple behaviors such as phototaxis (movement toward or away from light), which provides insights into neuronal function and sensory processing [84].

3.3. Drug Screening and Toxicology

One of the primary advantages of this model system is the transparency of zebrafish embryos. It allows for real-time imaging of developmental processes in live embryos, such as cell division, organogenesis, and neuronal activity. Researchers can track the movement of individual cells, visualize gene expression patterns, and monitor the effects of drugs or genetic modifications on developmental processes. Fluorescent proteins and other markers are frequently used to track specific cell populations or tissues, allowing for detailed visualization of developmental processes in vivo [76, 77].

Zebrafish embryos are highly amenable to genetic manipulation, a significant advantage for researchers. Techniques such as CRISPR-Cas9 and morpholino oligonucleotides can knock out or knock down genes, allowing researchers to investigate gene function in the context of development and disease. Transgenic zebrafish models, in which genes are inserted or modified to express fluorescent proteins or other markers, have been developed to study gene function and disease processes [89].

Zebrafish embryos develop rapidly, with significant organs forming within 24 hours. This rapid development allows researchers to observe developmental events quickly, making zebrafish ideal for high-throughput screening and rapid experimental workflows. Additionally, zebrafish are prolific breeders, with a female capable of laying hundreds of eggs per week. This high reproductive capacity allows for large-scale experiments and the generation of numerous embryos for genetic screening and drug testing [84].

Chapter Four: Comparative Study of Chelating Agents in the Treatment of Heavy Metal Poisoning on Early Zebrafish Embryo Development Followed by quantitative-PCR Studies

4.1. Aim of the Study

Heavy metals, such as mercury, lead, and cadmium, are some of the most toxic and relevant species concerning public health. These metals tend to access the central nervous system and accumulate in the kidney and liver, which causes severe damage or fatality. When the maximum tolerated dose is exceeded in the human body, the so-called chelation therapy is recommended, where traditional sulfur-based compounds such as alpha-lipoic acid (ALA), dimercaptosuccinic acid (DMSA), dimercatopropanesulfonic acid (DMPS), cysteine (L-Cys) and glutathione (L-GSH), are orally introduced in the body to chelate metal (II) ions. Little is known for the most effective chelating agents to treat heavy metal poisoning. To investigate these compounds, we utilized the rapidly growing and experimentally tractable zebrafish, a model that has been widely used for toxicological studies.

First, we investigated the oxidation rate of the organic compounds in zebrafish embryo medium (E3) by Nuclear Magnetic Resonance. Second, we identified the lowest toxic concentration of the heavy metals in early developing zebrafish embryos. Lastly, we compared the efficacy of different commercially available and clinically approved chelating agents in controlling heavy metal toxicity. In our evaluation, we found out that (i) the organic compounds are stable for the time the embryos were incubated, (ii) Pb can be tolerated at higher concentrations than Cd (II) (iii) DMSA, DMPS, cysteine, and glutathione successfully rescue mercury-poisoned zebrafish embryo, while LA does not (iv) DMSA and DMPS rescue cadmium-poisoned zebrafish embryo, while LA, cysteine, and glutathione do not (v) qPCR analysis of genetic material extracted from the poisoned embryos revealed alterations in specific pathways, which can be reversed by chelation therapy.

Keywords: Toxicology · Nuclear Magnetic Resonance (NMR) · Oxidation Kinetics · Chelating Agents · Mercury · Lead · Cadmium · Zebrafish Embryo · qPCR · RNA

Graphical Abstract

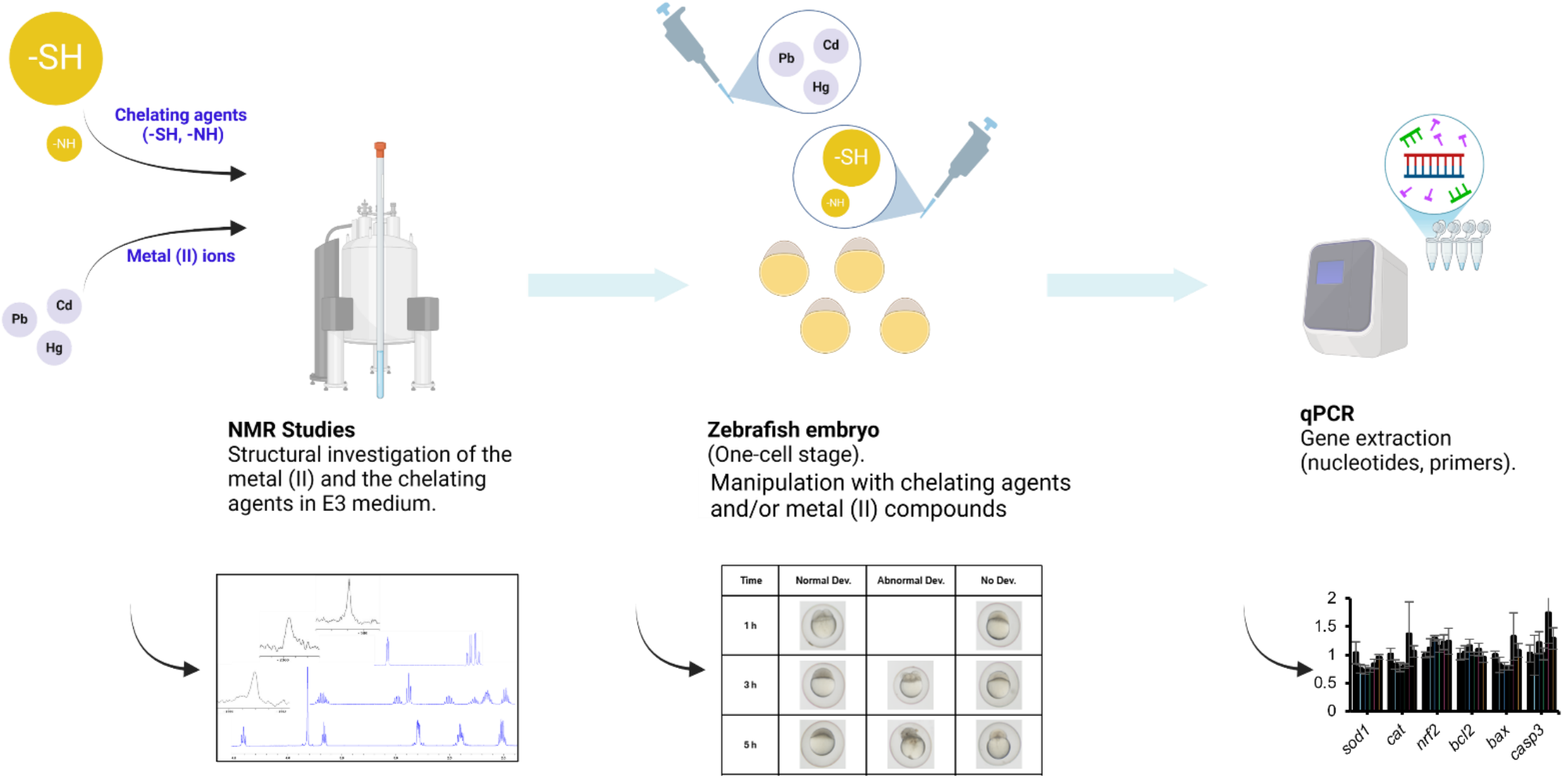

4.3. Experimental Part

Materials and methods

ALA (Alpha-lipoic acid) was purchased from Tokyo chemical industry (TCI), Germany, NaCl from ITW Reagents, Germany potassium chloride (KCl), calcium chloride dihydrate ($CaCl_2 \cdot 2H_2O$), magnesium sulfate heptahydrate ($MgSO_4 \cdot 7\ H_2O$), Methylene Blue zinc chloride double salt ($C_{16}H_{18}ClN_3S \cdot 0.5\ ZnCl_2 \cdot xH_2O$) DMSA, DMPS, L-CYS, L-GSH, mercury chloride ($HgCl_2$), lead chloride ($PbCl_2$) and cadmium chloride ($CdCl_2$) were obtained from Sigma Aldrich. Deuterated water (D_2O) was purchased from Deutero GmbH, and deuterated DMSO-*d*$_6$ from Eurisotop. All chemicals were used as received unless otherwise stated.

Instruments

Nuclear Magnetic Resonance (NMR) experiments were conducted on two different NMR instruments, a Bruker Avance III equipped with a 5 mm ATM BBFO probehead for metallic experiments, and a Bruker Avance II with 5 mm DUL S1 probehead for the organic compounds (metal chelators), both instruments operating at a nominal ^1H frequency of 400.13 Hz. All experiments were regulated at ambient conditions (298 K), except for lead chloride, 378 K was used. The data arrangements were processed using TopSpin 4.2.0 (Bruker) and Dynamics Center 2.8.6 (Bruker).

Preparation of E3 Medium

The E3 medium was freshly prepared in 1L from distilled H_2O or deuterated D_2O, consisting of 5 µL NaCl, 0.17 µL KCl, 0.33 µL $CaCl_2 \cdot 2\ H_2O$, 0.33 µL $MgSO_4 \cdot 7\ H_2O$, and 300 µL (0.1%) methylene blue.

NMR studies of free Hg, Pb, and Cd

Each metal compound was prepared in E3 medium from deuterated H_2O, 10 mM for mercury(II) chloride, 35.5 mM for lead(II) chloride, and 0.1 M cadmium(II) chloride (2.7 mg/ml $HgCl_2$, 9.3 mg/ml $PbCl_2$, and 18.3 mg/ml $CdCl_2$).

NMR studies of the Ligands

Each organic compound was prepared prior to 10 mM in E3 medium from deuterated H_2O (2.06 mg/ml LA, 1.82 mg/ml DMSA, 2.28 mg/ml, L-Cys 1.21 mg/ml and 3.07 mg/ml L-GSH). The ligands were initially dissolved before adding DMSO-*d*$_6$ (55 µL), followed by instant NMR experiments.

Preparation of Metals and Chelating Agents for Zebrafish Embryos

Heavy metals and chelating agents were freshly prepared before each set/replicate of experiments using E3 medium (distilled H_2O), producing one mM stock solutions, followed by dilution for the desired concentration.

Zebrafish Husbandry

The zebrafish (Danio rerio) AB strain was kept as described in [90]. Zebrafish embryos were kept in an E3 medium. Staging of the zebrafish embryonic development was conducted following the guidelines of previous studies [90].

Evaluation of heavy metals toxicity and chelation efficacy in Zebrafish embryos

AB strain zebrafish were crossed, and the embryos were harvested and incubated at the described time points with various concentrations of the heavy metals in the E3 medium. The development of the zebrafish was investigated and imaged using a Nikon SMZ18 stereo microscope. The observed phenotypes were then categorized into four distinct classes, "normal development," "abnormal development," "no development," and "dead" (see **Figure 1.4.4**). The efficacy of the chelators in rescuing the observed phenotypes was assessed by adding an equimolar chelator solution two hours post-heavy metal treatment.

RNA extraction and qPCR

RNA was extracted using TRIZOL, as previously described [91]. Briefly, 20-30 embryos were homogenized in 1 ml Trizol reagent (Sigma) with a pestle, and 200 µl bromochloropropane was added; samples were then vortexed and centrifuged at 16000 g at 4 °C for 30 mins. Subsequently, the aqueous phase was separated, and RNA precipitation was performed using 0.8 volume of 100 % Isopropanol. Any DNA traces were removed by treating the RNA with TURBO™ DNase (Ambion) following the manufacturer's protocols. RNA was then reverse transcribed using GoScriptTM Reverse Transcriptase (Promega) according to the manufacturer's instructions. Quantitative real-time PCR (qPCR) was performed using Applied BiosystemsTM ABI 7500 or QIAGEN Rotor-Gene Q, using the KAPA SYBR® FAST kit (Sigma). GAPDH expression levels were used to control the expression levels of target genes.

Table 1.4.1: q-PCR primer sequences

Primer	Sequence	Reference
BE_2171_sod1_F	GGCCAACCGATAGTGTGAGA	[92]
BE_2172_sod1_R	CCAGCGTTGCCAGTTTTAAG	
BE_2173_catalase_F	AGGGCAACTGGGATCTTACA	
BE_2174_catalase_R	TTTATGGGACCAGACCTTGG	
BE_2175_bax_F	GGCTATTTCAACCAGGGTTCC	
BE_2176_bax_R	TGCGAATCACCAATGCTGT	
BE_2177_casp3_F	CCGCTGCCCATCACTA	[93]
BE_2178_casp3_R	ATCCTTACACGACCATCT	
BE_2179_nrf2_F	TCGGGTTTGTCCCTAGATG	
BE_2180_nrf2_R	AGGTTTGGAGTGTCCGCTA	
BE_2181_bcl2_F	CACTGGATGACTGACTACCTGAA	
BE_2182_bcl2_R	CCTGCAGTCCTCATTCTGTAT	
BE_235_zfGAPDH_F	GTGCAGGAGGCATTGCTTACA	[92]
BE_236_zfGAPDH_R	GTGCAGGCATTGCTTACA	

4.4. Results and Discussions

Spectroscopic evaluation of free Hg, Pb, and Cd

In contrast to the compounds' solubility, we have considered the optimal concentrations for NMR experiments (see **Figure 1.4.1)**. Mercury (II) chloride was highly soluble in water with the presence of Ca and Mg ions (E3 medium), whereas lead (II) chloride and cadmium chloride had a lower solubility. Therefore, depending on their maximum water solubility, cadmium, and lead chloride were of higher concentrations.

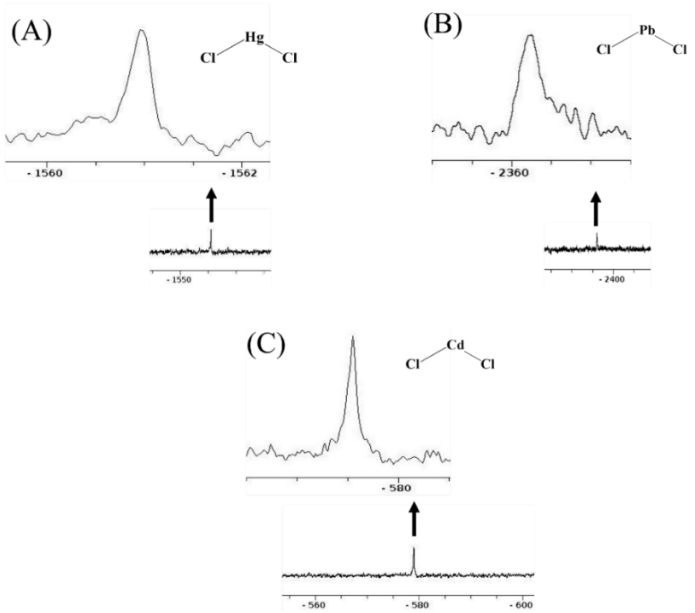

Figure 1.4.1: Chemical shift range of metal (II) ions in E3 medium at ambient conditions. **(A)** 10 mM mercury (II) chloride **(B)** 35.5 mM lead (II) chloride at 323 K **(C)** 0.1 M mercury (Acquisition Parameters; Supplementary Information Figure S1.9).

Spectroscopic evaluation of free Metal Chelators

Expectedly, concerning ALA, no changes were observed as ALA exists in the oxidized form (see **Figure 1.4.2**).

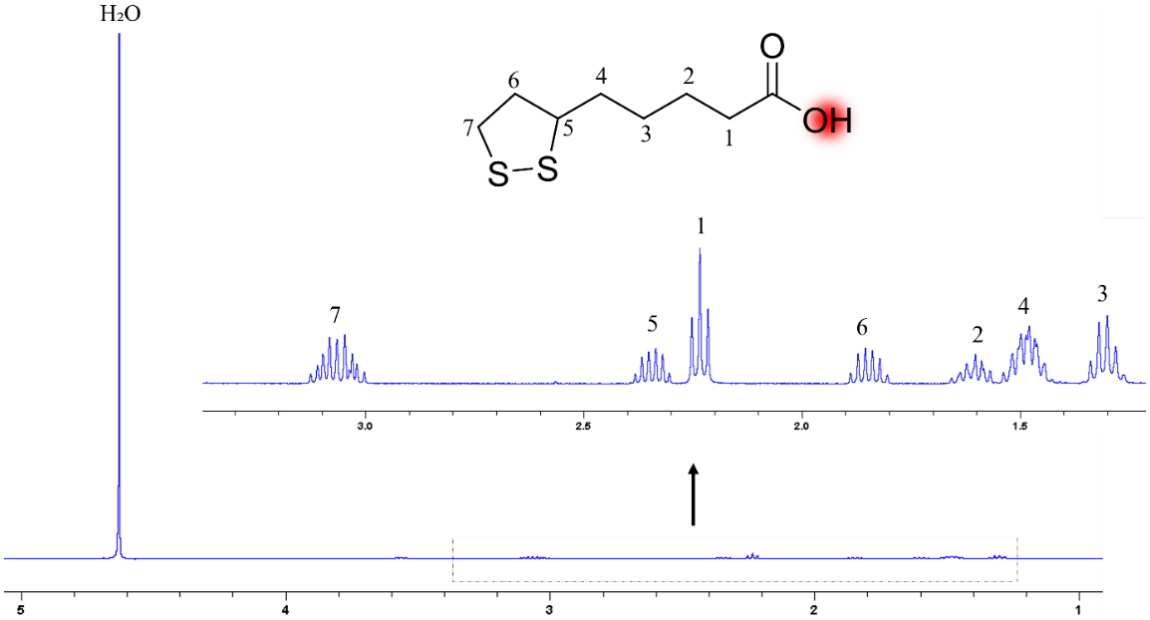

Figure 1.4.2: Superimposed ^{1}H NMR spectra of alpha-lipoic acid (10 mM) at ambient conditions before adding the oxidizing agent (DMSO-d_6) (NMR acquisition Parameters; see Supplementary Information Figures S1.1-S4.4).

Kinetics Oxidation of Chelating Agents

The oxidation state of the chelating agents was a step taken to ensure the ligands' stability during the embryos' incubation time. The oxidation of the ligands was monitored using ^{1}H NMR spectroscopy, providing insights into the stability of the metal(II) and the organic compounds. The recorded spectra over 24 hours (see **Figure 1.4.3a**) show extremely gradual progression of oxidation of the compounds, evidenced by the appearance of no new peaks and the shifting of proton signals corresponding to the oxidized forms of DMSA, DMPS, Cys, and GSH (Supplementary Information Figures S1.1-1.4). This suggests that the organic compounds undergo very slow oxidation under ambient conditions.

The addition of 10% DMSO significantly altered the oxidation profile, as seen in the NMR spectra recorded over 4 hours for DMSA, DMPS, L-Cys, and GSH (see **Figure 1.4.3b**, Supplementary Information Figures S1.5-1.8). The spectrum at time 0.05 h. (167 sec.) represents the system's state before adding DMSO and shows no significant oxidation.

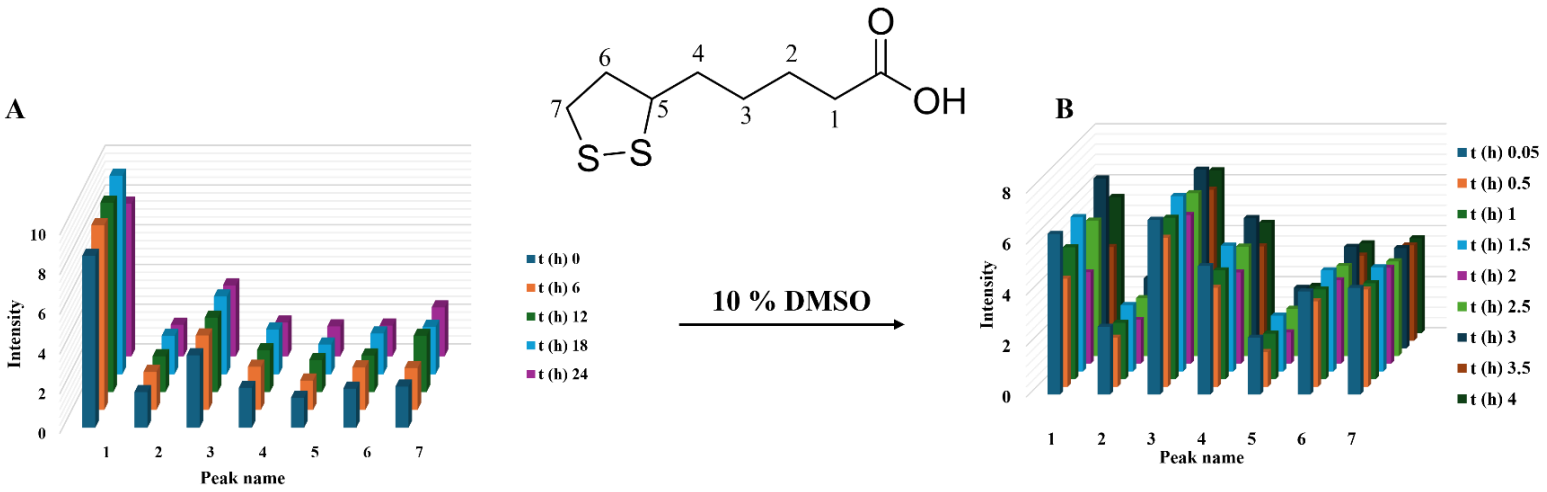

Figure 1.4.3: Oxidation data for lipoic acid monitored through ^{1}H NMR spectroscopy at ambient conditions. **(A)** ^{1}H NMR spectra were recorded over 24 hours, with one spectrum collected each hour. **(B)** ^{1}H NMR spectra were recorded for 4 hours after adding 10% DMSO, with one spectrum collected every 0.5 hours. The spectrum at 0.05 hours represents the ^{1}H NMR spectrum before DMSO is added.

To ensure the stability of the metal and organic compounds used in the incubation of zebrafish embryos, it is essential to prevent oxidation during experimental procedures. The NMR analysis confirmed that the compounds remain stable in the E3 medium for at least 12 hours, indicating that the compounds are not prone to oxidation under standard experimental conditions. This stability is crucial when assessing the biological effects of these compounds on zebrafish embryos, as it ensures that the observed biological outcomes are due to the intended compounds and not their oxidized derivatives. Moreover, adding an oxidizing agent allowed us to observe apparent changes in the NMR spectra, confirming that the compounds are susceptible to oxidation

under certain conditions. These changes are reflected in the corresponding graphs (see **Figure 1.4.3a-b**). These findings are essential for reproducing and reliability in zebrafish embryo studies, mainly when working with metal-containing compounds or sulfur-based antioxidants.

Despite DMSO's destabilizing effect, complete inhibition of oxidation was not observed. This suggests that other factors, such as pH, oxygen concentration, and the sample's specific environment, may influence the oxidation rate. Future studies should explore the impact of these parameters to gain a more comprehensive understanding of the oxidation mechanism of lipoic acid and other compounds in various conditions.

Profiling the toxicity of $HgCl_2$, $CdCl_2$, and $PbCl_2$ on the zebrafish early development

To identify the lowest toxic concentrations of $HgCl_2$, $CdCl_2$, and $PbCl_2$ in the early-developing zebrafish embryos, newly born embryos were incubated with various dilutions of the three heavy metals in the E3 medium. The zebrafish embryos were classified into three categories based on their responses to the test of heavy metals: normal development, abnormal development, and no development classes (see **Figure 1.4.4**). In contrast to $CdCl_2$ and $PbCl_2$, $HgCl_2$ exhibited higher toxicity in the developing zebrafish embryos. As early as 3 hours post-treatment (hpt), developmental defects were evident in more than 50% of the embryos upon exposure to $HgCl_2$ at a concentration of 5 µM (Supplementary Information Table S1.1). Higher $HgCl_2$ concentrations have resulted in a substantially increased toxicity with doses of 50 µM and 100 µM leading to early lethality at just one hpt (Supplementary Information Table S1.1). Although lower HgCl2 concentrations of 1-2 µM did not induce any toxicity at the first hours post-treatment, prolonged incubation for 24 hours has resulted in either developmental defects in up to 50% of the treated larvae with one µM $HgCl_2$ or almost complete lethality at two µM (see **Figure 1.4.5a**). On the other hand, the embryos exhibited high tolerance to concentrations as high as 150 µM $CdCl_2$ and 120 µM $PbCl_2$, with a lethality rate of only 10-25% at 24-hour post-treatment (see **Figures 1.4.5b** and **1.4.5c**). Furthermore, none of the tested concentrations of $CdCl_2$ and $PbCl_2$ have resulted in significant early developmental defects in the first few hours post-treatment (see **Figures 1.4.5b, c**, Supplementary Information Table S1.1).

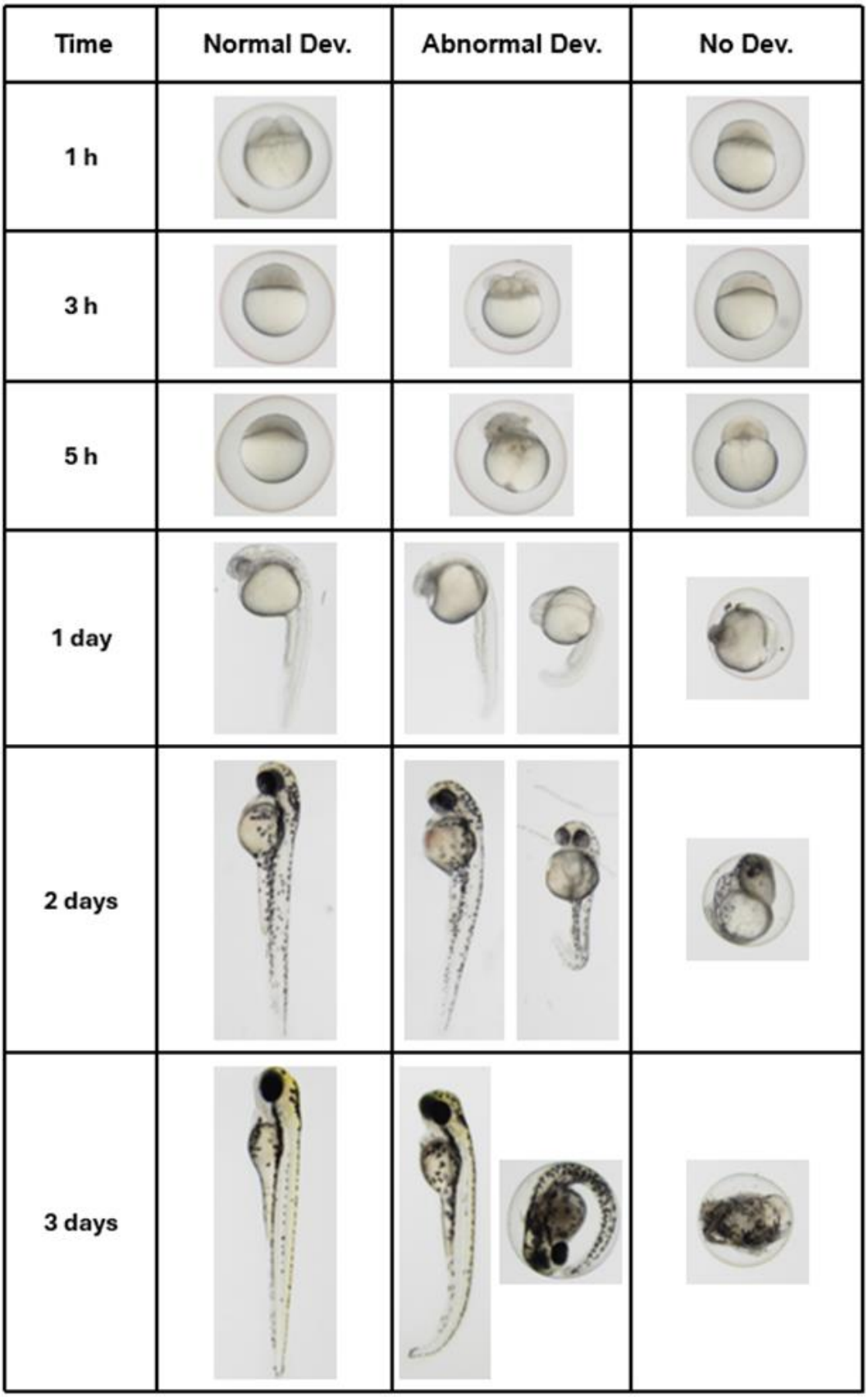

Figure 1.4.4: Classification of different development categorized upon heavy metal exposure. The presented classes include normal, abnormal, and no development (Normal Dev, abnormal Dev, and No Dev).

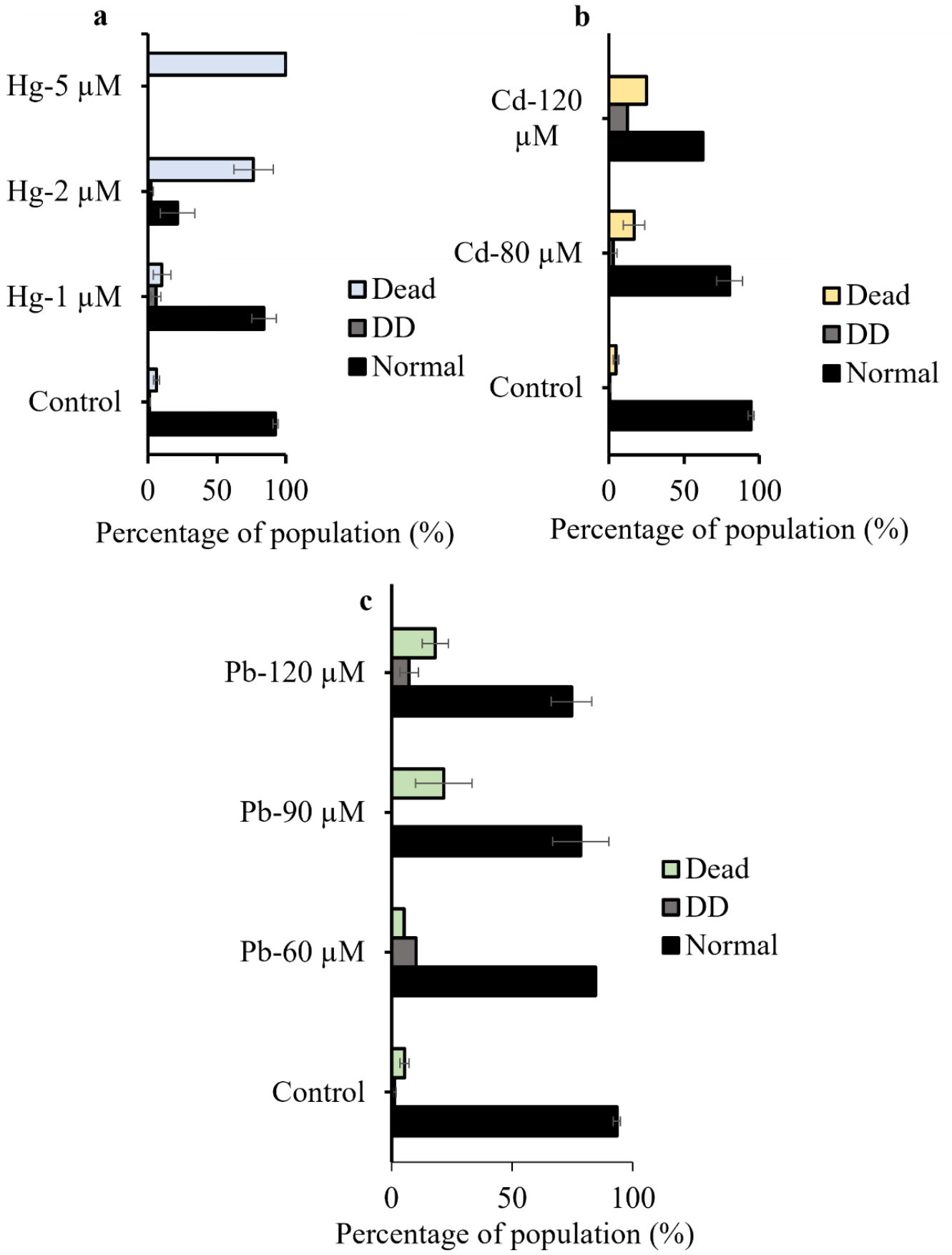

Figure 1.4.5: Acute toxicity assessment of different heavy metals concentrations at 24 hours post-treatment (24-hpt). Investigation of the toxicity of 1, 2, and 5 µM $HgCl_2$ (a), 80, 120 and 150 µM $CdCl_2$ (b) and 60, 90, 120 and 150 µM $PbCl_2$ (c). DD Developmental defects, error bars represent standard error of the mean.

Clinically approved heavy metal chelators have variable efficiencies

To evaluate the efficiency of the clinically approved chelators (LA, DMPS, DMSA, cysteine, and GSH), the embryos were preincubated with 1-2 µM $HgCl_2$, 80 µM $CdCl_2$, and 120 µM $PbCl_2$ for 2 hours before adding the chelators at a molar ratio of 1:1. The incidence of lethality and developmental defects was investigated at 24-hpt (see **Figure 1.4.6 a-d**). Surprisingly, LA was not able to mitigate developmental defects or the lethal effect of heavy metal exposure (see **Figure 1.4.7 a-d**). Apart from the one µM concentration, which resulted in approximately 50% lethality, the coadministration of LA with any of the three heavy metals at 2-120 µM has resulted in complete lethality (see **Figure 1.4.6a-d**). This suggests potential additional toxicity of this chelator in the early-developing zebrafish embryos. Nevertheless, all DMPS, DMSA, cysteine, and GSH successfully alleviated the heavy metal developmental and lethal effects to a comparable degree (see **Figure 1.4.7a-d**).

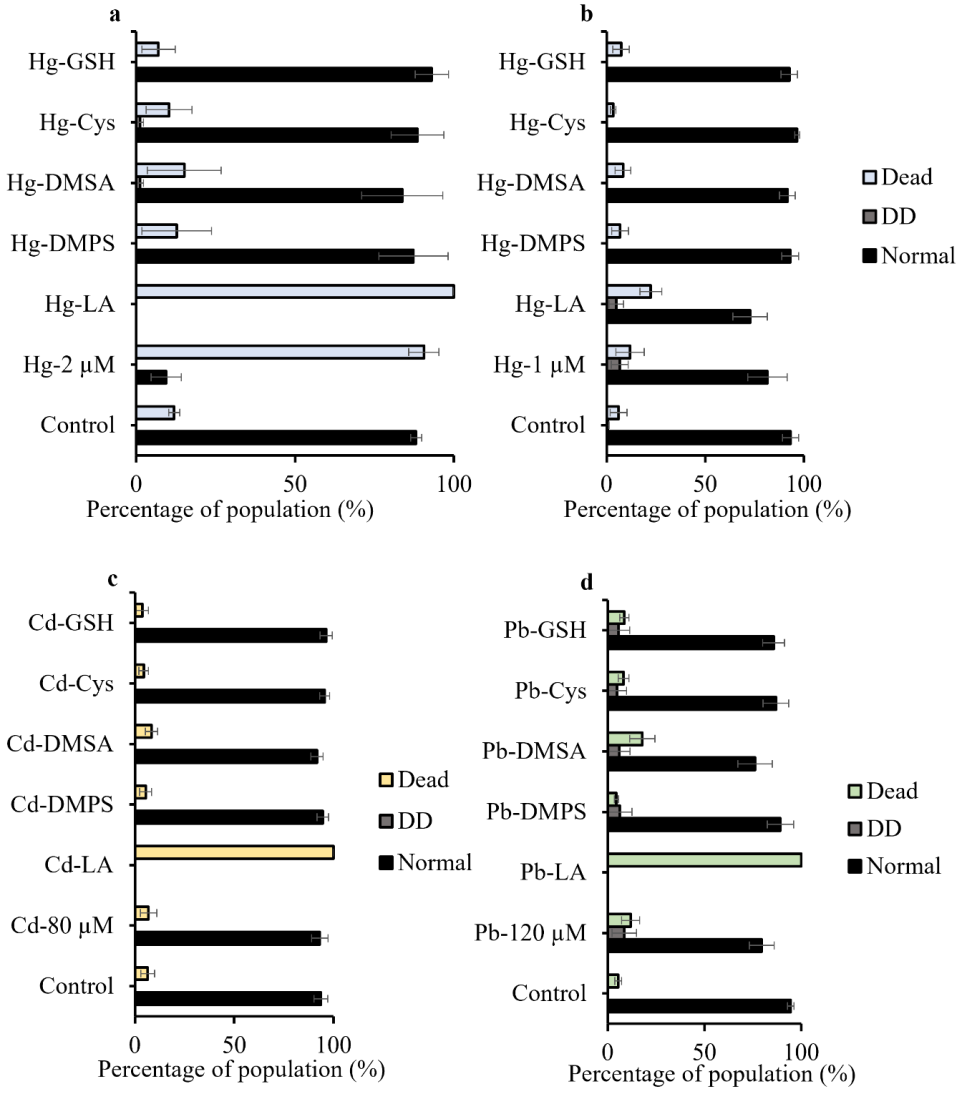

Figure 1.4.6: Assessment of various chelators' efficacy in rescuing heavy metals toxicity. The ability of LA, DMPS, DMSA, Cysteine (Cys), and glutathione (GSH) to rescue the toxicity of 1 (a) or 2 (b) µM $HgCl_2$, 80

μM $CdCl_2$ (c) and 120 μM $PbCl_2$ (d). DD developmental defects, error bars represent the standard error of the mean.

Distinct mechanisms of heavy metals toxicity and chelation therapy efficacy

To identify the molecular mechanisms underlying the observed lethality and the test chelators' ability to counteract such mechanisms, quantitative real-time PCR (qPCR) was employed to determine the expression levels of the antioxidant genes (*sod1, catalase,* and *nrf2*), the antiapoptotic factor (*bcl2*) and the proapoptotic factors (*bax* and *casp3*) at 24-hpt, both with and without the chelators. These experiments revealed that all three heavy metals reduce antioxidant activity with a particularly pronounced reduction of the highly expressed antioxidant, *sod1* (see **Figure 1.4.7 a-c**). Interestingly, the response to chelation therapy varied depending on the specific heavy metal used. While all the different test chelators could not counteract the reduction of *sod1* by $HgCl_2$ poisoning, both cysteine and GSH efficiently reversed *sod1* downregulation in the case of $CdCl_2$ and $PbCl_2$. Furthermore, the antioxidant gene catalase was downregulated in response to both $CdCl_2$ and $PbCl_2$ toxicity, an effect that was consistently rescued by cysteine and GSH in the case of Cd poisoning. In contrast, DMPS, DMSA, and cysteine could reverse catalase downregulation upon Pb poisoning (see **Figures 1.4.7b** and **1.4.7c**). Although the expression of the third antioxidant gene, *nrf2,* was only slightly reduced under $HgCl_2$ toxicity, it exhibited an upregulation during $CdCl_2$ and $PbCl_2$ poisoning. Additionally, chelation therapy with DMPS, DMSA, and cysteine comparably rescued the downregulation of *nrf2* during $HgCl_2$ exposure.

In contrast to both $CdCl_2$ and $HgCl_2$, $PbCl_2$ induced a remarkable increase in apoptosis, as illustrated by the downregulation of the antiapoptotic factor, *bcl2,* and upregulation of the proapoptotic genes, *bax,* and *casp3*, suggesting uncontrolled apoptosis as a major player in the Pb toxicity (see **Figures 1.4.7a-c**). Essentially, the upregulation of *casp3* was the only effect successfully rescued by all four chelators. To our surprise, chelation therapy in conjunction with specific heavy metal toxicity resulted in increased apoptosis, as demonstrated by further downregulation of *bcl2* during pb poisoning upon treatment with DMPS, DMSA, cysteine, and GSH (see **Figure 1.4.7c**). Furthermore, upregulation of both *bax* and *casp3* was detectable upon cysteine and GSH treatment during Cd poisoning (see **Figure 1.4.7b**). Collectively, these results highlight the multifaceted efficacy and the potential for additional toxicity of the clinically approved chelators in managing heavy metal toxicity in aquatic organisms.

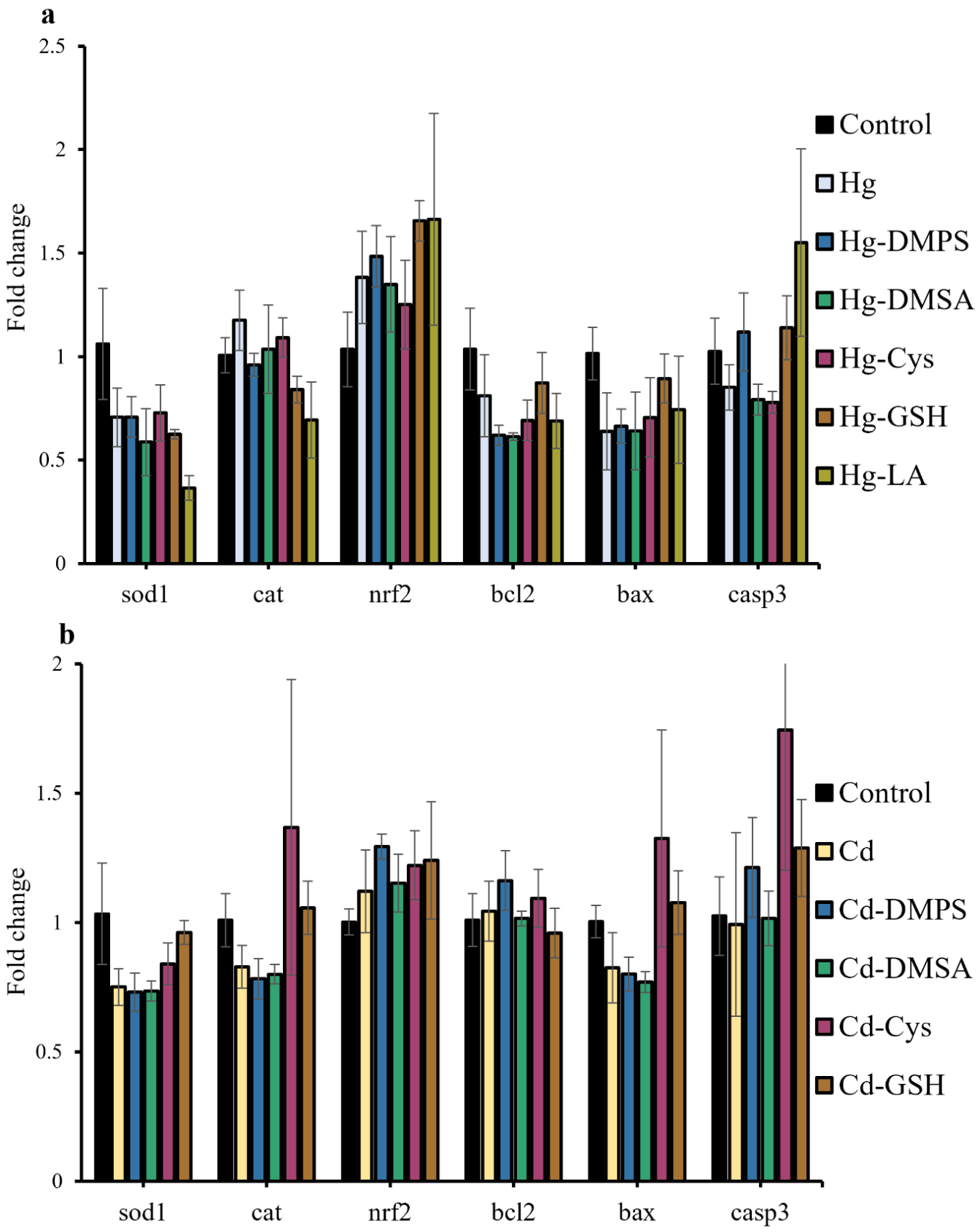
a
Fold change
2.5
2
1.5
1
0.5
0
sod1
cat
nrf2
bcl2
bax
casp3
Control
Hg
Hg-DMPS
Hg-DMSA
Hg-Cys
Hg-GSH
Hg-LA
b
Fold change
2
1.5
1
0.5
0
sod1
cat
nrf2
bcl2
bax
casp3
Control
Cd
Cd-DMPS
Cd-DMSA
Cd-Cys
Cd-GSH

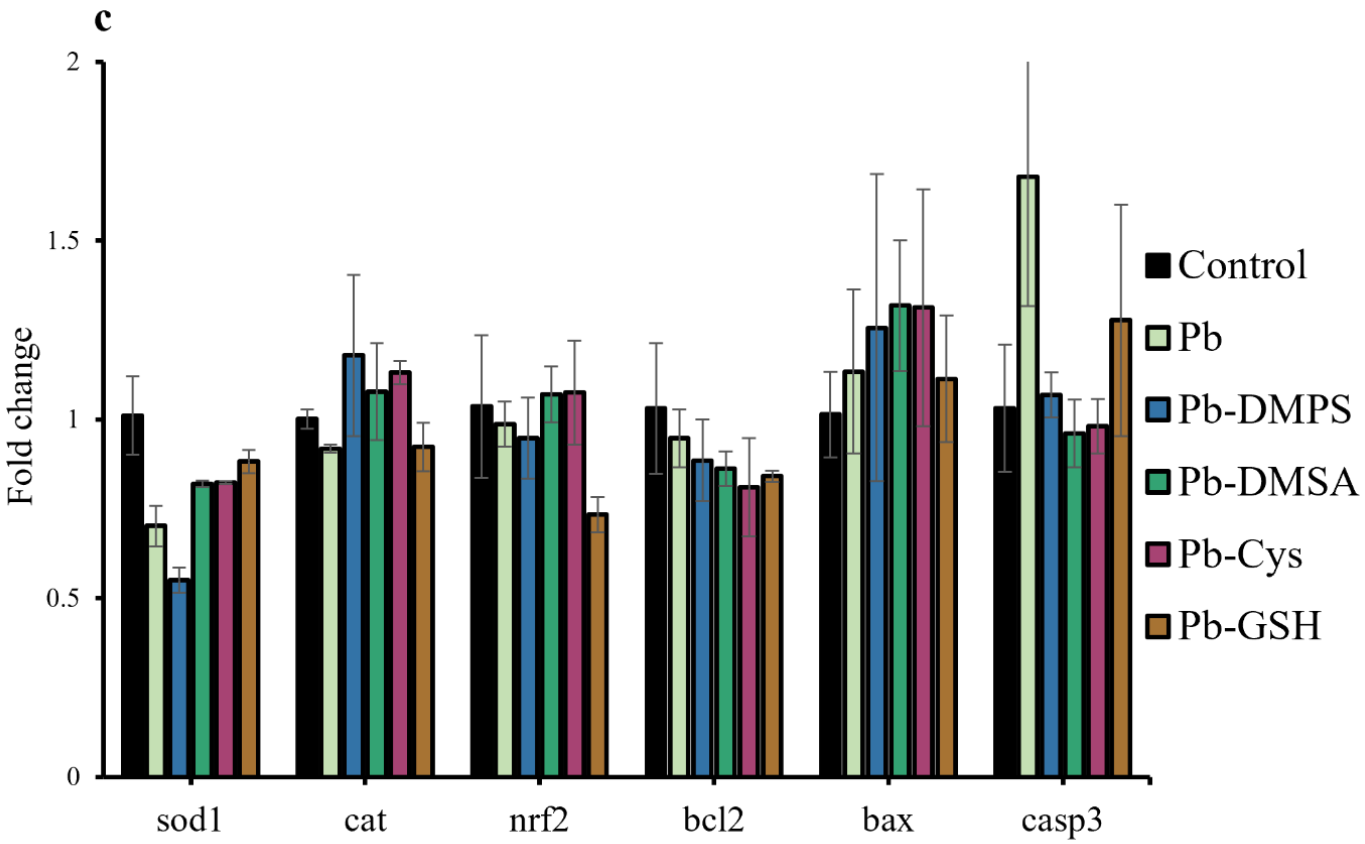

Figure 1.4.7: Variable capacity of the clinically approved chelators LA, DMPS, DMSA, Cysteine (Cys), and glutathione (GSH) in rescuing the toxicity of 1 µM $HgCl_2$ (a), 80 µM $CdCl_2$ (c) and 120 µM $PbCl_2$ (d). error bars represent the standard error of the mean.

4.5. Conclusions

In conclusion, using NMR spectroscopy provided valuable insights into the time-dependent oxidation of ligands and the effect of DMSO. These findings confirm the stability of metal and organic compounds in an E3 medium for at least 12 hours before the addition of the oxidizing agent, which is critical for zebrafish embryo studies. The results also emphasize monitoring oxidation states to ensure accurate biological interpretations. These findings contribute to the broader understanding of stabilization strategies for sulfur-containing antioxidants and metal compounds, with important implications in pharmaceutical and biomedical applications.

We have also investigated the efficacy of various commercially available and clinically approved chelating agents in rescuing heavy metal toxicity in zebrafish. We identified toxic doses of Hg, Cd, and Pb in the E3 medium and used equimolar concentrations of the different chelators to prevent toxicity. We found out that $HgCl_2$ exhibited the highest toxicity with a dose of 1 µM sufficient to induce complete fatality at 24-hpt. This is consistent with published research where it was demonstrated that Hg is highly toxic to zebrafish embryos, with concentrations as low as 16 µg/L (0.059 µM), inducing developmental defects [94]. On the other hand, $CdCl_2$ and $PbCl_2$

demonstrated a higher tolerance threshold, with doses ranging from 40-80 µM exhibiting no significant gross morphological defects or early lethality. Similarly, earlier studies have shown that Cd has no significant toxic effects on embryos at up to 50 µM concentrations [93]. Furthermore, studies on Pb poisoning in zebrafish have demonstrated no severe morphological defects, while long-term exposure induces central nervous system defects [95, 96]. Mechanistically, we uncovered that the three heavy metals can induce oxidative stress, as illustrated by the downregulation of the antioxidant gene *sod1* (see **Figure 1.4.7a-c**). Downregulation of antioxidant genes was similarly observed in earlier studies of Hg and Cd poisoning in zebrafish [91, 94, 97]. Surprisingly, rescue experiments using various chelators revealed that LA is toxic to zebrafish embryos when administered during heavy metal poisoning (Supplementary Information Figures S1.11 and 1.12). Indeed, human cases of LA-induced multiorgan failure and fatality have been reported [98]. This underscores the necessity for meticulous investigation to ascertain the precise cause of lethality. Furthermore, the efficacies of all DMPS, DMSA, cysteine, and GSH were variable, and even cysteine and GSH further increased the expression of the proapoptotic factors *bax* and *casp3* during Cd poisoning. This finding suggests the possibility of additional toxic effects of the chelation therapy at certain concentrations in conjunction with specific heavy metals. Further experimentation in different systems is required to investigate the specificity of these effects on zebrafish and ascertain safe dose ranges for these chelators.

PART II: DRUG DELIVERY SYSTEMS (DDS)

Chapter One: Background and Knowledge of Anticancer Drugs

1.0. Human Cancer – From Discovery to Advances

Cancer continues to be one of the leading causes of mortality worldwide, making it necessary for the continuous development of innovative therapies [99]. Its discovery dates back to ancient civilizations and is referred to as a condition with no known cure [100]. In the 19th century, the invention of microscopes established that cancer arose from abnormal cell growth and was understood as a cellular disease. Later, monumental advancements were made, including the discovery of genetic mutations, carcinogens, and viruses linked to cancer. The transformation of cancer treatment was established by the establishment of oncology combined with chemotherapy, radiation therapy, and surgical techniques [101].

Among anticancer drugs, platinum-based organometallic compounds have gained much attention due to their effectiveness against various cancers [102]. In biology, cancer develops when normal cells undergo genetic mutations that disrupt their regulatory mechanisms, allowing uncontrolled growth and division. Key hallmarks of cancer include self-sufficiency in growth signals, resistance to cell death, sustained angiogenesis (formation of blood vessels), tissue invasion, and metastasis [103]. In genetic factors, cancer arises from mutations in critical genes, including oncogenes, tumor suppressor genes, and Deoxyribonucleic Acid (DNA) repair genes. For example, Tumour Protein 53 (TP53) tumour suppressor gene mutations are found in over 50% of cancers [104]. Advances in genomics have identified specific genetic changes associated with various cancers, paving the way for targeted therapies [105-107]. In addition, cancer can also arise from environmental and lifestyle factors, including tobacco smoke, ultraviolet radiation, asbestos, and certain chemicals. Lifestyle factors such as diet, physical inactivity, and alcohol consumption also contribute to cancer risk. The interplay between genetic predisposition and environmental exposure remains a critical study area [108]. However, certain viruses, such as human papillomavirus (HPV), hepatitis B and C, and Epstein-Barr, are linked to cancer development [109]. Vaccines, such as the HPV vaccine, have emerged as practical tools for cancer prevention [110, 111].

1.1. Research and Therapy

Over the years, significant advancements in diagnostic tools have revolutionized oncology. Advances in cancer diagnosis have emerged, leading to accurate diagnoses and effective cancer management. Imaging such as X-rays, Computed Tomography (CT) scans, and Magnetic Resonance Imaging (MRI) are traditional techniques that provide detailed insights into tumour biology. For example, Positron Emission Tomography Scans (PET) scans use radiolabelled

glucose to detect metabolically active cancer cells [112]. Biopsy, the gold standard for cancer diagnosis, involves the microscopic examination of tissue samples. Advances in histopathology, including immunohistochemistry, allow identifying specific biomarkers that guide treatment decisions [113]. Liquid biopsy is a groundbreaking technique that analyses circulating tumour DNA (ctDNA) and other biomarkers in blood samples. This non-invasive method offers the potential for early detection, monitoring treatment response, and detecting recurrence [114]. Genomic and molecular diagnostics are next-generation sequencing (NGS) technologies that have enabled comprehensive genomic profiling of tumors. This approach identifies genetic mutations, enabling personalized treatment strategies and prognostic predictions [115]. Surgery for the removal of tumors has been a cornerstone of cancer treatment. Advances in minimally invasive techniques, such as laparoscopy and robotic-assisted surgery, have improved precision and reduced recovery times [116].

Radiation therapy uses high-energy rays to destroy cancer cells. Advanced techniques, such as Intensity-Modulated Radiation Therapy (IMRT) and proton therapy, enable precise tumour targeting while minimizing damage to healthy tissue [117]. Chemotherapy, first introduced in the mid-20th century, employs cytotoxic drugs to eliminate rapidly dividing cells. Although effective, it often causes significant side effects. The development of combination regimens and supportive therapies has improved outcomes. Targeted therapies revolutionized cancer treatment by selectively targeting molecular abnormalities in cancer cells. For example, trastuzumab (Herceptin) targets HER2-positive breast cancer. At the same time, imatinib (Gleevec) inhibits the BCR-ABL fusion protein in chronic myeloid leukemia (CML) [118]. Chimeric Antigen Receptor (CAR) T-cell therapy, another breakthrough, engineers patients' T cells to recognize and destroy cancer cells [119]. Hormone therapy is effective against hormone-sensitive cancers such as breast and prostate cancer. Drugs like tamoxifen and aromatase inhibitors block hormonal signals that fuel cancer growth [120]. Precision medicine is also a medical approach that customizes treatment for individual patients by considering their genetic and molecular. This personalized approach minimizes side effects and maximizes efficacy [121]. Stem cell transplants restore bone marrow function after high-dose chemotherapy. This approach is particularly valuable in hematologic cancers like leukemia and lymphoma [122].

Vaccines such as the HPV and hepatitis B vaccines, prevent cancer-associated infections. Extensive vaccination programs have significantly decreased the incidence of cervical and liver cancers [123]. Emerging techniques like low-dose CT scans for lung cancer screening hold promise for high-risk populations [124].

Screening programs, such as mammography for breast cancer and colonoscopy for colorectal cancer, facilitate early detection and improve survival rates by promoting smoking

cessation, healthy diets, physical activity, and reduced alcohol consumption have demonstrated success in preventing cancer [125]. Epigenetic modifications contribute to cancer progression, including DNA methylation and histone acetylation. Epigenetic therapies, such as HDAC inhibitors and DNA methyltransferase inhibitors, are being investigated as potential treatment options.[126].

Nanotechnology offers innovative solutions for drug delivery, imaging, and diagnostics. Nanoparticles enable targeted chemotherapy delivery to tumors, minimizing systemic toxicity while enhancing treatment efficacy [127].

1.2. Platinum-Based complexes - Cisplatin, Carboplatin and Oxaliplatin

The journey of platinum compounds as anticancer drugs began in the 1960s (see **Figure 2.1.1**). Their cytotoxic properties were sparked when platinum electrodes were used in bacterial cultures to inhibit cell division. This discovery promoted extensive research, and they were then clinically used in 1978 [128, 129]. Since then, cisplatin has been used for cancer treatment, in particular for ovarian, testicular, bladder, and lung cancers [130]. However, despite its revolutionary success, its limitations are still controversial. These include severe effects such as nephrotoxicity, neurotoxicity, and ototoxicity. Its acquired drug resistance has pushed scientists to develop second—and third-generation platinum analogs [131]. The development of second-generation platinum drugs was needed to overcome cisplatin's resistance and side effects. The generation included carboplatin and nedaplatin, which were in need [131].

Advances in medicinal chemistry have produced a plethora of novel platinum complexes with unique properties [131]. Key strategies include modifying the coordination sphere to enhance selectivity and developing platinum(IV) prodrugs.[132] Platinum(IV) complexes, characterized by their octahedral geometry, exhibit improved stability in the bloodstream and can be activated in the reductive environment of tumor cells [132]. This approach aims to minimize systemic toxicity and improves the therapeutic index [133].

Carboplatin's bidentate dicarboxylate ligand reduces its reactivity compared to cisplatin. This modification translates into a better safety profile, notably lower nephrotoxicity, without significantly compromising efficacy [132].

Third-generation platinum complexes, including oxaliplatin, were designed to expand the spectrum of activity and address resistance mechanisms [128]. Oxaliplatin incorporates a bulky diaminocyclohexane (DACH) ligand, which enhances its activity against cisplatin-resistant tumors [130]. It has shown remarkable efficacy in colorectal cancer treatment and is less prone to nephrotoxicity and ototoxicity [133].

Recent advancements in medicinal chemistry have led to the development of numerous novel platinum complexes with distinct properties [131].

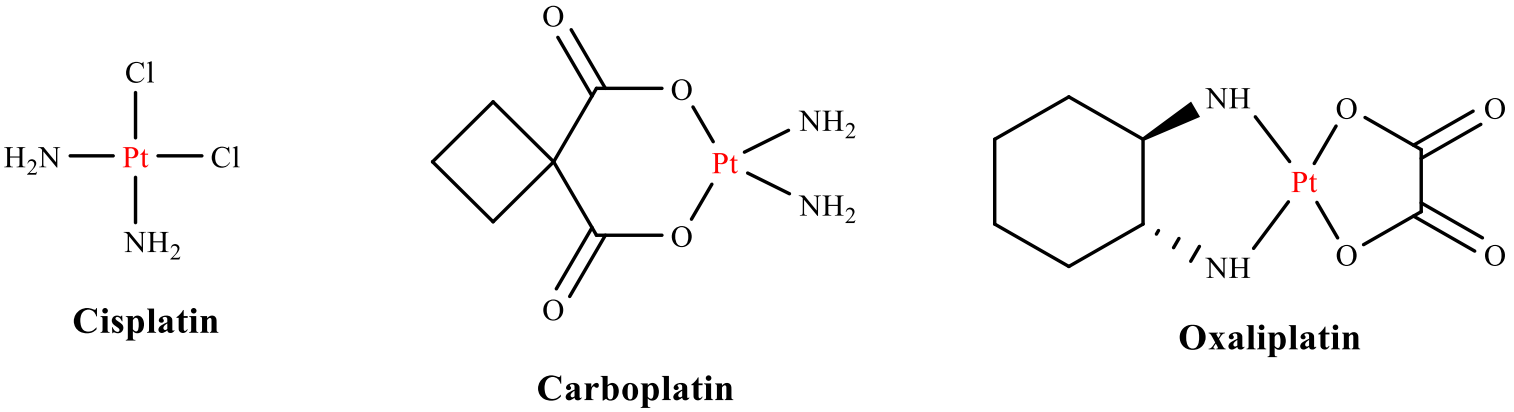

Figure 2.1.1: Chemical structures of the first discovered platinum-based compounds as anticancer drugs, including cisplatin (cis-diamminedichloroplatinum(II), CDDP), which was the first FDA-approved platinum drug for cancer therapy. Figure created by Author using Chemdraw.

Platinum complexes exert their anticancer effects primarily through interactions with DNA. Upon administration, cisplatin undergoes aquation, replacing its chloride ligands with water molecules. The resulting positively charged complex readily binds to nucleophilic sites on DNA, particularly at the N7 position of guanine residues. This binding induces the formation of intrastrand and interstrand crosslinks, disrupting the DNA double helix's structure and function. These platinum-DNA adducts impede transcription and replication, triggering cellular stress response. Persistent DNA damage activates apoptotic pathways, leading to programmed cell death [134]. Although cisplatin predominantly targets DNA, recent studies suggest that it may also interact with proteins and Ribonucleic Acid (RNA), contributing to its multifaceted mechanisms of action [135].

1.3. Ruthenium-Based Complexes - NAMI-A, NKP-1339 and -1019

Ruthenium (II) complexes have received increasing attention as chemotherapeutic drugs due to their distinctive photochemical, photophysical, and biological properties. Despite their promising therapeutic profile, most of these complexes have exhibited high cytotoxic activity, but it has poor water solubility and poor selectivity toward cancer cells [136]. Ruthenium is one of the rarest elements found in the Earth's crust. It was discovered by the Russian chemist Karl Klaus in the late 18th century and is currently the subject of intense research. Its coordination chemistry is yet the most varied among all transition metals. Ruthenium is a distinctive catalyst in oxidation reactions due to its broad range of oxidation states from +2 to +8 [137]. It primarily exists in two stable oxidation states (II and III), which can coordinate with various auxiliary ligands to form a diverse array of Ru(II/III) complexes with different steric and electronic properties [138].

With the discovery of platinum-based compounds such as cisplatin, followed by its analogs carboplatin and oxaliplatin, which can potentially resist tumour cells, the search for other metals was considered. Scientists have focused on developing non-platinum metal complexes with cytotoxic effects without causing severe toxicity. Ruthenium complexes have emerged as promising candidates among the many metal compounds investigated (see **Figure 2.1.2**). Ruthenium compounds have been shown as alternatives to platinum drugs due to their versatile synthetic and coordination chemistry and their existence in at least two stable oxidation states under physiological conditions. Some ruthenium compounds have demonstrated in vitro and in vivo anticancer activity with low systemic toxicity [139].

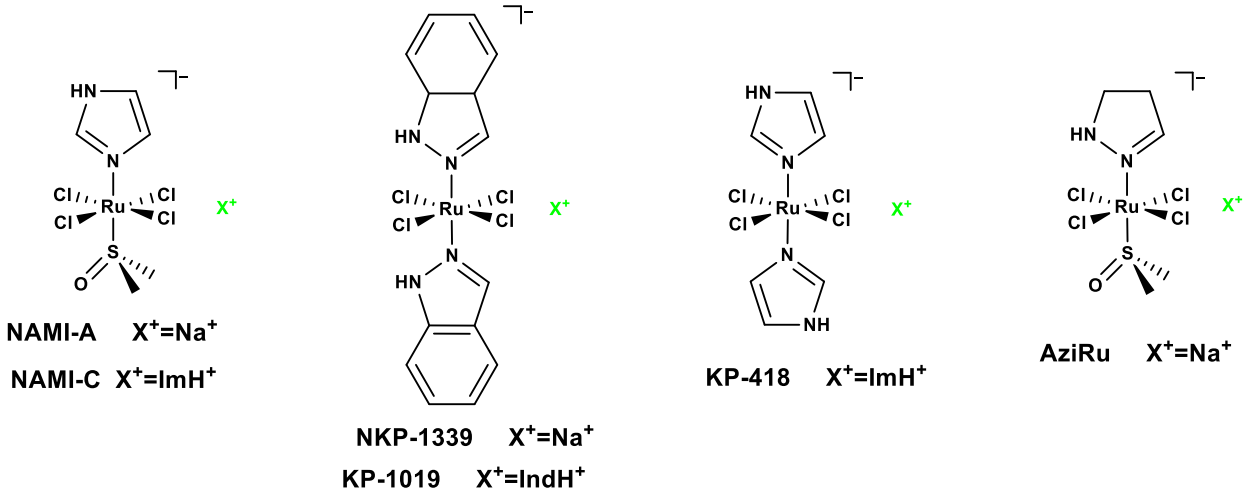

Figure 2.1.2: Chemical structures of the first ruthenium-based complexes as anticancer drugs, including NAMI-A and NAMI-C, were among the first anti-metastatic ruthenium(III) compounds, while KP1019 and its sodium derivative NKP-1339 advanced as cytotoxic agents, with NKP-1339 reaching clinical trials. KP418, an early ruthenium(II) arene complex, contributed to the development of organo-ruthenium drugs, while Azi-Ru, a ruthenium(II)-azithromycin conjugate, was explored for dual anticancer and antimicrobial effects. These compounds offer promising alternatives to platinum-based chemotherapy, with unique properties for improved cancer treatment.

Ruthenium-catalyzed functionalization and C–H bond activation are commonly used in modern synthetic strategies, owing to the foundational work of researchers [140]. In 1993, the first Ru(0)-complex-mediated coupling of olefins with aromatic ketones, which was then followed by the work on C–C bond formation using Ru-complexes with ortho-metalated triphenyl phosphite ligands [141]. With these features, various catalytic reactions, and affordability, ruthenium compounds have become preferred over platinum-group compounds such as Pt, Pd, Ir, and Rh. Moreover, ruthenium compounds are gaining more attention as potential pharmaceuticals due to their outstanding biocompatibility compared to other metallodrugs [142].

The medicinal properties of ruthenium are currently in clinical trials, and promising results have been obtained against resistant tumors. Much research on organometallic compounds has been conducted on their anti-tumor effects. At the same time, cisplatin remains the treatment of

choice in cancer treatment, facing significant challenges due to drug resistance and various side effects. Ruthenium-based compounds, such as New Anti-tumor Metallodrug – Italy A (NAMI-A), New Anti-tumor Metallodrug – Italy C (NAMI-C), and Keppler 1019 (KP1019), are currently in phase 2 clinical trials for their anticancer properties and notable anticancer potential [143]. Ruthenium complexes such as Ru-1 and Ru-2, the very first anticancer drugs in history, have shown vigorous anticancer activity, particularly Ru-2, against MCF-7 breast cancer cells [144].

It is widely accepted that the cytotoxic activity of some well-researched Ru compounds arises from their binding to DNA, making it their primary or classical target. However, researchers have not yet fully identified all the pharmacological targets in intra- and extracellular antitumor ruthenium complexes.

1.4. Tritholato-bridged Dinuclear Ruthenium (II)-Arene Complexes

In 1992, symmetric trithiolato-bridged dinuclear ruthenium(II)-arene complexes with the general formula $[(\eta^6\text{-arene})_2Ru_2(\mu_2\text{-SR})_3]^+$ were discovered, and since then, a plethora of those compounds were synthesized [145-148]. Due to the the promising anti-cancer properties of ruthenium(III) complexes such as KP-1339 (sodium trans-[tetrachloridobis(1H-indazole)ruthenate(III)]) and NAMI-A (imidazolium [trans-[tetrachlorido(S-dimethylsulfoxide)-(1H-imidazole)ruthenate(III)]), along with ruthenium(II) complexes like RAPTA-C ($[Ru(II)(\eta^6\text{-}p\text{-}MeC_6H_4Pr^i)Cl_2(PTA)]$, PTA = 1,3,5-triaza-7-phosphoadamantane) and RM175 ($[Ru(II)(\eta^6\text{-biphenyl})Cl(en)]PF_6$, en = 1,2-ethylenediamine), symmetrical trithiolato-bridged ruthenium(II)-arene complexes have been the focus of extensive in vitro anti-cancer studies.

Previous studies have investigated eight symmetrical trithiolato-bridged dinuclear ruthenium(II)-arene complexes, which included thiophenol or 4-hydroxythiophenol as bridging ligands and two types of functionalized diene-arenes. Additionally, they evaluated $[(\eta^6\text{-}C_6H_6)_2Ru_2(\mu_2\text{-SPh})_3]+$, $[(\eta^6\text{-p-}MeC_6H4Pr^i)_2Ru_2(\mu_2\text{-SPh})_3]^+$, $[(\eta^6\text{-}C_6Me_6)_2Ru_2(\mu_2\text{-SPh})_3]^+$, and $[(\eta^6\text{-}p\text{-}MeC_6H_4Pr^i)_2Ru_2(\mu_2\text{-S-p-}C_6H_4Me)_3]^+$. These complexes were evaluated against the A2780 human ovarian cancer cell line and its cisplatin-resistant counterpart, A2780cisR. All compounds displayed toxicity with IC50 values ranging from 0.08 to 132 μM in both cell lines. Complexes containing thiophenol were more cytotoxic than those with 4-hydroxythiophenol. While the type of arene moiety influenced IC_{50} values, no clear or consistent relationship was observed with lipophilicity or substituent size [149].

However, targeted delivery systems represent a significant advancement in platinum-based chemotherapy. Nanocarriers such as liposomes, dendrimers, and polymeric nanoparticles have been engineered to encapsulate platinum complexes, facilitating their accumulation in tumor tissues via the enhanced permeability and retention (EPR) effect. For example, liposomal

formulations of cisplatin (e.g., Lipoplatin) have shown promise in clinical trials, offering reduced toxicity and enhanced efficacy [131].

In recent years, efforts have been made to address these limitations by synthesizing and testing novel lipophilic platinum(II) complexes designed for intravenous administration via encapsulation into liposomes [150-154]. These complexes generally have the structure [DACH-Pt-R2], where DACH represents 1,2-diamino cyclohexane, and R denotes a lipophilic carboxylate group. The primary compound evaluated in preclinical and early clinical studies was NDDP [cis-bis-neodecanoato-trans-R, R-1,2-diamino cyclohexane platinum (II)], encapsulated in multilamellar vesicles composed of dimyristoyl phosphatidylcholine (DMPC) and dimyristoyl phosphatidylglycerol (DMPG). Liposomal NDDP (L-NDDP) demonstrated no cross-resistance with cisplatin in both in vitro and in vivo studies, was non-nephrotoxic in mice and dogs, and exhibited enhanced efficacy against in vivo models of liver metastases [153, 155]. Its ability to overcome cisplatin resistance was linked to comparable drug accumulation and DNA plastination in sensitive and resistant cells—a phase I trial revealed that L-NDDP was non-nephrotoxic, with myelosuppression identified as its dose-limiting toxicity [154, 156].

Recently, our group has focused on synthesizing and characterizing ruthenium (II) complexes (see **Figure 2.1.3**) [157-160]. Ruthenium chemistry is comprehensive and diverse, with new fields in catalysis, such as photocatalysis, continuously emerging. Ruthenium-based catalysis has become a crucial tool in synthetic chemistry. Generally, ruthenium metal is much more affordable than iridium, being approximately ten times cheaper [161].

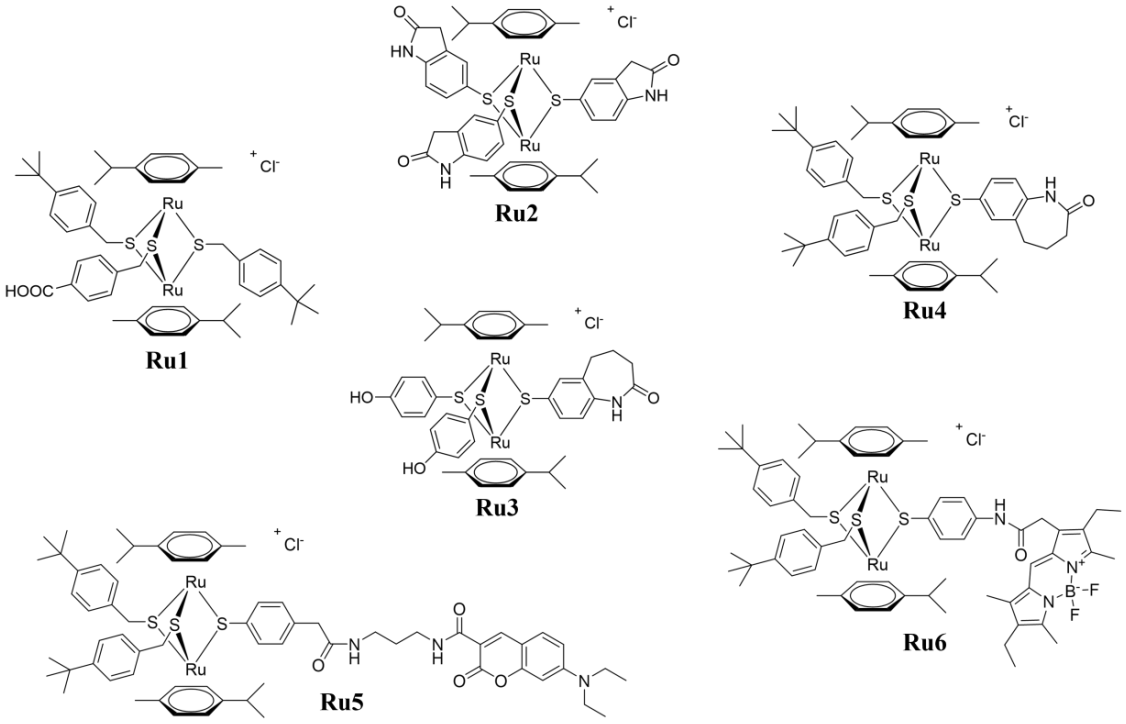

Figure 2.1.3: Chemical structures of some tritholato-bridged dinuclear ruthenium (II)-Arene Complexes, initially synthesized by our Group.

Chapter Two: A Review on Novel Liposomes

2.0. Introduction to Nanosized-Liposomes

2.1. Background and Discovery

Liposomes are spherical nano-sized vesicles, closed structures composed of amphiphilic phospholipids with hydrophilic heads and hydrophobic tails, which help to self-seal liposomes in aqueous media. Liposomes provide several advantages as drug delivery systems, including high biocompatibility, minimal immune response, and natural biodegradability, and improve drug delivery efficiency, thereby reducing systemic toxicity. In addition, liposomes shield sensitive compounds from degradation, enhancing pharmacokinetics and therapeutic effectiveness. From the discovery of A. D. Bangham in 1965, it was concluded that phospholipid molecules can form a closed bilayer vesicles in aqueous medium, in which it then was used for the encapsulation of hydrophilic and hydrophobic drugs into the lipid bilayer and aqueous core (see **Figure 2.2.1**) [162].

Drug delivery systems (DDS) have gained significant attention over the past six decades, focusing on enhancing humans' and livestock's health and well-being. In the past, researchers have focused on the delivery of antibiotics, antifungal, anti-inflammatory, anti-cancer drugs, and genes, which have also become beneficial in many biological, medical, and pharmaceutical fields.[163-172].

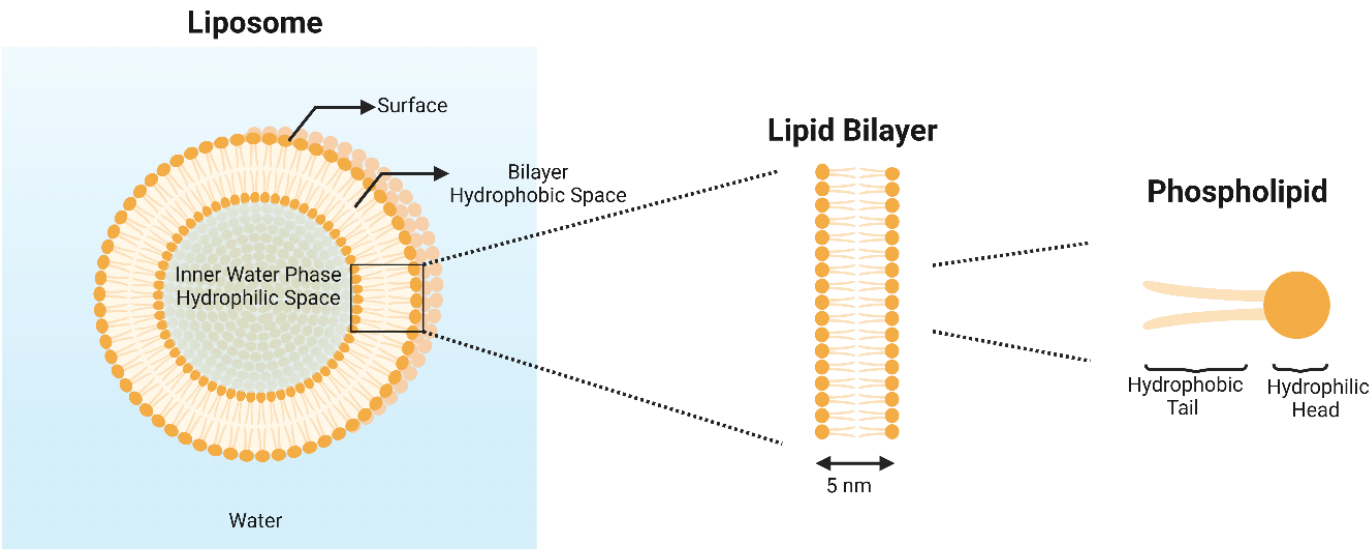

Figure 2.2.1: Scheme of a liposome formed by phospholipids. A spherical vesicle composed of phospholipid bilayers. The amphiphilic nature of phospholipids enables self-assembly in an aqueous environment, with the hydrophilic (polar) head groups oriented outward towards the surrounding water and the hydrophobic (non-polar) tails facing inward, forming a closed bilayer. This bilayer structure encloses an aqueous core, encapsulating hydrophilic molecules, while the lipid membrane can incorporate hydrophobic compounds. Figure created by Author using biorender.com.

The first liposome-encapsulated drug entered clinical trials in 1985 [173], and 40 liposome-based formulations entered the market from various clinical stages. Liposomes are generally classified into multilamellar, unilamellar, oligolamellar, and multi-vesicular vesicles, depending on the number of phospholipid bilayers, as shown in **Figure 2.2.2**:

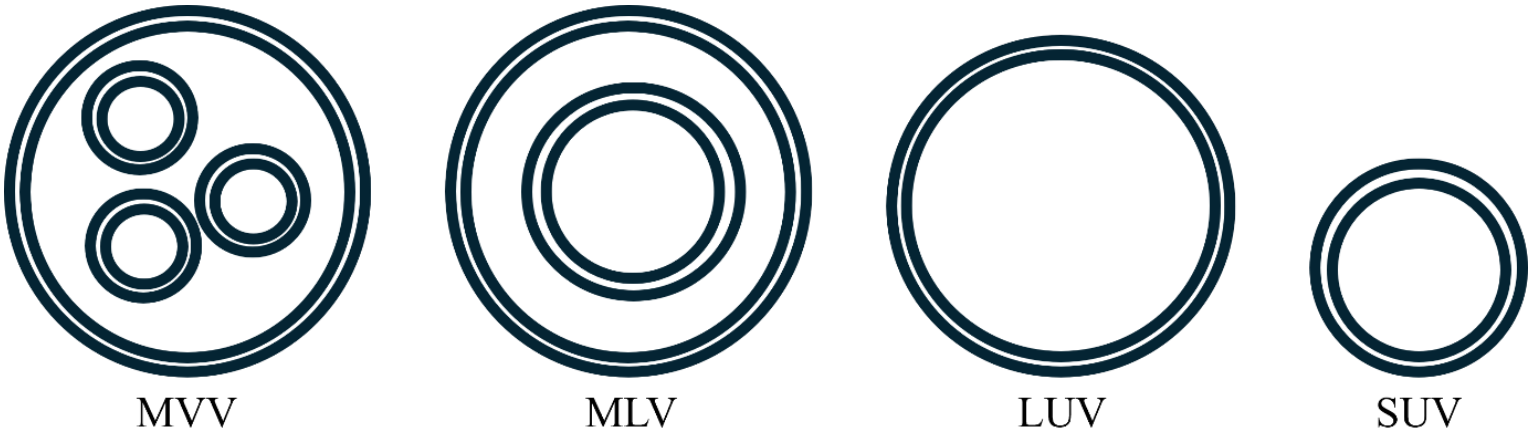

Figure 2.2.2: Classification and Composition of Liposomes.

The desirable size of liposomes drug delivery applications ranges between 50 and 200 nm (see Table 1).

Table 2.2.1: Classes of liposomes by their size.

Class of liposomes	**Particle size**	**Number of lamellae**
Multi vesicular vesicles (MVVs)	> 1 µm	1
Oligo lamellar vesicles (OLVs)	100 – 1000 nm	2-5
Multi lamellar vesicles (MLVs)	> 500 nm	> 5
Giant unilamellar vesicles (GUVs)	> 1 µm	1
Large unilamellar vesicles (LUVs)	> 100 nm	1
Small unilamellar vesicles (SUVs)	20-100 nm	1

The size of liposomes plays a crucial role in ensuring effective drug delivery within the body. It greatly influences the pharmacokinetics of both the liposomes and the drugs they carry, as well as their ability to accumulate in tumor cells [174, 175].

2.2. Characterization of Nanoparticles

The number of particles in an aqueous solution is a critical factor in drug delivery systems, affecting both quality assurance and pharmacodynamics. Beyond size alone, the number of particles per unit volume plays a significant role in determining how liposomes are absorbed,

distributed, and cleared by the body. A precise understanding of particle quantity is essential for accurately assessing drug concentration in solid, rigid formulations (such as liposomes made from lipids with high phase transition temperatures) and more flexible, liquid-based formulations. The distribution and concentration of the bioactive agent determine whether the system exists in a dissolved or dispersed state, ultimately shaping the kinetics and mechanisms of drug release.

Nanoparticle Tracking Analysis (NTA) is a precise technique for quantifying particle numbers by tracking and measuring their movement caused by Brownian motion [176]. This high-resolution method is particularly effective for analyzing the size, size distribution, and concentration of colloidal and particulate drug delivery systems, targeting particles within the 30–1000 nm range [177].

Vesicular drug delivery carriers include liposomes, nanoliposomes, micelles, tocosomes, niosomes, solid lipid nanoparticles, and archaeosomes [178]. Among these, liposomes and nanoliposomes are the most used encapsulation systems, with numerous approved products available for human application. Structurally, liposomes are bilayer phospholipid vesicles primarily composed of lipids, phospholipids, and water molecules. These vesicles consist mainly of amphiphilic lipid or phospholipid molecules, enabling the entrapment and controlled release of water-soluble, lipid-soluble, and amphipathic substances. This structure enhances the efficacy of pharmaceuticals, nutraceuticals, and other bioactive compounds while allowing targeted drug delivery to specific cells or tissues [179].

A simple mathematical approach has recently been developed to calculate the number of phospholipid vesicles, particularly for unilamellar vesicles per liter (L), using the following equation, *Eq 1* [180]:

$$N_{ves} = [M_{ing} \times N_A] \div [N_{tot} \times 1000]$$

$M_{ing} = M_{conc}$
$N_A = 6.02 \times 10^{23}$
$N_{tot} = Ing_{tot}$

$$N_{tot} = [4\pi\left(\frac{d}{2}\right)^2 + 4\pi[\left(\frac{d}{2}\right)^2 - h]^2$$

$4\pi\left(\frac{d}{2}\right)^2$ = SA
d = diameter (nm)
h = bilayer (nm)m

2.3. Methodologies and Formulations

Conventional methods for preparing liposomes include the Bangham method (thin film hydration), reverse evaporation, ether/EtOH injection, detergent depletion, microfluidic channel method, heating method, sonication method, homogenization method, and membrane extrusion method [162].

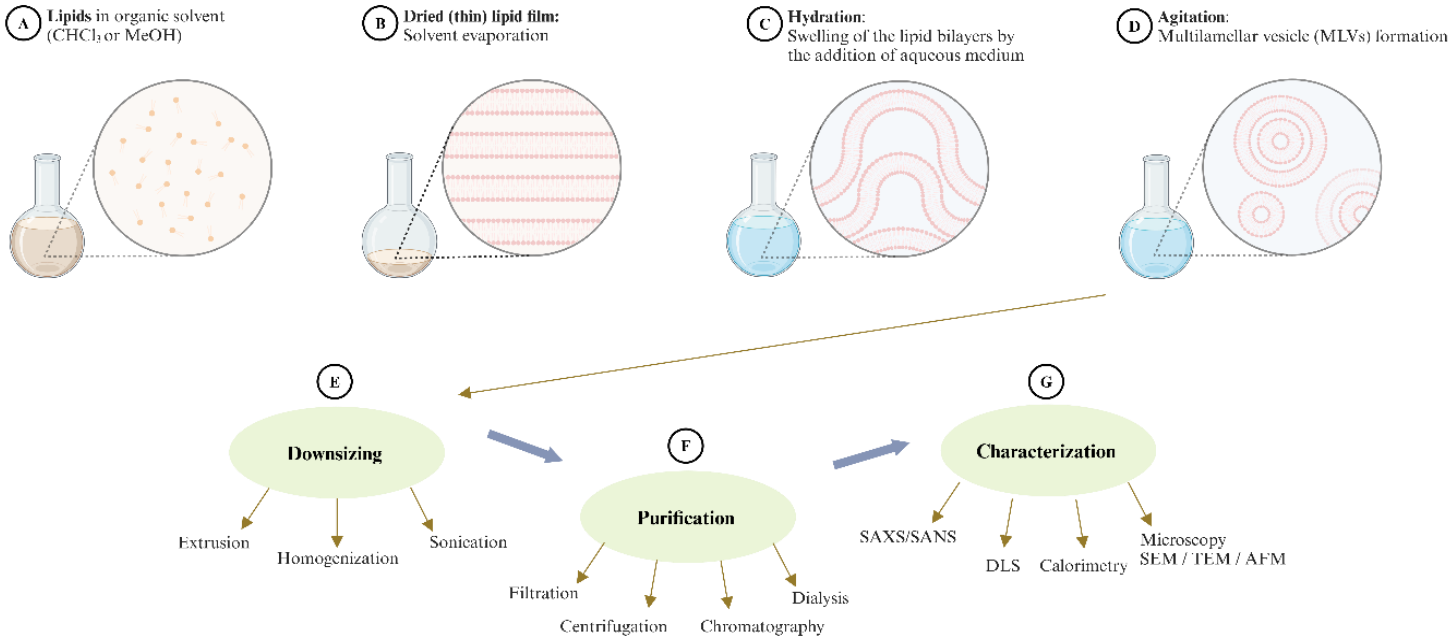

Figure 2.2.3: The Bangham method. Phospholipids are first dissolved in an organic solvent, evaporating to form a thin lipid film. Upon hydration with an aqueous buffer, the lipid film forms multilamellar vesicles (MLVs). These MLVs can be further processed by sonication or extrusion to produce small unilamellar vesicles (SUVs) or large unilamellar vesicles (LUVs) with more uniform size distributions. Figure created by Author using biorender.com.

The Bangham method is the first and most used method for the preparation of liposomes, in which lipids are dissolved in an organic solvent ($CHCl_3$, CH_2Cl_2, EtOH, or $CHCl_3$/MeOH mixture and followed by evaporation under vacuum at 45-60 °C for solvent removal, to form a thin lipid film. The lipid film is then hydrated in aqueous media by continuous agitation for up to 2h at a temperature ranging from 60-70 °C. This method is simple, straightforward, and applicable to various lipid mixtures.

The ethanol injection method was first described in 1973 [181]. In this method, lipids are dissolved in an organic solvent and injected into an aqueous phase at 55-65°C to form liposomes.

Table 2.2.1: Advantages and disadvantages of liposome preparation techniques.

Methods	Advantages	Disadvantages
Bangham	Simple and easy	Low entrapment efficiency for water-soluble drugs Difficulty in solvent removal Produces large vesicles with no control over particle size It is time-consuming and requires sterilization
EtOH/Ether injection	Rapid, reproducible High entrapment efficiency with the ether method	Risk of producing heterogeneous liposomes due to improper mixing Difficult removal of ethanol Biologically active macromolecules may become inactive with ethanol

Chapter Three: Monitoring the Optimization for the Preparation of Multilamellar and Small Unilamellar Vesicles by Nuclear Magnetic Resonance (NMR) and Dynamic Light Scattering (DLS) Spectroscopy Techniques

3.1. Aim of the Study

Nanosized liposomes' molecular structure and size play a crucial role in their stability, biodistribution, and in vivo behavior, making them essential in pharmaceutical and biomedical applications. First, we have investigated the structural and dynamic properties of liposomes prepared from DOPC, POPC, and DPPC phospholipids, focusing on multilamellar vesicles (MLVs) to small unilamellar vesicles (SUVs). Advanced characterization techniques, including Dynamic Light Scattering (DLS) for size distribution and Nuclear Magnetic Resonance (NMR) spectroscopy for molecular interactions, were utilized to optimize liposomal formulations.

The results demonstrate that optimized process parameters are essential for maintaining stable and well-defined liposomal structures, which are crucial for drug delivery and various industrial applications. This study highlights the importance of precise liposomal size and stability tuning to improve drug efficacy and ensure formulation reproducibility. It highlights the importance of fine-tuning liposome preparation methods and applying advanced analytical techniques to enhance formulation efficiency and performance.

Extrusion techniques were optimized to control liposomal size and achieve monodisperse populations, and the SUVs remained intact for over three months under optimized conditions. The molecular composition and size distribution of liposomes were evaluated using DLS and High-Resolution Magic Angle Spinning (HR-MAS) NMR spectroscopy.

Keywords: liposomes · MLVs · SUVs · dynamic light scattering (DLS) · nuclear magnetic resonance (NMR) · hydrodynamic radius · polydispersity index (PDI) · drug formulation · diffusion coefficient

Graphical Abstarct

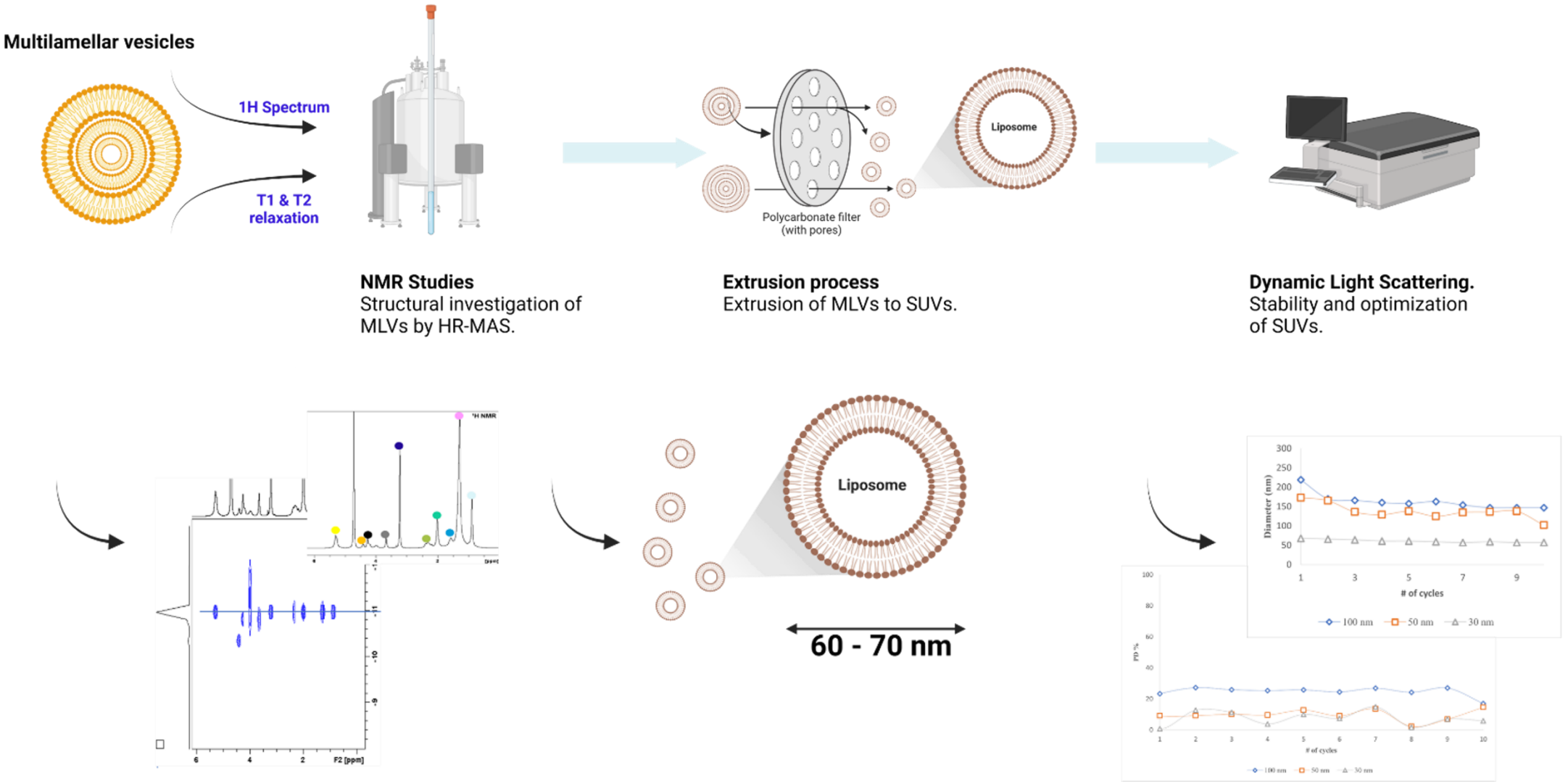

3.2. Experimental part

Chemicals

1,2-dioleoyl-*sn*-glycero-3-phosphocholine (DOPC), 1-palmitoyl-2-oleoyl-*sn*- glycero -3-phosphocholine (POPC), and 1,2-dipalmitoyl-*sn*-glycero-3-phosphocholine (DPPC) were received from Avant Polar Lipids Inc., USA.

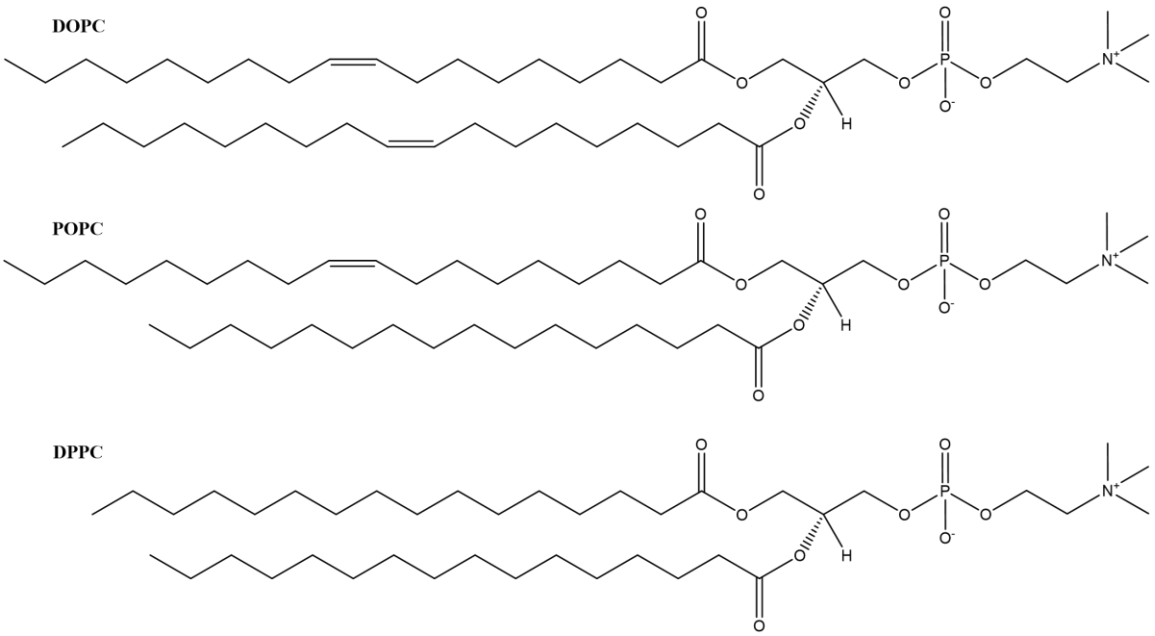

Figure 2.3.1: Chemical structures of the three phospholipids (DOPC, POPC, and DPPC).

NaCl, KH_2PO_4, and Na_2HPO_4 were obtained from Sigma Aldrich, Switzerland. Chloroform (stab./EtOH) of HPLC grade was obtained from Biosolve Chimie SARL, from France, MeOH of HPLC grade from Fisher Scientific, Belgium, and deuterated solvents from Cambridge Isotope Laboratories Inc, UK. All chemicals were used without further purification unless otherwise stated. For all the experiments, phosphate-buffered saline (PBS) solution was freshly prepared from aliquots of 50 mM KH_2PO_4 and 50 mM Na_2HPO_4 containing 0.9% NaCl in distilled H_2O, reaching a pH of 7.4. For NMR experiments, PBS was prepared from deuterated H_2O.

Instruments

Dynamic Light Scattering

Dynamic Light Scattering (DLS) was used to determine the vesicles' size distribution and diffusion coefficient. It was conducted on an Anton Paar Litesizer, using disposable acrylic cuvettes (1 cm path length) and a 600 nm laser in backscattering mode 175°. Ten runs (time/run: 10 sec.) were performed, and the data obtained were processed by Kalliope 2.8.3.

Nuclear Magnetic Resonance

All HR-MAS NMR experiments were performed on a Bruker Avance II spectrometer (Bruker BioSpin) operating at a resonance frequency of 500.13 MHz for ^{1}H nuclei. The instrument had a 4 mm HR-MAS dual inverse $^{1}H/^{13}C$ probe with a magic angle gradient. The samples were inclined around the magic angle (54.7°), spinning at 5000 Hz, and the temperature was set to 295 K (nominal), except for DPPC MLVs, the temperature was set to 323 K due to its T_m (transition temperature, 41.6 °C). Data acquisition was performed on Bruker software 4.2.0 TopSpin.

Cryo-Transmission Electron Microscopy

Vitrification of the liposome samples for cryo-EM was carried out using a Vitrobot Mark IV (Thermo Fisher Scientific) set at 10°C and 100% chamber humidity. Lacey carbon grids (Cu, 200-mesh, Quantifoil) were glow-discharged for 30 seconds at 10 mA using a CTA010 device (Balzers Union) prior to sample application. A 4 µl aliquot of the liposome suspension was gently pipetted onto the grids, followed by the Vitrobot procedure with a 4-second wait time, blot force of -7, and a blotting time of 4 seconds. The vitrified grids were then stored in liquid nitrogen until further use. Image acquisition was performed on a Tecnai F20 transmission electron microscope (Thermo Fisher Scientific) operating at 200 kV, equipped with a Falcon III direct electron detector and a Gatan 626 cryo-holder. Images were acquired using EPU software (Thermo Fisher Scientific) with a defocus range of -2 to -3 µm, a total dose of 50 e-/Å², and at a magnification of 50,000x, corresponding to a pixel size of 2.065 Å.

Preparation of Multilamellar Vesicles for HR-MAS

All the liposomes were freshly prepared before each set of experiments. The lipids were initially dissolved in $CHCl_3$ followed by solvent removal using a rotary evaporator and left under vacuum overnight to obtain a thin lipid film. The lipid film was then hydrated with the desired PBS, followed by a vortex and a water bath at 50 °C for complete dissolution. After hydration with PBS, MLVs were obtained and used for characterization without further purification.

For NMR structural studies, the lipids were prepared prior to 20 mM (DOPC 15.72 mg/ml, POPC 15.2 mg/ml, and DPPC 14.68 mg/ml) in PBS (from deuterated H_2O). The liposome suspension was carefully filled in a 50 µL HR-MAS, ensuring proper filling to optimize signal quality.

Preparation of Multilamellar Vesicle for DLS

For DLS experiments, the phospholipids were prepared at 10 mM (DOPC 7.86 mg/ml, POPC 7.6 mg/ml, and DPPC 7.34 mg/ml) in PBS. The lipids were prepared initially prepared as described above.

To obtain SUVs, the multilamellar vesicles were homogenized by freeze/thaw (6 cycles). The mixture was then extruded through three polycarbonate membranes, 100, 50, and 30 nm (10 cycles for each membrane).

3.3. Results and Discussions

^{1}H HR-MAS of Multilamellar Vesicles (MLVs)

HR-MAS NMR provided good resolution of the multilamellar vesicles (MLVs) composed of DOPC, POPC, or DPPC (see **Figures 2.3.2-2.3.4**). This technique provided clear spectral resolution, enabling the identification and differentiation of lipid components within the vesicles. HR-MAS detected distinct peaks corresponding to the headgroup and acyl chain regions of DOPC, POPC, and DPPC, generating precise, well-resolved spectra that captured the structural characteristics of each lipid. DOPC, with its unsaturated acyl chains, exhibited unique shifts in the olefinic region. At the same time, DPPC and POPC displayed distinct spectral features in the glycerol backbone and chain methylene regions, reflecting their structural and packing differences.

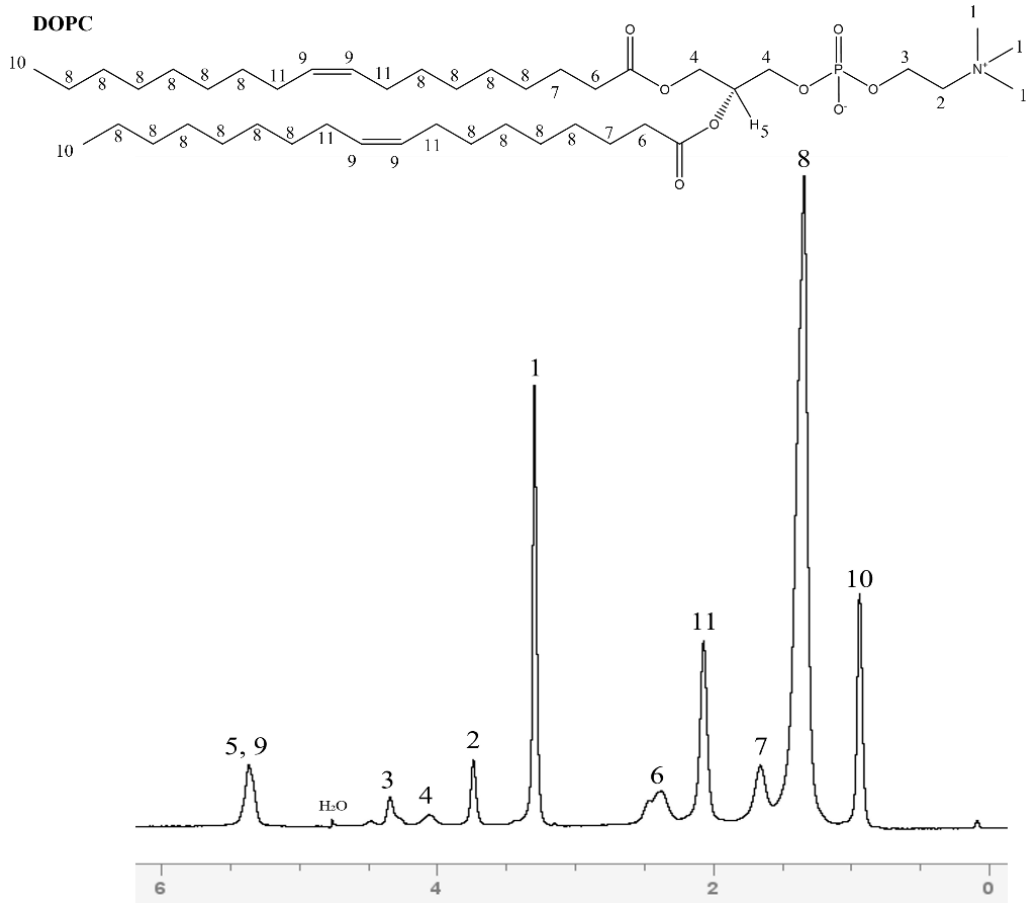

Figure 2.3.2: Superimposed ^{1}H HR-MAS NMR spectra of DOPC MLVs (20 mM) in PBS at ambient temperature. NMR acquisition parameters (see Supplementary Information **Figure S2.1**).

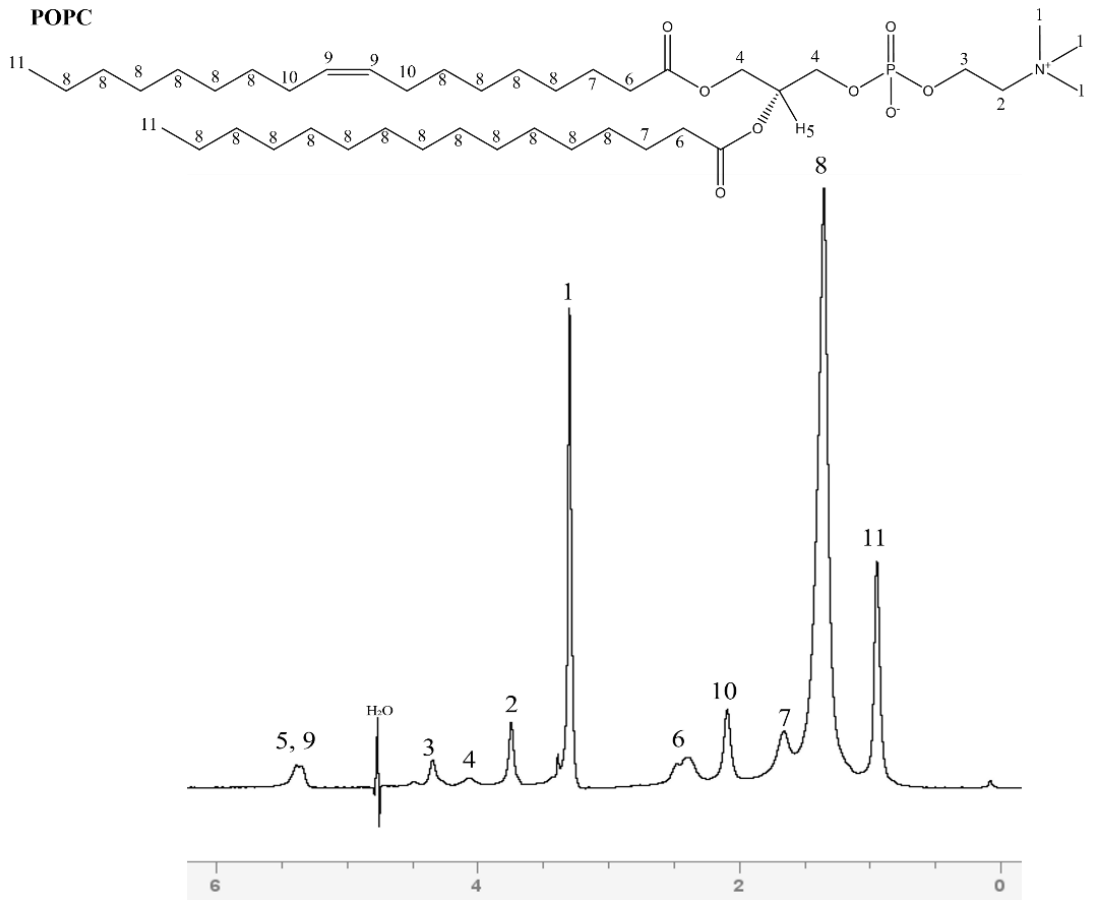

Figure 2.3.3: Superimposed ^{1}H HR-MAS NMR spectra of POPC MLVs (20 mM) in PBS at ambient temperature.

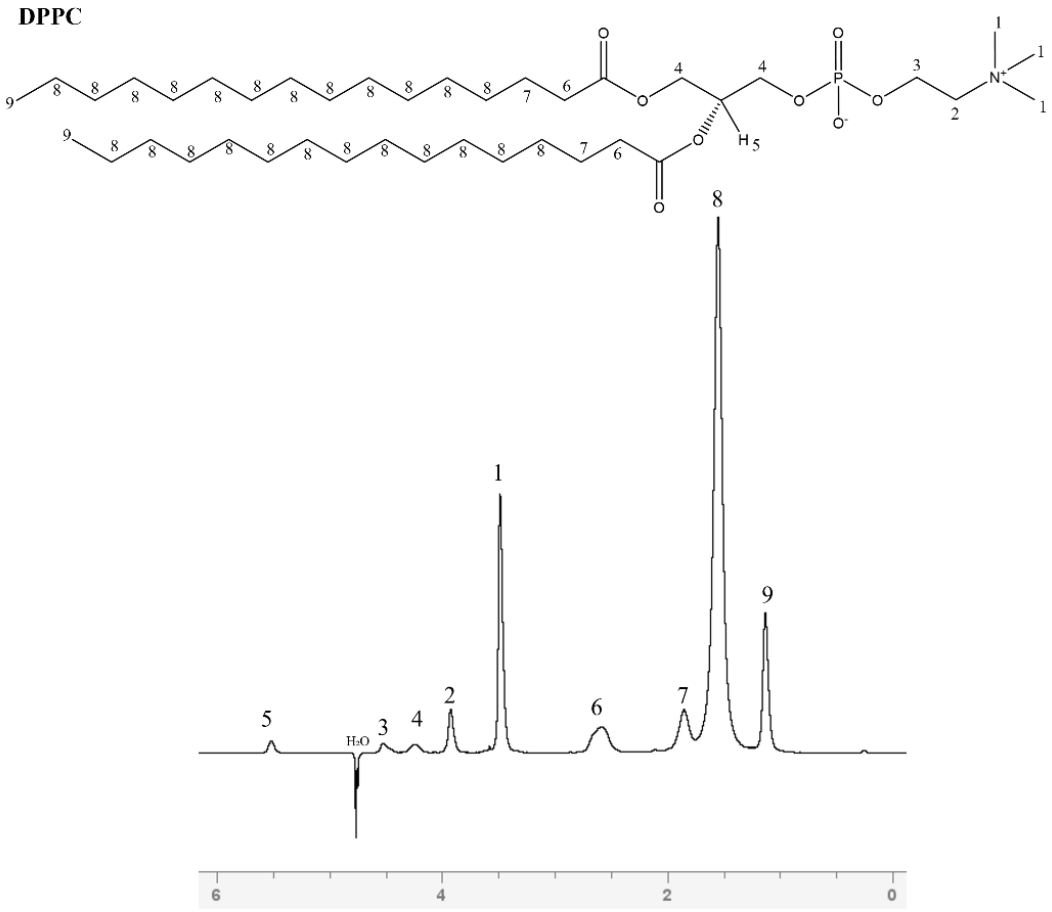

Figure 2.3.4: Superimposed ^{1}H HR-MAS NMR spectra of DPPC MLVs (20 mM) in PBS at ambient temperature.

Mass Spectrometry (MS)

The same liposome suspension was also considered for mass spectrometry and has shown that using mass spectrometry (MS) for analyzing multilamellar vesicles (MLVs) composed of DOPC, POPC, and DPPC only provided molecular weight data and identified the associated counter ions for each lipid species. While limited in the scope of structural details, this information is critical for confirming the lipids' molecular identity and validating the vesicle formulations' purity.

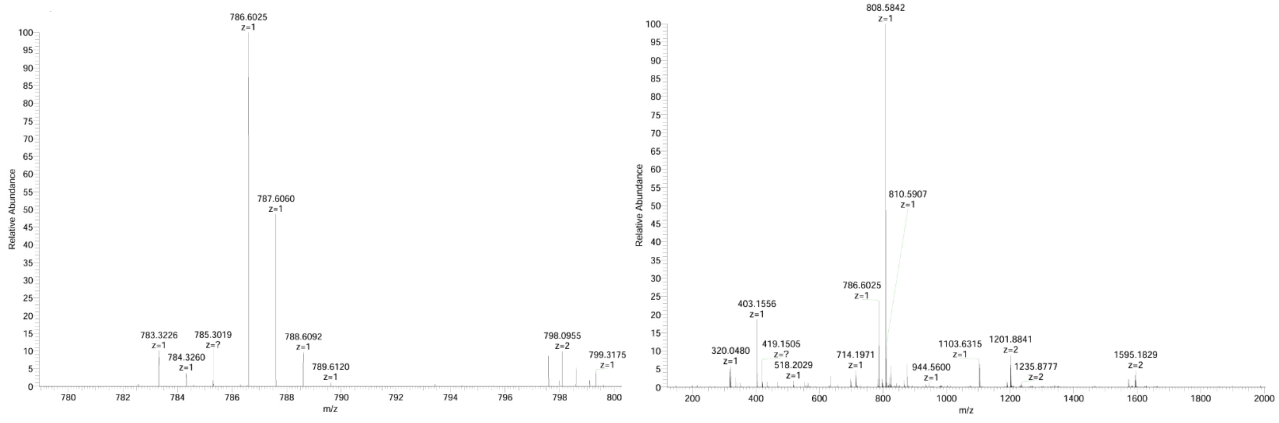

Figure 2.3.5: ESI-MS in ACN/MeOH of MLVs DOPC in PBS. On the left, the peak corresponds to DOPC, and on the right, the peak corresponds to DOPC with the addition of Na^{+} counter ion.

Optimization of Small Unilamellar Vesicle (SUV) Size Through Extrusion

The MLVs (10 mM) prepared for DLS experiments were first subject to freeze/thaw six times. After this process, the MLVs were extruded subsequently through three membrane filters, 100, 50, and 30 nm, to obtain SUVs finally. After each cycle through the membrane, 0.05 ml was collected and diluted with 0.950 ml milli-q water. As illustrated (**Figures 2.3.6-2.3.8**), the size distribution and polydispersity of small unilamellar vesicles (SUVs) were evaluated using different membrane pore sizes (100 nm, 50 nm, and 30 nm) in extrusion-based preparation, to assess how membrane filtration and preparation methods influence liposome size uniformity and polydispersity index (PDI), key parameters for stability and drug delivery applications. Additionally, according to the Stokes-Einstein equation, the diffusion coefficient directly correlates with the hydrodynamic diameter, providing valuable insights into vesicle size and stability.

When small unilamellar vesicles are prepared by sonication, a commonly used method, they exhibit higher polydispersity and broader size distributions, indicating heterogeneous vesicle populations. In contrast to the sonication techniques [182], [183], it has been shown that extrusion through membrane filters significantly improved liposome size definition, resulting in more uniform vesicle populations with lower PDI values.

By forcing the lipid suspension through well-defined pore-sized membranes, the extrusion technique facilitated the production of highly homogeneous SUVs, reducing the occurrence of large vesicles. Moreover, SUVs prepared via extrusion exhibited greater size consistency across multiple measurements, confirming the method's superior reproducibility and precise control over vesicle dimensions.

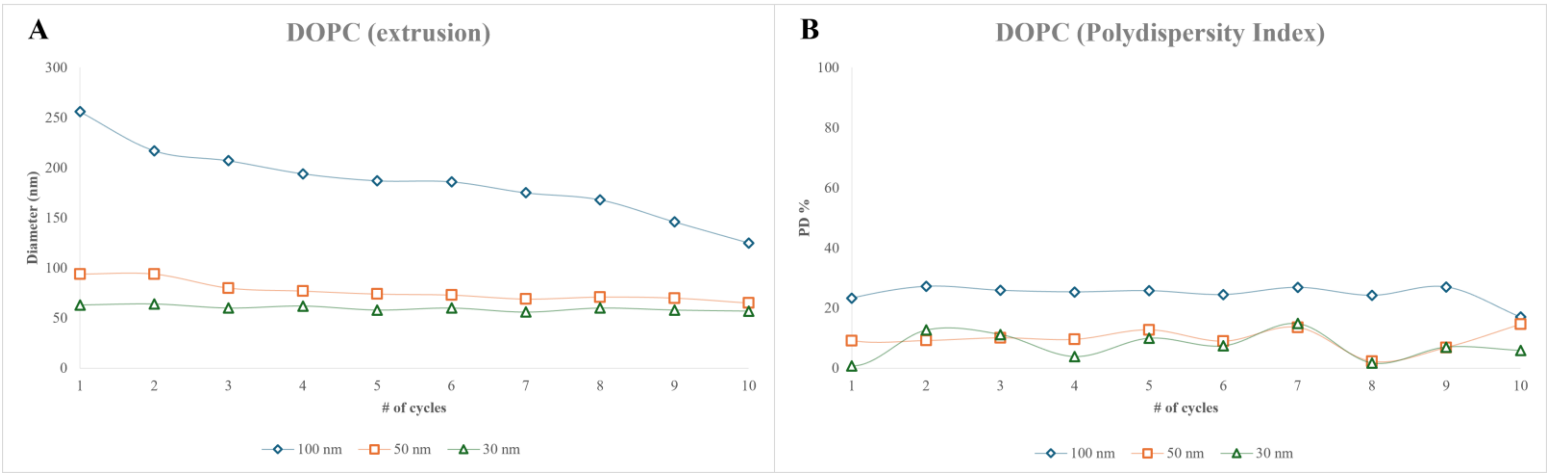

Figure 2.3.6: Dynamic light scattering. **(A)** The hydrodynamic diameters of the **DOPC** (0.5 mM) MLVs to SUVs in aqueous suspension provide insights after collecting initial cycles of extrusion techniques, their mean size, polydispersity index (PDI), and size distribution profile. **(B)** The PDI values correspond to each cycle of the **DOPC** MLVs in aqueous suspension. The PDI value represents the size distribution and homogeneity of the liposomal formulation, where lower PDI values (<0.2) indicate monodisperse and uniform vesicles, while higher values suggest polydispersity and potential aggregation.

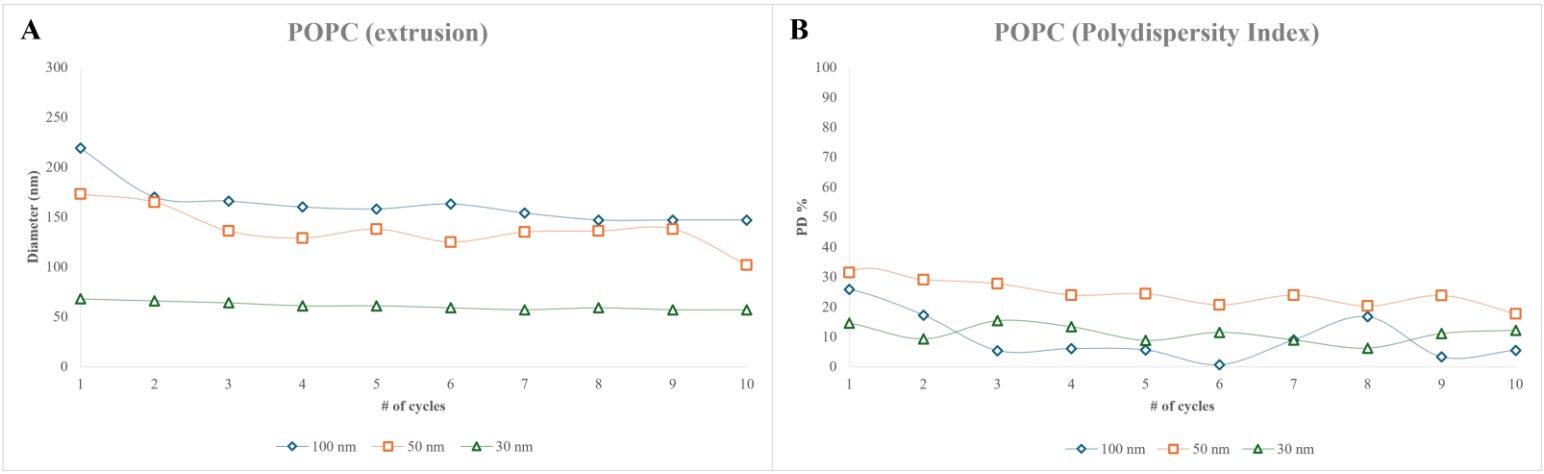

Figure 2.3.7: Dynamic light scattering. **(A)** The hydrodynamic diameters of the **POPC** (0.5 mM) MLVs to SUVs in aqueous suspension provide insights after collecting initial cycles of extrusion techniques, their mean size, polydispersity index (PDI), and size distribution profile. **(B)** The PDI values correspond to each cycle of the **POPC** MLVs in aqueous suspension. The PDI value represents the size distribution and homogeneity of the liposomal formulation, where lower PDI values (<0.2) indicate monodisperse and uniform vesicles, while higher values suggest polydispersity and potential aggregation.

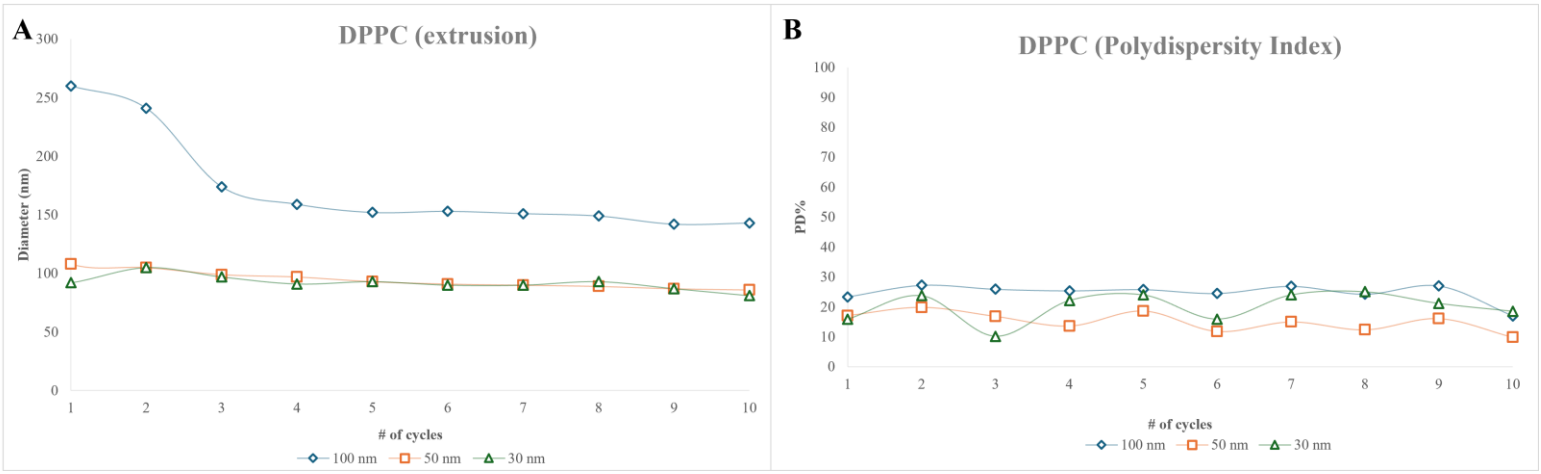

Figure 2.3.8: Dynamic light scattering. **(A)** The hydrodynamic diameters of the **DPPC** (0.5 mM) MLVs to SUVs in aqueous suspension provide insights after collecting initial cycles of extrusion techniques, their mean size, polydispersity index (PDI), and size distribution profile. **(B)** The PDI values correspond to each cycle of the DPPC MLVs in aqueous suspension. The PDI value represents the size distribution and homogeneity of the liposomal formulation, where lower PDI values (<0.2) indicate monodisperse and uniform vesicles, while higher values suggest polydispersity and potential aggregation. All experiments were regulated at ambient temperature.

After each extrusion cycle, the liposomes demonstrated faster movement and indicated better uniformity and structural definition. This behavior suggests that the extrusion process minimizes size variability, resulting in more homogeneous and spherical vesicles than SUVs prepared via sonication.

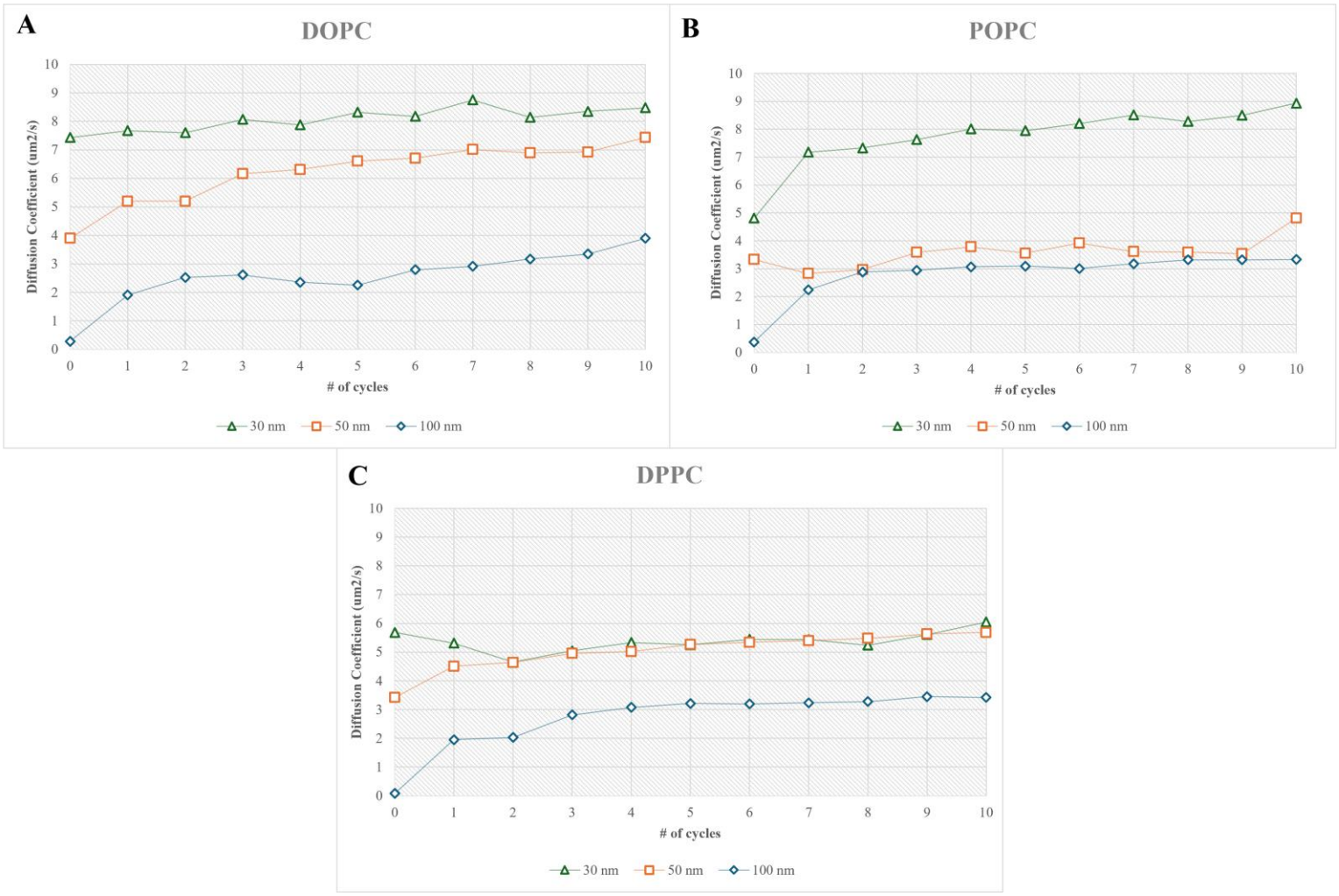

Figure 2.3.9: Dynamic light scattering. The diffusion coefficient **(A)** DOPC (0.5 mM), **(B)** POPC (0.5 mM), **(C)** and DPPC (0.5 mM) of each cycle reflect the mobility of liposomes in solution, which is influenced by their size, shape, and interactions with the surrounding medium.

These findings highlight the advantages of extrusion over sonication alone for preparing small, well-defined liposomes with improved stability and uniformity. Such improvements are significant and relevant for nanomedicine applications, where precise control over liposome size is crucial for enhancing drug loading efficiency, cellular uptake, and in vivo biodistribution.

Stability vs time for SUVs

The prepared small unilamellar vesicles (SUVs) composed of DOPC, POPC, and DPPC were monitored over three months (stored at +4°C) using Dynamic Light Scattering (DLS) to investigate their stability. Weekly measurements of the same sample showed consistent size and polydispersity, with no signs of aggregation or structural changes, and remained stable throughout the study period (see **Figure 2.3.10**).

The properties of the lipid components and the preparation process explain the SUVs' long-term stability. DPPC, with its high phase transition temperature, adds rigidity to the bilayer, while the unsaturated lipids DOPC and POPC contribute flexibility, creating a balanced and stable structure. The extrusion process during preparation further enhanced uniformity, reducing size variability and minimizing aggregation risk.

These findings also confirm that SUVs composed of DOPC, POPC, and DPPC exhibit high robustness. This makes them well-suited for applications requiring long-term stability and essential for drug delivery and encapsulation technologies.

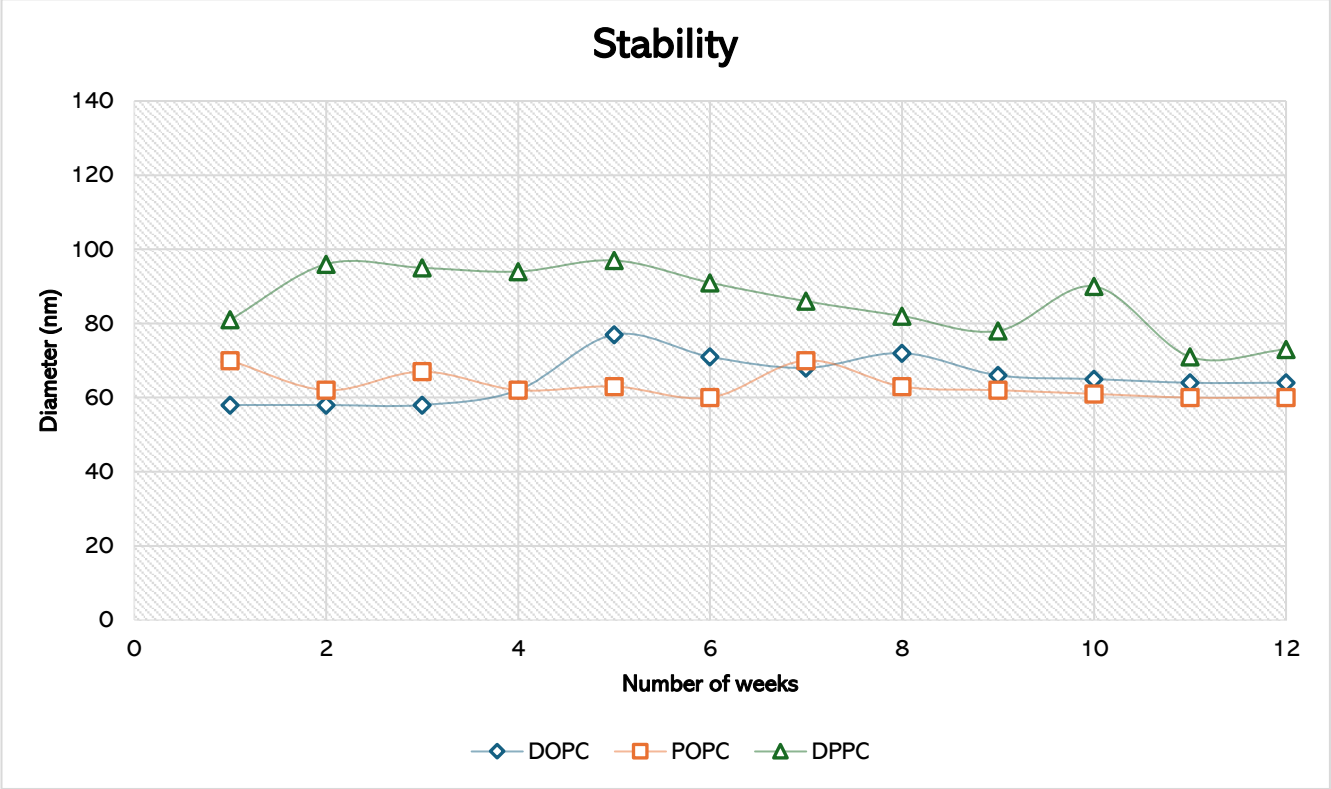

Figure 2.3.10: Dynamic light scattering. DLS measurements of Small Unilamellar Vesicles (SUVs) (0.5 mM) of the three phospholipids over a three-month period, assessing their size stability and polydispersity. The hydrodynamic diameter and polydispersity index (PDI) were monitored to evaluate any changes in vesicle integrity, aggregation, or degradation over time.

Optimum Concentration for the Size-Distribution

Among DOPC, POPC, and DPPC, surprisingly DPPC is more likely to form larger vesicles at very low concentrations in aqueous medium. This behavior is primarily due to Tm, whereas the experiments were regulated at RT.

DPPC has a high T*m* (~41°C), meaning it remains in a more ordered gel phase at lower temperatures and the lipids chains are more stretched, resulting in larger vesicle diameter. DOPC and POPC, with lower T*m* values, exist in the liquid crystalline phase at ambient temperature. This higher fluidity results in smaller, more dynamic vesicles less prone to forming larger aggregates.

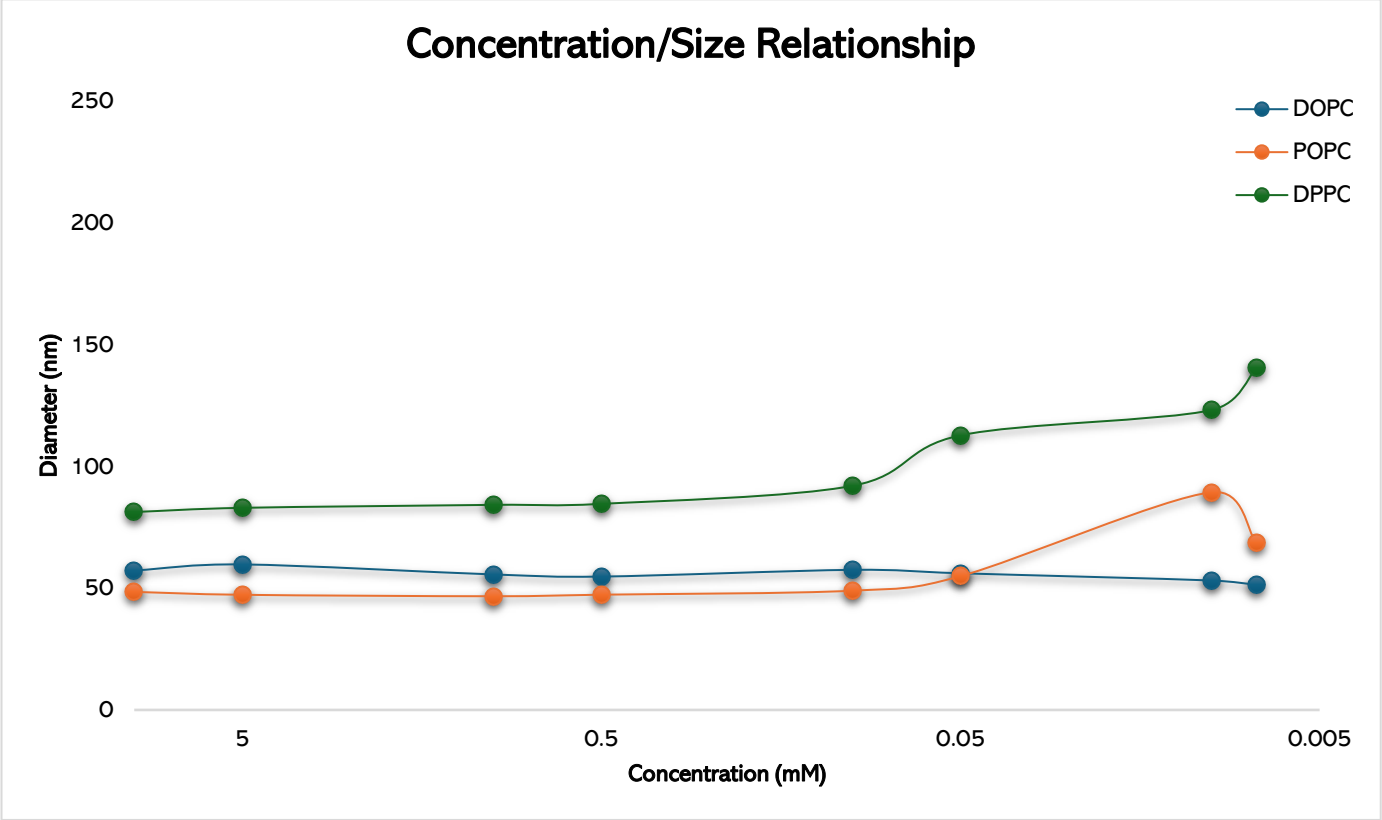

Figure 2.3.11: Dynamic light scattering. DLS measurements of Small Unilamellar Vesicles (SUVs) at varying concentrations, assessing their size distribution and stability. All experiments were regulated at ambient temperature.

In theory, unsaturated phospholipids (POPC, liquid-crystalline phase at RT) tend to form larger vesicles at very low concentration in aqueous medium. Unsaturated phospholipids possess low-packing density and high membrane flexibility, which makes them more flexible to form larger vesicles. Whereas saturated phospholipids (DPPC, gel phase at RT), the lipid-chain are more rigid which makes it unlikely to form larger vesicles.

Cryo-Transmission Electron Microscopy (Cryo-TEM)

Cryogenic Transmission Electron Microscopy was utilized to visualize the morphology, lamellarity, and size distribution of multilamellar vesicles (MLVs) and small unilamellar vesicles (SUVs) formed from DOPC, POPC, and DPPC. Cryo-TEM provides a high-resolution structural assessment of vesicles in their near-native hydrated state, allowing for a detailed comparison of lipid-dependent vesicle formation (see **Figures 2.3.12-2.3.17**). Multilamellar vesicles from DOPC are generally the highest due to their fluidity. In contrast to DOPC MLVs, POPC is similar in size but slightly different and more stable due to its partial saturation, and DPPC MLVs are the smallest, unless hydrated above the T_m (41.6 °C). The scale of all the MLVs indicated in the images, is highlighted, ranges in 50 nm.

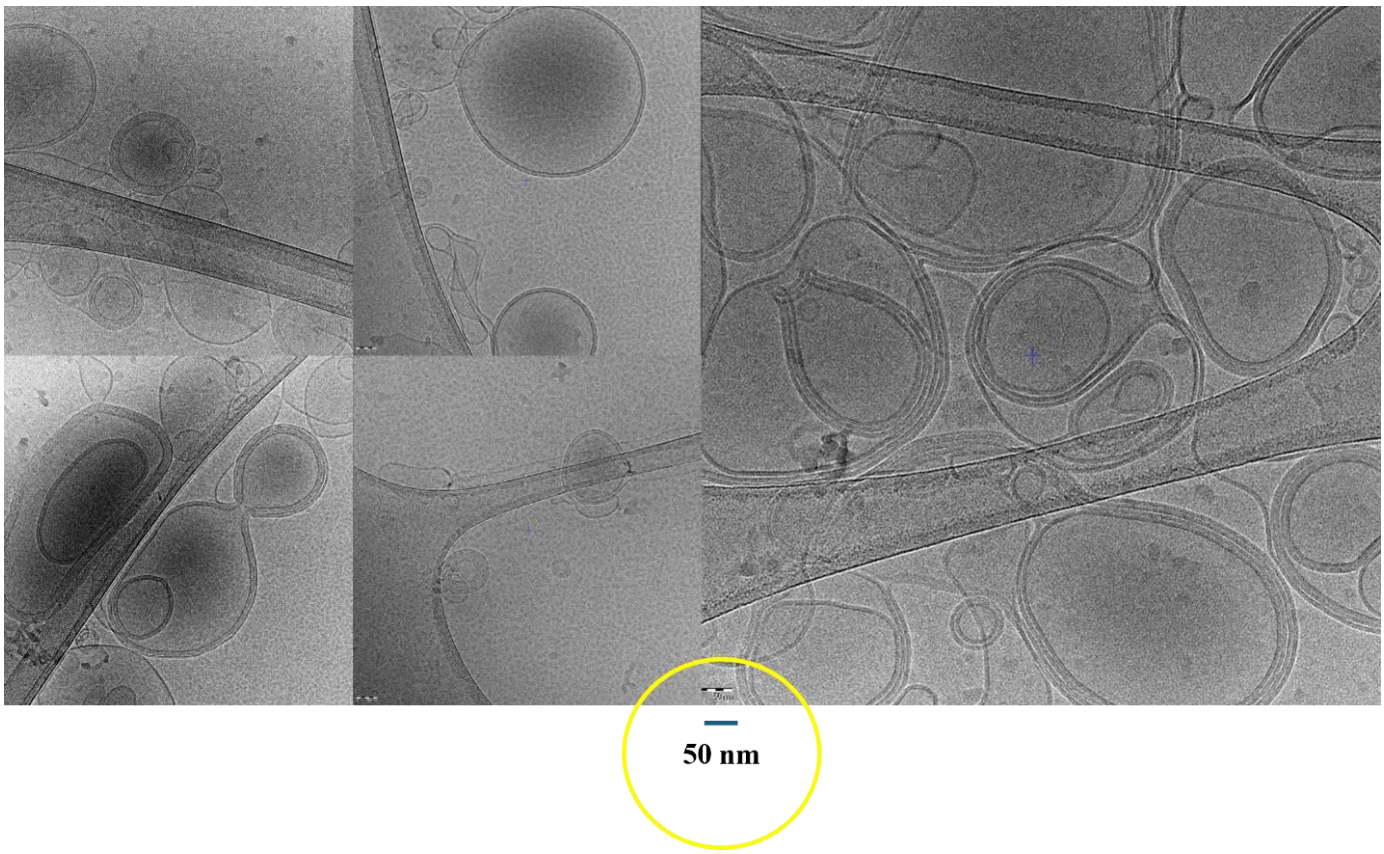

Figure 2.3.12: Cryogenic-Transmission Electron Microscopy. Cryo-TEM images of DOPC multilamellar vesicles (MLVs) more than 1µm nm in diameter at a concentration of 1 mM, providing detailed visualization of their morphology, lamellarity, and structural integrity. The one mM concentration ensures an adequate lipid-to-buffer ratio, maintaining vesicle stability while enabling high-resolution imaging.

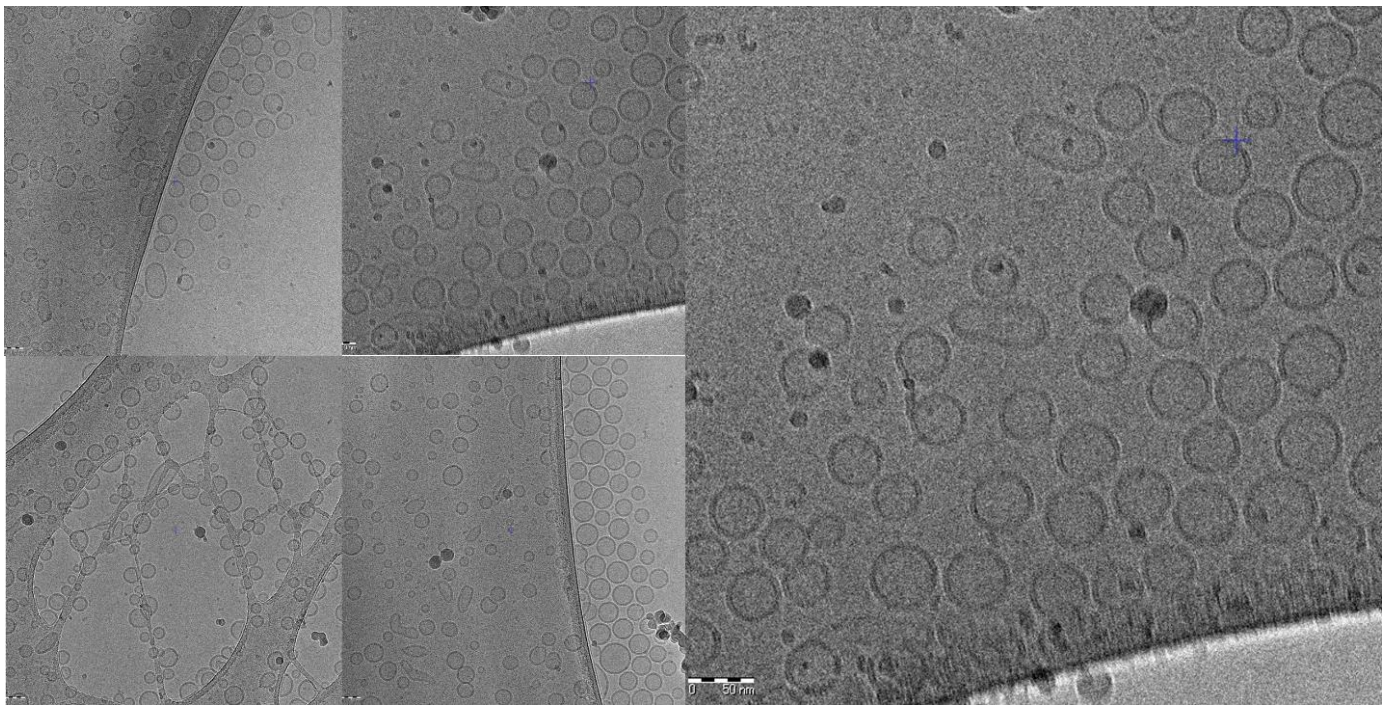

Figure 2.3.13: Cryogenic-Transmission Electron microscopy. Cryo-TEM images of DOPC small unilamellar vesicles (SUVs) less than 50 nm in diameter at a five mM concentration provide detailed visualization of their morphology, lamellarity, and structural integrity. The five mM concentration ensures an adequate lipid-to-buffer ratio, maintaining vesicle stability while enabling high-resolution imaging.

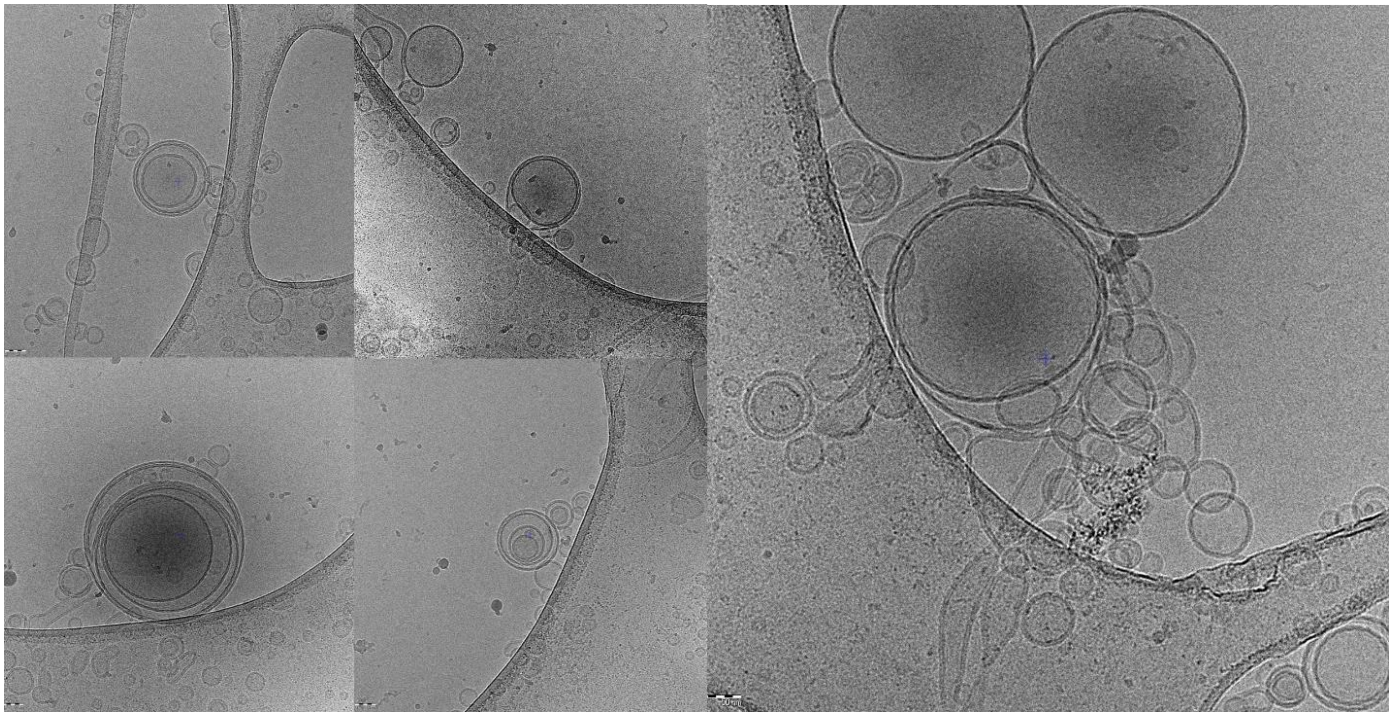

Figure 2.3.14: Cryogenic-Transmission Electron Microscopy. Cryo-TEM images of POPC multilamellar vesicles (MLVs) less than 1 µm in diameter at a concentration of 1 mM, providing detailed visualization of their morphology, lamellarity, and structural integrity. The one mM concentration

ensures an adequate lipid-to-buffer ratio, maintaining vesicle stability while enabling high-resolution imaging.

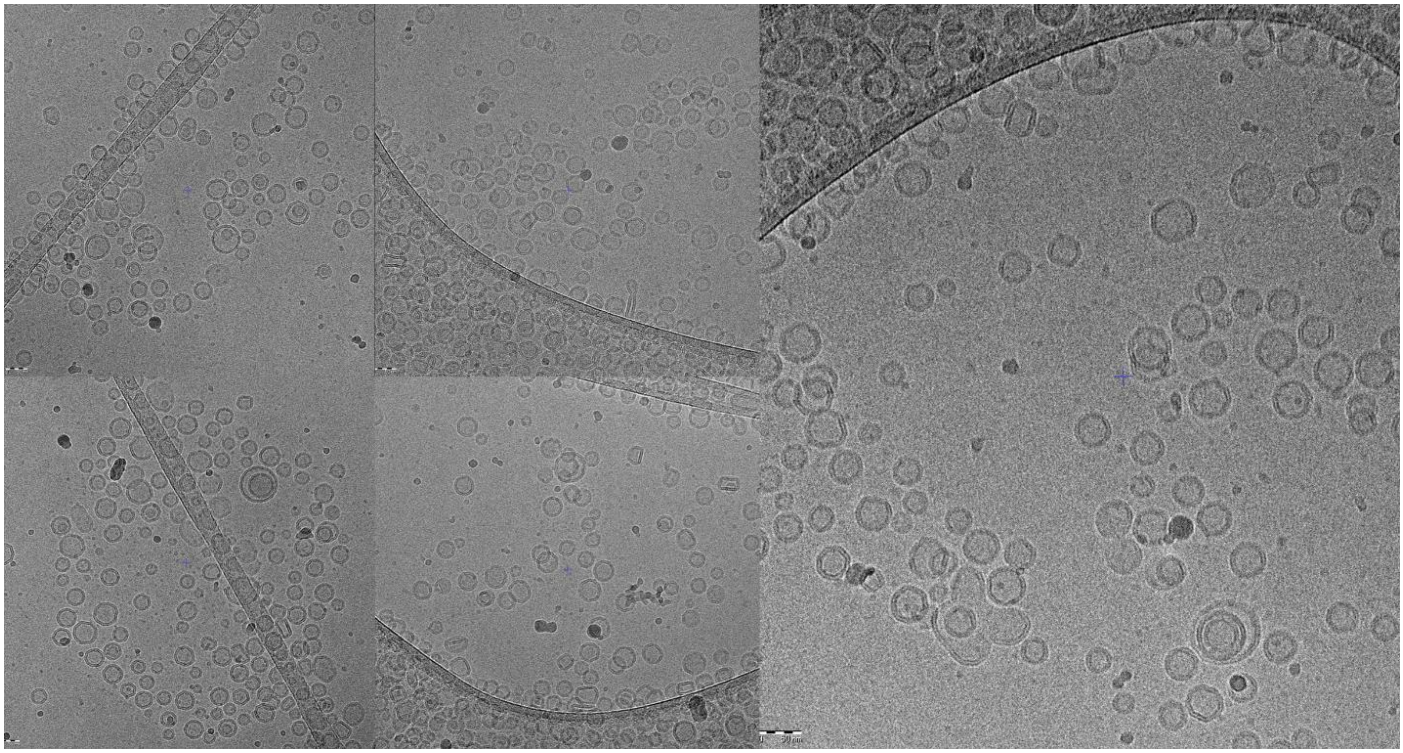

Figure 2.3.15: Cryogenic-Transmission Electron Microscopy. Cryo-TEM images of POPC small unilamellar vesicles (SUVs) less than 50 nm in diameter at a five mM concentration provide detailed visualization of their morphology, lamellarity, and structural integrity. The five mM concentration ensures an adequate lipid-to-buffer ratio, maintaining vesicle stability while enabling high-resolution imaging.

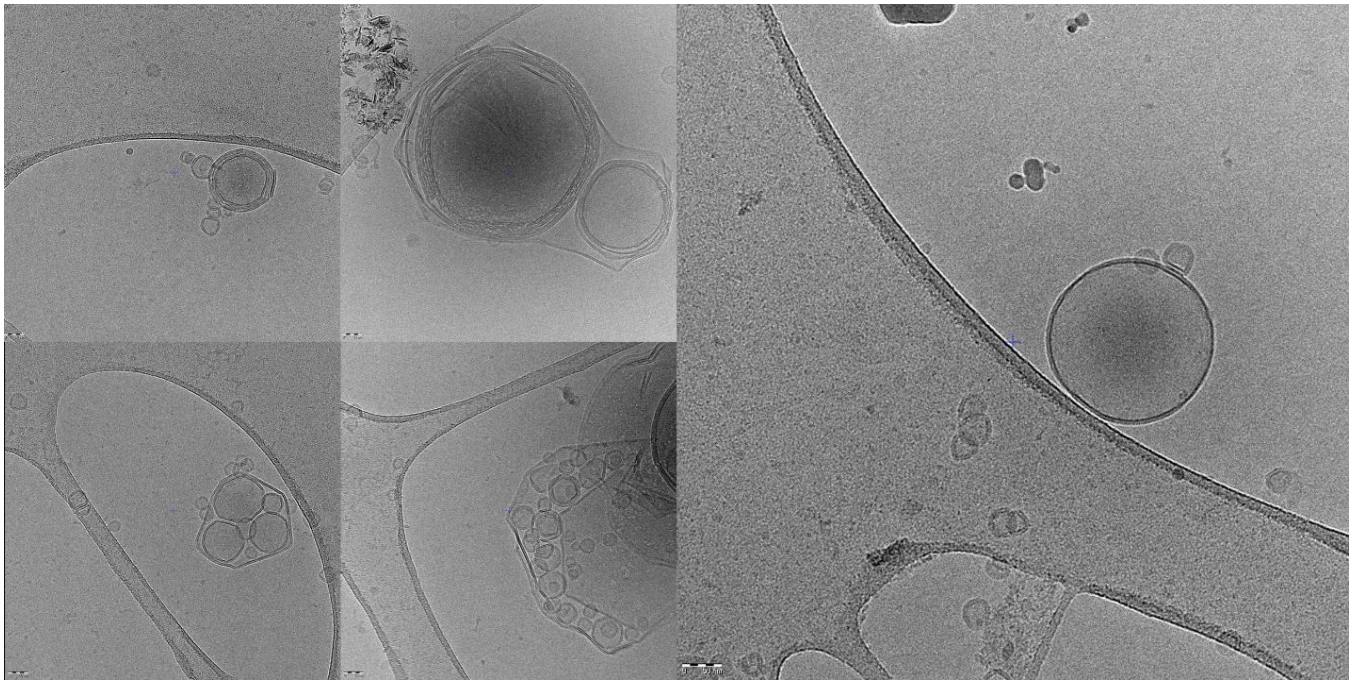

Figure 2.3.16: Cryogenic-Transmission Electron Microscopy. Cryo-TEM images of DPPC multilamellar vesicles (MLVs) less than 1µm in diameter at a concentration of 1 mM, providing detailed

visualization of their morphology, lamellarity, and structural integrity. The one mM concentration ensures an adequate lipid-to-buffer ratio, maintaining vesicle stability while enabling high-resolution imaging.

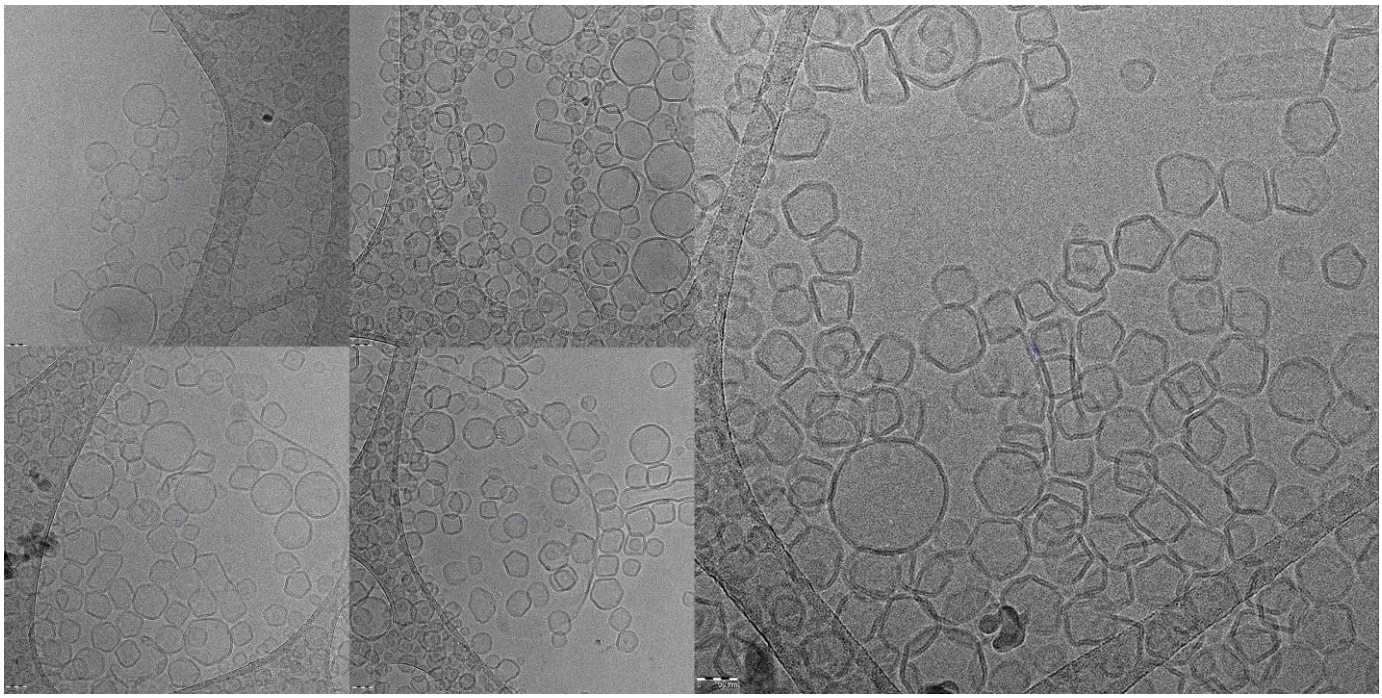

Figure 2.3.17: Cryogenic-Transmission Electron microscopy. Cryo-TEM images of DPPC small unilamellar vesicles (SUVs) less than 50 nm in diameter at a five mM concentration provide detailed visualization of their morphology, lamellarity, and structural integrity. The five mM concentration ensures an adequate lipid-to-buffer ratio, maintaining vesicle stability while enabling high-resolution imaging.

3.4. Conclusions

This study used advanced analytical techniques to investigate the properties, stability, and behavior of multilamellar vesicles (MLVs) and small unilamellar vesicles (SUVs) composed of DOPC, POPC, and DPPC.

High-Resolution Magic Angle Spinning (HR-MAS) NMR successfully characterized the lipid components of the MLVs, providing high-resolution spectra that revealed the distinct chemical environments of the lipids. This analysis demonstrated the utility of HR-MAS for studying complex lipid systems and their phase behavior, providing foundational knowledge for optimizing liposome formulations.

A three-month stability study of SUVs, monitored weekly using Dynamic Light Scattering (DLS), confirmed their remarkable stability. The SUVs maintained consistent size and polydispersity, with no aggregation or structural changes observed. The stability can be attributed to the balanced composition of DOPC, POPC, and DPPC, where the high phase transition temperature of DPPC provided structural rigidity, and the unsaturated DOPC and POPC

contributed flexibility. This robustness underscores the suitability of these lipid systems for applications requiring long-term stability, such as drug delivery.

Surprisingly, DPPC was found to form larger vesicles at very low lipid concentrations compared to DOPC and POPC. This behavior could be attributed to DPPC's high phase transition temperature. In contrast, DOPC and POPC, with their unsaturated chains and lower phase transition temperatures, produced more diminutive and more dynamic vesicles, reflecting their greater membrane fluidity at normal conditions. These findings highlight the influence of lipid composition and phase behavior in regulating vesicle size and structural properties across different conditions.

These results help assess liposomal integrity, aggregation tendencies, and suitability for biomedical applications. Integrating HR-MAS NMR, DLS, and lipid behavior analysis at low concentrations provides a comprehensive understanding of lipid vesicles' structural and dynamic properties. These insights are critical for optimizing liposome formulations for specific applications, including drug delivery and encapsulation systems. Future studies could further explore temperature- and pH-dependent effects to refine vesicle design and performance.

Chapter Four: Interactions of Cationic Dinuclear Trithiolato-bridged Arene Ruthenium (II) Complexes with MLVs Studied by HR-MAS Spectroscopy

4.1. Aim of the Study

Over the last decade, our research group has focused on the synthesis and characterization of novel cationic dinuclear thiolato-bridged arene ruthenium(II) complexes, followed by in vitro and in vivo evaluations for their potential as anticancer and antiparasitic agents. Diruthenium complexes with the general chemical formulas $[(\eta^6\text{-arene})_2Ru_2(\mu\text{-}SR)_3]^+$ and $[(\eta^6\text{-arene})_2Ru_2(\mu\text{-}SR_1)_2(\mu\text{-}SR_2)]^+$ have progressed to clinical trials for tumor treatment, demonstrating significant cytotoxicity against ovarian cancer cell lines (A2780) and their cisplatin-resistant counterparts (A2780cisR). While these complexes exhibit stability under physiological conditions, their precise interaction mechanisms remain unclear.

This study aims to explore the interactions of six cytotoxic cationic dinuclear thiolato-bridged arene ruthenium(II) complexes with multilamellar vesicles (MLVs) composed of two different phospholipids: 1,2-dioleoyl-*sn*-glycero-3-phosphocholine (DOPC), 1-palmitoyl-2-oleoyl-*sn*-glycero-3-phosphocholine (POPC) and 1,2-dipalmitoyl-*sn*-glycero-3-phosphocholine (DPPC)**.** Given their unique amphiphilic properties, liposomes have gained significant interest as targeted drug delivery systems, making them a promising vehicle for improving the efficacy and selectivity of ruthenium-based anticancer therapies.

These interactions were investigated using high-resolution magic angle spinning (HR-MAS) NMR, employing 1D and 2D techniques such as ^{1}H HR-MAS-Nuclear Overhauser effect (NOE), and diffusion-ordered spectroscopy (DOSY).

The results indicate that (i) specific interactions exist between the ruthenium complexes and the MLVs (ii) both the dinuclear Ru(II) complexes and the MLV structures remain intact, suggesting minimal perturbation, (iii) localization of the Ru-complexes within the phospholipid bilayer is dependent on their chemical structure, (iv) intermolecular forces play a role in these interactions.

Keywords: Drug delivery systems (DDS) · Ruthenium (II) complexes · phospholipids · MLVs · Nuclear Magnetic Resonance (NMR) · High Resolution – Magic Angle Spinning (HR-MAS)

Graphical Abstarct

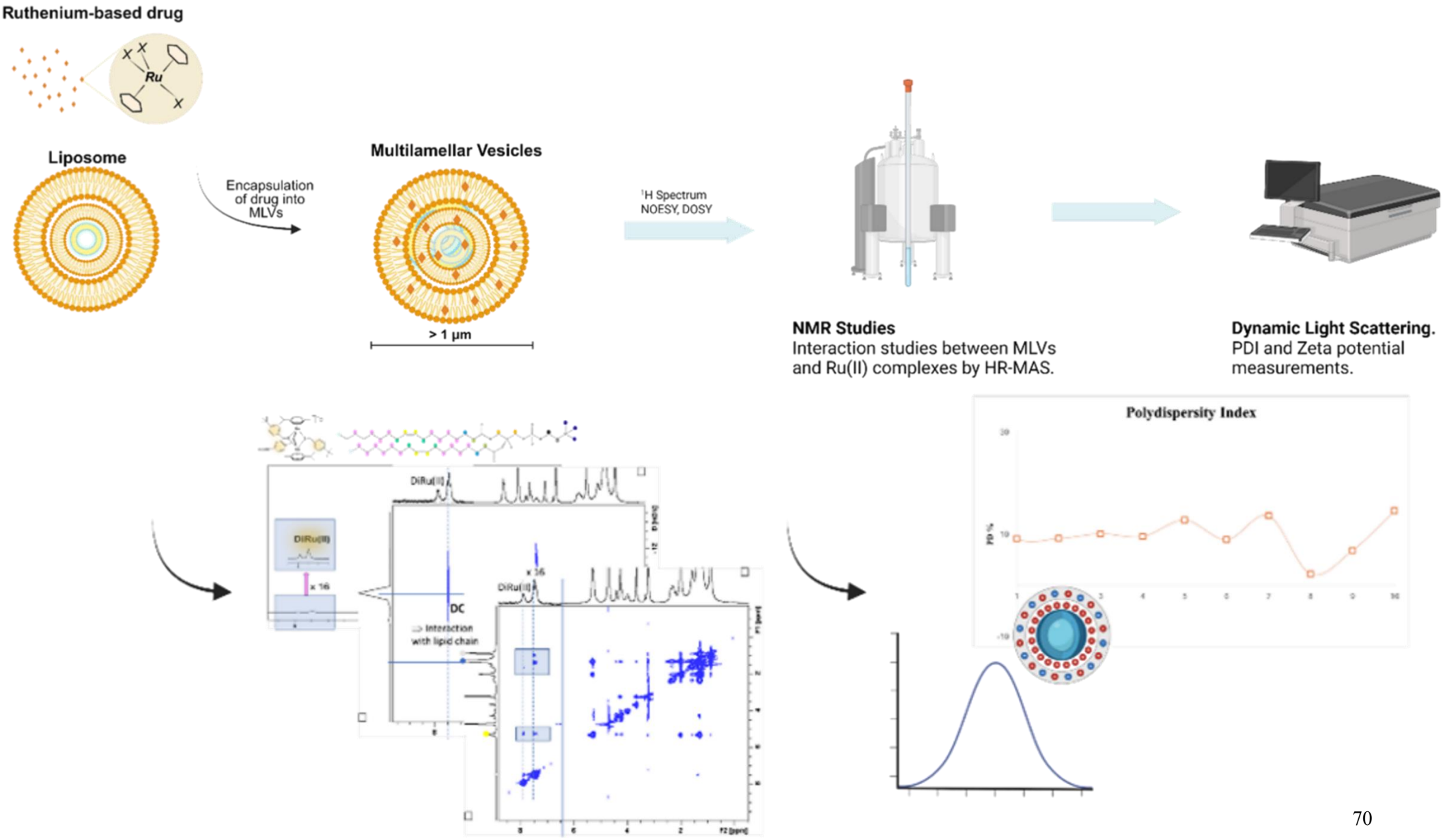

4.2. Experimental Part

Materials and Methods

The six diruthenium complexes, 1–6, were synthesized and characterized according to previous work. [59, 60, 62].

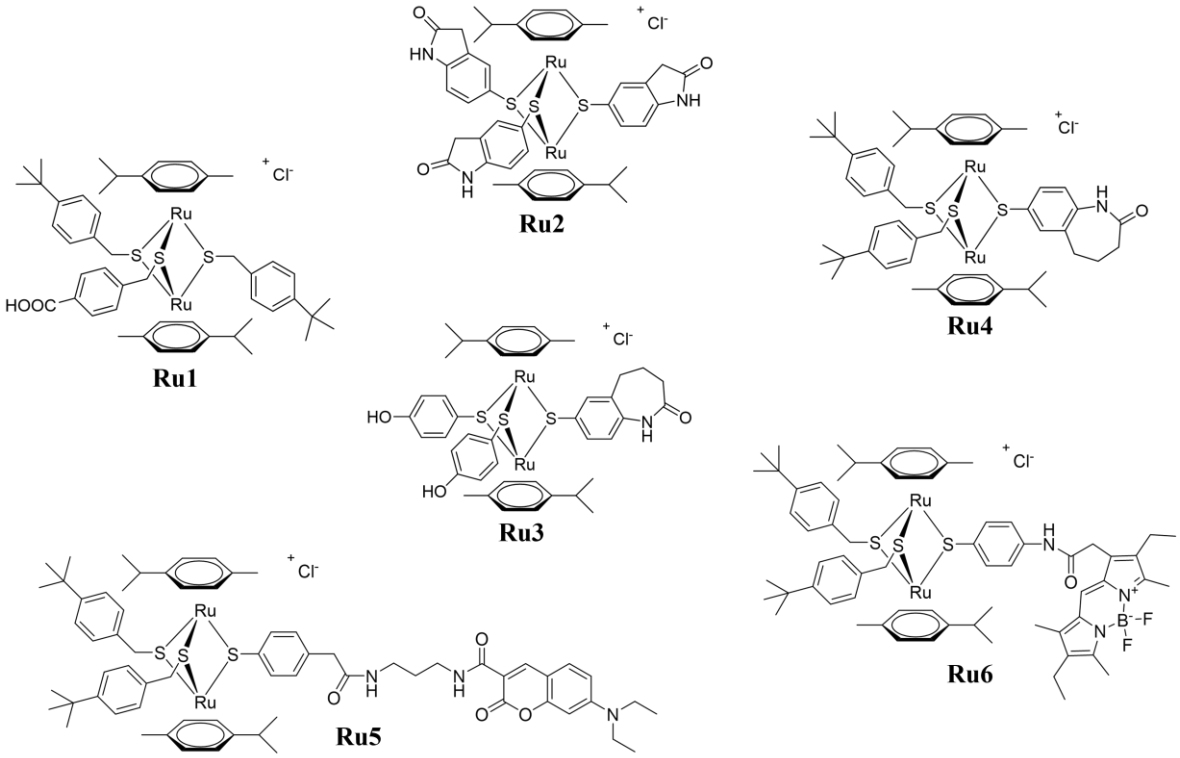

Figure 4.2.1: Molecular structures of the six diruthenium complexes **(1-6)** investigated in this work.

1,2-dioleoyl-*sn*-glycero-3-phosphocholine (DOPC), 1-palmitoyl-2-oleoyl-*sn*- glycero -3-phosphocholine (POPC) and 1,2-dipalmitoyl-*sn*-glycero-3-phosphocholine (DPPC) were received from Avant Polar Lipids Inc., USA. NaCl, KH_2PO_4, and Na_2HPO_4 were obtained from Sigma Aldrich, Switzerland, and deuterated solvents from Cambridge Isotope Laboratories Inc, UK. Phosphate-buffered saline (PBS) solution was freshly prepared from aliquots of 50 mM KH_2PO_4 and 50 mM Na_2HPO_4 containing 0.9% NaCl in D_2O, reaching a pH of 7.4. All chemicals were used without further purification unless otherwise stated

Instruments

Nuclear Magnetic Resonance

All HR-MAS NMR experiments were performed on a Bruker Avance II spectrometer (Bruker BioSpin) operating at a resonance frequency of 500.13 MHz for ^1H nuclei. The instrument had a 4 mm HR-MAS dual inverse $^1H/^{13}C$ probe with a magic angle gradient. The samples were inclined around the magic angle (54.7°), spun at 5000 Hz, and the temperature was set to 293 K

(nominal), except for DPPC, 323 K was considered. Data acquisition was performed on Bruker software 4.2.0 TopSpin. For each sample, the following spectra were recorded: (i) ^{1}H spectra using a 1D NOESY (Nuclear Overhauser Enhancement Spectroscopy) pulse sequence ("noesygppr1d" from the Bruker pulse-program library) with spoil gradients for water suppression. (ii) 2D Nuclear Overhauser effect (noesyph, Bruker library), and (iii) ^{1}H diffusion edited spectra applying the 1D DOSY (Diffusion Ordered Spectroscopy, ledbpcpgp2scprol.bi).

Mixtures of MLVs and Ruthenium Complexes (1-6)

DOPC, POPC or DPPC vesicles were freshly prepared before each new set of experiments. DOPC, POPC or DPPC was dissolved in chloroform, followed by subsequent evaporation upon an Ar stream for a uniform gel-like lipid film. The residual solvent was removed and dried in a vacuum overnight. The homogenized film was then hydrated in the prepared PBS for a final concentration of 20 mM, followed by sonication and vortex.

Diruthenium complexes 1 – 6 were dissolved in MeOH-d4 to a final concentration of 5 mM. To study the interaction of DOPC, POPC and DPPC with the diruthenium complexes, a ratio concentration of 20:5 mM (lipid:drug) was considered. The lipids were dissolved in CHCl3 and DiRu(II) in MeOH and then mixed, resulting in a final mixture of 75% v/v $CHCl_3$ and 25% v/v MeOH. The gel-like film was then hydrated with PBS (in deuterated H_2O).

4.3. Results and Discussions

^{1}H HR-MAS of encapsulated Ru1 into DOPC MLVs

For the interaction studies, 1D ^{1}H HR-MAS NMR spectra of the individual phospholipids were initially recorded, followed by the acquisition of 1D ^{1}H HR-MAS NMR spectra of the mixtures. Based on previous studies, the chemical shifts of the different protons of the individual components are due to the difference in solvent [83-85]. Broad peaks of the ruthenium complexes were observed in the region containing the protons of the thiol ligand and the p-cymene (**Figure 4.2.2**, Supplementary Information **Figures S2.1 – 2.17**) for all the six ruthenium complexes, indicating weak, noncovalent bonds with the MLVs.

ESI-MS has also suggested the absence of covalent bonds (Supplementary Information **Figure S2.52**).

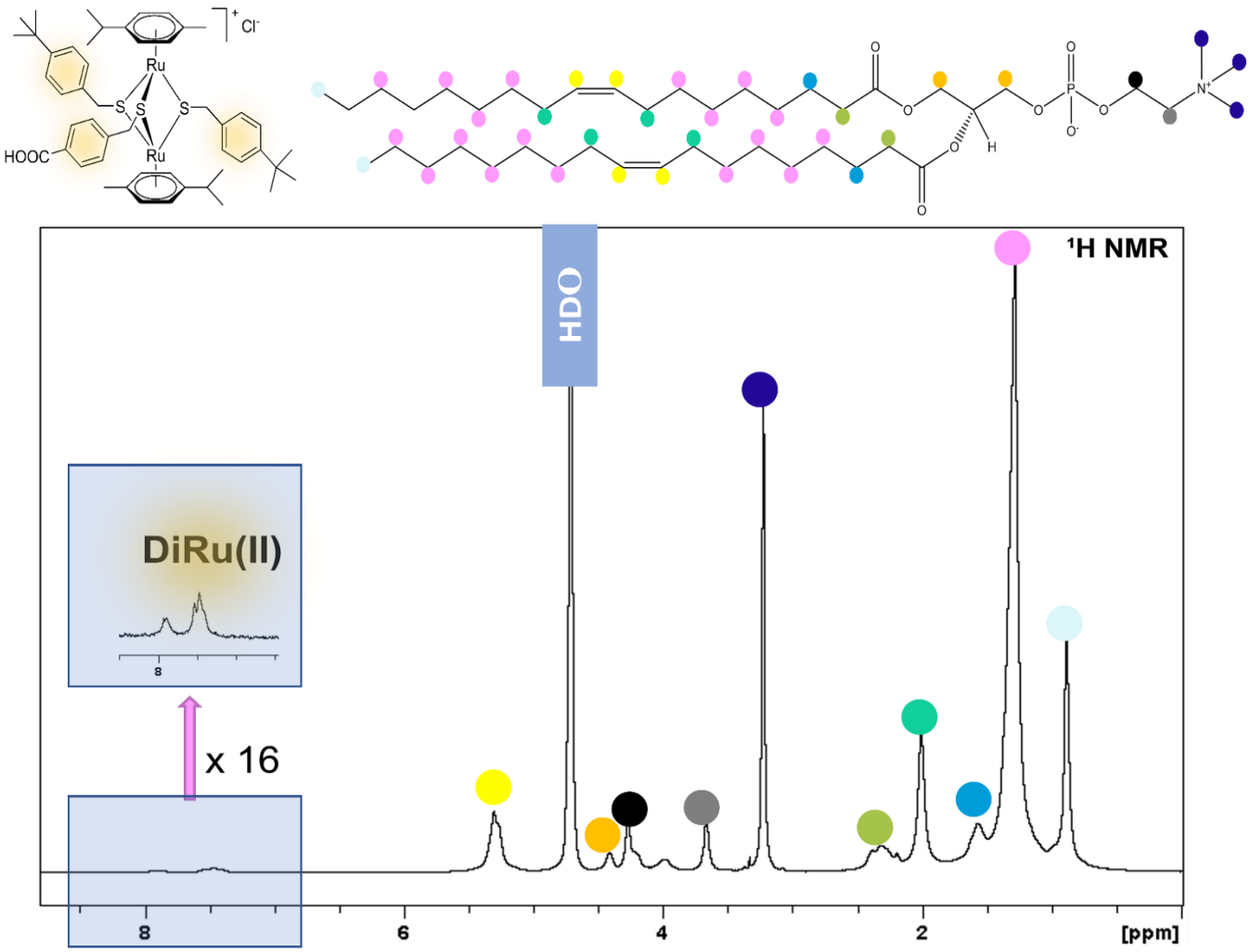

Figure 4.2.2: ^{1}H HR-MAS NMR spectrum of DOPC:Ru1 MLVs in PBS.

To investigate the spatial proximity between the ruthenium complex and the phospholipid bilayer in MLVs, we performed 2D NOESY experiments, to axcquire and support the attribution of the protons. NOE experiments have long been known to provide 1D difference spectra or 2D chemical shift correlation maps, enabling the identification of through-space interactions. Thus, we utilized NOE experiments to investigate the localization of the complexes (1-6) at the interface of the multilamellar vesicles, and the resulting spectra exhibited clear intermolecular NOE cross-peaks, indicating through-space interactions between the complex and specific lipid components, confirming their proximity within 5 Å. (**Figure 4.2.3**, Supplementary Information **Figures S2.1 – 2.17**).

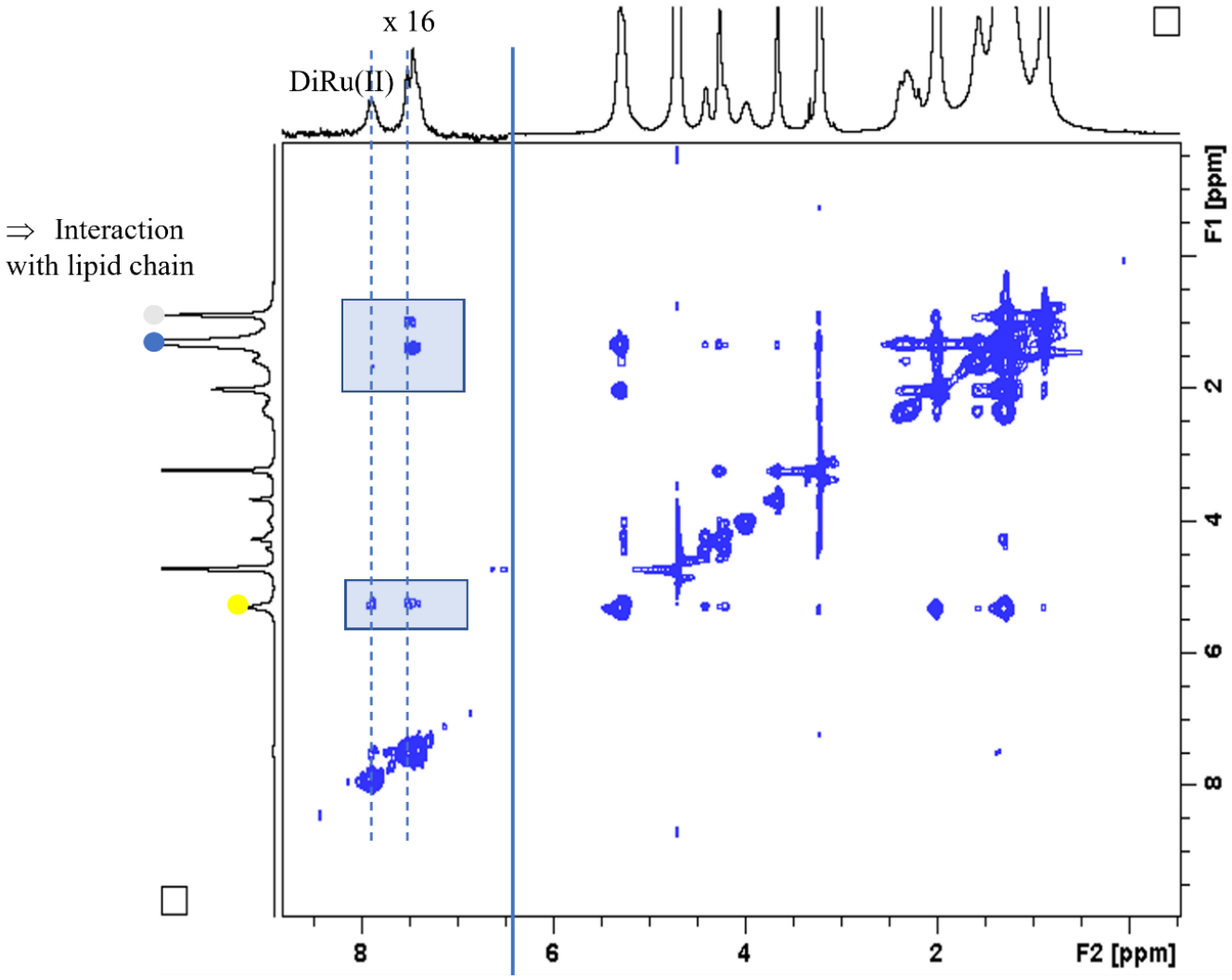

Figure 4.2.3: 2D NOESY NMR spectra of DOPC:Ru1 MLVs in PBS.

This interaction highlights that the complex preferentially localizes within the lipid chain environment, likely stabilized by van der Waals and hydrophobic interactions, due to the hydrophobicity of the diruthenium complexes.

Furthermore, we have also investigated the interaction and encapsulation of the ruthenium complexes within the multilamellar vesicles (MLVs), where Diffusion-Ordered Spectroscopy (DOSY) was performed. DOSY provided a diffusion coefficient (*D*), which is inversely related to the size of the molecular species in the solution. This allowed us to compare vesicles' adequate size and aggregation behavior before and after encapsulating the ruthenium complex. The results suggest that upon encapsulation of the ruthenium complex, a significant decrease in the diffusion coefficient was compared to empty MLVs ($D_{Ru\text{-}vesicle} < D_{empty}$) (**Figure 4.2.4**, Supplementary Information **Figures 2.18 – 2.34**).

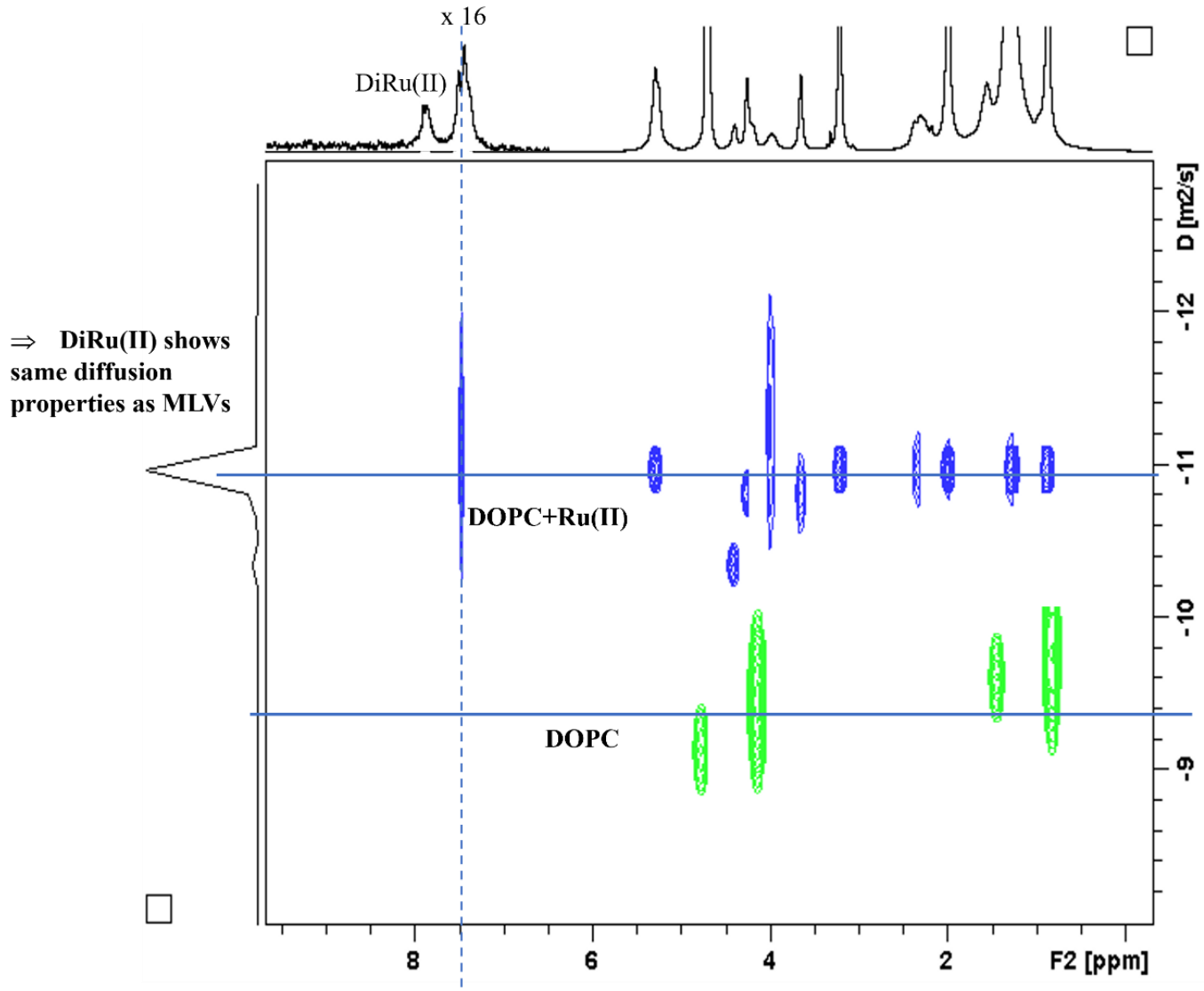

Figure 4.2.4: Overlay of DOSY HR-MAS NMR spectra of DOPC and DOPC:Ru1 MLVs in PBS.

In the case of the MLVs composed from POPC and DPPC phospholipids encapsulated with ruthenium complexes (Supplementary Information **Figures 2.35-2.51**), the diffusion coefficient was very similar to the free-POPC vesicles, and this can be explained by differences in lipid bilayer dynamics, membrane packing, and the degree of interaction between the ruthenium complex and the lipid chains (less encapsulation of the drug).

4.4. Conclusions

We have evaluated the interactions of the six diruthenium complexes with phospholipid membrane models using HR-MAS spectroscopy. Depending on the 1D NMR spectra, we have concluded that the diruthenium complexes strongly interact with the phospholipids DOPC, POPC and DPPC. The interaction between multilamellar vesicles (MLVs) composed of DOPC, POPC, and DPPC with ruthenium-based molecules was observed using HR-MAS ^{1}H NMR. Distinct chemical shift changes in the spectra indicated the incorporation or association of the ruthenium molecules with the lipid bilayers.

2D NOE (Nuclear Overhauser Effect) NMR spectra offer a decisive advantage in characterizing the interaction between multilamellar vesicles (MLVs) and ruthenium molecules. NOE data indicated that the complexes interact with the lipid chain and are located in the hydrophobic region of the vesicle, the lipid chain. This technique provides detailed insights into spatial proximity at the atomic level by detecting through-space interactions between protons. In the context of MLVs and ruthenium molecules, 2D NOE allows for precise mapping of how and where the ruthenium complexes interact with the lipid bilayer—whether at the hydrophilic headgroups, within the hydrophobic core, or both. Furthermore, it enables the differentiation between intramolecular and intermolecular interactions, elucidating the system's binding dynamics and structural organization.

DOSY (Diffusion-Ordered Spectroscopy) NMR provides a unique advantage in studying the interactions between multilamellar vesicles (MLVs) and ruthenium molecules by enabling the measurement of molecular diffusion coefficients. This technique distinguishes between free and vesicle-bound ruthenium molecules based on their diffusion rates, as larger MLV-bound molecules diffuse more slowly than free species in solution. DOSY also helps assess the strength and extent of interaction by observing changes in the diffusion behavior of the ruthenium molecules in the presence of MLVs. This method offers a quantitative understanding of how the interaction affects molecular mobility and vesicle dynamics.

Future research in drug delivery systems should prioritize enhancing vesicle precision by incorporating targeting moieties such as ligands or antibodies to improve selectivity for specific cells or tissues. Better methods for loading drugs into the vesicles and tracking their behavior in the body could make these systems even more effective. Lastly, combining ruthenium-based compounds with other medications might create powerful new therapies, especially for treating cancer.

Bibliography

[1] World Health Organization, 'Ten Chemicals of Major Health Concern', WHO: Geneva, Switzerland. Accessed: Dec. 25, 2024. [Online]. Available: https://www.who.int/news-room/photo-story/photo-story-detail/10-chemicals-of-public-health-concern

[2] Agency for Toxic Substances and Disease Registry, 'Substance Priority List', ATDSR: Atlanta, GA, USA. Accessed: Dec. 25, 2025. [Online]. Available: https://www.atsdr.cdc.gov/

[3] A. Kabata-Pendias and A. B. Mukherjee, *Trace Elements from Soil to Human*. Berlin, Heidelberg: Springer Berlin Heidelberg, 2007. doi: 10.1007/978-3-540-32714-1.

[4] K. Hans Wedepohl, 'The composition of the continental crust', *Geochimica et Cosmochimica Acta*, vol. 59, no. 7, pp. 1217–1232, Apr. 1995, doi: 10.1016/0016-7037(95)00038-2.

[5] S. R. Taylor and S. M. McLennan, 'The geochemical evolution of the continental crust', *Reviews of Geophysics*, vol. 33, no. 2, pp. 241–265, May 1995, doi: 10.1029/95RG00262.

[6] J. O. Nriagu, 'A global assessment of natural sources of atmospheric trace metals', *Nature*, vol. 338, no. 6210, pp. 47–49, Mar. 1989, doi: 10.1038/338047a0.

[7] L. Meyer, S. Guyot, M. Chalot, and N. Capelli, 'The potential of microorganisms as biomonitoring and bioremediation tools for mercury-contaminated soils', *Ecotoxicology and Environmental Safety*, vol. 262, p. 115185, Sep. 2023, doi: 10.1016/j.ecoenv.2023.115185.

[8] D. C. Adriano, *Trace Elements in Terrestrial Environments*. New York, NY: Springer New York, 2001. doi: 10.1007/978-0-387-21510-5.

[9] B. J. Alloway, Ed., *Heavy Metals in Soils: Trace Metals and Metalloids in Soils and their Bioavailability*, vol. 22. in Environmental Pollution, vol. 22. Dordrecht: Springer Netherlands, 2013. doi: 10.1007/978-94-007-4470-7.

[10] N. Pirrone *et al.*, 'Global mercury emissions to the atmosphere from anthropogenic and natural sources', *Atmos. Chem. Phys.*, vol. 10, no. 13, pp. 5951–5964, Jul. 2010, doi: 10.5194/acp-10-5951-2010.

[11] E. G. Pacyna, J. M. Pacyna, F. Steenhuisen, and S. Wilson, 'Global anthropogenic mercury emission inventory for 2000', *Atmospheric Environment*, vol. 40, no. 22, pp. 4048–4063, Jul. 2006, doi: 10.1016/j.atmosenv.2006.03.041.

[12] D. G. Streets, Q. Zhang, and Y. Wu, 'Projections of Global Mercury Emissions in 2050', *Environ. Sci. Technol.*, vol. 43, no. 8, pp. 2983–2988, Apr. 2009, doi: 10.1021/es802474j.

[13] N. E. Selin, 'Global Biogeochemical Cycling of Mercury: A Review', *Annu. Rev. Environ. Resour.*, vol. 34, no. 1, pp. 43–63, Nov. 2009, doi: 10.1146/annurev.environ.051308.084314.

[14] S. Lindberg *et al.*, 'A Synthesis of Progress and Uncertainties in Attributing the Sources of Mercury in Deposition', *AMBIO: A Journal of the Human Environment*, vol. 36, no. 1, pp. 19–33, Feb. 2007, doi: 10.1579/0044-7447(2007)36[19:ASOPAU]2.0.CO;2.

[15] W. H. Schroeder and J. Munthe, 'Atmospheric mercury—An overview', *Atmospheric Environment*, vol. 32, no. 5, pp. 809–822, Mar. 1998, doi: 10.1016/S1352-2310(97)00293-8.

[16] X. Feng and G. N. Bigham, 'Mercury biogeochemical cycling in mercury contaminated environments', *Applied Geochemistry*, vol. 26, no. 2, p. 153, Feb. 2011, doi: 10.1016/j.apgeochem.2010.11.012.

[17] P. A. Ariya *et al.*, 'Mercury Physicochemical and Biogeochemical Transformation in the Atmosphere and at Atmospheric Interfaces: A Review and Future Directions', *Chem. Rev.*, vol. 115, no. 10, pp. 3760–3802, May 2015, doi: 10.1021/cr500667e.

[18] Y. Zhang, L. Jaeglé, L. Thompson, and D. G. Streets, ‘Six centuries of changing oceanic mercury’, *Global Biogeochemical Cycles*, vol. 28, no. 11, pp. 1251–1261, Nov. 2014, doi: 10.1002/2014GB004939.
[19] M. Boldyrev, ‘Lead: properties, history, and applications’, *Wiki J Sci*, vol. 1, no. 2, p. 7, Jul. 2018, doi: 10.15347/wjs/2018.007.
[20] K. R. Mahaffey, ‘Environmental lead toxicity: nutrition as a component of intervention.’, *Environ Health Perspect*, vol. 89, pp. 75–78, Nov. 1990, doi: 10.1289/ehp.908975.
[21] H. Needleman, ‘Lead Poisoning’, *Annu. Rev. Med.*, vol. 55, no. 1, pp. 209–222, Feb. 2004, doi: 10.1146/annurev.med.55.091902.103653.
[22] F. Degryse, E. Smolders, and D. R. Parker, ‘Partitioning of metals (Cd, Co, Cu, Ni, Pb, Zn) in soils: concepts, methodologies, prediction and applications – a review’, *European J Soil Science*, vol. 60, no. 4, pp. 590–612, Aug. 2009, doi: 10.1111/j.1365-2389.2009.01142.x.
[23] T. Watanabe, M. Kasahara, H. Nakatsuka, and M. Ikeda, ‘Cadmium and lead contents of cigarettes produced in various areas of the world1’, *The Science of The Total Environment*, vol. 66, pp. 29–37, Oct. 1987, doi: 10.1016/0048-9697(87)90074-X.
[24] M. S. Sonmez and R. V. Kumar, ‘Leaching of waste battery paste components. Part 1: Lead citrate synthesis from PbO and PbO2’, *Hydrometallurgy*, vol. 95, no. 1–2, pp. 53–60, Jan. 2009, doi: 10.1016/j.hydromet.2008.04.012.
[25] B. P. Lanphear, ‘Cognitive Deficits Associated with Blood Lead Concentrations <10 microg/dL in US Children and Adolescents’, *Public Health Reports*, vol. 115, no. 6, pp. 521–529, Dec. 2000, doi: 10.1093/phr/115.6.521.
[26] H. W. Mielke and P. L. Reagan, ‘Soil is an important pathway of human lead exposure.’, *Environ Health Perspect*, vol. 106, no. suppl 1, pp. 217–229, Feb. 1998, doi: 10.1289/ehp.98106s1217.
[27] A. Jonsson, M. Lindström, and B. Bergbäck, ‘Phasing out cadmium and lead—emissions and sediment loads in an urban area’, *Science of The Total Environment*, vol. 292, no. 1–2, pp. 91–100, Jun. 2002, doi: 10.1016/S0048-9697(02)00029-3.
[28] J. O. Nriagu and J. M. Pacyna, ‘Quantitative assessment of worldwide contamination of air, water and soils by trace metals’, *Nature*, vol. 333, no. 6169, pp. 134–139, May 1988, doi: 10.1038/333134a0.
[29] F. Crea, C. Foti, D. Milea, and S. Sammartano, ‘Speciation of Cadmium in the Environment’, in *Cadmium: From Toxicity to Essentiality*, vol. 11, A. Sigel, H. Sigel, and R. K. Sigel, Eds., in Metal Ions in Life Sciences, vol. 11. , Dordrecht: Springer Netherlands, 2013, pp. 63–83. doi: 10.1007/978-94-007-5179-8_3.
[30] A. Chen, K. N. Dietrich, X. Huo, and S. Ho, ‘Developmental Neurotoxicants in E-Waste: An Emerging Health Concern’, *Environ Health Perspect*, vol. 119, no. 4, pp. 431–438, Apr. 2011, doi: 10.1289/ehp.1002452.
[31] G. Nordberg, B. Sandstrom, G. Becking, and R. A. Goyer, ‘Essentiality and toxicity of trace elements: Principles and methods for assessment of risk from human exposure to essential trace elements’, *J. Trace Elem. Exp. Med.*, vol. 13, no. 1, pp. 141–153, 2000, doi: 10.1002/(SICI)1520-670X(2000)13:1<141::AID-JTRA15>3.0.CO;2-A.
[32] Q. Peng, B. K. Greenfield, F. Dang, and H. Zhong, ‘Human exposure to methylmercury from crayfish (Procambarus clarkii) in China’, *Environ Geochem Health*, vol. 38, no. 1, pp. 169–181, Feb. 2016, doi: 10.1007/s10653-015-9701-4.
[33] K. G. Homme *et al.*, ‘New science challenges old notion that mercury dental amalgam is safe’, *Biometals*, vol. 27, no. 1, pp. 19–24, Feb. 2014, doi: 10.1007/s10534-013-9700-9.
[34] M. Berlin, R. K. Zalups, and B. A. Fowler, ‘Mercury’, in *Handbook on the Toxicology of Metals*, Elsevier, 2015, pp. 1013–1075. doi: 10.1016/B978-0-444-59453-2.00046-9.

[35] A. L. V. Milioni, B. V. Nagy, A. L. A. Moura, E. C. Zachi, M. T. S. Barboni, and D. F. Ventura, 'Neurotoxic impact of mercury on the central nervous system evaluated by neuropsychological tests and on the autonomic nervous system evaluated by dynamic pupillometry', *NeuroToxicology*, vol. 59, pp. 263–269, Mar. 2017, doi: 10.1016/j.neuro.2016.04.010.

[36] T. W. Clarkson, 'The Toxicology of Mercury', *Critical Reviews in Clinical Laboratory Sciences*, vol. 34, no. 4, pp. 369–403, Jan. 1997, doi: 10.3109/10408369708998098.

[37] PREDIMED Study Investigators *et al.*, 'Mercury exposure and risk of cardiovascular disease: a nested case-control study in the PREDIMED (PREvention with MEDiterranean Diet) study', *BMC Cardiovasc Disord*, vol. 17, no. 1, p. 9, Dec. 2017, doi: 10.1186/s12872-016-0435-8.

[38] H. A. Roman *et al.*, 'Evaluation of the Cardiovascular Effects of Methylmercury Exposures: Current Evidence Supports Development of a Dose–Response Function for Regulatory Benefits Analysis', *Environ Health Perspect*, vol. 119, no. 5, pp. 607–614, May 2011, doi: 10.1289/ehp.1003012.

[39] S. Bose-O'Reilly, K. M. McCarty, N. Steckling, and B. Lettmeier, 'Mercury Exposure and Children's Health', *Current Problems in Pediatric and Adolescent Health Care*, vol. 40, no. 8, pp. 186–215, Sep. 2010, doi: 10.1016/j.cppeds.2010.07.002.

[40] T. Michael *et al.*, 'Prenatal exposure to heavy metal mixtures and anthropometric birth outcomes: a cross-sectional study', *Environ Health*, vol. 21, no. 1, p. 139, Dec. 2022, doi: 10.1186/s12940-022-00950-z.

[41] R. Levin *et al.*, 'Lead Exposures in U.S. Children, 2008: Implications for Prevention', *Environ Health Perspect*, vol. 116, no. 10, pp. 1285–1293, Oct. 2008, doi: 10.1289/ehp.11241.

[42] D. C. Bellinger, 'Very low lead exposures and children's neurodevelopment', *Current Opinion in Pediatrics*, vol. 20, no. 2, pp. 172–177, Apr. 2008, doi: 10.1097/MOP.0b013e3282f4f97b.

[43] A. Navas-Acien, E. Guallar, E. K. Silbergeld, and S. J. Rothenberg, 'Lead Exposure and Cardiovascular Disease—A Systematic Review', *Environ Health Perspect*, vol. 115, no. 3, pp. 472–482, Mar. 2007, doi: 10.1289/ehp.9785.

[44] R. J. Person, E. J. Tokar, Y. Xu, R. Orihuela, N. N. O. Ngalame, and M. P. Waalkes, 'Chronic cadmium exposure in vitro induces cancer cell characteristics in human lung cells', *Toxicology and Applied Pharmacology*, vol. 273, no. 2, pp. 281–288, Dec. 2013, doi: 10.1016/j.taap.2013.06.013.

[45] S. Moon *et al.*, 'Association between environmental cadmium exposure and increased mortality in the U.S. National Health and Nutrition Examination Survey (1999–2018)', *J Expo Sci Environ Epidemiol*, vol. 33, no. 6, pp. 874–882, Nov. 2023, doi: 10.1038/s41370-023-00556-8.

[46] L. Järup, 'Hazards of heavy metal contamination', *British Medical Bulletin*, vol. 68, no. 1, pp. 167–182, Dec. 2003, doi: 10.1093/bmb/ldg032.

[47] K. M. Marano *et al.*, 'Cadmium exposure and tobacco consumption: Biomarkers and risk assessment', *Regulatory Toxicology and Pharmacology*, vol. 64, no. 2, pp. 243–252, Nov. 2012, doi: 10.1016/j.yrtph.2012.07.008.

[48] Agency for Toxic Substances and Disease Registry, 'U.S. Department of Health and Human Services'. Accessed: Dec. 25, 2024. [Online]. Available: www.atsdr.cdc.gov/toxprofiles/tp5.pdf](https://www.atsdr.cdc.gov/toxprofiles/tp5.pdf)

[49] M. Hernandez, M. Schuhmacher, J. D. Fernandez, J. L. Domingo, and J. M. Llobet, 'Urinary cadmium levels during pregnancy and postpartum: A longitudinal study', *Biol Trace Elem Res*, vol. 53, no. 1–3, pp. 205–212, Jun. 1996, doi: 10.1007/BF02784556.

[50] M. Nishijo *et al.*, 'Effects of maternal exposure to cadmium on pregnancy outcome and breast milk', *Occup Environ Med*, vol. 59, no. 6, pp. 394–397, Jun. 2002, doi: 10.1136/oem.59.6.394.
[51] L. Zhao *et al.*, 'Reproductive effects of cadmium on sperm function and early embryonic development in vitro', *PLoS ONE*, vol. 12, no. 11, p. e0186727, Nov. 2017, doi: 10.1371/journal.pone.0186727.
[52] J. Aaseth, M. A. Skaug, Y. Cao, and O. Andersen, 'Chelation in metal intoxication—Principles and paradigms', *Journal of Trace Elements in Medicine and Biology*, vol. 31, pp. 260–266, Jul. 2015, doi: 10.1016/j.jtemb.2014.10.001.
[53] H. Dapul and D. Laraque, 'Lead poisoning in children', *Adv Pediatr*, vol. 61, no. 1, pp. 313–333, Aug. 2014, doi: 10.1016/j.yapd.2014.04.004.
[54] S. Jacob *et al.*, 'Enhancement of glucose disposal in patients with type 2 diabetes by alpha-lipoic acid', *Arzneimittelforschung*, vol. 45, no. 8, pp. 872–874, Aug. 1995.
[55] M. J. Kosnett, 'Unithiol (DMPS)', in *Critical Care Toxicology*, J. Brent, K. Burkhart, P. Dargan, B. Hatten, B. Megarbane, and R. Palmer, Eds., Cham: Springer International Publishing, 2016, pp. 1–4. doi: 10.1007/978-3-319-20790-2_21-1.
[56] L. Gerhardsson and J. Aaseth, 'Guidance for Clinical Treatment of Metal Poisonings—Use and Misuse of Chelating Agents', in *Chelation Therapy in the Treatment of Metal Intoxication*, Elsevier, 2016, pp. 313–341. doi: 10.1016/B978-0-12-803072-1.00007-9.
[57] California Poison Control System (CPCS), 'Antidote Chart'. [Online]. Available: http://www.calpoison.org/hcp/CPCS_antidote_chart.pdf
[58] Illinois Poison Center, 'IPC Poison Antidote Stocking Chart'. [Online]. Available: https://www.illinoispoisoncenter.org/getmedia/f7c14fba-03bf-44b8-b589-32f6f552f6c7/ipc-antidote-stocking-list-2022_final-edit.pdf
[59] L. Packer, E. H. Witt, and H. J. Tritschler, 'Alpha-lipoic acid as a biological antioxidant', *Free Radical Biology and Medicine*, vol. 19, no. 2, pp. 227–250, Aug. 1995, doi: 10.1016/0891-5849(95)00017-R.
[60] G. Bjørklund, J. Aaseth, G. Crisponi, Md. M. Rahman, and S. Chirumbolo, 'Insights on alpha lipoic and dihydrolipoic acids as promising scavengers of oxidative stress and possible chelators in mercury toxicology', *Journal of Inorganic Biochemistry*, vol. 195, pp. 111–119, Jun. 2019, doi: 10.1016/j.jinorgbio.2019.03.019.
[61] M. T. Muhammad and M. N. Khan, 'Kinetics, mechanistic and synergistic studies of Alpha lipoic acid with hydrogen peroxide', *Journal of Saudi Chemical Society*, vol. 21, no. 2, pp. 123–131, Feb. 2017, doi: 10.1016/j.jscs.2015.01.008.
[62] C. Pagano, P. Calarco, M. Ceccarini, T. Beccari, M. Ricci, and L. Perioli, 'Development and Characterization of New Topical Hydrogels Based on Alpha Lipoic Acid—Hydrotalcite Hybrids', *Cosmetics*, vol. 6, no. 2, p. 35, Jun. 2019, doi: 10.3390/cosmetics6020035.
[63] M. D. Coleman, R. C. Eason, and C. J. Bailey, 'The therapeutic use of lipoic acid in diabetes: a current perspective', *Environmental Toxicology and Pharmacology*, vol. 10, no. 4, pp. 167–172, Sep. 2001, doi: 10.1016/s1382-6689(01)00080-1.
[64] P. Keattanong, N. Wasukan, M. Kuno, and S. Srisung, 'Synthesis, structural characterization, computational studies and stability evaluations of metal ions and ZnONPs complexes with dimercaptosuccinic acid', *Heliyon*, vol. 7, no. 1, p. e05962, Jan. 2021, doi: 10.1016/j.heliyon.2021.e05962.
[65] X. Fang, F. Hua, and Q. Fernando, 'Comparison of *rac* - and *meso* -2,3-Dimercaptosuccinic Acids for Chelation of Mercury and Cadmium Using Chemical Speciation Models', *Chem. Res. Toxicol.*, vol. 9, no. 1, pp. 284–290, Jan. 1996, doi: 10.1021/tx950096o.

[66] X. Fang, F. Hua, and Q. Fernando, ‘Comparison of *rac* - and *meso* -2,3-Dimercaptosuccinic Acids for Chelation of Mercury and Cadmium Using Chemical Speciation Models’, *Chem. Res. Toxicol.*, vol. 9, no. 1, pp. 284–290, Jan. 1996, doi: 10.1021/tx950096o.
[67] J. R. Campbell, ‘The Therapeutic Use of 2,3-Dimercaptopropane-1-Sulfonate in Two Cases of Inorganic Mercury Poisoning’, *JAMA*, vol. 256, no. 22, p. 3127, Dec. 1986, doi: 10.1001/jama.1986.03380220093029.
[68] S. Maheshwari, Y. Li, and M. J. Janik, ‘The Fe_2 O_3 (0001) Surface Under Electroreduction Conditions: A DFT Study of L-Cysteine Adsorption’, *J. Electrochem. Soc.*, vol. 169, no. 6, p. 064513, Jun. 2022, doi: 10.1149/1945-7111/ac7826.
[69] R. Matsui *et al.*, ‘Redox Regulation *via* Glutaredoxin-1 and Protein *S* -Glutathionylation’, *Antioxidants & Redox Signaling*, vol. 32, no. 10, pp. 677–700, Apr. 2020, doi: 10.1089/ars.2019.7963.
[70] N. Ballatori and M. W. Lieberman, ‘N-Acetylcysteine as an Antidote in Methylmercury Poisoning’, *Environmental Health Perspectives*, vol. 106, no. 5, 1998.
[71] M. E. Sears, ‘Chelation: Harnessing and Enhancing Heavy Metal Detoxification—A Review’, *The Scientific World Journal*, vol. 2013, no. 1, p. 219840, Jan. 2013, doi: 10.1155/2013/219840.
[72] H. Kimura, ‘Hydrogen Sulfide and Polysulfides as Biological Mediators’, *Molecules*, vol. 19, no. 10, pp. 16146–16157, Oct. 2014, doi: 10.3390/molecules191016146.
[73] C. K. Mathews and K. E. Van Holde, *Biochemistry*, 2nd ed. Menlo Park, Calif: Benjamin/Cummings Pub. Co., Inc, 1996.
[74] G. Wu, J. R. Lupton, N. D. Turner, Y.-Z. Fang, and S. Yang, ‘Glutathione Metabolism and Its Implications for Health’, *The Journal of Nutrition*, vol. 134, no. 3, pp. 489–492, Mar. 2004, doi: 10.1093/jn/134.3.489.
[75] S. C. Lu, ‘Regulation of glutathione synthesis’, *Molecular Aspects of Medicine*, vol. 30, no. 1–2, pp. 42–59, Feb. 2009, doi: 10.1016/j.mam.2008.05.005.
[76] A. Meister and M. E. Anderson, ‘GLUTATHIONE’, *Annu. Rev. Biochem.*, vol. 52, no. 1, pp. 711–760, Jun. 1983, doi: 10.1146/annurev.bi.52.070183.003431.
[77] J. Reedijk, Ed., *Comprehensive inorganic chemistry II: from elements to applications*, 2. ed. Amsterdam: Elsevier, 2013.
[78] J. Aaseth, ‘Recent Advance in the Therapy of Metal Poisonings with Chelating Agents’, *Human Toxicology*, vol. 2, no. 2, pp. 257–272, Apr. 1983, doi: 10.1177/096032718300200214.
[79] O. Andersen and J. Aaseth, ‘Molecular mechanisms of in vivo metal chelation: implications for clinical treatment of metal intoxications.’, *Environ Health Perspect*, vol. 110, no. suppl 5, pp. 887–890, Oct. 2002, doi: 10.1289/ehp.02110s5887.
[80] R. G. Pearson, ‘**Hard and Soft Acids and Bases**’, *J. Am. Chem. Soc.*, vol. 85, no. 22, pp. 3533–3539, Nov. 1963, doi: 10.1021/ja00905a001.
[81] G. N. Lewis, ‘Acids and bases’, *Journal of the Franklin Institute*, vol. 226, no. 3, pp. 293–313, Sep. 1938, doi: 10.1016/S0016-0032(38)91691-6.
[82] D. J. Grunwald and J. S. Eisen, ‘Headwaters of the zebrafish — emergence of a new model vertebrate’, *Nat Rev Genet*, vol. 3, no. 9, pp. 717–724, Sep. 2002, doi: 10.1038/nrg892.
[83] K. Howe *et al.*, ‘The zebrafish reference genome sequence and its relationship to the human genome’, *Nature*, vol. 496, no. 7446, pp. 498–503, Apr. 2013, doi: 10.1038/nature12111.
[84] L. I. Zon and R. T. Peterson, ‘In vivo drug discovery in the zebrafish’, *Nat Rev Drug Discov*, vol. 4, no. 1, pp. 35–44, Jan. 2005, doi: 10.1038/nrd1606.

[85] R. M. Warga and C. Nüsslein-Volhard, ‘Origin and development of the zebrafish endoderm’, *Development*, vol. 126, no. 4, pp. 827–838, Feb. 1999, doi: 10.1242/dev.126.4.827.
[86] L. U. Sneddon *et al.*, ‘Response to: Responses of larval zebrafish to low pH immersion assay. Comment on Lopez-Luna et al.’, *Journal of Experimental Biology*, vol. 220, no. 17, pp. 3192–3194, Sep. 2017, doi: 10.1242/jeb.163451.
[87] M. M. Adams and H. Kafaligonul, ‘Zebrafish—A Model Organism for Studying the Neurobiological Mechanisms Underlying Cognitive Brain Aging and Use of Potential Interventions’, *Front. Cell Dev. Biol.*, vol. 6, p. 135, Nov. 2018, doi: 10.3389/fcell.2018.00135.
[88] P. J. Keller, A. D. Schmidt, J. Wittbrodt, and E. H. K. Stelzer, ‘Reconstruction of Zebrafish Early Embryonic Development by Scanned Light Sheet Microscopy’, *Science*, vol. 322, no. 5904, pp. 1065–1069, Nov. 2008, doi: 10.1126/science.1162493.
[89] Y. Wang, M. Rovira, S. Yusuff, and M. J. Parsons, ‘Genetic inducible fate mapping in larval zebrafish reveals origins of adult insulin-producing β-cells’, *Development*, vol. 138, no. 4, pp. 609–617, Feb. 2011, doi: 10.1242/dev.059097.
[90] C. B. Kimmel, W. W. Ballard, S. R. Kimmel, B. Ullmann, and T. F. Schilling, ‘Stages of embryonic development of the zebrafish’, *Developmental Dynamics*, vol. 203, no. 3, pp. 253–310, Jul. 1995, doi: 10.1002/aja.1002030302.
[91] S. M. Peterson and J. L. Freeman, ‘RNA Isolation from Embryonic Zebrafish and cDNA Synthesis for Gene Expression Analysis’, *JoVE*, no. 30, p. 1470, Aug. 2009, doi: 10.3791/1470-v.
[92] R. Wang, K. Liu, Y. Zhang, X. Chen, and X. Wang, ‘Evaluation of the Developmental Toxicity Induced by E804 in Zebrafish Embryos’, *Front. Pharmacol.*, vol. 11, p. 32, Feb. 2020, doi: 10.3389/fphar.2020.00032.
[93] D. Di Paola *et al.*, ‘Combined Toxicity of Xenobiotics Bisphenol A and Heavy Metals on Zebrafish Embryos (Danio rerio)’, *Toxics*, vol. 9, no. 12, p. 344, Dec. 2021, doi: 10.3390/toxics9120344.
[94] Q.-F. Zhang, Y.-W. Li, Z.-H. Liu, and Q.-L. Chen, ‘Exposure to mercuric chloride induces developmental damage, oxidative stress and immunotoxicity in zebrafish embryos-larvae’, *Aquatic Toxicology*, vol. 181, pp. 76–85, Dec. 2016, doi: 10.1016/j.aquatox.2016.10.029.
[95] Z. Wang *et al.*, ‘Early-life lead exposure induces long-term toxicity in the central nervous system: From zebrafish larvae to juveniles and adults’, *Science of The Total Environment*, vol. 804, p. 150185, Jan. 2022, doi: 10.1016/j.scitotenv.2021.150185.
[96] N. H. Bui Thi *et al.*, ‘Chronic Exposure to Low Concentration Lead Chloride-Induced Anxiety and Loss of Aggression and Memory in Zebrafish’, *IJMS*, vol. 21, no. 5, p. 1844, Mar. 2020, doi: 10.3390/ijms21051844.
[97] F. F. Cruz *et al.*, ‘Assessment of mercury chloride-induced toxicity and the relevance of P2X7 receptor activation in zebrafish larvae’, *Comparative Biochemistry and Physiology Part C: Toxicology & Pharmacology*, vol. 158, no. 3, pp. 159–164, Sep. 2013, doi: 10.1016/j.cbpc.2013.07.003.
[98] Z. Halabi *et al.*, ‘Alpha Lipoic Acid Toxicity: The First Reported Mortality in an Adult Patient After Multiorgan Failure’, *The Journal of Emergency Medicine*, vol. 64, no. 2, pp. 190–194, Feb. 2023, doi: 10.1016/j.jemermed.2022.12.016.
[99] F. Bray *et al.*, ‘Global cancer statistics 2022: GLOBOCAN estimates of incidence and mortality worldwide for 36 cancers in 185 countries’, *CA A Cancer J Clinicians*, vol. 74, no. 3, pp. 229–263, May 2024, doi: 10.3322/caac.21834.

[100] A. R. David and M. R. Zimmerman, ‘Cancer: an old disease, a new disease or something in between?’, *Nat Rev Cancer*, vol. 10, no. 10, pp. 728–733, Oct. 2010, doi: 10.1038/nrc2914.
[101] P. A. Marks, ‘The Emperor of All Maladies (2010, Scribner): By Siddhartha Mukherjee’, *FASEB j.*, vol. 25, no. 6, pp. 1786–1787, Jun. 2011, doi: 10.1096/fj.11-0603ufm.
[102] N. J. Wheate, S. Walker, G. E. Craig, and R. Oun, ‘The status of platinum anticancer drugs in the clinic and in clinical trials’, *Dalton Trans.*, vol. 39, no. 35, p. 8113, 2010, doi: 10.1039/c0dt00292e.
[103] D. Hanahan and R. A. Weinberg, ‘Hallmarks of Cancer: The Next Generation’, *Cell*, vol. 144, no. 5, pp. 646–674, Mar. 2011, doi: 10.1016/j.cell.2011.02.013.
[104] B. J. Aubrey, G. L. Kelly, A. Janic, M. J. Herold, and A. Strasser, ‘How does p53 induce apoptosis and how does this relate to p53-mediated tumour suppression?’, *Cell Death Differ*, vol. 25, no. 1, pp. 104–113, Jan. 2018, doi: 10.1038/cdd.2017.169.
[105] B. Vogelstein, N. Papadopoulos, V. E. Velculescu, S. Zhou, L. A. Diaz, and K. W. Kinzler, ‘Cancer Genome Landscapes’, *Science*, vol. 339, no. 6127, pp. 1546–1558, Mar. 2013, doi: 10.1126/science.1235122.
[106] K. H. Vousden and D. P. Lane, ‘p53 in health and disease’, *Nat Rev Mol Cell Biol*, vol. 8, no. 4, pp. 275–283, Apr. 2007, doi: 10.1038/nrm2147.
[107] A. Lewandowska, M. Rudzki, S. Rudzki, T. Lewandowski, and B. Laskowska, ‘Environmental risk factors for cancer – review paper’, *Ann Agric Environ Med.*, vol. 26, no. 1, pp. 1–7, Mar. 2019, doi: 10.26444/aaem/94299.
[108] World Health Organization, ‘Cancer’. [Online]. Available: https://www.who.int/news-room/fact-sheets/detail/cancer
[109] Y. Hatano *et al.*, ‘Virus-Driven Carcinogenesis’, *Cancers*, vol. 13, no. 11, p. 2625, May 2021, doi: 10.3390/cancers13112625.
[110] M. Schiffman, P. E. Castle, J. Jeronimo, A. C. Rodriguez, and S. Wacholder, ‘Human papillomavirus and cervical cancer’, *The Lancet*, vol. 370, no. 9590, pp. 890–907, Sep. 2007, doi: 10.1016/S0140-6736(07)61416-0.
[111] H. Zur Hausen, ‘Papillomaviruses in the causation of human cancers — a brief historical account’, *Virology*, vol. 384, no. 2, pp. 260–265, Feb. 2009, doi: 10.1016/j.virol.2008.11.046.
[112] S. S. Gambhir, ‘Molecular imaging of cancer with positron emission tomography’, *Nat Rev Cancer*, vol. 2, no. 9, pp. 683–693, Sep. 2002, doi: 10.1038/nrc882.
[113] J. A. Ramos-Vara, ‘Technical Aspects of Immunohistochemistry’, *Vet Pathol*, vol. 42, no. 4, pp. 405–426, Jul. 2005, doi: 10.1354/vp.42-4-405.
[114] J. C. M. Wan *et al.*, ‘Liquid biopsies come of age: towards implementation of circulating tumour DNA’, *Nat Rev Cancer*, vol. 17, no. 4, pp. 223–238, Apr. 2017, doi: 10.1038/nrc.2017.7.
[115] E. R. Mardis, ‘The Impact of Next-Generation Sequencing on Cancer Genomics: From Discovery to Clinic’, *Cold Spring Harb Perspect Med*, vol. 9, no. 9, p. a036269, Sep. 2019, doi: 10.1101/cshperspect.a036269.
[116] K. Reddy, P. Gharde, H. Tayade, M. Patil, L. S. Reddy, and D. Surya, ‘Advancements in Robotic Surgery: A Comprehensive Overview of Current Utilizations and Upcoming Frontiers’, *Cureus*, Dec. 2023, doi: 10.7759/cureus.50415.
[117] D. De Ruysscher, G. Niedermann, N. G. Burnet, S. Siva, A. W. M. Lee, and F. Hegi-Johnson, ‘Radiotherapy toxicity’, *Nat Rev Dis Primers*, vol. 5, no. 1, p. 13, Feb. 2019, doi: 10.1038/s41572-019-0064-5.
[118] S. J. Baker and E. P. Reddy, ‘Targeted Inhibition of Kinases in Cancer Therapy’, *Mount Sinai J Medicine*, vol. 77, no. 6, pp. 573–586, Nov. 2010, doi: 10.1002/msj.20220.

[119] C. H. June, R. S. O'Connor, O. U. Kawalekar, S. Ghassemi, and M. C. Milone, 'CAR T cell immunotherapy for human cancer', *Science*, vol. 359, no. 6382, pp. 1361–1365, Mar. 2018, doi: 10.1126/science.aar6711.
[120] V. C. Jordan, 'Tamoxifen: a most unlikely pioneering medicine', *Nat Rev Drug Discov*, vol. 2, no. 3, pp. 205–213, Mar. 2003, doi: 10.1038/nrd1031.
[121] A. J. Vargas and C. C. Harris, 'Biomarker development in the precision medicine era: lung cancer as a case study', *Nat Rev Cancer*, vol. 16, no. 8, pp. 525–537, Aug. 2016, doi: 10.1038/nrc.2016.56.
[122] E. A. Copelan, 'Hematopoietic Stem-Cell Transplantation', *N Engl J Med*, vol. 354, no. 17, pp. 1813–1826, Apr. 2006, doi: 10.1056/NEJMra052638.
[123] V. Lim and S. C. Eppes, 'Vaccines', *Delaware Journal of Public Health*, vol. 10, no. 3, pp. 12–14, Aug. 2024, doi: 10.32481/djph.2024.08.05.
[124] The National Lung Screening Trial Research Team, 'Reduced Lung-Cancer Mortality with Low-Dose Computed Tomographic Screening', *N Engl J Med*, vol. 365, no. 5, pp. 395–409, Aug. 2011, doi: 10.1056/NEJMoa1102873.
[125] A. Lewandowska, M. Rudzki, S. Rudzki, T. Lewandowski, and B. Laskowska, 'Environmental risk factors for cancer – review paper', *Ann Agric Environ Med.*, vol. 26, no. 1, pp. 1–7, Mar. 2019, doi: 10.26444/aaem/94299.
[126] A. Urruticoechea, R. Alemany, J. Balart, A. Villanueva, F. Vinals, and G. Capella, 'Recent Advances in Cancer Therapy: An Overview', *CPD*, vol. 16, no. 1, pp. 3–10, Jan. 2010, doi: 10.2174/138161210789941847.
[127] O. C. Farokhzad and R. Langer, 'Impact of Nanotechnology on Drug Delivery', *ACS Nano*, vol. 3, no. 1, pp. 16–20, Jan. 2009, doi: 10.1021/nn900002m.
[128] A.-M. Florea and D. Büsselberg, 'Cisplatin as an Anti-Tumor Drug: Cellular Mechanisms of Activity, Drug Resistance and Induced Side Effects', *Cancers*, vol. 3, no. 1, pp. 1351–1371, Mar. 2011, doi: 10.3390/cancers3011351.
[129] B. Rosenberg, L. Van Camp, and T. Krigas, 'Inhibition of Cell Division in Escherichia coli by Electrolysis Products from a Platinum Electrode', *Nature*, vol. 205, no. 4972, pp. 698–699, Feb. 1965, doi: 10.1038/205698a0.
[130] L. Kelland, 'The resurgence of platinum-based cancer chemotherapy', *Nat Rev Cancer*, vol. 7, no. 8, pp. 573–584, Aug. 2007, doi: 10.1038/nrc2167.
[131] T. C. Johnstone, K. Suntharalingam, and S. J. Lippard, 'The Next Generation of Platinum Drugs: Targeted Pt(II) Agents, Nanoparticle Delivery, and Pt(IV) Prodrugs', *Chem. Rev.*, vol. 116, no. 5, pp. 3436–3486, Mar. 2016, doi: 10.1021/acs.chemrev.5b00597.
[132] X. Wang and Z. Guo, 'Targeting and delivery of platinum-based anticancer drugs', *Chem. Soc. Rev.*, vol. 42, no. 1, pp. 202–224, 2013, doi: 10.1039/C2CS35259A.
[133] S. Dasari and P. Bernard Tchounwou, 'Cisplatin in cancer therapy: Molecular mechanisms of action', *European Journal of Pharmacology*, vol. 740, pp. 364–378, Oct. 2014, doi: 10.1016/j.ejphar.2014.07.025.
[134] C. R. R. Rocha, M. M. Silva, A. Quinet, J. B. Cabral-Neto, and C. F. M. Menck, 'DNA repair pathways and cisplatin resistance: an intimate relationship', *Clinics*, vol. 73, p. e478s, 2018, doi: 10.6061/clinics/2018/e478s.
[135] S. V. Melnikov, D. Söll, T. A. Steitz, and Y. S. Polikanov, 'Insights into RNA binding by the anticancer drug cisplatin from the crystal structure of cisplatin-modified ribosome', *Nucleic Acids Res*, vol. 44, no. 10, pp. 4978–4987, Jun. 2016, doi: 10.1093/nar/gkw246.
[136] S. Y. Lee, C. Y. Kim, and T.-G. Nam, 'Ruthenium Complexes as Anticancer Agents: A Brief History and Perspectives', *DDDT*, vol. Volume 14, pp. 5375–5392, Dec. 2020, doi: 10.2147/DDDT.S275007.

[137] V. Paradiso, C. Costabile, and F. Grisi, 'Ruthenium-based olefin metathesis catalysts with monodentate unsymmetrical NHC ligands', *Beilstein J. Org. Chem.*, vol. 14, pp. 3122–3149, Dec. 2018, doi: 10.3762/bjoc.14.292.
[138] A. Jabłońska-Wawrzycka, P. Rogala, S. Michałkiewicz, M. Hodorowicz, and B. Barszcz, 'Ruthenium complexes in different oxidation states: synthesis, crystal structure, spectra and redox properties', *Dalton Trans.*, vol. 42, no. 17, p. 6092, 2013, doi: 10.1039/c3dt32214a.
[139] K. Lin, Z.-Z. Zhao, H.-B. Bo, X.-J. Hao, and J.-Q. Wang, 'Applications of Ruthenium Complex in Tumor Diagnosis and Therapy', *Front. Pharmacol.*, vol. 9, p. 1323, Nov. 2018, doi: 10.3389/fphar.2018.01323.
[140] L. Ackermann, A. Althammer, and R. Born, '[RuCl3(H2O)n]-catalyzed direct arylations', *Tetrahedron*, vol. 64, no. 26, pp. 6115–6124, Jun. 2008, doi: 10.1016/j.tet.2008.01.050.
[141] M. Sonoda, F. Kakiuchi, N. Chatani, and S. Murai, 'Directing effect of functional groups in ruthenium-catalyzed addition of substituted acetophonones to an olefin', *Journal of Organometallic Chemistry*, vol. 504, no. 1–2, pp. 151–152, Nov. 1995, doi: 10.1016/0022-328X(95)05607-Q.
[142] M. A. W. Lawrence, J. L. Bullock, and A. A. Holder, 'Basic Coordination Chemistry of Ruthenium', in *Ruthenium Complexes*, 1st ed., W. R. Browne, A. A. Holder, M. A. Lawrence, J. L. Bullock Jr, and L. Lilge, Eds., Wiley, 2018, pp. 25–41. doi: 10.1002/9783527695225.ch2.
[143] A. D'Amato *et al.*, 'Complexes of Ruthenium(II) as Promising Dual-Active Agents against Cancer and Viral Infections', *Pharmaceuticals*, vol. 16, no. 12, p. 1729, Dec. 2023, doi: 10.3390/ph16121729.
[144] Pragti *et al.*, 'Pyrene-based fluorescent Ru(II)-arene complexes for significant biological applications: catalytic potential, DNA/protein binding, two photon cell imaging and *in vitro* cytotoxicity', *Dalton Trans.*, vol. 51, no. 10, pp. 3937–3953, 2022, doi: 10.1039/D1DT04093F.
[145] F. Chérioux, C. M. Thomas, T. Monnier, and G. Süss-Fink, 'Specific reactivity of SH versus OH functions towards dinuclear arene ruthenium units: synthesis of cationic complexes of the type [(arene)2Ru2(SR)3]+', *Polyhedron*, vol. 22, no. 4, pp. 543–548, Feb. 2003, doi: 10.1016/S0277-5387(02)01376-1.
[146] A. P. Basto *et al.*, 'Characterization of the Activities of Dinuclear Thiolato-Bridged Arene Ruthenium Complexes against Toxoplasma gondii', *Antimicrob Agents Chemother*, vol. 61, no. 9, pp. e01031-17, Sep. 2017, doi: 10.1128/AAC.01031-17.
[147] F. Giannini *et al.*, 'Highly cytotoxic trithiophenolatodiruthenium complexes of the type [(η6-p-MeC6H4Pr i)2Ru2(SC6H4-p-X)3]+: synthesis, molecular structure, electrochemistry, cytotoxicity, and glutathione oxidation potential', *J Biol Inorg Chem*, vol. 17, no. 6, pp. 951–960, Aug. 2012, doi: 10.1007/s00775-012-0911-2.
[148] F. Giannini *et al.*, 'Tuning the in vitro cell cytotoxicity of dinuclear arene ruthenium trithiolato complexes: Influence of the arene ligand', *Journal of Organometallic Chemistry*, vol. 783, pp. 40–45, May 2015, doi: 10.1016/j.jorganchem.2015.02.010.
[149] M. Gras, B. Therrien, G. Süss-Fink, O. Zava, and P. J. Dyson, 'Thiophenolato-bridged dinuclear arene ruthenium complexes: a new family of highly cytotoxic anticancer agents', *Dalton Trans.*, vol. 39, no. 42, p. 10305, 2010, doi: 10.1039/c0dt00887g.
[150] K. Vadiei, Z. H. Siddik, A. R. Khokhar, S. Al-Baker, F. Sampedro, and R. Perez-Soler, 'Pharmacokinetics of liposome-entrappedcis-bis-neodecanoato-trans-R,R-1,2-diaminocyclohexane platinum(II) and cisplatin given i.v. and i.p. in the rat', *Cancer Chemother. Pharmacol.*, vol. 30, no. 5, pp. 365–369, 1992, doi: 10.1007/BF00689964.

[151] A. R. Knokhar, S. Al-Baker, I. H. Krakoff, and R. Perez-Soler, ‘Toxicity and antitumor activity of cis-bis-carboxylato(trans-R,R-1,2-diaminocyclohexane) platinum(II) complexes entrapped in liposomes’, *Cancer Chemother. Pharmacol.*, vol. 23, no. 4, pp. 219–224, 1989, doi: 10.1007/BF00451645.
[152] R. Perez-Solerl, I. Hanl, S. AI-Baker, and A. R. Khokhar, ‘Lipophilic platinum complexes entrapped in liposomes: improved stability and preserved antitumor activity with complexes containing linear alkyl carboxylato leaving groups’.
[153] R. Perez-Soler, A. R. Khokhar, and G. Lopez-Berestein, ‘Treatment and prophylaxis of experimental liver metastases of M5076 reticulosarcoma with cis-bis-neodecanoato-trans-R,R-1,2-diaminocyclohexaneplatinum (II) encapsulated in multilamellar vesicles’, *Cancer Res*, vol. 47, no. 24 Pt 1, pp. 6462–6466, Dec. 1987.
[154] R. Perez-Soler *et al.*, ‘Phase I clinical and pharmacological study of liposome-entrapped cis-bis-neodecanoato-trans-R,R-1,2-diaminocyclohexane platinum(II)’, *Cancer Res*, vol. 50, no. 14, pp. 4254–4259, Jul. 1990.
[155] R. Perez-Soler, J. Lautersztain, L. C. Stephens, K. Wright, and A. R. Khokhar, ‘Preclinical toxicity and pharmacology of liposome-entrapped cis-bis-neodecanoato-trans-R,R-1,2-diaminocyclohexane platinum(II)’, *Cancer Chemother. Pharmacol.*, vol. 24, no. 1, Jul. 1989, doi: 10.1007/BF00254097.
[156] I. Han, Y. H. Ling, S. al-Baker, A. R. Khokhar, and R. Perez-Soler, ‘Cellular pharmacology of liposomal cis-bis-neodecanoato-trans-R,R-1,2-diaminocyclohexaneplatinum(II) in A2780/S and A2780/PDD cells’, *Cancer Res*, vol. 53, no. 20, pp. 4913–4919, Oct. 1993.
[157] O. Desiatkina, ‘Synthesis, Photophysical Properties and Biological Evaluation of New Conjugates BODIPY: Dinuclear Trithiolato-Bridged Ruthenium(II)-Arene Complexes’.
[158] Q. Bugnon *et al.*, ‘*In vitro* antibacterial activity of dinuclear thiolato-bridged ruthenium(II)-arene compounds’, *Microbiol Spectr*, vol. 11, no. 6, pp. e00954-23, Dec. 2023, doi: 10.1128/spectrum.00954-23.
[159] H. Primasová, M. Vermathen, and J. Furrer, ‘Interactions of Cationic Diruthenium Trithiolato Complexes with Phospholipid Membranes Studied by NMR Spectroscopy’, *J. Phys. Chem. B*, vol. 124, no. 40, pp. 8822–8834, Oct. 2020, doi: 10.1021/acs.jpcb.0c05133.
[160] E. Păunescu *et al.*, ‘The quest of the best – A SAR study of trithiolato-bridged dinuclear Ruthenium(II)-Arene compounds presenting antiparasitic properties’, *European Journal of Medicinal Chemistry*, vol. 222, p. 113610, Oct. 2021, doi: 10.1016/j.ejmech.2021.113610.
[161] D. L. Gerlach *et al.*, ‘Ruthenium (II) and iridium (III) complexes of N-heterocyclic carbene and pyridinol derived bidentate chelates: Synthesis, characterization, and reactivity’, *Inorganica Chimica Acta*, vol. 466, pp. 442–450, Sep. 2017, doi: 10.1016/j.ica.2017.06.063.
[162] A. D. Bangham, M. M. Standish, and J. C. Watkins, ‘Diffusion of univalent ions across the lamellae of swollen phospholipids’, *Journal of Molecular Biology*, vol. 13, no. 1, pp. 238-IN27, Aug. 1965, doi: 10.1016/S0022-2836(65)80093-6.
[163] J. K. De Oliveira *et al.*, ‘Liposome-based nanocarrier loaded with a new quinoxaline derivative for the treatment of cutaneous leishmaniasis’, *Materials Science and Engineering: C*, vol. 110, p. 110720, May 2020, doi: 10.1016/j.msec.2020.110720.
[164] Y. Cha, B. Son, and S. Ryu, ‘Effective removal of staphylococcal biofilms on various food contact surfaces by Staphylococcus aureus phage endolysin LysCSA13’, *Food Microbiology*, vol. 84, p. 103245, Dec. 2019, doi: 10.1016/j.fm.2019.103245.

[165] V. Marchianò, M. Matos, E. Serrano-Pertierra, G. Gutiérrez, and M. C. Blanco-López, 'Vesicles as antibiotic carrier: State of art', *International Journal of Pharmaceutics*, vol. 585, p. 119478, Jul. 2020, doi: 10.1016/j.ijpharm.2020.119478.
[166] C. Liu *et al.*, 'Barriers and Strategies of Cationic Liposomes for Cancer Gene Therapy', *Molecular Therapy - Methods & Clinical Development*, vol. 18, pp. 751–764, Sep. 2020, doi: 10.1016/j.omtm.2020.07.015.
[167] B. Dos Santos Rodrigues, T. Kanekiyo, and J. Singh, 'In vitro and in vivo characterization of CPP and transferrin modified liposomes encapsulating pDNA', *Nanomedicine: Nanotechnology, Biology and Medicine*, vol. 28, p. 102225, Aug. 2020, doi: 10.1016/j.nano.2020.102225.
[168] C. F. Bezerra *et al.*, 'Antifungal Effect of Liposomal α-Bisabolol and When Associated with Fluconazole', *Cosmetics*, vol. 8, no. 2, p. 28, Apr. 2021, doi: 10.3390/cosmetics8020028.
[169] Y. Zhang *et al.*, 'Dimeric artesunate phospholipid-conjugated liposomes as promising anti-inflammatory therapy for rheumatoid arthritis', *International Journal of Pharmaceutics*, vol. 579, p. 119178, Apr. 2020, doi: 10.1016/j.ijpharm.2020.119178.
[170] Z. J. Zhang and B. Michniak-Kohn, 'Flavosomes, novel deformable liposomes for the co-delivery of anti-inflammatory compounds to skin', *International Journal of Pharmaceutics*, vol. 585, p. 119500, Jul. 2020, doi: 10.1016/j.ijpharm.2020.119500.
[171] L. Bai *et al.*, 'Liposomes encapsulated iridium(III) polypyridyl complexes enhance anticancer activity in vitro and in vivo', *Journal of Inorganic Biochemistry*, vol. 205, p. 111014, Apr. 2020, doi: 10.1016/j.jinorgbio.2020.111014.
[172] Y. Li *et al.*, 'Enhanced anticancer effect of doxorubicin by TPGS-coated liposomes with Bcl-2 siRNA-corona for dual suppression of drug resistance', *Asian Journal of Pharmaceutical Sciences*, vol. 15, no. 5, pp. 646–660, Sep. 2020, doi: 10.1016/j.ajps.2019.10.003.
[173] J. R. Morgan, L. A. Williams, and C. B. Howard, 'Technetium-labelled liposome imaging for deep-seated infection', *BJR*, vol. 58, no. 685, pp. 35–39, Jan. 1985, doi: 10.1259/0007-1285-58-685-35.
[174] F. Paltauf and A. Hermetter, 'Phospholipids — Natural, Semisynthetic, Synthetic', in *Phospholipids*, I. Hanin and G. Pepeu, Eds., Boston, MA: Springer US, 1990, pp. 1–12. doi: 10.1007/978-1-4757-1364-0_1.
[175] M. C. Woodle, 'Sterically stabilized liposome therapeutics', *Advanced Drug Delivery Reviews*, vol. 16, no. 2–3, pp. 249–265, Sep. 1995, doi: 10.1016/0169-409X(95)00028-6.
[176] M. Danaei *et al.*, 'Probing nanoliposomes using single particle analytical techniques: effect of excipients, solvents, phase transition and zeta potential', *Heliyon*, vol. 4, no. 12, p. e01088, Dec. 2018, doi: 10.1016/j.heliyon.2018.e01088.
[177] V. Filipe, A. Hawe, and W. Jiskoot, 'Critical Evaluation of Nanoparticle Tracking Analysis (NTA) by NanoSight for the Measurement of Nanoparticles and Protein Aggregates', *Pharm Res*, vol. 27, no. 5, pp. 796–810, May 2010, doi: 10.1007/s11095-010-0073-2.
[178] G. Amoabediny *et al.*, 'Overview of preparation methods of polymeric and lipid-based (niosome, solid lipid, liposome) nanoparticles: A comprehensive review', *International Journal of Polymeric Materials and Polymeric Biomaterials*, vol. 67, no. 6, pp. 383–400, Apr. 2018, doi: 10.1080/00914037.2017.1332623.
[179] B. Maherani, E. Arab-Tehrany, M. R. Mozafari, C. Gaiani, and M. Linder, 'Liposomes: A Review of Manufacturing Techniques and Targeting Strategies', *CNANO*, vol. 7, no. 3, pp. 436–452, Jun. 2011, doi: 10.2174/157341311795542453.

[180] M. R. Mozafari, E. Mazaheri, and K. Dormiani, ‘Simple Equations Pertaining to the Particle Number and Surface Area of Metallic, Polymeric, Lipidic and Vesicular Nanocarriers’, *Sci. Pharm.*, vol. 89, no. 2, p. 15, Mar. 2021, doi: 10.3390/scipharm89020015.
[181] R. W. Kriftner, ‘Liposome Production: The Ethanol Injection Technique and the Development of the First Approved Liposome Dermatic’, in *Liposome Dermatics*, O. Braun-Falco, H. C. Korting, and H. I. Maibach, Eds., Berlin, Heidelberg: Springer Berlin Heidelberg, 1992, pp. 91–100. doi: 10.1007/978-3-642-48391-2_10.
[182] N.-J. Cho, L. Hwang, J. Solandt, and C. Frank, ‘Comparison of Extruded and Sonicated Vesicles for Planar Bilayer Self-Assembly’, *Materials*, vol. 6, no. 8, pp. 3294–3308, Aug. 2013, doi: 10.3390/ma6083294.
[183] S. Ong, M. Chitneni, K. Lee, L. Ming, and K. Yuen, ‘Evaluation of Extrusion Technique for Nanosizing Liposomes’, *Pharmaceutics*, vol. 8, no. 4, p. 36, Dec. 2016, doi: 10.3390/pharmaceutics8040036.
[184] Z. Zhou, B. G. Sayer, D. W. Hughes, R. E. Stark, and R. M. Epand, ‘Studies of Phospholipid Hydration by High-Resolution Magic-Angle Spinning Nuclear Magnetic Resonance’, *Biophysical Journal*, vol. 76, no. 1, pp. 387–399, Jan. 1999, doi: 10.1016/S0006-3495(99)77205-X.
[185] D. Stíbal *et al.*, ‘Chlorambucil conjugates of dinuclear p-cymene ruthenium trithiolato complexes: synthesis, characterization and cytotoxicity study in vitro and in vivo’, *J Biol Inorg Chem*, vol. 21, no. 4, pp. 443–452, Jul. 2016, doi: 10.1007/s00775-016-1353-z.
[186] F. Giannini, L. E. H. Paul, J. Furrer, B. Therrien, and G. Süss-Fink, ‘Highly cytotoxic diruthenium trithiolato complexes of the type [(η6-p-MeC6H4Pri)2Ru2(μ2-SR)3]+: synthesis, characterization, molecular structure and in vitro anticancer activity’, *New J. Chem.*, vol. 37, no. 11, p. 3503, 2013, doi: 10.1039/c3nj00476g.

Supplementary Information for Part One

Contents

Figure S1.1: Superimposed ^{1}H NMR spectra of DMSA (10 mM) before adding the oxidizing agent DMSO-d_6. Acquisition Parameters: pulse program zg30 (Bruker library), 65536 TD data points, 64 scans, 9973.404 Hz spectral width, acquisition time 3 s, relaxation delay 6 s. Rough estimation is indicated in red.

Figure S1.2: Superimposed ^{1}H NMR spectra of DMPS (10 mM) before adding the oxidizing agent DMSO-d_6. Acquisition Parameters: pulse program zg30 (Bruker library), 65536 TD data points, 64 scans, 9973.404 Hz spectral width, acquisition time 3 s, relaxation delay 6 s. Rough estimation is indicated in red.

Figure S1.3: Superimposed ^{1}H NMR spectra of L-Cys (10 mM) before adding the oxidizing agent DMSO-d_6. Acquisition Parameters: pulse program zg30 (Bruker library), 65536 TD data points, 64 scans, 9973.404 Hz spectral width, acquisition time 3 s, relaxation delay 6 s. Rough estimation is indicated in red.

Figure S1.4: Superimposed ^{1}H NMR spectra of L-GSH (10 mM) before adding the oxidizing agent DMSO-d_6. Acquisition Parameters: pulse program zg30 (Bruker library), 65536 TD data points, 64 scans, 9973.404 Hz spectral width, acquisition time 3 s, relaxation delay 6 s. Rough estimation indicated in red.

Figure S1.5: Oxidation data for DMSA monitored through ^{1}H NMR spectroscopy. **(A)** ^{1}H NMR spectra were recorded over 24 hours, with one spectrum collected each hour. **(B)** ^{1}H NMR spectra were recorded for 4 hours after adding 10% DMSO, with one spectrum collected every 0.5 hours. The spectrum at 0.05 hours represents the ^{1}H NMR spectrum before DMSO is added.

Figure S1.6: Oxidation data for DMPS monitored through ^{1}H NMR spectroscopy. **(A)** ^{1}H NMR spectra were recorded over 24 hours, with one spectrum collected each hour. **(B)** ^{1}H NMR spectra were recorded for 4 hours after adding 10% DMSO, with one spectrum collected every 0.5 hours. The spectrum at 0.05 hours represents the ^{1}H NMR spectrum before DMSO is added.

Figure S1.7: Oxidation data for L-Cys monitored through ^{1}H NMR spectroscopy. **(A)** ^{1}H NMR spectra were recorded over 24 hours, with one spectrum collected each hour. **(B)** ^{1}H NMR

spectra were recorded for 4 hours after adding 10% DMSO, with one spectrum collected every 0.5 hours. The spectrum at 0.05 hours represents the ^{1}H NMR spectrum before DMSO is added.

Figure S1.8: Oxidation data for L-GSH monitored through ^{1}H NMR spectroscopy. (A) ^{1}H NMR spectra were recorded over 24 hours, with one spectrum collected each hour. (B) ^{1}H NMR spectra were recorded for 4 hours after adding 10% DMSO, with one spectrum collected every 0.5 hours. The spectrum at 0.05 hours represents the ^{1}H NMR spectrum before DMSO is added.

Figure 1.9: Chemical shift range of metal (II) ions in E3 medium. **(A)** 10 mM mercury (II) chloride at RT (Nuclei ^{199}Hg, -1560.98 ppm). Acquisition Parameters: pulse program zg (Bruker library), 65536 TD data points, 1k scans, 144230.766 Hz spectral width, acquisition time 227 ms, relaxation delay 300 ms. **(B)** 35.5 mM lead (II) chloride at 323 K (Nuclei ^{207}Pb - 579.8981 ppm). Acquisition Parameters: pulse program zg (Bruker library), 131072 TD data points, 1k scans, 166666.672 Hz spectral width, acquisition time 393 ms, relaxation delay 300 ms. **(C)** 100 mM cadmium (II) chloride at RT (Nuclei ^{113}Cd) Acquisition Parameters: pulse program zg (Bruker library), 131072 TD data points, 1k scans, 178571.422 Hz spectral width, acquisition time 367 ms, relaxation delay 500 ms.

Figure S1.10: Clinically approved heavy metal chelators inhibit zebrafish swim bladder development. LA, DMPS, DMSA, Cysteine and GSH all inhibit the inflation of the swim bladder at 4 dpf. Arrowhead indicates the swim bladder of untreated control larvae at 4 dpf.

Table S1.1: Practical experiments of the zebrafish embryo with metal (II) ions and chelating agents before different concentrations.

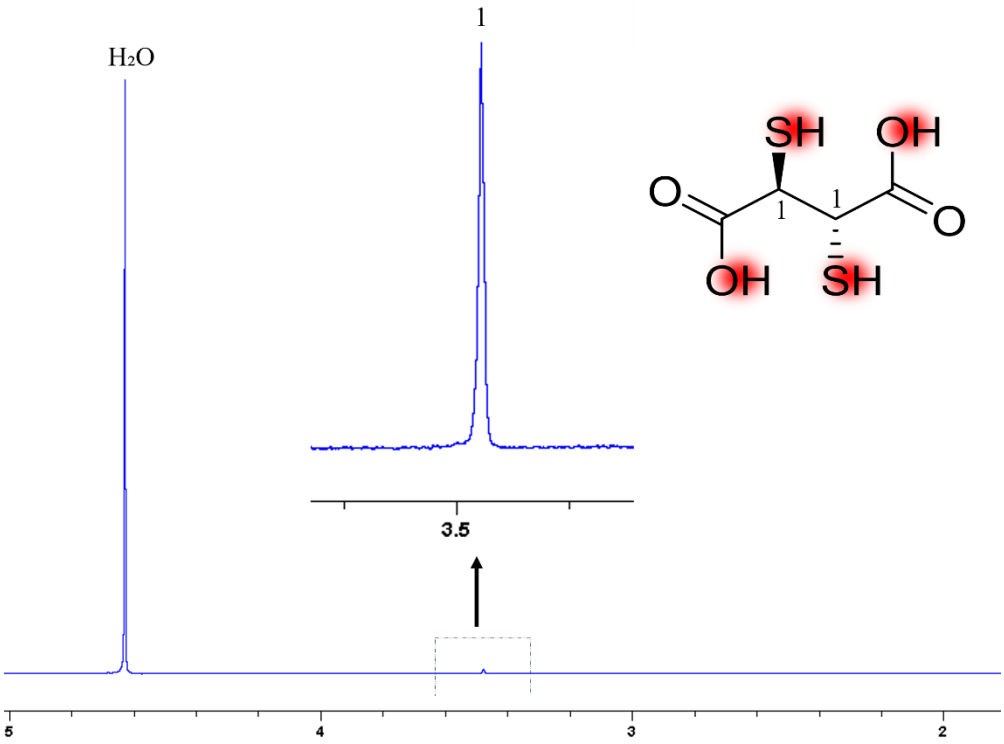

Figure S1.1: Superimposed ^{1}H NMR spectra of DMSA (10 mM) before adding the oxidizing agent DMSO-d_6. Acquisition Parameters: pulse program zg30 (Bruker library), 65536 TD data points, 64 scans, 9973.404 Hz spectral width, acquisition time 3 s, relaxation delay 6 s. Rough estimation indicated in red.

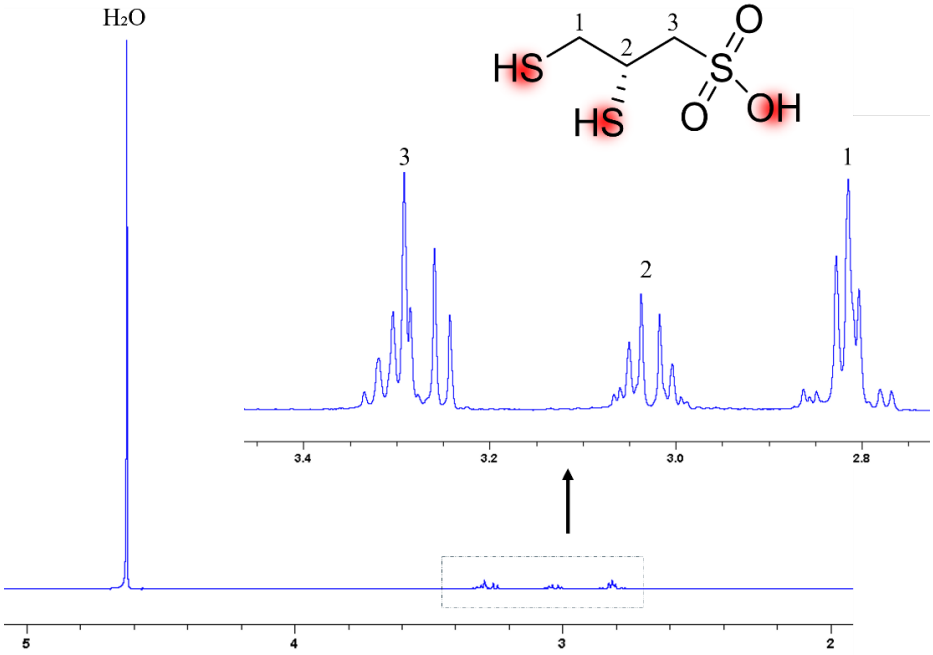

Figure S1.2: Superimposed ^{1}H NMR spectra of DMPS (10 mM) before adding the oxidizing agent DMSO-d_6. Acquisition Parameters: pulse program zg30 (Bruker library), 65536 TD data points, 64 scans, 9973.404 Hz spectral width, acquisition time 3 s, relaxation delay 6 s.. Rough estimation indicated in red.

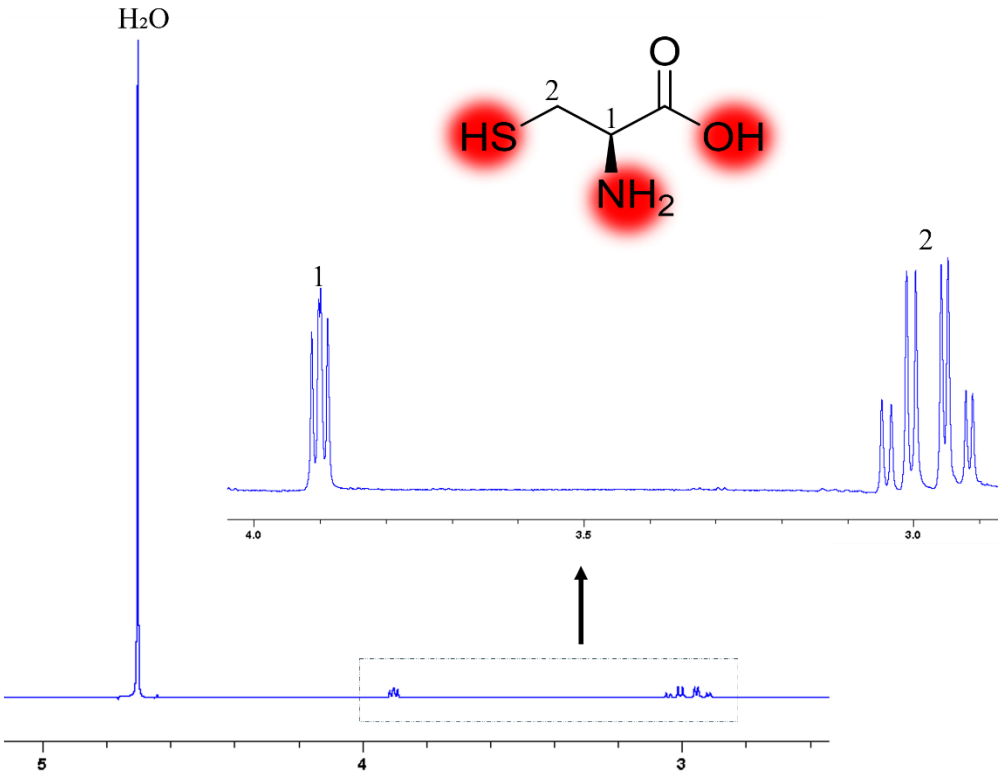

Figure S1.3: Superimposed ^{1}H NMR spectra of L-Cys (10 mM) before adding the oxidizing agent DMSO-d_6. Acquisition Parameters: pulse program zg30 (Bruker library), 65536 TD data points, 64 scans, 9973.404 Hz spectral width, acquisition time 3 s, relaxation delay 6 s. Rough estimation indicated in red.

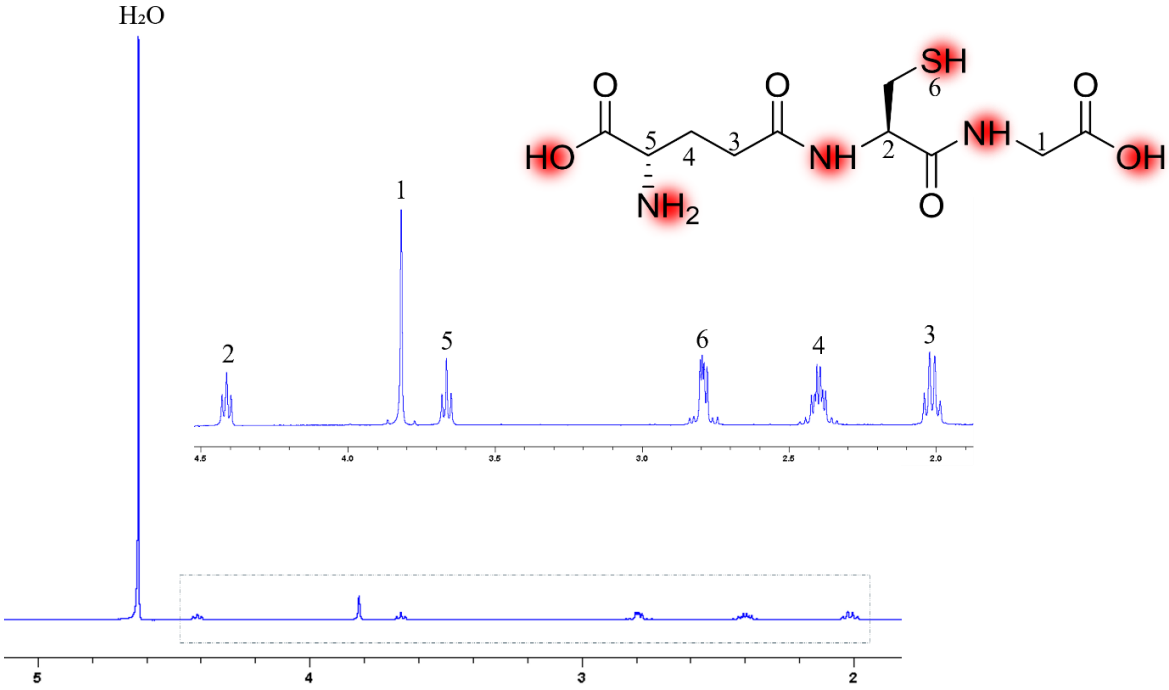

Figure S1.4: Superimposed ^{1}H NMR spectra of L-GSH (10 mM) before adding the oxidizing agent DMSO-d_6. Acquisition Parameters: pulse program zg30 (Bruker library), 65536 TD data points, 64 scans, 9973.404 Hz spectral width, acquisition time 3 s, relaxation delay 6 s. Rough estimation indicated in red.

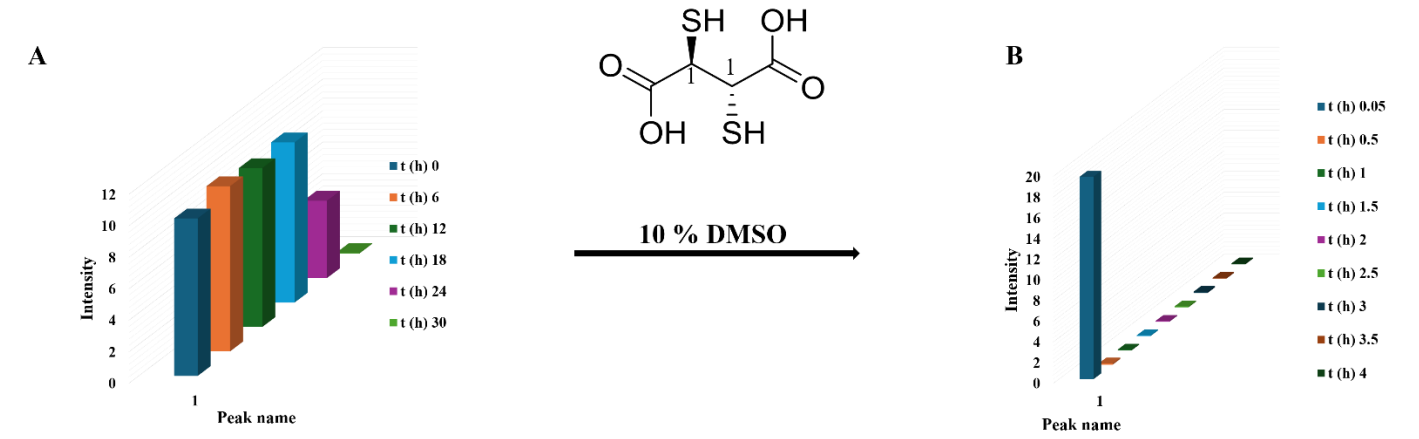

Figure S1.5: Oxidation data for DMSA monitored through ^{1}H NMR spectroscopy. **(A)** ^{1}H NMR spectra were recorded over 24 hours, with one spectrum collected each hour. **(B)** ^{1}H NMR spectra were recorded for 4 hours after adding 10% DMSO, with one spectrum collected every 0.5 hours. The spectrum at 0.05 hours represents the ^{1}H NMR spectrum before DMSO is added.

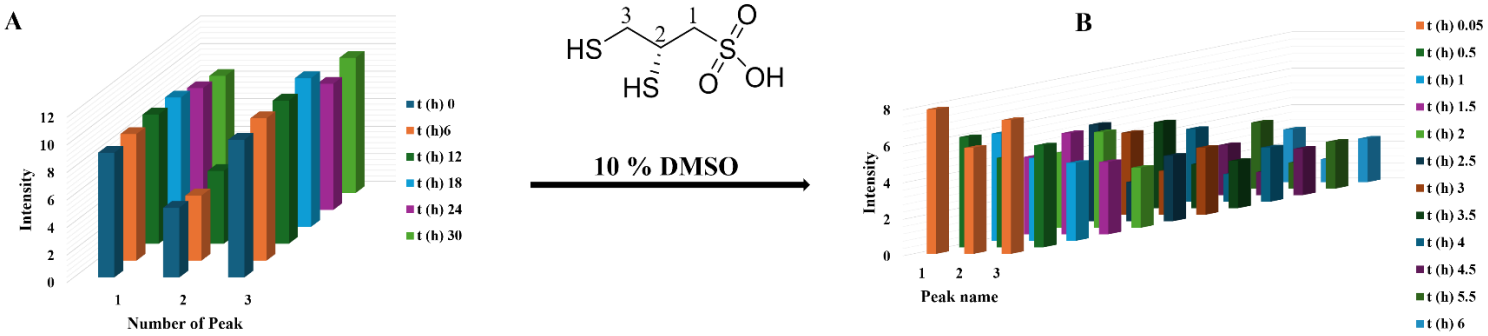

Figure S1.6: Oxidation data for DMPS monitored through ^{1}H NMR spectroscopy. **(A)** ^{1}H NMR spectra were recorded over 24 hours, with one spectrum collected each hour. **(B)** ^{1}H NMR spectra were recorded for 4 hours after adding 10% DMSO, with one spectrum collected every 0.5 hours. The spectrum at 0.05 hours represents the ^{1}H NMR spectrum before DMSO is added.

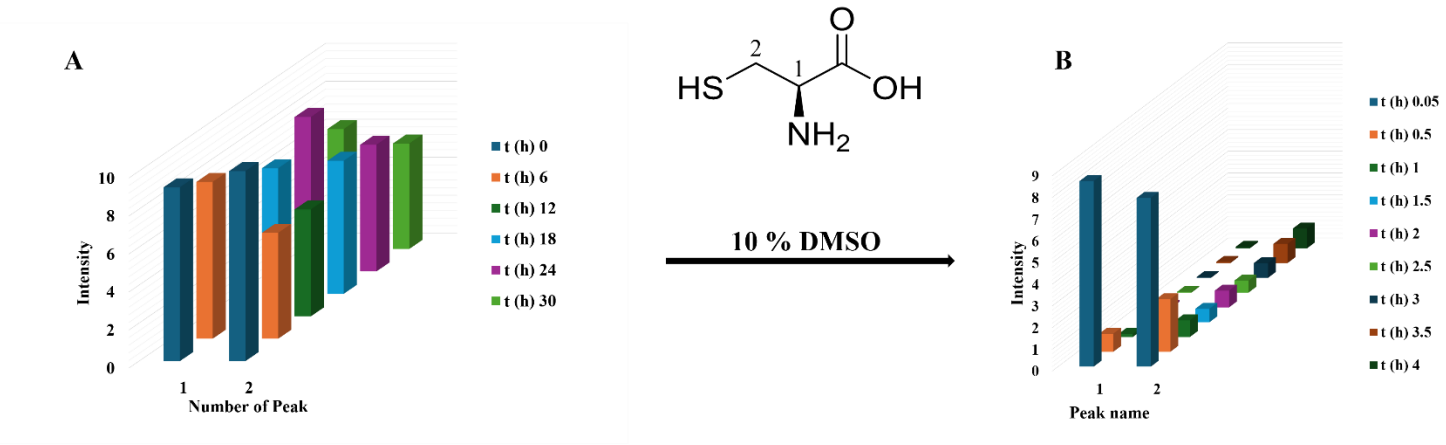

Figure S1.7: Oxidation data for L-Cys monitored through ^{1}H NMR spectroscopy. **(A)** ^{1}H NMR spectra were recorded over 24 hours, with one spectrum collected each hour. **(B)** ^{1}H NMR spectra were recorded for 4 hours after adding 10% DMSO, with one spectrum collected every 0.5 hours. The spectrum at 0.05 hours represents the ^{1}H NMR spectrum before DMSO is added.

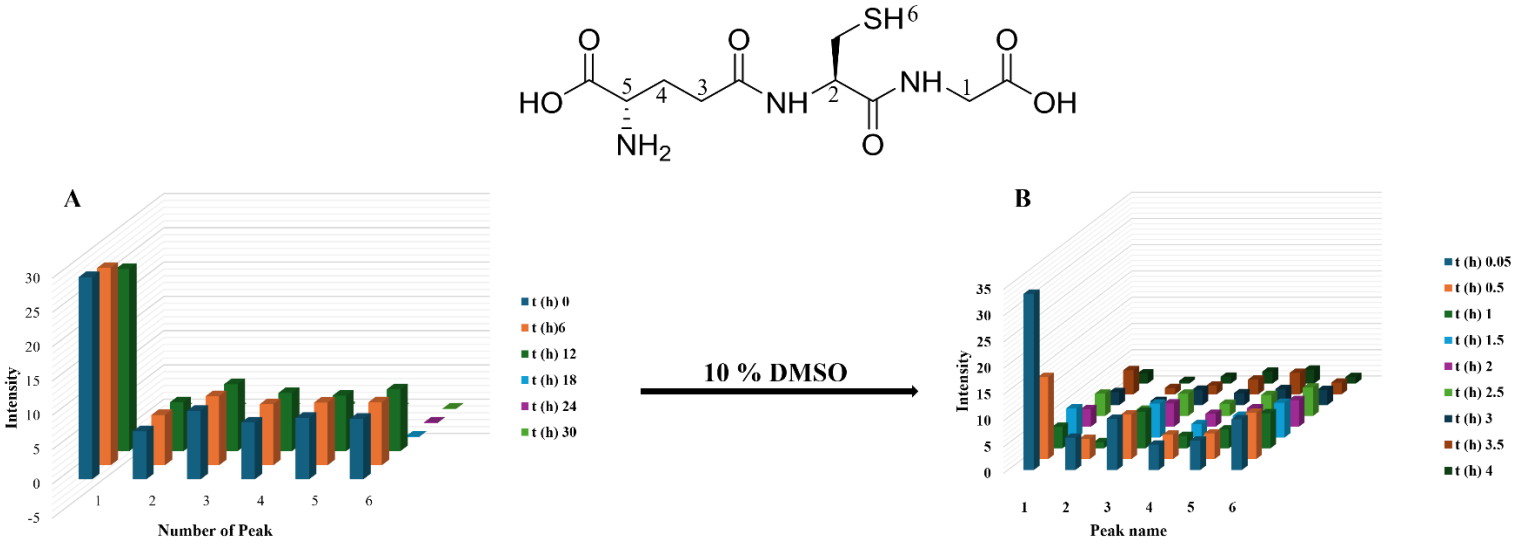

Figure S1.8: Oxidation data for L-GSH monitored through ^{1}H NMR spectroscopy. **(A)** ^{1}H NMR spectra were recorded over 24 hours, with one spectrum collected each hour. **(B)** ^{1}H NMR spectra were recorded for 4 hours after adding 10% DMSO, with one spectrum collected every 0.5 hours. The spectrum at 0.05 hours represents the ^{1}H NMR spectrum before DMSO is added.

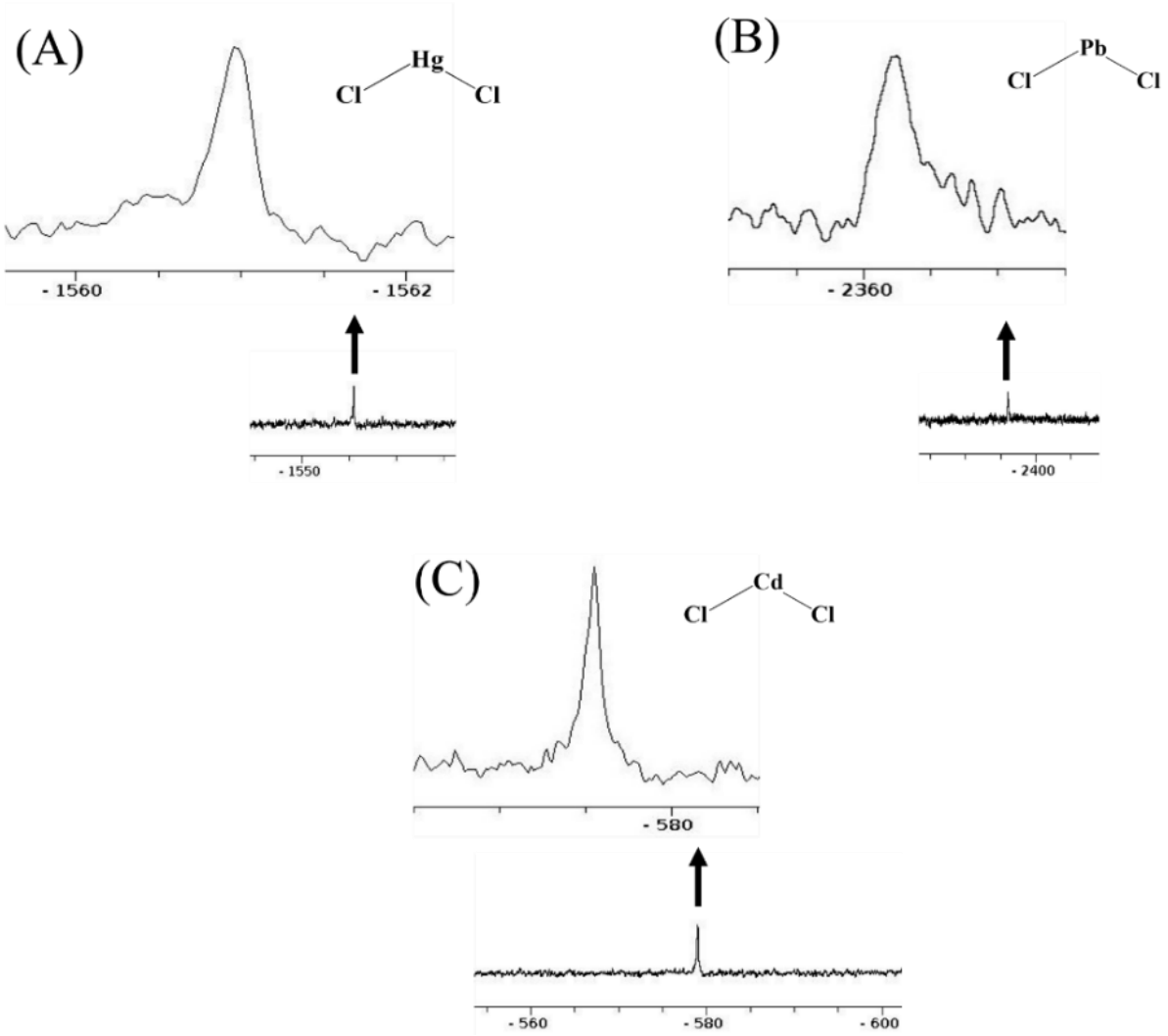

Figure S1.9 : Chemical shift range of metal (II) ions in E3 medium. **(A)** 10 mM mercury (II) chloride (Nuclei ^{199}Hg, -1560.98 ppm). Acquisition Parameters: pulse program zg (Bruker library), 65536 TD data points, 1k scans, 144230.766 Hz spectral width, acquisition time 227 ms, relaxation delay 300 ms. **(B)** 35.5 mM lead (II) chloride (Nuclei ^{207}Pb -579.8981 ppm). Acquisition Parameters: pulse program zg (Bruker library), 131072 TD data points, 1k scans, 166666.672 Hz spectral width, acquisition time 393 ms, relaxation delay 300 ms. **(C)** 100 mM cadmium (II) chloride (Nuclei ^{113}Cd) Acquisition Parameters: pulse program zg (Bruker library), 131072 TD data points, 1k scans, 178571.422 Hz.

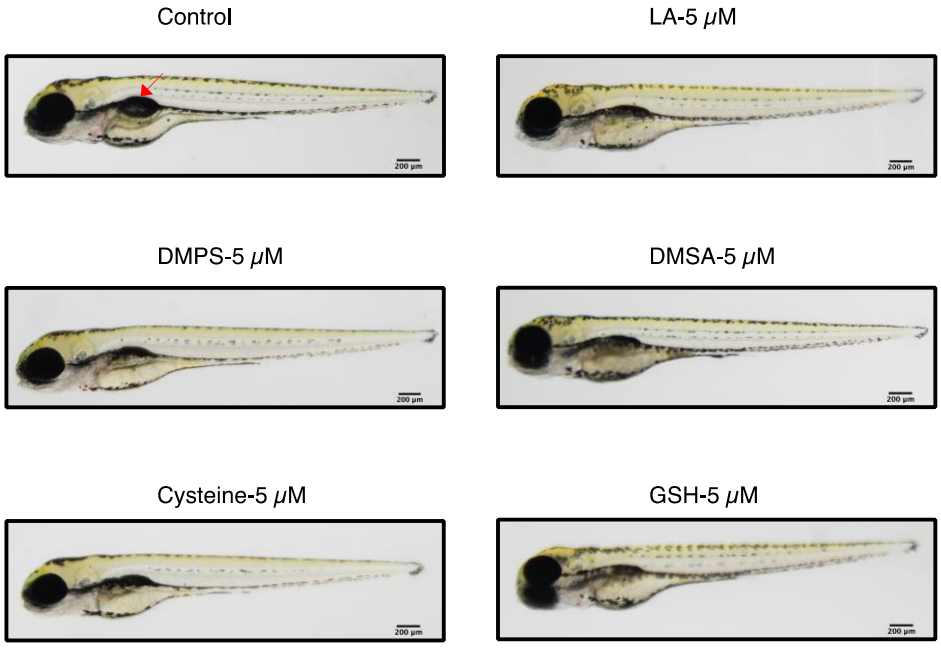

Figure S1.10: Clinically approved heavy metal chelators inhibit zebrafish swim bladder development. LA, DMPS, DMSA, Cysteine and GSH all inhibit the inflation of the swim bladder at 4 dpf. Arrowhead indicates the swim bladder of untreated control larvae at 4 dpf.

Table S1.1: Practical experiments of the zebrafish embryo with metal (II) ions and chelating agents prior to different concentrations.

Experiment	Clutch	Control	Toxin	Chelator	Conc. (µM)	Time	Total Fish	Normal Dev.	Total Abnormal Dev.	Dead
1.0	1	Control 1	No	No	0	1h	27	24	0	0
1.0	1	Control 1	No	No	0	3h	27	24	0	0
1.0	1	Control 1	No	No	0	1d	27	24	0	0
1.0	1	Control 1	No	No	0	2d	27	24	0	0
1.0	1	Control 1	No	No	0	3d	27	23	3	3
1.0	2	Control 2	No	No	0	1h	20	20	0	0
1.0	2	Control 2	No	No	0	3h	20	20	0	0
1.0	2	Control 2	No	No	0	1d	20	20	0	0
1.0	2	Control 2	No	No	0	2d	20	20	0	0
1.0	2	Control 2	No	No	0	3d	20	20	0	0
1.0	1	No	$HgCl_2$	No	0.01	1h	20	16	0	0
1.0	1	No	$HgCl_2$	No	0.01	3h	20	16	0	0
1.0	1	No	$HgCl_2$	No	0.01	1d	20	11	0	0
1.0	1	No	$HgCl_2$	No	0.01	2d	20	10	0	0
1.0	1	No	$HgCl_2$	No	0.01	3d	20	10	0	0
1.0	1	No	$HgCl_2$	No	0.1	1h	16	12	1	1
1.0	1	No	$HgCl_2$	No	0.1	3h	16	12	1	1
1.0	1	No	$HgCl_2$	No	0.1	1d	16	12	0	0
1.0	1	No	$HgCl_2$	No	0.1	2d	16	13	0	0
1.0	1	No	$HgCl_2$	No	0.1	3d	16	12	0	0
1.0	1	No	$HgCl_2$	No	0.5	1h	20	16	0	0
1.0	1	No	$HgCl_2$	No	0.5	3h	20	16	0	0
1.0	1	No	$HgCl_2$	No	0.5	1d	20	14	0	0
1.0	1	No	$HgCl_2$	No	0.5	2d	20	15	0	0

Experiment	Clutch	Control	Toxin	Chelator	Conc. (µM)	Time	Total Fish	Normal Dev.	Total Abnormal Dev.	Dead
1.0	1	No	$HgCl_2$	No	0.5	3d	18	7	4	4
1.0	1	No	$HgCl_2$	No	1	1h	19	16	0	0
1.0	1	No	$HgCl_2$	No	1	3h	19	16	0	0
1.0	1	No	$HgCl_2$	No	1	1d	19	16	0	0
1.0	1	No	$HgCl_2$	No	1	2d	19	17	0	0
1.0	1	No	$HgCl_2$	No	1	3d	20	2	0	0
1.0	2	No	$PbCl_2$	No	0.36	1h	20	20	0	0
1.0	2	No	$PbCl_2$	No	0.36	3h	20	20	0	0
1.0	2	No	$PbCl_2$	No	0.36	1d	19	19	0	0
1.0	2	No	$PbCl_2$	No	0.36	2d	19	18	0	0
1.0	2	No	$PbCl_2$	No	0.36	3d	19	14	0	0
1.0	2	No	$PbCl_2$	No	1.8	1h	20	20	0	0
1.0	2	No	$PbCl_2$	No	1.8	3h	20	20	0	0
1.0	2	No	$PbCl_2$	No	1.8	1d	17	17	0	0
1.0	2	No	$PbCl_2$	No	1.8	2d	18	18	0	0
1.0	2	No	$PbCl_2$	No	1.8	3d	18	17	0	0
1.0	1	No	$PbCl_2$	No	5.6	1h	20	14	0	0
1.0	1	No	$PbCl_2$	No	5.6	3h	20	14	0	0
1.0	1	No	$PbCl_2$	No	5.6	1d	20	13	0	0
1.0	1	No	$PbCl_2$	No	5.6	2d	20	12	0	0
1.0	1	No	$PbCl_2$	No	5.6	3d	20	11	0	0
1.0	1	No	$PbCl_2$	No	17.98	1h	20	12	2	2
1.0	1	No	$PbCl_2$	No	17.98	3h	20	12	2	2
1.0	1	No	$PbCl_2$	No	17.98	1d	20	14	0	0
1.0	1	No	$PbCl_2$	No	17.98	2d	20	14	0	0
1.0	1	No	$PbCl_2$	No	17.98	3d	20	13	0	0

Experiment	Clutch	Control	Toxin	Chelator	Conc. (µM)	Time	Total Fish	Normal Dev.	Total Abnormal Dev.	Dead
1.0	2	No	$CdCl_2$	No	1	1h	20	20	0	0
1.0	2	No	$CdCl_2$	No	1	3h	20	20	0	0
1.0	2	No	$CdCl_2$	No	1	1d	20	18	0	0
1.0	2	No	$CdCl_2$	No	1	2d	20	18	0	0
1.0	2	No	$CdCl_2$	No	1	3d	20	20	0	0
1.0	2	No	$CdCl_2$	No	10	1h	20	20	0	0
1.0	2	No	$CdCl_2$	No	10	3h	20	20	0	0
1.0	2	No	$CdCl_2$	No	10	1d	19	18	0	0
1.0	2	No	$CdCl_2$	No	10	2d	19	14	0	0
1.0	2	No	$CdCl_2$	No	10	3d	19	19	0	0
1.0	2	No	$CdCl_2$	No	50	1h	20	20	0	0
1.0	2	No	$CdCl_2$	No	50	3h	20	20	0	0
1.0	2	No	$CdCl_2$	No	50	1d	20	19	0	0
1.0	2	No	$CdCl_2$	No	50	2d	20	20	0	0
1.0	2	No	$CdCl_2$	No	50	3d	17	9	0	0
1.0	2	No	$CdCl_2$	No	100	1h	20	20	0	0
1.0	2	No	$CdCl_2$	No	100	2d	20	0	20	20
1.0	2	No	$CdCl_2$	No	100	3d	20	0	20	20
1.0	2	No	$CdCl_2$	No	100	3h	20	20	0	0
1.0	2	No	$CdCl_2$	No	100	1d	20	0	20	20
1.0	0	No	$CdCl_2$	No	60	1d	20	11	9	9
1.0	0	No	$CdCl_2$	No	60	3h	19	17	0	0
1.1	0	Control	No	No	0	1h	19	19	0	0
1.1	0	Control	No	No	0	3h	19	18	0	0
1.1	0	Control	No	No	0	1d	21	19	0	0
1.1	0	Control	No	No	0	5d	20	17	2	2

Experiment	Clutch	Control	Toxin	Chelator	Conc. (µM)	Time	Total Fish	Normal Dev.	Total Abnormal Dev.	Dead
1.1	0	No	$HgCl_2$	No	10	1h	20	15	0	0
1.1	0	No	$HgCl_2$	No	10	3h	20	0	2	2
1.1	0	No	$HgCl_2$	No	10	5d	20	0	20	20
1.1	0	No	$HgCl_2$	No	50	1h	20	0	20	20
1.1	0	No	$HgCl_2$	No	50	3h	20	0	20	20
1.1	0	No	$HgCl_2$	No	50	5d	20	0	20	20
1.1	0	No	$HgCl_2$	No	100	1h	20	0	20	20
1.1	0	No	$HgCl_2$	No	100	3h	20	0	20	20
1.1	0	No	$HgCl_2$	No	100	5d	20	0	20	20
1.1	0	No	$PbCl_2$	No	30	1h	20	15	0	0
1.1	0	No	$PbCl_2$	No	30	3h	19	14	0	0
1.1	0	No	$PbCl_2$	No	30	5d	20	14	6	6
1.1	0	No	$PbCl_2$	No	60	1h	18	15	0	0
1.1	0	No	$PbCl_2$	No	60	3h	20	18	0	0
1.1	0	No	$PbCl_2$	No	60	5d	20	0	3	3
1.1	0	No	$PbCl_2$	No	100	1h	20	20	0	0
1.1	0	No	$PbCl_2$	No	100	3h	20	19	0	0
1.1	0	No	$PbCl_2$	No	100	5d	20	0	13	13
1.1	0	No	$CdCl_2$	No	60	1h	19	17	0	0
1.1	0	No	$CdCl_2$	No	60	5d	20	8	12	12
1.1	0	No	$CdCl_2$	No	80	1h	19	16	0	0
1.1	0	No	$CdCl_2$	No	80	3h	20	5	10	10
1.1	0	No	$CdCl_2$	No	80	1d	20	0	20	20
1.1	0	No	$CdCl_2$	No	80	5d	20	0	20	20
1.1	0	No	$HgCl_2$	No	10	1d	20	0	20	20
1.1	0	No	$PbCl_2$	No	30	1d	20	14	6	6

Experiment	Clutch	Control	Toxin	Chelator	Conc. (µM)	Time	Total Fish	Normal Dev.	Total Abnormal Dev.	Dead
1.1	0	No	$HgCl_2$	No	50	1d	20	0	20	20
1.1	0	No	$PbCl_2$	No	60	1d	20	17	0	0
1.1	0	No	$HgCl_2$	No	100	1d	20	0	20	20
1.1	0	No	$PbCl_2$	No	100	1d	21	10	11	11
1.1	0	No	$CdCl_2$	No	60	1d	19	10	6	6
1.1	0	No	$HgCl_2$	No	1	1d	19	16	2	2
1.1	0	No	$PbCl_2$	No	20	1d	19	14	3	3
1.1	0	No	$HgCl_2$	No	5	1d	20	20	0	0
1.1	0	No	$PbCl_2$	No	40	1d	19	14	3	3
1.1	0	No	$HgCl_2$	No	10	1d	20	0	20	20
1.1	0	No	$PbCl_2$	No	60	1d	19	16	2	2
1.1	0	No	$CdCl_2$	No	60	3h	19	16	0	0
1.1	0	No	$CdCl_2$	No	80	1d	20	0	20	20
1.2	0	Control	No	No	0	1h	19	19	0	0
1.2	0	Control	No	No	0	3h	19	18	0	0
1.2	0	Control	No	No	0	1d	20	16	0	0
1.2	0	Control	No	No	0	2d	17	15	1	1
1.2	0	Control	No	No	0	3d	21	14	1	1
1.2	0	No	$HgCl_2$	No	1	1h	19	19	0	0
1.2	0	No	$HgCl_2$	No	1	3h	19	19	0	0
1.2	0	No	$HgCl_2$	No	1	2d	19	17	2	2
1.2	0	No	$HgCl_2$	No	1	3d	17	11	0	0
1.2	0	No	$HgCl_2$	No	5	1h	20	20	0	0
1.2	0	No	$HgCl_2$	No	5	3h	20	20	0	0
1.2	0	No	$HgCl_2$	No	5	2d	20	0	20	20
1.2	0	No	$HgCl_2$	No	5	3d	20	0	20	20

Experiment	Clutch	Control	Toxin	Chelator	Conc. (µM)	Time	Total Fish	Normal Dev.	Total Abnormal Dev.	Dead
1.2	0	No	$HgCl_2$	No	10	1h	20	19	0	0
1.2	0	No	$HgCl_2$	No	10	3h	20	18	0	0
1.2	0	No	$HgCl_2$	No	10	2d	20	0	20	20
1.2	0	No	$HgCl_2$	No	10	3d	20	0	20	20
1.2	0	No	$PbCl_2$	No	20	1h	20	20	0	0
1.2	0	No	$PbCl_2$	No	20	3h	20	17	0	0
1.2	0	No	$PbCl_2$	No	20	2d	20	16	4	4
1.2	0	No	$PbCl_2$	No	20	3d	20	15	3	3
1.2	0	No	$PbCl_2$	No	40	1h	20	17	0	0
1.2	0	No	$PbCl_2$	No	40	3h	20	17	0	0
1.2	0	No	$PbCl_2$	No	80	1d	19	12	3	3
1.2	0	No	$PbCl_2$	No	40	2d	18	13	4	4
1.2	0	No	$PbCl_2$	No	40	3d	18	13	3	3
1.2	0	No	$PbCl_2$	No	60	1h	20	20	0	0
1.2	0	No	$PbCl_2$	No	60	3h	19	18	0	0
1.2	0	No	$PbCl_2$	No	60	2d	19	16	2	2
1.2	0	No	$PbCl_2$	No	60	3d	20	13	3	3
1.2	0	No	$PbCl_2$	No	80	1h	20	19	0	0
1.2	0	No	$PbCl_2$	No	80	3h	20	19	0	0
1.2	0	No	$PbCl_2$	No	80	2d	19	10	4	4
1.2	0	No	$PbCl_2$	No	80	3d	18	9	5	5
1.2	0	No	$PbCl_2$	No	100	1h	20	20	0	0
1.2	0	No	$PbCl_2$	No	100	3h	19	15	0	0
1.2	0	No	$PbCl_2$	No	100	1d	19	6	12	12
1.2	0	No	$PbCl_2$	No	100	2d	18	5	10	10
1.2	0	No	$PbCl_2$	No	100	3d	17	4	12	12

Experiment	Clutch	Control	Toxin	Chelator	Conc. (µM)	Time	Total Fish	Normal Dev.	Total Abnormal Dev.	Dead
1.2	0	No	$CdCl_2$	No	60	1h	20	20	0	0
1.2	0	No	$CdCl_2$	No	80	3h	20	12	0	0
1.2	0	No	$CdCl_2$	No	60	2d	20	12	7	7
1.2	0	No	$CdCl_2$	No	60	3d	20	11	8	8
1.2	0	No	$CdCl_2$	No	80	1h	20	20	0	0
1.2	0	No	$CdCl_2$	No	80	2d	20	0	20	20
1.2	0	No	$CdCl_2$	No	80	3d	20	0	20	20
1.3	0	Control	No	No	0	2d	20	20	0	0
1.3	0	Control	No	No	0	3d	20	19	0	0
1.3	0	No	$HgCl_2$	No	1	2d	20	0	0	0
1.3	0	No	$HgCl_2$	No	1	3d	20	0	6	6
1.3	0	No	$HgCl_2$	No	5	2d	20	0	20	20
1.3	0	No	$HgCl_2$	No	5	3d	20	0	20	20
1.3	0	No	$HgCl_2$	No	10	2d	20	0	20	20
1.3	0	No	$HgCl_2$	No	10	3d	20	0	20	20
1.3	0	No	$PbCl_2$	No	20	2d	20	20	0	0
1.3	0	No	$PbCl_2$	No	20	3d	20	20	0	0
1.3	0	No	$PbCl_2$	No	40	2d	20	20	0	0
1.3	0	No	$PbCl_2$	No	40	3d	20	20	0	0
1.3	0	No	$PbCl_2$	No	60	2d	20	20	0	0
1.3	0	No	$PbCl_2$	No	60	3d	20	19	1	1
1.3	0	No	$PbCl_2$	No	80	2d	20	20	0	0
1.3	0	No	$PbCl_2$	No	80	3d	20	20	0	0
1.3	0	No	$PbCl_2$	No	100	2d	20	20	0	0
1.3	0	No	$PbCl_2$	No	100	3d	20	19	1	1
1.3	0	No	$CdCl_2$	No	60	2d	20	20	0	0

Experiment	Clutch	Control	Toxin	Chelator	Conc. (µM)	Time	Total Fish	Normal Dev.	Total Abnormal Dev.	Dead
1.3	0	No	$CdCl_2$	No	60	3d	20	20	0	0
1.3	0	No	$CdCl_2$	No	80	2d	20	20	0	0
1.3	0	No	$CdCl_2$	No	80	3d	20	19	0	0
2.0	0	Control	No	No	0	1h	19	19	0	0
2.0	0	Control	No	No	0	3h	19	18	0	0
2.0	0	Control	No	No	0	1d	21	19	0	0
2.0	0	Control	No	No	0	5d	20	17	2	2
2.0	0	No	No	LA	100	1h	20	12	0	0
2.0	0	No	No	LA	100	3h	18	6	0	0
2.0	0	No	No	LA	100	1d	20	0	20	20
2.0	0	No	No	LA	100	5d	20	0	20	20
2.0	0	No	No	DMSA	100	1h	20	18	0	0
2.0	0	No	No	DMSA	100	3h	20	17	0	0
2.0	0	No	No	DMSA	100	1d	20	16	4	4
2.0	0	No	No	DMSA	100	5d	20	16	4	4
2.0	0	No	No	DMPS	100	1h	20	13	0	0
2.0	0	No	No	DMPS	100	3h	20	13	0	0
2.0	0	No	No	DMPS	100	1d	20	13	7	7
2.0	0	No	No	DMPS	100	5d	20	13	7	7
2.1	0	Control	No	No	0	1h	20	20	0	0
2.1	0	Control	No	No	0	3h	23	23	0	0
2.1	0	Control	No	No	0	1d	23	23	0	0
2.1	0	Control	No	No	0	4d	23	23	0	0
2.1	0	No	No	LA	5	1h	19	18	0	0
2.1	0	No	No	LA	5	3h	19	18	0	0
2.1	0	No	No	LA	5	1d	19	18	1	1

Experiment	Clutch	Control	Toxin	Chelator	Conc. (µM)	Time	Total Fish	Normal Dev.	Total Abnormal Dev.	Dead
2.1	0	No	No	LA	5	4d	19	1	1	1
2.1	0	No	No	LA	60	1h	20	20	0	0
2.1	0	No	No	LA	60	3h	20	20	0	0
2.1	0	No	No	LA	60	1d	20	20	0	0
2.1	0	No	No	LA	60	4d	20	0	20	20
2.1	0	No	No	LA	100	1h	21	21	0	0
2.1	0	No	No	LA	100	3h	21	21	0	0
2.1	0	No	No	LA	100	1d	21	21	0	0
2.1	0	No	No	LA	100	4d	20	0	20	20
2.1	0	No	No	DMSA	5	1h	20	20	0	0
2.1	0	No	No	DMSA	5	3h	20	20	0	0
2.1	0	No	No	DMSA	5	1d	20	20	0	0
2.1	0	No	No	DMSA	5	4d	20	5	0	0
2.1	0	No	No	DMSA	60	1h	21	21	0	0
2.1	0	No	No	DMSA	60	3h	21	21	0	0
2.1	0	No	No	DMSA	60	1d	21	21	0	0
2.1	0	No	No	DMSA	60	4d	21	4	0	0
2.1	0	No	No	DMSA	100	1h	20	20	0	0
2.1	0	No	No	DMSA	100	3h	20	20	0	0
2.1	0	No	No	DMSA	100	1d	20	20	0	0
2.1	0	No	No	DMSA	100	4d	20	5	0	0
2.1	0	No	No	DMPS	5	1h	19	18	0	0
2.1	0	No	No	DMPS	5	3h	19	17	0	0
2.1	0	No	No	DMPS	5	1d	19	17	2	2
2.1	0	No	No	DMPS	5	4d	19	1	2	2
2.1	0	No	No	DMPS	60	1h	20	19	0	0

Experiment	Clutch	Control	Toxin	Chelator	Conc. (µM)	Time	Total Fish	Normal Dev.	Total Abnormal Dev.	Dead
2.1	0	No	No	DMPS	60	3h	20	19	0	0
2.1	0	No	No	DMPS	60	1d	20	19	1	1
2.1	0	No	No	DMPS	60	4d	20	2	1	1
2.1	0	No	No	DMPS	100	1h	20	20	0	0
2.1	0	No	No	DMPS	100	3h	20	20	0	0
2.1	0	No	No	DMPS	100	1d	20	20	0	0
2.1	0	No	No	DMPS	100	4d	20	6	0	0
2.1	0	No	No	Cysteine	5	1h	20	19	0	0
2.1	0	No	No	Cysteine	5	3h	20	19	0	0
2.1	0	No	No	Cysteine	5	1d	20	19	1	1
2.1	0	No	No	Cysteine	5	4d	20	1	1	1
2.1	0	No	No	Cysteine	60	1h	19	19	0	0
2.1	0	No	No	Cysteine	60	3h	19	19	0	0
2.1	0	No	No	Cysteine	60	1d	19	19	0	0
2.1	0	No	No	Cysteine	60	4d	19	0	0	0
2.1	0	No	No	Cysteine	100	1h	19	18	0	0
2.1	0	No	No	Cysteine	100	3h	19	18	0	0
2.1	0	No	No	Cysteine	100	1d	19	18	1	1
2.1	0	No	No	Cysteine	100	4d	19	0	1	1
2.1	0	No	No	Glutathione	5	1h	20	19	0	0
2.1	0	No	No	Glutathione	5	3h	20	19	0	0
2.1	0	No	No	Glutathione	5	1d	20	19	1	1
2.1	0	No	No	Glutathione	5	4d	20	0	1	1
2.1	0	No	No	Glutathione	60	1h	20	20	0	0
2.1	0	No	No	Glutathione	60	3h	20	19	0	0
2.1	0	No	No	Glutathione	60	1d	20	19	1	1

Experiment	Clutch	Control	Toxin	Chelator	Conc. (µM)	Time	Total Fish	Normal Dev.	Total Abnormal Dev.	Dead
2.1	0	No	No	Glutathione	60	4d	20	0	1	1
2.1	0	No	No	Glutathione	100	1h	20	20	0	0
2.1	0	No	No	Glutathione	100	3h	20	20	0	0
2.1	0	No	No	Glutathione	100	1d	20	20	0	0
2.1	0	No	No	Glutathione	100	4d	20	3	0	0
3.0	0	Control	No	No	0	1h	19	19	0	0
3.0	0	Control	No	No	0	3h	19	19	0	0
3.0	0	Control	No	No	0	1d	20	20	0	0
3.0	0	Control	No	No	0	2d	20	20	0	0
3.0	0	Control	No	No	0	3d	20	17	0	0
3.0	0	Control	$HgCl_2$	No	10	1h	20	20	0	0
3.0	0	Control	$HgCl_2$	No	10	3h	20	20	0	0
3.0	0	Control	$HgCl_2$	No	10	2d	20	0	20	20
3.0	0	Control	$HgCl_2$	No	10	3d	20	0	20	20
3.0	0	Control	No	LA	10	1h	20	20	0	0
3.0	0	Control	No	LA	10	3h	20	20	0	0
3.0	0	Control	No	LA	10	2d	20	20	0	0
3.0	0	Control	No	LA	10	3d	20	20	0	0
3.0	0	No	$HgCl_2$	LA	10	1h	20	19	0	0
3.0	0	No	$HgCl_2$	LA	10	3h	20	19	0	0
3.0	0	No	$HgCl_2$	LA	10	1d	20	0	20	20
3.0	0	No	$HgCl_2$	LA	10	2d	20	0	20	20
3.0	0	No	$HgCl_2$	LA	10	3d	20	0	20	20
3.0	0	Control	No	DMSA	10	1h	20	20	0	0
3.0	0	Control	No	DMSA	10	3h	20	20	0	0
3.0	0	Control	$HgCl_2$	No	10	1d	20	0	20	20

Experiment	Clutch	Control	Toxin	Chelator	Conc. (µM)	Time	Total Fish	Normal Dev.	Total Abnormal Dev.	Dead
3.0	0	Control	No	DMSA	10	2d	20	20	0	0
3.0	0	Control	No	DMSA	10	3d	20	20	0	0
3.0	0	No	$HgCl_2$	DMSA	10	1h	20	20	0	0
3.0	0	No	$HgCl_2$	DMSA	10	3h	20	20	0	0
3.0	0	No	$HgCl_2$	DMSA	10	2d	20	20	0	0
3.0	0	No	$HgCl_2$	DMSA	10	3d	20	18	0	0
3.0	0	Control	No	DMPS	10	1h	18	18	0	0
3.0	0	Control	No	DMPS	10	3h	18	18	0	0
3.0	0	Control	No	DMPS	10	2d	18	18	0	0
3.0	0	Control	No	DMPS	10	3d	18	18	0	0
3.0	0	No	$HgCl_2$	DMPS	10	1h	20	20	0	0
3.0	0	No	$HgCl_2$	DMPS	10	3h	20	20	0	0
3.0	0	No	$HgCl_2$	DMPS	10	2d	20	20	0	0
3.0	0	No	$HgCl_2$	DMPS	10	3d	20	20	0	0
3.1	0	Control	No	Cysteine	10	1h	20	20	0	0
3.1	0	Control	No	Cysteine	10	3h	20	20	0	0
3.1	0	Control	No	Cysteine	10	2d	20	20	0	0
3.1	0	Control	No	Cysteine	10	3d	20	20	0	0
3.1	0	No	$HgCl_2$	Cysteine	10	1h	20	20	0	0
3.1	0	No	$HgCl_2$	Cysteine	10	3h	20	20	0	0
3.1	0	No	$HgCl_2$	Cysteine	10	2d	20	20	0	0
3.1	0	No	$HgCl_2$	Cysteine	10	3d	20	10	0	0
3.1	0	Control	No	Glutathione	10	1h	20	20	0	0
3.1	0	Control	No	Glutathione	10	3h	20	20	0	0
3.1	0	Control	No	No	0	1d	21	21	0	0
3.1	0	Control	No	Glutathione	10	2d	20	20	0	0

Experiment	Clutch	Control	Toxin	Chelator	Conc. (µM)	Time	Total Fish	Normal Dev.	Total Abnormal Dev.	Dead
3.1	0	Control	No	Glutathione	10	3d	20	20	0	0
3.1	0	No	$HgCl_2$	Glutathione	10	1h	20	20	0	0
3.1	0	No	$HgCl_2$	Glutathione	10	3h	20	20	0	0
3.1	0	No	$HgCl_2$	DMSA	10	1d	20	20	0	0
3.1	0	No	$HgCl_2$	Glutathione	10	2d	20	4	16	16
3.1	0	No	$HgCl_2$	Glutathione	10	3d	20	0	20	20
3.1	0	Control	No	No	0	1d	20	20	0	0
3.1	0	Control	No	LA	10	1d	20	20	0	0
3.1	0	No	$HgCl_2$	DMPS	10	1d	20	20	0	0
3.1	0	No	$HgCl_2$	Cysteine	10	1d	20	20	0	0
3.1	0	Control	No	LA	10	1d	20	18	2	2
3.1	0	Control	No	LA	10	1d	20	20	0	0
3.1	0	No	$HgCl_2$	Glutathione	10	1d	20	20	0	0
3.1	0	Control	No	DMSA	10	1d	20	20	0	0
3.1	0	No	$HgCl_2$	LA	10	1d	20	0	20	20
3.1	0	Control	$HgCl_2$	No	10	1d	18	0	18	18
3.1	0	Control	No	No	0	3h	21	21	0	0
3.1	0	Control	No	DMSA	10	1d	20	19	0	0
3.1	0	Control	No	No	0	4d	21	20	0	0
3.1	0	Control	$HgCl_2$	No	10	3h	18	18	0	0
3.1	0	Control	$HgCl_2$	No	10	4d	18	0	18	18
3.1	0	Control	No	LA	10	3h	20	20	0	0
3.1	0	Control	No	LA	10	4d	20	17	2	2
3.1	0	No	$HgCl_2$	LA	10	3h	20	20	0	0
3.1	0	No	$HgCl_2$	DMSA	10	1d	20	20	0	0
3.1	0	No	$HgCl_2$	LA	10	4d	20	0	20	20

Experiment	Clutch	Control	Toxin	Chelator	Conc. (µM)	Time	Total Fish	Normal Dev.	Total Abnormal Dev.	Dead
3.1	0	Control	No	DMSA	10	3h	20	19	0	0
3.1	0	Control	No	DMSA	10	1d	20	18	2	2
3.1	0	Control	No	DMSA	10	4d	20	19	0	0
3.1	0	No	$HgCl_2$	DMSA	10	3h	20	20	0	0
3.1	0	No	$HgCl_2$	DMSA	10	4d	20	19	1	1
3.1	0	Control	No	DMPS	10	3h	19	19	0	0
3.1	0	Control	No	DMPS	10	4d	19	17	2	2
3.1	0	No	$HgCl_2$	DMPS	10	3h	20	18	0	0
3.1	0	No	$HgCl_2$	DMPS	10	4d	19	2	17	17
3.1	0	Control	No	Cysteine	10	3h	20	19	0	0
3.1	0	Control	No	Cysteine	10	4d	20	18	2	2
3.1	0	No	$HgCl_2$	Cysteine	10	3h	20	20	0	0
3.1	0	No	$HgCl_2$	Cysteine	10	4d	20	0	20	20
3.1	0	Control	No	Glutathione	10	3h	19	18	0	0
3.1	0	Control	No	DMPS	10	1d	18	18	0	0
3.1	0	Control	No	Glutathione	10	4d	19	18	1	1
3.1	0	No	$HgCl_2$	Glutathione	10	3h	20	19	0	0
3.1	0	No	$HgCl_2$	DMPS	10	1d	20	18	0	0
3.1	0	No	$HgCl_2$	Glutathione	10	4d	18	0	9	9
3.1	0	Control	No	DMPS	10	1d	19	18	0	0
3.1	0	No	$HgCl_2$	Cysteine	10	1d	20	0	20	20
3.1	0	Control	No	DMPS	10	1d	20	20	0	0
3.1	0	No	$HgCl_2$	Glutathione	10	1d	20	17	3	3
3.2	0	Control	No	No	0	1h	20	12	0	0
3.2	0	Control	No	No	0	3h	20	12	0	0
3.2	0	Control	No	No	0	3d	20	7	10	10

Experiment	Clutch	Control	Toxin	Chelator	Conc. (µM)	Time	Total Fish	Normal Dev.	Total Abnormal Dev.	Dead
3.2	0	Control	$PbCl_2$	No	60	1h	20	17	0	0
3.2	0	Control	$PbCl_2$	No	60	3h	20	17	0	0
3.2	0	Control	$PbCl_2$	No	60	3d	20	3	17	17
3.2	0	Control	No	LA	60	1h	20	17	0	0
3.2	0	Control	No	LA	60	3h	20	17	0	0
3.2	0	Control	No	LA	60	3d	18	5	4	4
3.2	0	No	$PbCl_2$	LA	60	1h	13	13	0	0
3.2	0	No	$PbCl_2$	LA	60	3h	13	13	0	0
3.2	0	No	$PbCl_2$	LA	60	3d	13	0	13	13
3.2	0	Control	No	DMSA	60	1h	20	15	0	0
3.2	0	Control	No	DMSA	60	3h	20	15	0	0
3.2	0	Control	No	DMSA	60	3d	20	12	7	7
3.2	0	No	$PbCl_2$	DMSA	60	1h	19	12	0	0
3.2	0	No	$PbCl_2$	DMSA	60	3h	19	10	0	0
3.2	0	No	$PbCl_2$	DMSA	60	3d	19	1	16	16
3.2	0	Control	No	DMPS	60	1h	20	11	0	0
3.2	0	Control	No	DMPS	60	3h	20	10	0	0
3.2	0	Control	No	DMPS	60	3d	20	10	10	10
3.2	0	No	$PbCl_2$	DMPS	60	1h	14	12	0	0
3.2	0	No	$PbCl_2$	DMPS	60	3h	14	12	0	0
3.2	0	No	$PbCl_2$	DMPS	60	3d	14	6	7	7
3.3	1	Control	No	No	0	1h	19	19	0	0
3.3	1	Control	No	No	0	3h	19	19	0	0
3.3	1	Control	No	No	0	5h	19	19	0	0
3.3	1	Control	No	No	0	1d	19	19	0	0
3.3	1	Control	No	No	0	2d	19	19	0	0

Experiment	Clutch	Control	Toxin	Chelator	Conc. (µM)	Time	Total Fish	Normal Dev.	Total Abnormal Dev.	Dead
3.3	2	Control	No	No	0	1h	19	16	0	0
3.3	2	Control	No	No	0	3h	19	16	0	0
3.3	2	Control	No	No	0	5h	19	16	3	3
3.3	2	Control	No	No	0	1d	19	16	3	3
3.3	2	Control	No	No	0	2d	19	16	3	3
3.3	1	Control	$CdCl_2$	No	80	1h	20	20	0	0
3.3	1	Control	$CdCl_2$	No	80	3h	20	20	0	0
3.3	1	Control	$CdCl_2$	No	80	5h	18	9	1	1
3.3	1	Control	$CdCl_2$	No	80	2d	20	0	20	20
3.3	1	Control	No	LA	80	1h	20	20	0	0
3.3	1	Control	No	LA	80	3h	20	20	0	0
3.3	1	Control	No	LA	80	5h	20	20	0	0
3.3	1	Control	No	LA	80	2d	20	0	5	5
3.3	1	No	$CdCl_2$	LA	80	1h	20	20	0	0
3.3	1	No	$CdCl_2$	LA	80	3h	20	20	0	0
3.3	1	No	$CdCl_2$	LA	80	5h	20	0	7	7
3.3	1	No	$CdCl_2$	LA	80	1d	20	0	20	20
3.3	1	No	$CdCl_2$	LA	80	2d	20	0	20	20
3.3	1	Control	No	DMSA	80	1h	20	20	0	0
3.3	1	Control	No	DMSA	80	3h	20	19	0	0
3.3	1	Control	No	DMSA	80	5h	20	19	1	1
3.3	1	Control	$CdCl_2$	No	80	1d	20	0	20	20
3.3	1	Control	No	DMSA	80	2d	20	19	1	1
3.3	1	No	$CdCl_2$	DMSA	80	1h	20	17	0	0
3.3	1	No	$CdCl_2$	DMSA	80	3h	20	16	0	0
3.3	1	No	$CdCl_2$	DMSA	80	5h	20	16	1	1

Experiment	Clutch	Control	Toxin	Chelator	Conc. (µM)	Time	Total Fish	Normal Dev.	Total Abnormal Dev.	Dead
3.3	1	No	$CdCl_2$	DMSA	80	2d	20	15	5	5
3.3	2	Control	No	DMPS	80	1h	20	17	0	0
3.3	2	Control	No	DMPS	80	3h	20	16	0	0
3.3	2	Control	No	DMPS	80	5h	20	16	0	0
3.3	2	Control	No	DMPS	80	2d	20	15	5	5
3.3	1	No	$CdCl_2$	DMPS	80	1h	20	20	0	0
3.3	1	No	$CdCl_2$	DMPS	80	3h	20	19	0	0
3.3	1	No	$CdCl_2$	DMPS	80	5h	20	19	0	0
3.3	1	No	$CdCl_2$	DMPS	80	2d	20	0	5	5
3.3	2	Control	No	Cysteine	80	1h	20	17	0	0
3.3	2	Control	No	Cysteine	80	3h	20	17	0	0
3.3	2	Control	No	Cysteine	80	5h	20	17	0	0
3.3	2	Control	No	Cysteine	80	2d	20	16	4	4
3.3	2	No	$CdCl_2$	Cysteine	80	1h	20	18	0	0
3.3	2	No	$CdCl_2$	Cysteine	80	3h	20	18	0	0
3.3	2	No	$CdCl_2$	Cysteine	80	5h	20	18	1	1
3.3	1	No	$CdCl_2$	DMSA	80	1d	20	15	5	5
3.3	2	No	$CdCl_2$	Cysteine	80	2d	20	0	20	20
3.3	2	Control	No	Glutathione	80	1h	17	17	0	0
3.3	2	Control	No	Glutathione	80	3h	17	16	0	0
3.3	2	Control	No	Glutathione	80	5h	17	16	0	0
3.3	1	Control	No	LA	80	1d	20	0	5	5
3.3	2	Control	No	Glutathione	80	2d	17	15	2	2
3.3	2	No	$CdCl_2$	Glutathione	80	1h	19	18	0	0
3.3	2	No	$CdCl_2$	Glutathione	80	3h	19	17	0	0
3.3	2	No	$CdCl_2$	Glutathione	80	5h	19	9	6	6

Experiment	Clutch	Control	Toxin	Chelator	Conc. (µM)	Time	Total Fish	Normal Dev.	Total Abnormal Dev.	Dead
3.3	2	No	$CdCl_2$	Glutathione	80	2d	20	0	20	20
3.3	1	No	$CdCl_2$	DMPS	80	1d	20	15	5	5
3.3	2	No	$CdCl_2$	Cysteine	80	1d	20	0	20	20
3.3	2	No	$CdCl_2$	Glutathione	80	1d	20	0	20	20
3.4	1	Control	No	DMSA	80	1d	20	19	1	1
3.4	2	Control	No	DMPS	80	1d	20	15	5	5
3.4	2	Control	No	Cysteine	80	1d	20	16	4	4
3.4	2	Control	No	Glutathione	80	1d	17	15	2	2
3.4	0	No	$HgCl_2$	LA	10	1d	20	0	20	20
3.4	0	No	$HgCl_2$	DMSA	10	1d	20	0	19	19
3.4	0	Control	No	No	0	3h	19	16	0	0
3.4	0	Control	No	No	0	1d	19	16	3	3
3.4	0	Control	No	No	0	2d	19	16	3	3
3.4	0	Control	$HgCl_2$	No	10	3h	19	17	0	0
3.4	0	Control	$HgCl_2$	No	10	1d	19	0	19	19
3.4	0	Control	$HgCl_2$	No	10	2d	19	0	19	19
3.4	0	Control	No	LA	10	3h	20	19	0	0
3.4	0	Control	No	LA	10	1d	20	18	2	2
3.4	0	Control	No	LA	10	2d	20	18	2	2
3.4	0	No	$HgCl_2$	LA	10	3h	20	14	0	0
3.4	0	No	$HgCl_2$	DMPS	10	1d	9	9	0	0
3.4	0	No	$HgCl_2$	LA	10	2d	20	0	20	20
3.4	0	Control	No	DMSA	10	3h	16	13	0	0
3.4	0	Control	No	DMSA	10	1d	16	12	4	4
3.4	0	Control	No	DMSA	10	2d	16	11	5	5
3.4	0	No	$HgCl_2$	DMSA	10	3h	20	18	0	0

Experiment	Clutch	Control	Toxin	Chelator	Conc. (µM)	Time	Total Fish	Normal Dev.	Total Abnormal Dev.	Dead
3.4	0	No	$HgCl_2$	DMSA	10	2d	20	0	20	20
3.4	0	Control	No	DMPS	10	3h	18	16	0	0
3.4	0	Control	No	DMPS	10	1d	18	14	4	4
3.4	0	Control	No	DMPS	10	2d	18	13	5	5
3.4	0	No	$HgCl_2$	DMPS	10	3h	9	9	0	0
3.4	0	No	$HgCl_2$	DMPS	10	2d	9	9	0	0
3.5	0	Control	No	No	0	3h	20	17	0	0
3.5	0	Control	No	No	0	1d	20	17	3	3
3.5	0	Control	No	No	0	2d	20	17	3	3
3.5	0	Control	No	No	0	3d	20	11	3	3
3.5	0	Control	No	No	0	5d	20	17	3	3
3.5	0	Control	$PbCl_2$	No	90	3h	20	18	0	0
3.5	0	Control	$PbCl_2$	No	90	2d	20	17	2	2
3.5	0	Control	$PbCl_2$	No	90	3d	20	14	2	2
3.5	0	Control	$PbCl_2$	No	90	5d	20	0	20	20
3.5	0	Control	No	LA	90	3h	20	17	0	0
3.5	0	Control	No	LA	90	2d	20	0	8	8
3.5	0	Control	No	LA	90	3d	20	0	20	20
3.5	0	Control	No	LA	90	5d	20	0	20	20
3.5	0	No	$PbCl_2$	LA	90	3h	20	15	2	2
3.5	0	No	$PbCl_2$	LA	90	1d	20	0	20	20
3.5	0	No	$PbCl_2$	LA	90	2d	20	0	20	20
3.5	0	No	$PbCl_2$	LA	90	3d	20	0	20	20
3.5	0	No	$PbCl_2$	LA	90	5d	20	0	20	20
3.5	0	Control	No	DMSA	90	3h	20	19	0	0
3.5	0	Control	No	DMSA	90	2d	20	19	1	1

Experiment	Clutch	Control	Toxin	Chelator	Conc. (µM)	Time	Total Fish	Normal Dev.	Total Abnormal Dev.	Dead
3.5	0	Control	No	DMSA	90	3d	20	15	1	1
3.5	0	Control	No	DMSA	90	5d	20	19	1	1
3.5	0	No	$PbCl_2$	DMSA	90	3h	20	11	9	9
3.5	0	No	$PbCl_2$	DMSA	90	2d	20	2	18	18
3.5	0	No	$PbCl_2$	DMSA	90	3d	20	2	18	18
3.5	0	No	$PbCl_2$	DMSA	90	5d	20	2	18	18
3.5	0	Control	No	DMPS	90	3h	20	17	0	0
3.5	0	Control	$PbCl_2$	No	90	1d	20	18	2	2
3.5	0	Control	No	DMPS	90	2d	20	17	3	3
3.5	0	Control	No	DMPS	90	3d	20	17	3	3
3.5	0	Control	No	DMPS	90	5d	20	17	3	3
3.5	0	No	$PbCl_2$	DMPS	90	3h	20	15	5	5
3.5	0	No	$PbCl_2$	DMPS	90	2d	20	11	9	9
3.5	0	No	$PbCl_2$	DMPS	90	3d	20	11	9	9
3.5	0	No	$PbCl_2$	DMPS	90	5d	20	0	20	20
3.5	0	Control	No	Cysteine	90	3h	20	18	0	0
3.5	0	Control	No	Cysteine	90	2d	20	17	3	3
3.5	0	Control	No	Cysteine	90	3d	20	17	3	3
3.5	0	Control	No	Cysteine	90	5d	20	17	3	3
3.5	0	No	$PbCl_2$	Cysteine	90	3h	20	15	0	0
3.5	0	No	$PbCl_2$	DMSA	90	1d	20	2	18	18
3.5	0	No	$PbCl_2$	Cysteine	90	2d	20	15	5	5
3.5	0	No	$PbCl_2$	Cysteine	90	3d	20	15	5	5
3.5	0	No	$PbCl_2$	Cysteine	90	5d	20	0	20	20
3.5	0	Control	No	Glutathione	90	3h	20	18	0	0
3.5	0	Control	No	Glutathione	90	2d	20	17	3	3

Experiment	Clutch	Control	Toxin	Chelator	Conc. (µM)	Time	Total Fish	Normal Dev.	Total Abnormal Dev.	Dead
3.5	0	Control	No	Glutathione	90	3d	20	17	3	3
3.5	0	Control	No	Glutathione	90	5d	20	17	3	3
3.5	0	No	$PbCl_2$	Glutathione	90	3h	20	9	0	0
3.5	0	No	$PbCl_2$	Glutathione	90	2d	20	7	12	12
3.5	0	No	$PbCl_2$	Glutathione	90	3d	20	6	12	12
3.5	0	No	$PbCl_2$	Glutathione	90	5d	20	18	2	2
3.5	1	Control	No	No	0	1d	20	12	8	8
3.5	2	Control	No	No	0	1d	20	19	1	1
3.5	0	No	$PbCl_2$	DMPS	90	1d	20	11	9	9
3.5	0	Control	No	No	0	1d	20	19	1	1
3.5	0	No	$PbCl_2$	Cysteine	90	1d	20	15	5	5
3.5	0	Control	No	LA	90	1d	20	0	5	5
3.5	2	Control	No	LA	90	1d	20	0	20	20
3.5	0	No	$PbCl_2$	Glutathione	90	1d	20	8	12	12
3.6	0	Control	No	No	0	1d	20	17	3	3
3.6	0	Control	$CdCl_2$	No	80	1d	20	0	20	20
3.6	0	No	$CdCl_2$	LA	80	1d	20	0	20	20
3.6	0	No	$CdCl_2$	DMSA	80	1d	20	19	1	1
3.6	0	Control	No	No	0	5h	20	17	0	0
3.6	0	Control	No	LA	80	1d	20	0	20	20
3.6	0	Control	No	No	0	2d	20	17	3	3
3.6	0	Control	No	No	0	3d	20	12	3	3
3.6	0	Control	$CdCl_2$	No	80	5h	20	14	4	4
3.6	0	Control	$CdCl_2$	No	80	2d	20	0	20	20
3.6	0	Control	$CdCl_2$	No	80	3d	20	0	20	20
3.6	0	Control	No	LA	80	5h	20	18	0	0

Experiment	Clutch	Control	Toxin	Chelator	Conc. (µM)	Time	Total Fish	Normal Dev.	Total Abnormal Dev.	Dead
3.6	0	Control	No	LA	80	2d	20	0	20	20
3.6	0	Control	No	LA	80	3d	20	0	20	20
3.6	0	No	$CdCl_2$	LA	80	5h	20	3	17	17
3.6	0	No	$CdCl_2$	LA	80	2d	20	0	20	20
3.6	0	No	$CdCl_2$	LA	80	3d	20	0	20	20
3.6	0	Control	No	DMSA	80	5h	20	18	0	0
3.6	0	Control	No	DMSA	80	1d	20	18	2	2
3.6	0	Control	No	DMSA	80	2d	20	18	2	2
3.6	0	Control	No	DMSA	80	3d	20	14	2	2
3.6	0	No	$CdCl_2$	DMSA	80	5h	20	20	0	0
3.6	0	No	$CdCl_2$	DMSA	80	2d	20	19	1	1
3.6	0	No	$CdCl_2$	DMSA	80	3d	20	19	1	1
3.6	0	Control	No	DMPS	80	5h	20	18	1	1
3.6	0	Control	No	DMPS	80	2d	20	17	3	3
3.6	0	Control	No	DMPS	80	3d	20	14	3	3
3.6	0	No	$CdCl_2$	DMPS	80	5h	20	20	0	0
3.6	0	No	$CdCl_2$	DMPS	80	1d	20	19	1	1
3.6	0	No	$CdCl_2$	DMPS	80	2d	20	19	1	1
3.6	0	No	$CdCl_2$	DMPS	80	3d	20	17	1	1
3.6	0	Control	No	Cysteine	80	5h	20	18	0	0
3.6	0	Control	No	Cysteine	80	2d	20	17	3	3
3.6	0	Control	No	Cysteine	80	3d	20	12	4	4
3.6	0	No	$CdCl_2$	Cysteine	80	5h	20	16	4	4
3.6	0	No	$CdCl_2$	Cysteine	80	2d	20	0	18	18
3.6	0	No	$CdCl_2$	Cysteine	80	3d	20	1	19	19
3.6	0	Control	No	Glutathione	80	5h	20	18	0	0

Experiment	Clutch	Control	Toxin	Chelator	Conc. (µM)	Time	Total Fish	Normal Dev.	Total Abnormal Dev.	Dead
3.6	0	Control	No	DMPS	80	1d	20	18	2	2
3.6	0	Control	No	Glutathione	80	2d	20	18	2	2
3.6	0	Control	No	Glutathione	80	3d	20	14	2	2
3.6	0	No	$CdCl_2$	Glutathione	80	5h	20	17	3	3
3.6	0	No	$CdCl_2$	Glutathione	80	2d	20	1	18	18
3.6	0	No	$CdCl_2$	Glutathione	80	3d	20	1	19	19
3.6	0	No	$CdCl_2$	Cysteine	80	1d	20	2	17	17
3.6	0	No	$CdCl_2$	Glutathione	80	1d	20	3	16	16
3.7	0	Control	No	Cysteine	80	1d	20	18	2	2
3.7	0	Control	No	Glutathione	80	1d	20	18	2	2
3.7	0	Control	No	LA	90	1d	20	0	20	20
3.7	0	Control	No	DMSA	90	1d	20	19	1	1
3.7	2	No	$PbCl_2$	LA	90	1d	20	0	20	20
3.7	1	Control	$PbCl_2$	No	90	1d	20	11	9	9
3.7	1	No	$PbCl_2$	DMSA	90	1d	20	0	20	20
3.7	1	Control	No	No	0	5h	20	12	0	0
3.7	1	Control	No	No	0	2d	20	12	8	8
3.7	2	Control	No	No	0	5h	20	19	0	0
3.7	1	Control	No	DMSA	90	1d	20	15	5	5
3.7	2	Control	No	No	0	2d	20	19	1	1
3.7	1	Control	$PbCl_2$	No	90	5h	20	12	0	0
3.7	1	Control	$PbCl_2$	No	90	2d	20	11	9	9
3.7	2	Control	No	LA	90	5h	20	19	0	0
3.7	2	Control	No	LA	90	2d	20	0	20	20
3.7	2	No	$PbCl_2$	LA	90	5h	20	0	20	20
3.7	2	No	$PbCl_2$	LA	90	2d	20	0	20	20

Experiment	Clutch	Control	Toxin	Chelator	Conc. (µM)	Time	Total Fish	Normal Dev.	Total Abnormal Dev.	Dead
3.7	1	Control	No	DMSA	90	5h	20	15	0	0
3.7	0	Control	No	DMSA	90	1d	20	18	2	2
3.7	1	Control	No	DMSA	90	2d	20	15	5	5
3.7	1	No	$PbCl_2$	DMSA	90	5h	20	4	16	16
3.7	1	No	$PbCl_2$	DMSA	90	2d	20	0	20	20
3.7	1	Control	No	DMPS	90	5h	20	14	0	0
3.7	1	Control	No	DMPS	90	2d	20	14	6	6
3.7	1	No	$PbCl_2$	DMPS	90	5h	20	8	12	12
3.7	1	No	$PbCl_2$	DMPS	90	1d	20	8	12	12
3.7	1	No	$PbCl_2$	DMPS	90	2d	20	8	12	12
3.7	1	Control	No	Cysteine	90	5h	20	15	0	0
3.7	1	Control	No	Cysteine	90	2d	20	12	8	8
3.7	1	No	$PbCl_2$	Cysteine	90	5h	20	15	1	1
3.7	1	No	$PbCl_2$	Cysteine	90	2d	20	13	7	7
3.7	2	Control	No	Glutathione	90	5h	20	20	0	0
3.7	0	Control	No	DMPS	90	1d	20	17	3	3
3.7	2	Control	No	Glutathione	90	2d	20	20	0	0
3.7	2	No	$PbCl_2$	Glutathione	90	5h	20	19	1	1
3.7	2	No	$PbCl_2$	Glutathione	90	2d	20	18	2	2
3.7	1	Control	No	DMPS	90	1d	20	14	6	6
3.7	1	No	$PbCl_2$	Cysteine	90	1d	20	13	7	7
3.7	0	Control	No	DMPS	90	1d	20	20	0	0
3.7	2	No	$PbCl_2$	Glutathione	90	1d	20	18	2	2
3.7	0	Control	No	Cysteine	90	1d	20	18	2	2
3.7	0	No	$PbCl_2$	LA	90	1d	20	0	20	20
3.7	0	Control	$PbCl_2$	No	90	1d	20	18	2	2

Experiment	Clutch	Control	Toxin	Chelator	Conc. (µM)	Time	Total Fish	Normal Dev.	Total Abnormal Dev.	Dead
3.7	1	Control	No	Cysteine	90	1d	20	12	8	8
3.7	0	No	$PbCl_2$	DMSA	90	1d	20	16	4	4
3.7	0	Control	No	Cysteine	90	1d	20	19	1	1
3.7	0	No	$PbCl_2$	DMPS	90	1d	20	18	2	2
3.7	0	Control	No	No	0	5h	20	20	0	0
3.7	0	Control	No	Glutathione	90	1d	20	17	3	3
3.7	0	Control	No	No	0	2d	20	19	1	1
3.7	0	Control	$PbCl_2$	No	90	5h	20	18	0	0
3.7	0	Control	$PbCl_2$	No	90	2d	20	17	3	3
3.7	0	Control	No	LA	90	5h	20	19	1	1
3.7	0	Control	No	LA	90	2d	20	0	20	20
3.7	0	No	$PbCl_2$	LA	90	5h	20	4	16	16
3.7	0	No	$PbCl_2$	LA	90	2d	20	0	20	20
3.7	0	Control	No	DMSA	90	5h	20	18	0	0
3.7	2	Control	No	Glutathione	90	1d	20	20	0	0
3.7	0	Control	No	DMSA	90	2d	20	18	2	2
3.7	0	No	$PbCl_2$	DMSA	90	5h	20	16	4	4
3.7	0	No	$PbCl_2$	Cysteine	90	1d	19	19	0	0
3.7	0	No	$PbCl_2$	DMSA	90	2d	20	16	3	3
3.7	0	Control	No	DMPS	90	5h	20	20	0	0
3.7	0	Control	No	DMPS	90	2d	20	20	0	0
3.7	0	No	$PbCl_2$	DMPS	90	5h	20	18	2	2
3.7	0	No	$PbCl_2$	DMPS	90	2d	20	18	2	2
3.7	0	Control	No	Cysteine	90	5h	20	20	0	0
3.7	0	Control	No	Cysteine	90	2d	20	19	1	1
3.7	0	No	$PbCl_2$	Cysteine	90	5h	19	19	0	0

Experiment	Clutch	Control	Toxin	Chelator	Conc. (µM)	Time	Total Fish	Normal Dev.	Total Abnormal Dev.	Dead
3.7	0	No	$PbCl_2$	Cysteine	90	2d	19	18	1	1
3.7	0	Control	No	Glutathione	90	5h	20	18	0	0
3.7	0	Control	No	Glutathione	90	1d	20	18	2	2
3.7	0	Control	No	Glutathione	90	2d	20	18	2	2
3.7	0	No	$PbCl_2$	Glutathione	90	5h	20	19	1	1
3.7	0	No	$PbCl_2$	Glutathione	90	1d	20	19	1	1
3.7	0	No	$PbCl_2$	Glutathione	90	2d	20	17	3	3
3.7	0	Control	No	Cysteine	10	1d	20	20	0	0
3.7	0	Control	$HgCl_2$	No	10	1d	20	0	20	20
3.7	0	No	$HgCl_2$	LA	10	1d	20	0	20	20
3.8	0	Control	No	Cysteine	10	1d	20	19	0	0
3.8	0	Control	No	Cysteine	10	1d	20	20	0	0
3.8	0	No	$HgCl_2$	DMSA	10	1d	20	18	1	1
3.8	0	No	$HgCl_2$	DMPS	10	1d	20	20	0	0
3.8	0	Control	No	No	0	5h	20	20	0	0
3.8	0	Control	No	Glutathione	10	1d	20	20	0	0
3.8	0	Control	No	No	0	2d	20	20	0	0
3.8	0	Control	$HgCl_2$	No	10	5h	20	20	0	0
3.8	0	Control	$HgCl_2$	No	10	2d	20	0	20	20
3.8	0	Control	No	LA	10	5h	20	20	0	0
3.8	0	Control	No	LA	10	2d	20	19	1	1
3.8	0	No	$HgCl_2$	LA	10	5h	20	20	0	0
3.8	0	No	$HgCl_2$	LA	10	2d	20	0	20	20
3.8	0	Control	No	DMSA	10	5h	20	20	0	0
3.8	0	Control	No	Glutathione	10	1d	19	18	1	1
3.8	0	Control	No	DMSA	10	2d	20	18	2	2

Experiment	Clutch	Control	Toxin	Chelator	Conc. (µM)	Time	Total Fish	Normal Dev.	Total Abnormal Dev.	Dead
3.8	0	No	$HgCl_2$	DMSA	10	5h	20	20	0	0
3.8	0	No	$HgCl_2$	Cysteine	10	1d	20	20	0	0
3.8	0	No	$HgCl_2$	DMSA	10	2d	20	16	1	1
3.8	0	Control	No	DMPS	10	5h	20	20	0	0
3.8	0	Control	No	DMPS	10	2d	20	20	0	0
3.8	0	No	$HgCl_2$	DMPS	10	5h	20	20	0	0
3.8	0	No	$HgCl_2$	DMPS	10	2d	20	20	0	0
3.8	0	Control	No	Cysteine	10	5h	20	20	0	0
3.8	0	Control	No	Cysteine	10	2d	20	20	0	0
3.8	0	No	$HgCl_2$	Cysteine	10	5h	20	20	0	0
3.8	0	No	$HgCl_2$	Cysteine	10	2d	20	20	0	0
3.8	0	Control	No	Glutathione	10	5h	20	20	0	0
3.8	0	Control	No	Glutathione	10	1d	20	20	0	0
3.8	0	Control	No	Glutathione	10	2d	20	20	0	0
3.8	0	No	$HgCl_2$	Glutathione	10	5h	20	20	0	0
3.8	0	No	$HgCl_2$	Glutathione	10	1d	20	20	0	0
3.8	0	No	$HgCl_2$	Glutathione	10	2d	20	19	1	1
3.9	0	Control	No	No	0	1d	20	20	0	0
3.9	0	Control	$CdCl_2$	No	80	1d	20	13	7	7
3.9	0	Control	No	LA	80	1d	20	0	20	20
3.9	0	Control	No	DMSA	80	1d	20	18	2	2
3.9	0	Control	No	No	0	5h	20	20	0	0
3.9	0	Control	No	DMPS	80	1d	20	19	1	1
3.9	0	Control	$CdCl_2$	No	80	5h	20	19	1	1
3.9	0	No	$CdCl_2$	LA	80	1d	20	0	20	20
3.9	0	No	$CdCl_2$	LA	80	5h	20	11	9	9

Experiment	Clutch	Control	Toxin	Chelator	Conc. (µM)	Time	Total Fish	Normal Dev.	Total Abnormal Dev.	Dead
3.9	0	Control	No	LA	80	5h	20	20	0	0
3.9	0	No	$CdCl_2$	DMSA	80	1d	20	17	3	3
3.9	0	No	$CdCl_2$	DMSA	80	5h	20	19	1	1
3.9	0	Control	No	DMSA	80	5h	20	20	0	0
3.9	0	Control	No	Cysteine	80	1d	20	20	0	0
3.9	0	No	$CdCl_2$	DMPS	80	1d	20	17	2	2
3.9	0	No	$CdCl_2$	DMPS	80	5h	20	20	0	0
3.9	0	Control	No	DMPS	80	5h	20	20	0	0
3.9	0	No	$CdCl_2$	Cysteine	80	1d	20	14	6	6
3.9	0	No	$CdCl_2$	Cysteine	80	5h	20	20	0	0
3.9	0	Control	No	Cysteine	80	5h	20	20	0	0
3.9	0	No	$CdCl_2$	Glutathione	80	5h	20	19	1	1
3.9	0	No	$CdCl_2$	Glutathione	80	1d	20	12	8	8
3.9	0	Control	No	Glutathione	80	5h	20	20	0	0
3.9	0	Control	No	Glutathione	80	1d	20	19	1	1
4.0	1	Control	No	No	0	1d	25	25	0	0
4.0	2	Control	No	No	0	1d	20	19	1	0
4.0	1	No	$HgCl_2$	No	10	1d	20	0	0	20
4.0	2	No	$HgCl_2$	No	10	1d	20	0	0	20
4.0	1	No	$HgCl_2$	LA	10	1d	20	0	0	20
4.0	2	No	$HgCl_2$	LA	10	1d	20	0	0	20
4.0	1	No	$HgCl_2$	DMPS	10	1d	20	20	0	0
4.0	2	No	$HgCl_2$	DMPS	10	1d	20	19	1	0
4.0	1	No	$HgCl_2$	DMSA	10	1d	20	20	0	0
4.0	2	No	$HgCl_2$	DMSA	10	1d	20	18	1	1
4.0	1	No	$HgCl_2$	Cysteine	10	1d	20	20	0	0

Experiment	Clutch	Control	Toxin	Chelator	Conc. (µM)	Time	Total Fish	Normal Dev.	Total Abnormal Dev.	Dead
4.0	2	No	$HgCl_2$	Cysteine	10	1d	20	16	1	3
4.0	1	No	$HgCl_2$	Glutathione	10	1d	20	11	1	8
4.0	2	No	$HgCl_2$	Glutathione	10	1d	19	13	3	3
4.1	1	Control	No	No	0	1d	21	21	0	0
4.1	2	Control	No	No	0	1d	25	21	0	4
4.1	3	Control	No	No	0	1d	32	30	0	2
4.1	1	No	$HgCl_2$	No	5	1d	31	0	0	31
4.1	2	No	$HgCl_2$	No	5	1d	30	0	0	30
4.1	3	No	$HgCl_2$	No	5	1d	30	0	0	30
4.1	1	No	$HgCl_2$	LA	5	1d	30	0	0	30
4.1	2	No	$HgCl_2$	LA	5	1d	30	0	0	30
4.1	3	No	$HgCl_2$	LA	5	1d	23	0	0	23
4.1	1	No	$HgCl_2$	DMPS	5	1d	31	31	0	0
4.1	2	No	$HgCl_2$	DMPS	5	1d	30	29	0	1
4.1	3	No	$HgCl_2$	DMPS	5	1d	31	26	0	5
4.1	1	No	$HgCl_2$	DMSA	5	1d	29	28	0	1
4.1	2	No	$HgCl_2$	DMSA	5	1d	30	25	0	5
4.1	3	No	$HgCl_2$	DMSA	5	1d	30	24	0	6
4.1	1	No	$HgCl_2$	Cysteine	5	1d	29	28	0	1
4.1	2	No	$HgCl_2$	Cysteine	5	1d	30	24	4	2
4.1	3	No	$HgCl_2$	Cysteine	5	1d	30	27	0	3
4.1	1	No	$HgCl_2$	Glutathione	5	1d	30	28	1	1
4.1	2	No	$HgCl_2$	Glutathione	5	1d	30	29	0	1
4.1	3	No	$HgCl_2$	Glutathione	5	1d	23	22	0	1
4.2	1	Control	No	No	0	1d	23	22	0	1
4.2	1	No	$HgCl_2$	No	5	1d	25	0	0	25

Experiment	Clutch	Control	Toxin	Chelator	Conc. (µM)	Time	Total Fish	Normal Dev.	Total Abnormal Dev.	Dead
4.2	1	No	$HgCl_2$	No	2	1d	26	15	2	9
4.2	1	No	$HgCl_2$	No	1	1d	23	23	0	0
4.2	1	No	$HgCl_2$	No	0.5	1d	23	22	1	0
4.2	1	No	$PbCl_2$	No	120	1d	21	20	0	1
4.2	1	No	$PbCl_2$	No	200	1d	25	25	0	0
4.2	1	No	$PbCl_2$	No	300	1d	31	28	0	3
4.2	1	No	$CdCl_2$	No	150	1d	25	25	0	0
4.2	1	No	$CdCl_2$	No	200	1d	23	22	0	1
4.2	1	No	$CdCl_2$	No	300	1d	23	20	0	3
4.3	1	Control	No	No	0	1d	26	22	0	4
4.3	2	Control	No	No	0	1d	20	18	0	2
4.3	3	Control	No	No	0	1d	29	26	0	3
4.3	1	No	$HgCl_2$	No	2	1d	26	4	0	22
4.3	2	No	$HgCl_2$	No	2	1d	31	4	0	27
4.3	3	No	$HgCl_2$	No	2	1d	22	0	0	22
4.3	1	No	$HgCl_2$	LA	2	1d	31	0	0	31
4.3	2	No	$HgCl_2$	LA	2	1d	30	0	0	30
4.3	3	No	$HgCl_2$	LA	2	1d	30	0	0	30
4.3	1	No	$HgCl_2$	DMPS	2	1d	27	26	0	1
4.3	2	No	$HgCl_2$	DMPS	2	1d	28	28	0	0
4.3	3	No	$HgCl_2$	DMPS	2	1d	29	19	0	10
4.3	1	No	$HgCl_2$	DMSA	2	1d	27	25	0	2
4.3	2	No	$HgCl_2$	DMSA	2	1d	32	32	0	0
4.3	3	No	$HgCl_2$	DMSA	2	1d	29	17	1	11
4.3	1	No	$HgCl_2$	Cysteine	2	1d	29	27	0	2
4.3	2	No	$HgCl_2$	Cysteine	2	1d	30	30	0	0

Experiment	Clutch	Control	Toxin	Chelator	Conc. (µM)	Time	Total Fish	Normal Dev.	Total Abnormal Dev.	Dead
4.3	3	No	$HgCl_2$	Cysteine	2	1d	29	21	1	7
4.3	1	No	$HgCl_2$	Glutathione	2	1d	27	26	0	1
4.3	2	No	$HgCl_2$	Glutathione	2	1d	30	30	0	0
4.3	3	No	$HgCl_2$	Glutathione	2	1d	29	24	0	5
4.3	1	Control	No	No	0	1d	28	28	0	0
4.3	2	Control	No	No	0	1d	24	23	0	1
4.3	3	Control	No	No	0	1d	26	19	0	7
4.3	1	No	$HgCl_2$	No	1	1d	30	24	6	0
4.3	2	No	$HgCl_2$	No	1	1d	25	21	0	4
4.3	3	No	$HgCl_2$	No	1	1d	35	12	7	16
4.3	1	No	$HgCl_2$	LA	1	1d	28	25	0	3
4.3	2	No	$HgCl_2$	LA	1	1d	37	30	0	7
4.3	3	No	$HgCl_2$	LA	1	1d	13	4	3	6
4.3	1	No	$HgCl_2$	DMPS	1	1d	29	29	0	0
4.3	2	No	$HgCl_2$	DMPS	1	1d	27	26	0	1
4.3	3	No	$HgCl_2$	DMPS	1	1d	25	18	0	7
4.3	1	No	$HgCl_2$	DMSA	1	1d	32	31	0	1
4.3	2	No	$HgCl_2$	DMSA	1	1d	32	30	0	2
4.3	3	No	$HgCl_2$	DMSA	1	1d	26	19	0	7
4.3	1	No	$HgCl_2$	Cysteine	1	1d	29	29	0	0
4.3	2	No	$HgCl_2$	Cysteine	1	1d	25	25	0	0
4.3	3	No	$HgCl_2$	Cysteine	1	1d	25	23	0	2
4.3	1	No	$HgCl_2$	Glutathione	1	1d	32	32	0	0
4.3	2	No	$HgCl_2$	Glutathione	1	1d	26	24	0	2
4.3	3	No	$HgCl_2$	Glutathione	1	1d	27	20	0	7
4.3	1	Control	No	No	0	1d	30	30	0	0

Experiment	Clutch	Control	Toxin	Chelator	Conc. (µM)	Time	Total Fish	Normal Dev.	Total Abnormal Dev.	Dead
4.3	2	Control	No	No	0	1d	36	34	0	2
4.3	3	Control	No	No	0	1d	26	25	1	0
4.3	1	No	$HgCl_2$	No	1	1d	38	37	0	1
4.3	2	No	$HgCl_2$	No	1	1d	43	42	0	1
4.3	3	No	$HgCl_2$	No	1	1d	24	23	0	1
4.3	1	No	$HgCl_2$	LA	1	1d	30	21	0	9
4.3	2	No	$HgCl_2$	LA	1	1d	38	32	1	5
4.3	3	No	$HgCl_2$	LA	1	1d	26	21	1	4
4.3	1	No	$HgCl_2$	DMPS	1	1d	30	29	0	1
4.3	2	No	$HgCl_2$	DMPS	1	1d	33	32	0	1
4.3	3	No	$HgCl_2$	DMPS	1	1d	30	29	0	1
4.3	1	No	$HgCl_2$	DMSA	1	1d	31	31	0	0
4.3	2	No	$HgCl_2$	DMSA	1	1d	40	36	0	4
4.3	3	No	$HgCl_2$	DMSA	1	1d	28	27	0	1
4.3	1	No	$HgCl_2$	Cysteine	1	1d	32	30	0	2
4.3	2	No	$HgCl_2$	Cysteine	1	1d	40	39	0	1
4.3	3	No	$HgCl_2$	Cysteine	1	1d	29	28	0	1
4.3	1	No	$HgCl_2$	Glutathione	1	1d	30	30	0	0
4.3	2	No	$HgCl_2$	Glutathione	1	1d	38	34	0	4
4.3	3	No	$HgCl_2$	Glutathione	1	1d	27	27	0	0
4.4	1	Control	No	No	0	1d	24	24	0	0
4.4	2	Control	No	No	0	1d	35	30	0	5
4.4	1	No	$CdCl_2$	No	80	1d	26	22	0	4
4.4	2	No	$CdCl_2$	No	80	1d	27	25	0	2
4.4	1	No	$PbCl_2$	No	120	1d	23	9	7	7
4.4	2	No	$PbCl_2$	No	120	1d	23	11	4	8

Experiment	Clutch	Control	Toxin	Chelator	Conc. (µM)	Time	Total Fish	Normal Dev.	Total Abnormal Dev.	Dead
4.4	1	No	$PbCl_2$	DMPS	120	1d	24	22	0	2
4.4	2	No	$PbCl_2$	DMPS	120	1d	24	20	1	3
4.4	1	No	$PbCl_2$	DMSA	120	1d	23	13	1	9
4.4	2	No	$PbCl_2$	DMSA	120	1d	23	19	0	4
4.4	1	No	$PbCl_2$	Cysteine	120	1d	25	24	0	1
4.4	2	No	$PbCl_2$	Cysteine	120	1d	25	22	1	2
4.4	1	No	$PbCl_2$	Glutathione	120	1d	23	17	0	6
4.4	2	No	$PbCl_2$	Glutathione	120	1d	26	18	1	7
4.5	3	Control	No	No	0	1d	20	20	0	0
4.5	4	Control	No	No	0	1d	21	16	0	5
4.5	3	No	$CdCl_2$	No	80	1d	24	22	0	2
4.5	4	No	$CdCl_2$	No	80	1d	21	19	0	2
4.5	3	No	$CdCl_2$	LA	80	1d	21	0	0	21
4.5	4	No	$CdCl_2$	LA	80	1d	22	0	0	22
4.5	3	No	$CdCl_2$	DMPS	80	1d	20	19	0	1
4.5	4	No	$CdCl_2$	DMPS	80	1d	20	19	0	1
4.5	3	No	$CdCl_2$	DMSA	80	1d	20	17	0	3
4.5	4	No	$CdCl_2$	DMSA	80	1d	22	20	0	2
4.5	3	No	$CdCl_2$	Cysteine	80	1d	21	21	0	0
4.5	4	No	$CdCl_2$	Cysteine	80	1d	23	22	0	1
4.5	3	No	$CdCl_2$	Glutathione	80	1d	20	19	0	1
4.5	4	No	$CdCl_2$	Glutathione	80	1d	22	22	0	0
4.5	1	Control	No	No	0	1d	21	18	0	3
4.5	2	Control	No	No	0	1d	20	18	0	2
4.5	1	No	$PbCl_2$	No	120	1d	19	18	0	1
4.5	2	No	$PbCl_2$	No	120	1d	21	13	1	7

Experiment	Clutch	Control	Toxin	Chelator	Conc. (µM)	Time	Total Fish	Normal Dev.	Total Abnormal Dev.	Dead
4.5	1	No	$PbCl_2$	LA	120	1d	21	0	0	21
4.5	2	No	$PbCl_2$	LA	120	1d	22	0	0	22
4.5	1	No	$PbCl_2$	DMPS	120	1d	21	20	0	1
4.5	2	No	$PbCl_2$	DMPS	120	1d	20	18	0	2
4.5	1	No	$PbCl_2$	DMSA	120	1d	21	7	1	13
4.5	2	No	$PbCl_2$	DMSA	120	1d	20	19	0	1
4.5	1	No	$PbCl_2$	Cysteine	120	1d	22	22	0	0
4.5	2	No	$PbCl_2$	Cysteine	120	1d	22	19	0	3
4.5	1	No	$PbCl_2$	Glutathione	120	1d	24	23	0	1
4.5	2	No	$PbCl_2$	Glutathione	120	1d	21	16	0	5
4.6	1	Control	No	No	0	1d	24	24	0	0
4.6	1	No	$CdCl_2$	No	150	1d	24	16	2	6
4.6	1	No	$CdCl_2$	LA	150	1d	23	0	0	23
4.6	1	No	$CdCl_2$	DMPS	150	1d	26	22	4	0
4.6	1	No	$CdCl_2$	DMSA	150	1d	32	24	2	6
4.6	1	No	$CdCl_2$	Cysteine	150	1d	24	21	1	2
4.6	1	No	$CdCl_2$	Glutathione	150	1d	23	21	1	1
4.6	1	No	$CdCl_2$	No	200	1d	24	14	1	9
4.6	1	No	$CdCl_2$	No	120	1d	24	15	3	6
4.7	1	Control	No	No	0	1d	26	26	0	0
4.7	2	Control	No	No	0	1d	30	24	0	6
4.7	3	Control	No	No	0	1d	23	22	0	1
4.7	1	No	$CdCl_2$	No	80	1d	26	26	0	0
4.7	2	No	$CdCl_2$	No	80	1d	32	21	0	11
4.7	3	No	$CdCl_2$	No	80	1d	17	17	0	0
4.7	1	No	$CdCl_2$	LA	80	1d	20	0	0	20

Experiment	Clutch	Control	Toxin	Chelator	Conc. (µM)	Time	Total Fish	Normal Dev.	Total Abnormal Dev.	Dead
4.7	2	No	$CdCl_2$	LA	80	1d	26	0	0	26
4.7	1	No	$CdCl_2$	DMPS	80	1d	26	26	0	0
4.7	2	No	$CdCl_2$	DMPS	80	1d	24	18	0	6
4.7	3	No	$CdCl_2$	DMPS	80	1d	21	20	0	1
4.7	1	No	$CdCl_2$	DMSA	80	1d	28	28	0	0
4.7	2	No	$CdCl_2$	DMSA	80	1d	21	16	0	5
4.7	3	No	$CdCl_2$	DMSA	80	1d	20	20	0	0
4.7	1	No	$CdCl_2$	Cysteine	80	1d	26	24	0	2
4.7	2	No	$CdCl_2$	Cysteine	80	1d	25	20	0	5
4.7	3	No	$CdCl_2$	Cysteine	80	1d	21	21	0	0
4.7	1	No	$CdCl_2$	Glutathione	80	1d	26	26	0	0
4.7	2	No	$CdCl_2$	Glutathione	80	1d	32	24	0	8
4.7	3	No	$CdCl_2$	Glutathione	80	1d	20	20	0	0
4.8	1	Control	No	No	0	1d	40	40	0	0
4.8	2	Control	No	No	0	1d	38	37	0	1
4.8	3	Control	No	No	0	1d	20	20	0	0
4.8	1	No	$CdCl_2$	No	80	1d	36	35	0	1
4.8	2	No	$CdCl_2$	No	80	1d	35	35	0	0
4.8	3	No	$CdCl_2$	No	80	1d	20	20	0	0
4.8	1	No	$CdCl_2$	LA	80	1d	40	0	0	40
4.8	2	No	$CdCl_2$	LA	80	1d	37	0	0	37
4.8	3	No	$CdCl_2$	LA	80	1d	20	0	0	20
4.8	1	No	$CdCl_2$	DMPS	80	1d	29	28	0	1
4.8	2	No	$CdCl_2$	DMPS	80	1d	29	29	0	0
4.8	3	No	$CdCl_2$	DMPS	80	1d	25	25	0	0
4.8	1	No	$CdCl_2$	DMSA	80	1d	29	25	0	4

Experiment	Clutch	Control	Toxin	Chelator	Conc. (µM)	Time	Total Fish	Normal Dev.	Total Abnormal Dev.	Dead
4.8	2	No	$CdCl_2$	DMSA	80	1d	30	30	0	0
4.8	3	No	$CdCl_2$	DMSA	80	1d	20	19	0	1
4.8	1	No	$CdCl_2$	Cysteine	80	1d	29	28	0	1
4.8	2	No	$CdCl_2$	Cysteine	80	1d	25	25	0	0
4.8	3	No	$CdCl_2$	Cysteine	80	1d	18	18	0	0
4.8	1	No	$CdCl_2$	Glutathione	80	1d	29	29	0	0
4.8	2	No	$CdCl_2$	Glutathione	80	1d	27	27	0	0
4.8	3	No	$CdCl_2$	Glutathione	80	1d	20	20	0	0
4.9	1	Control	No	No	0	1d	29	27	0	2
4.9	2	Control	No	No	0	1d	20	19	0	1
4.9	3	Control	No	No	0	1d	34	33	0	1
4.9	1	No	$PbCl_2$	No	120	1d	36	36	0	0
4.9	2	No	$PbCl_2$	No	120	1d	20	14	0	6
4.9	3	No	$PbCl_2$	No	120	1d	35	29	2	4
4.9	1	No	$PbCl_2$	LA	120	1d	33	0	0	33
4.9	2	No	$PbCl_2$	LA	120	1d	35	0	0	35
4.9	1	No	$PbCl_2$	DMPS	120	1d	34	34	0	0
4.9	2	No	$PbCl_2$	DMPS	120	1d	22	21	0	1
4.9	3	No	$PbCl_2$	DMPS	120	1d	35	34	0	1
4.9	1	No	$PbCl_2$	DMSA	120	1d	36	33	0	3
4.9	2	No	$PbCl_2$	DMSA	120	1d	20	16	0	4
4.9	3	No	$PbCl_2$	DMSA	120	1d	35	31	0	4
4.9	1	No	$PbCl_2$	Cysteine	120	1d	36	36	0	0
4.9	2	No	$PbCl_2$	Cysteine	120	1d	20	16	0	4
4.9	3	No	$PbCl_2$	Cysteine	120	1d	34	33	0	1
4.9	1	No	$PbCl_2$	Glutathione	120	1d	38	34	0	4

Experiment	Clutch	Control	Toxin	Chelator	Conc. (µM)	Time	Total Fish	Normal Dev.	Total Abnormal Dev.	Dead
4.9	2	No	$PbCl_2$	Glutathione	120	1d	23	21	0	2
4.9	3	No	$PbCl_2$	Glutathione	120	1d	37	34	0	3
4.10	1	Control	No	No	0	1d	28	28	0	0
4.10	2	Control	No	No	0	1d	25	25	0	0
4.10	3	Control	No	No	0	1d	26	25	0	1
4.10	1	No	$PbCl_2$	No	120	1d	23	11	12	0
4.10	2	No	$PbCl_2$	No	120	1d	36	33	2	1
4.10	3	No	$PbCl_2$	No	120	1d	33	29	0	4
4.10	1	No	$PbCl_2$	DMPS	120	1d	26	11	13	2
4.10	2	No	$PbCl_2$	DMPS	120	1d	35	34	0	1
4.10	3	No	$PbCl_2$	DMPS	120	1d	31	30	0	1
4.10	1	No	$PbCl_2$	DMSA	120	1d	23	9	10	4
4.10	2	No	$PbCl_2$	DMSA	120	1d	41	37	0	4
4.10	3	No	$PbCl_2$	DMSA	120	1d	34	31	0	3
4.10	1	No	$PbCl_2$	Cysteine	120	1d	23	10	9	4
4.10	2	No	$PbCl_2$	Cysteine	120	1d	39	37	0	2
4.10	3	No	$PbCl_2$	Cysteine	120	1d	32	30	0	2
4.10	1	No	$PbCl_2$	Glutathione	120	1d	23	11	11	1
4.10	2	No	$PbCl_2$	Glutathione	120	1d	35	33	0	2
4.10	3	No	$PbCl_2$	Glutathione	120	1d	36	35	0	1

Supplementary Information for Part Two

Contents

Figure S2.13: Superimposed ^{1}H HR-MAS NMR spectrum of DPPC:R2 MLVs. Acquisition parameters: pulse program noesypr1d (Bruker library), 32767 TD data points, 32 scans, 7002.801 Hz spectral width, acquisition time 2.34 s, relaxation delay 4 s.

Figure S2.14: Superimposed ^{1}H HR-MAS NMR spectrum of DPPC:Ru3 MLVs. Acquisition parameters: pulse program noesypr1d (Bruker library), 32767 TD data points, 32 scans, 7002.801 Hz spectral width, acquisition time 2.34 s, relaxation delay 4 s.

Figure S2.15: Superimposed ^{1}H HR-MAS NMR spectrum of DPPC:Ru4 MLVs. Acquisition parameters: pulse program noesypr1d (Bruker library), 32767 TD data points, 32 scans, 7002.801 Hz spectral width, acquisition time 2.34 s, relaxation delay 4 s.

Figure S2.16: Superimposed ^{1}H HR-MAS NMR spectrum of DPPC:Ru5 MLVs. Acquisition parameters: pulse program noesypr1d (Bruker library), 32767 TD data points, 32 scans, 7002.801 Hz spectral width, acquisition time 2.34 s, relaxation delay 4 s.

Figure S2.17: Superimposed ^{1}H HR-MAS NMR spectrum of DPPC:Ru6 MLVs. Acquisition parameters: pulse program noesypr1d (Bruker library), 32767 TD data points, 32 scans, 7002.801 Hz spectral width, acquisition time 2.34 s, relaxation delay 4 s.

Figure S2.18: 2D NOESY NMR spectra of DOPC:Ru2 MLVs. Acquisition parameters: pulse program noesyph (Bruker library), 16 scans, relaxation delay 2 s, mixing time 100 ms.

Figure S2.19: 2D NOESY NMR spectra of DOPC:Ru3 MLVs. Acquisition parameters: pulse program noesyph (Bruker library), 16 scans, relaxation delay 2 s, mixing time 100 ms.

Figure S2.20: 2D NOESY NMR spectra of DOPC:Ru4 MLVs. Acquisition parameters: pulse program noesyph (Bruker library), 16 scans, relaxation delay 2 s, mixing time 100 ms.

Figure S2.21: 2D NOESY NMR spectra of DOPC:Ru5 MLVs. Acquisition parameters: pulse program noesyph (Bruker library), 16 scans, relaxation delay 2 s, mixing time 100 ms.

Figure S2.22: 2D NOESY NMR spectra of DOPC:Ru6 MLVs. Acquisition parameters: pulse program noesyph (Bruker library), 16 scans, relaxation delay 2 s, mixing time 100 ms.

Figure S2.23: 2D NOESY NMR spectra of POPC:Ru1 MLVs. Acquisition parameters: pulse program noesyph (Bruker library), 16 scans, relaxation delay 2 s, mixing time 100 ms.

Figure S2.24: 2D NOESY NMR spectra of POPC:Ru2 MLVs. Acquisition parameters: pulse program noesyph (Bruker library), 16 scans, relaxation delay 2 s, mixing time 100 ms.

Figure S2.25: 2D NOESY NMR spectra of POPC:Ru3 MLVs. Acquisition parameters: pulse program noesyph (Bruker library), 16 scans, relaxation delay 2 s, mixing time 100 ms.

Figure S2.26: 2D NOESY NMR spectra of POPC:Ru4 MLVs. Acquisition parameters: pulse program noesyph (Bruker library), 16 scans, relaxation delay 2 s, mixing time 100 ms.

Figure S2.27: 2D NOESY NMR spectra of POPC:Ru5 MLVs. Acquisition parameters: pulse program noesyph (Bruker library), 16 scans, relaxation delay 2 s, mixing time 100 ms.

Figure S2.28: 2D NOESY NMR spectra of POPC:Ru6 MLVs. Acquisition parameters: pulse program noesyph (Bruker library), 16 scans, relaxation delay 2 s, mixing time 100 ms.

Figure S2.29: 2D NOESY NMR spectra of DPPC:Ru1 MLVs. Acquisition parameters: pulse program noesyph (Bruker library), 16 scans, relaxation delay 2 s, mixing time 100 ms.

Figure S2.30: 2D NOESY NMR spectra of DPPC:Ru2 MLVs. Acquisition parameters: pulse program noesyph (Bruker library), 16 scans, relaxation delay 2 s, mixing time 100 ms.

Figure S2.31: 2D NOESY NMR spectra of DPPC:Ru3 MLVs. Acquisition parameters: pulse program noesyph (Bruker library), 16 scans, relaxation delay 2 s, mixing time 100 ms.

Figure S2.32: 2D NOESY NMR spectra of DPPC:Ru4 MLVs. Acquisition parameters: pulse program noesyph (Bruker library), 16 scans, relaxation delay 2 s, mixing time 100 ms.

Figure S2.33: 2D NOESY NMR spectra of DPPC:Ru5 MLVs. Acquisition parameters: pulse program noesyph (Bruker library), 16 scans, relaxation delay 2 s, mixing time 100 ms.

Figure S2.34: 2D NOESY NMR spectra of DPPC:Ru6 MLVs. Acquisition parameters: pulse program noesyph (Bruker library), 16 scans, relaxation delay 2 s, mixing time 100 ms.

Figure S2.35: Overlay of ^{1}H DOSY NMR spectra of DOPC and DOPC:Ru2 MLVs. Acquisition parameters: pulse program ledbpcpgp2scprol.bi (Bruker library), 16 scans, relaxation delay 2 s.

Figure S2.36: Overlay of ^{1}H DOSY NMR spectra of DOPC and DOPC:Ru3 MLVs. Acquisition parameters: pulse program ledbpcpgp2scprol.bi (Bruker library), 16 scans, relaxation delay 2 s.

Figure S2.37: Overlay of ^{1}H DOSY NMR spectra of DOPC and DOPC:Ru4 MLVs. Acquisition parameters: pulse program ledbpcpgp2scprol.bi (Bruker library), 16 scans, relaxation delay 2 s.

Figure S2.38: Overlay of ^{1}H DOSY NMR spectra of DOPC and DOPC:Ru5 MLVs. Acquisition parameters: pulse program ledbpcpgp2scprol.bi (Bruker library), 16 scans, relaxation delay 2 s.

Figure S2.39: Overlay of ^{1}H DOSY NMR spectra of DOPC and DOPC:Ru6 MLVs. Acquisition parameters: pulse program ledbpcpgp2scprol.bi (Bruker library), 16 scans, relaxation delay 2 s.

Figure S2.40: Overlay of ^{1}H DOSY NMR spectra of POPC and POPC:Ru1 MLVs. Acquisition parameters: pulse program ledbpcpgp2scprol.bi (Bruker library), 16 scans, relaxation delay 2 s.

Figure S2.41: Overlay of ^{1}H DOSY NMR spectra of POPC and POPC:Ru2 MLVs. Acquisition parameters: pulse program ledbpcpgp2scprol.bi (Bruker library), 16 scans, relaxation delay 2 s.

Figure S2.42: Overlay of ^{1}H DOSY NMR spectra of POPC and POPC:Ru3 MLVs. Acquisition parameters: pulse program ledbpcpgp2scprol.bi (Bruker library), 16 scans, relaxation delay 2 s.

Figure S2.43: Overlay of ^{1}H DOSY NMR spectra of POPC and POPC:Ru4 MLVs. Acquisition parameters: pulse program ledbpcpgp2scprol.bi (Bruker library), 16 scans, relaxation delay 2 s.

Figure S2.44: Overlay of ^{1}H DOSY NMR spectra of POPC and POPC:Ru5 MLVs. Acquisition parameters: pulse program ledbpcpgp2scprol.bi (Bruker library), 16 scans, relaxation delay 2 s.

Figure S2.45: Overlay of ^{1}H DOSY NMR spectra of POPC and POPC:Ru6 MLVs. Acquisition parameters: pulse program ledbpcpgp2scprol.bi (Bruker library), 16 scans, relaxation delay 2 s.

Figure S2.46: Overlay of ^{1}H DOSY NMR spectra of DPPC and DPPC:Ru1 MLVs. Acquisition parameters: pulse program ledbpcpgp2scprol.bi (Bruker library), 16 scans, relaxation delay 2 s.

Figure S2.47: Overlay of ^{1}H DOSY NMR spectra of DPPC and DPPC:Ru2 MLVs. Acquisition parameters: pulse program ledbpcpgp2scprol.bi (Bruker library), 16 scans, relaxation delay 2 s.

Figure S2.48: Overlay of ^{1}H DOSY NMR spectra of DPPC and DPPC:Ru3 MLVs. Acquisition parameters: pulse program ledbpcpgp2scprol.bi (Bruker library), 16 scans, relaxation delay 2 s.

Figure S2.49: Overlay of ^{1}H DOSY NMR spectra of DPPC and DPPC:Ru4 MLVs. Acquisition parameters: pulse program ledbpcpgp2scprol.bi (Bruker library), 16 scans, relaxation delay 2 s.

Figure S2.50: Overlay of ^{1}H DOSY NMR spectra of DPPC and DPPC:Ru5 MLVs. Acquisition parameters: pulse program ledbpcpgp2scprol.bi (Bruker library), 16 scans, relaxation delay 2 s.

Figure S2.51: Overlay of ^{1}H DOSY NMR spectra of DPPC and DPPC:Ru6 MLVs. Acquisition parameters: pulse program ledbpcpgp2scprol.bi (Bruker library), 16 scans, relaxation delay 2 s.

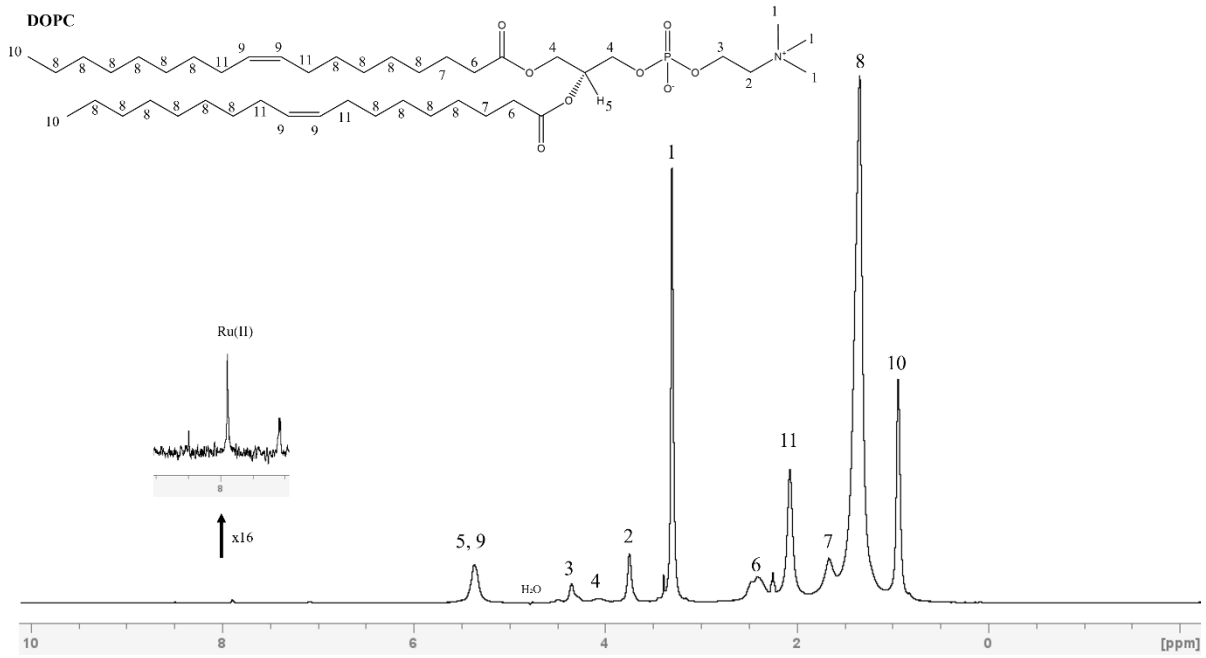

Figure S2.1: Superimposed ^{1}H HR-MAS NMR spectrum spectra of DOPC:Ru2 MLVs. Acquisition parameters: pulse program noesypr1d (Bruker library), 32767 TD data points, 32 scans, 7002.801 Hz spectral width, acquisition time 2.34 s, relaxation delay 4 s.

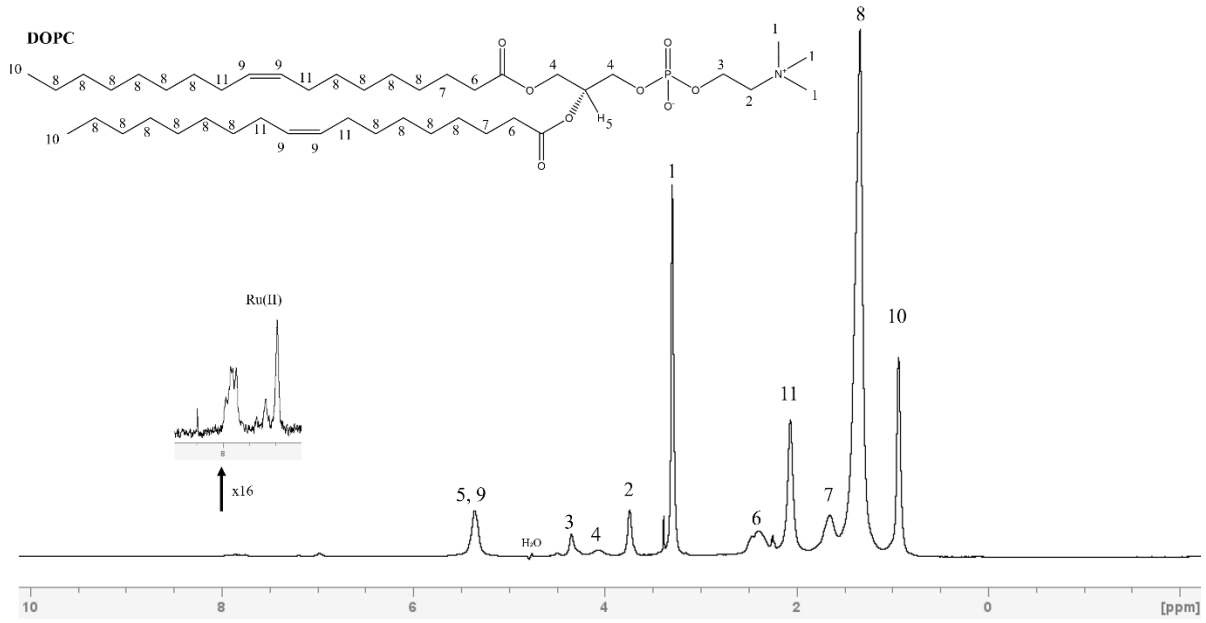

Figure S2.2: Superimposed ^{1}H HR-MAS NMR spectrum of DOPC:Ru3 MLVs. Acquisition parameters: pulse program noesypr1d (Bruker library), 32767 TD data points, 32 scans, 7002.801 Hz spectral width, acquisition time 2.34 s, relaxation delay 4 s.

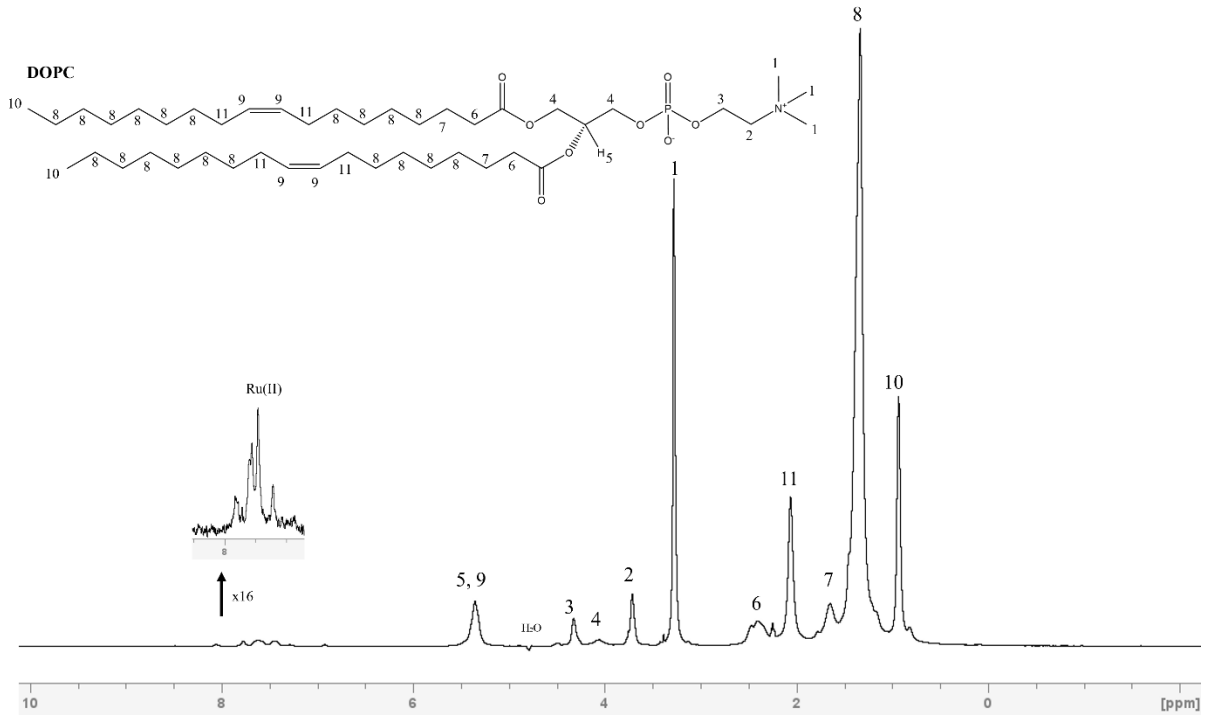

Figure S2.3: Superimposed ^{1}H HR-MAS NMR spectrum of DOPC:Ru4 MLVs. Acquisition parameters: pulse program noesypr1d (Bruker library), 32767 TD data points, 32 scans, 7002.801 Hz spectral width, acquisition time 2.34 s, relaxation delay 4 s.

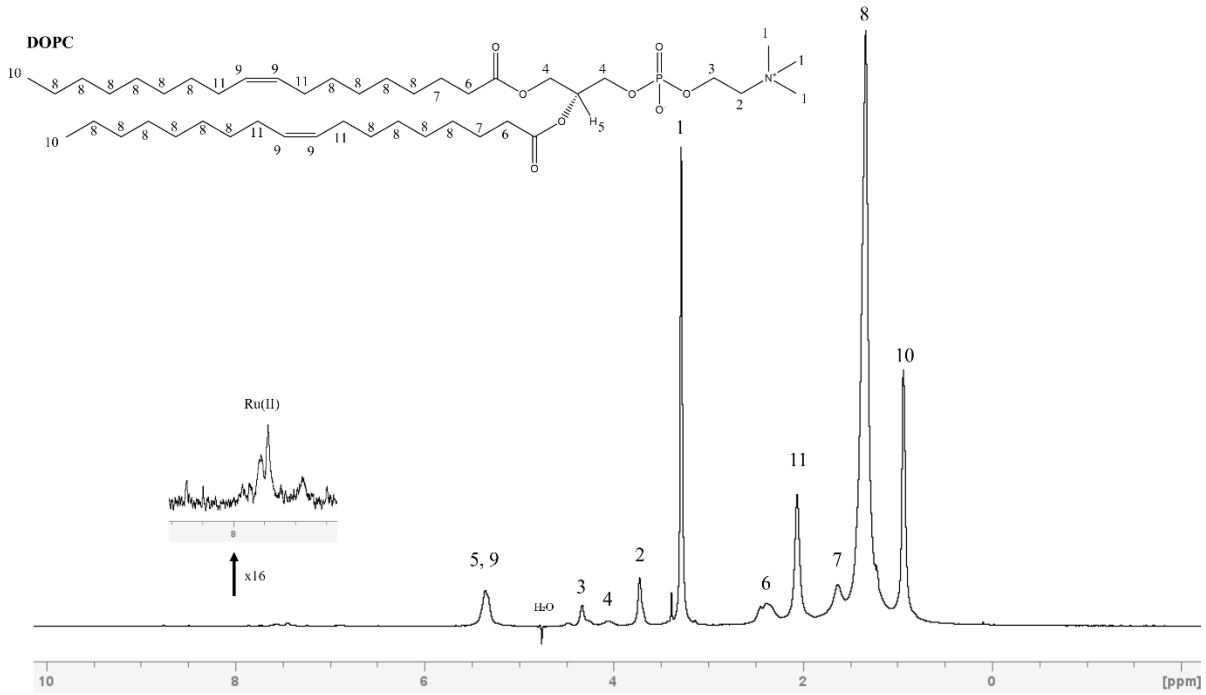

Figure S2.4: Superimposed ^{1}H HR-MAS NMR spectrum of DOPC:Ru5 MLVs. Acquisition parameters: pulse program noesypr1d (Bruker library), 32767 TD data points, 32 scans, 7002.801 Hz spectral width, acquisition time 2.34 s, relaxation delay 4 s.

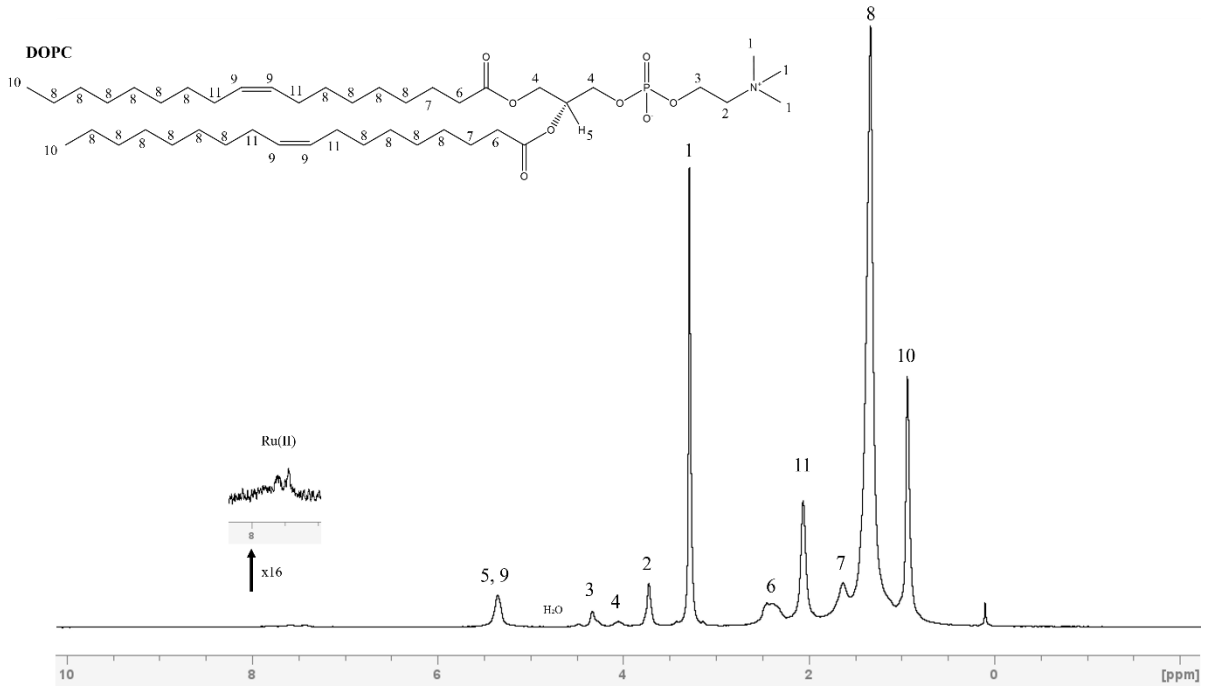

Figure S2.5: Superimposed ^{1}H HR-MAS NMR spectrum of DOPC:Ru6 MLVs. Acquisition parameters: pulse program noesypr1d (Bruker library), 32767 TD data points, 32 scans, 7002.801 Hz spectral width, acquisition time 2.34 s, relaxation delay 4 s.

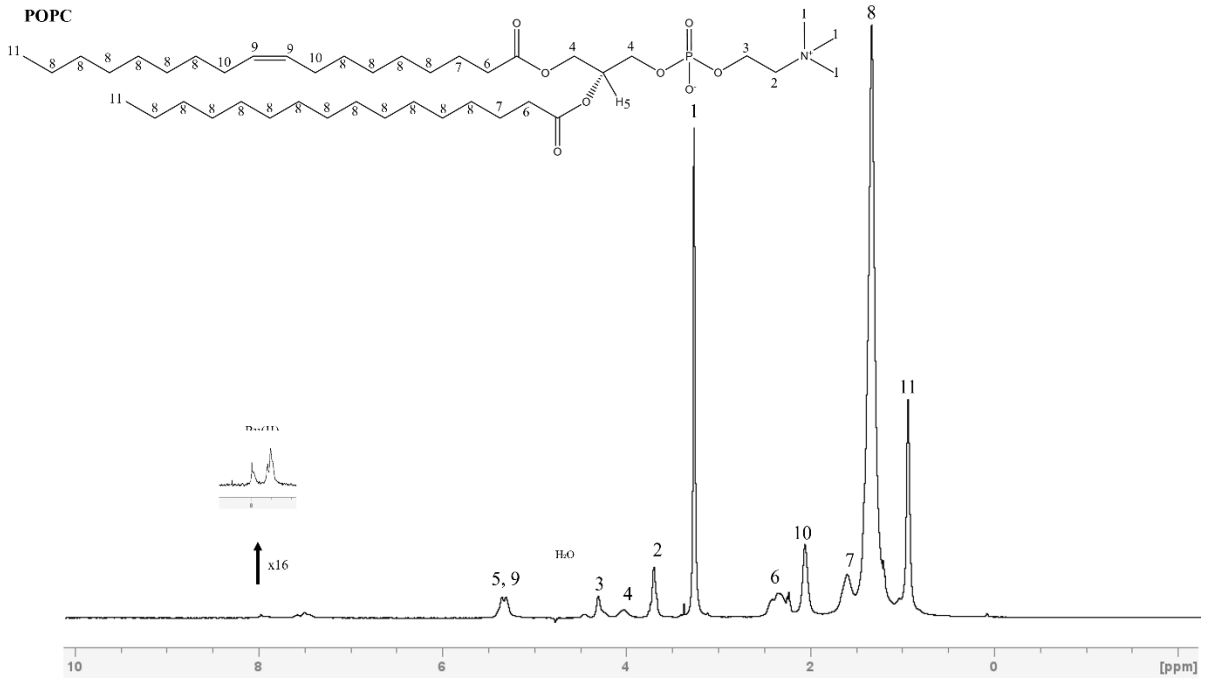

Figure S2.6: Superimposed ^{1}H HR-MAS NMR spectrum of POPC:Ru1 MLVs. Acquisition parameters: pulse program noesypr1d (Bruker library), 32767 TD data points, 32 scans, 7002.801 Hz spectral width, acquisition time 2.34 s, relaxation delay 4 s.

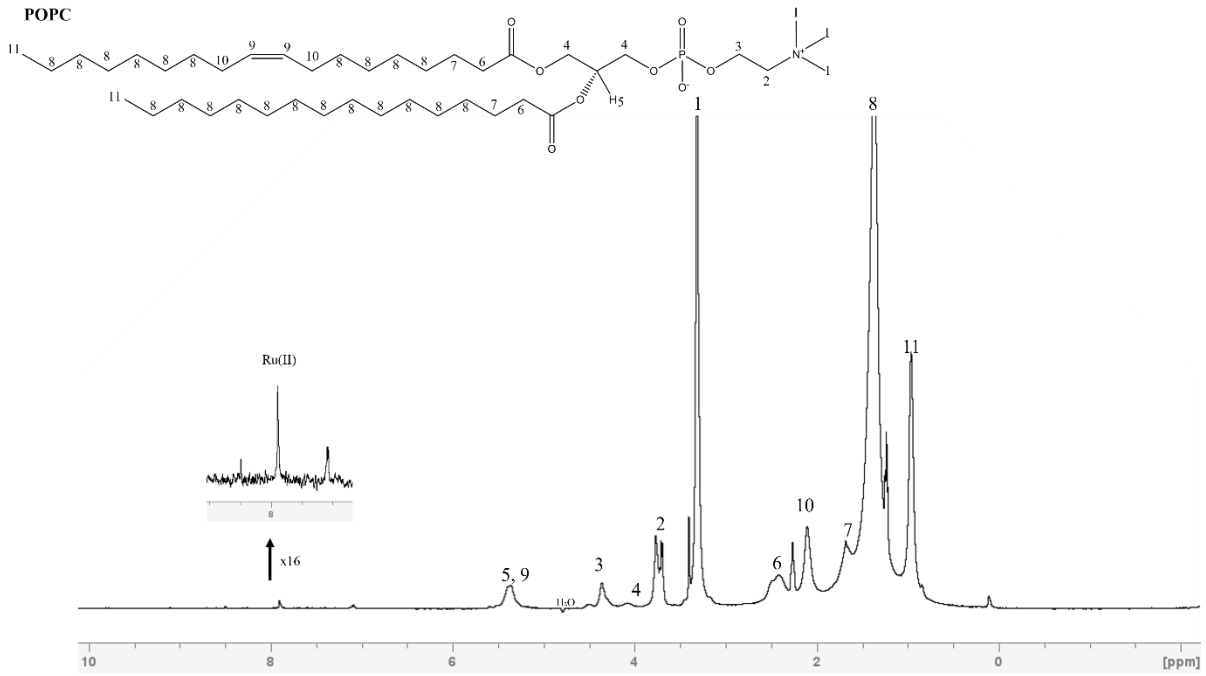

Figure S2.7: Superimposed ^{1}H HR-MAS NMR spectrum of POPC:R2 MLVs. Acquisition parameters: pulse program noesypr1d (Bruker library), 32767 TD data points, 32 scans, 7002.801 Hz spectral width, acquisition time 2.34 s, relaxation delay 4 s.

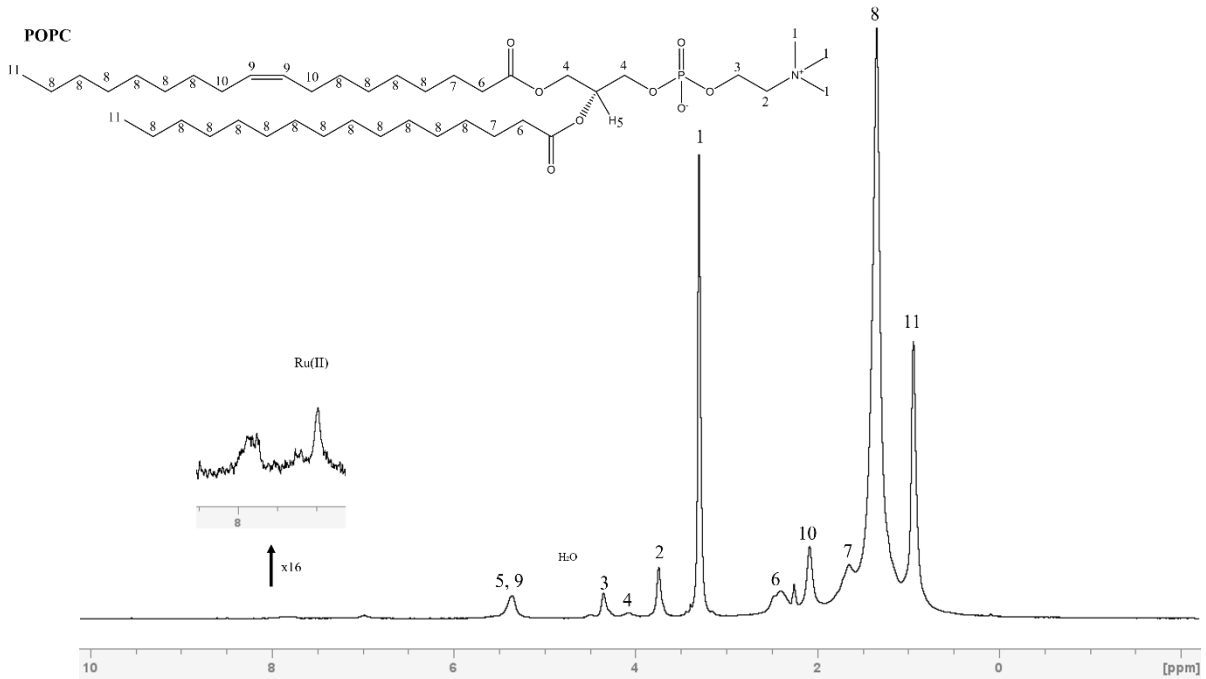

Figure S2.8: Superimposed ^{1}H HR-MAS NMR spectrum of POPC:Ru3 MLVs. Acquisition parameters: pulse program noesypr1d (Bruker library), 32767 TD data points, 32 scans, 7002.801 Hz spectral width, acquisition time 2.34 s, relaxation delay 4 s.

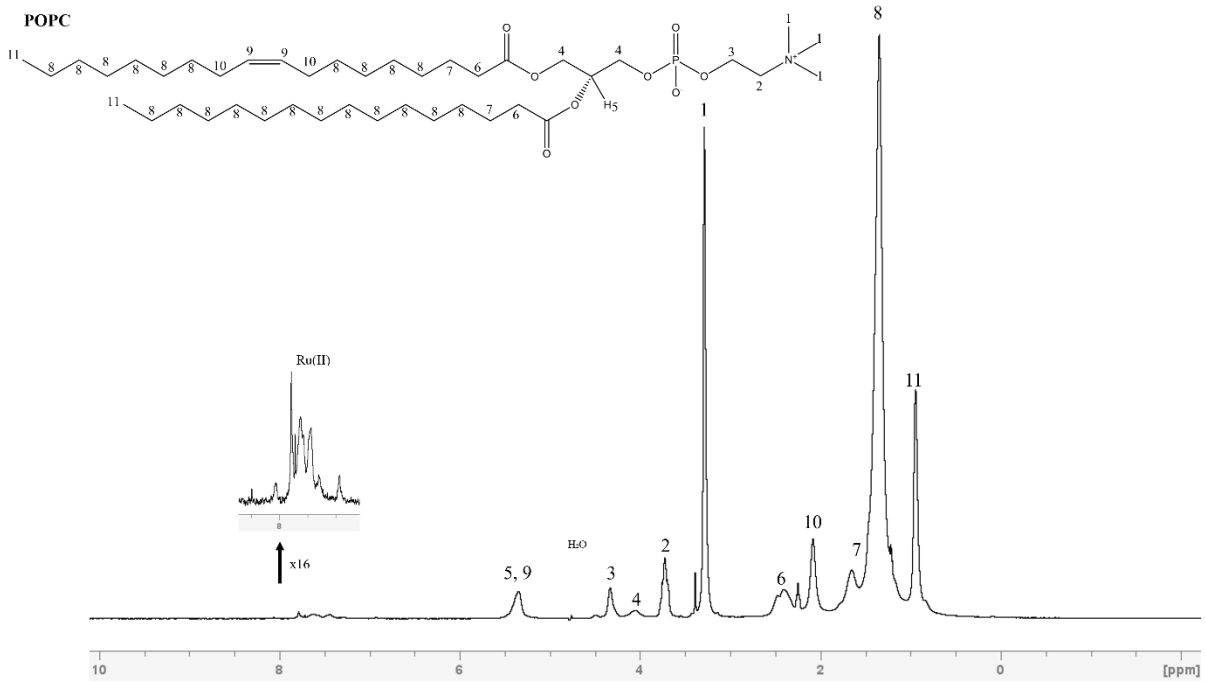

Figure S2.9: Superimposed ^{1}H HR-MAS NMR spectrum of POPC:Ru4 MLVs. Acquisition parameters: pulse program noesypr1d (Bruker library), 32767 TD data points, 32 scans, 7002.801 Hz spectral width, acquisition time 2.34 s, relaxation delay 4 s.

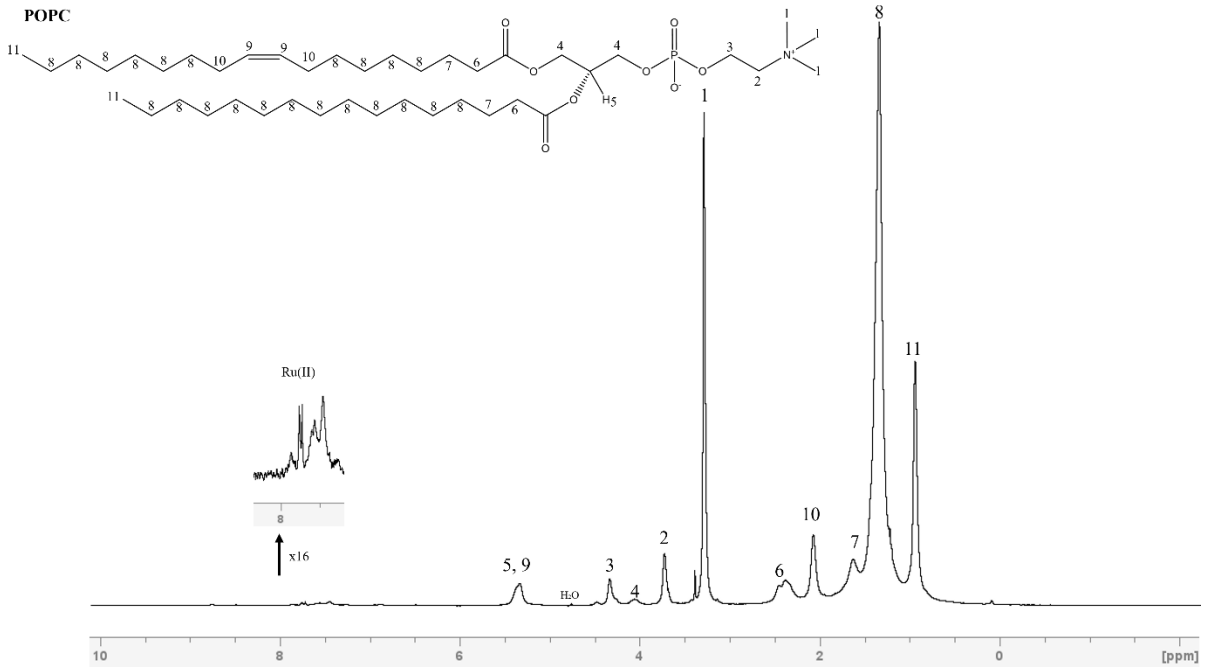

Figure S2.10: Superimposed ^{1}H HR-MAS NMR spectrum of POPC:Ru5 MLVs. Acquisition parameters: pulse program noesypr1d (Bruker library), 32767 TD data points, 32 scans, 7002.801 Hz spectral width, acquisition time 2.34 s, relaxation delay 4 s.

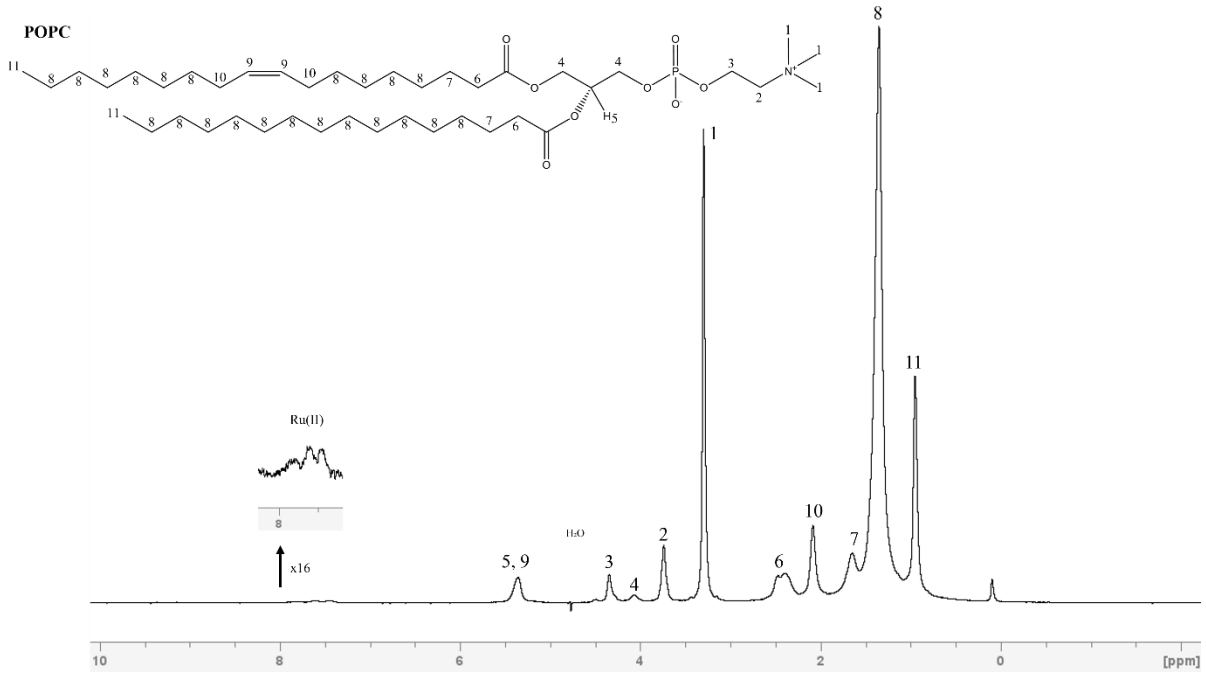

Figure S2.11: Superimposed ^{1}H HR-MAS NMR spectrum of POPC:Ru6 MLVs. Acquisition parameters: pulse program noesypr1d (Bruker library), 32767 TD data points, 32 scans, 7002.801 Hz spectral width, acquisition time 2.34 s, relaxation delay 4 s.

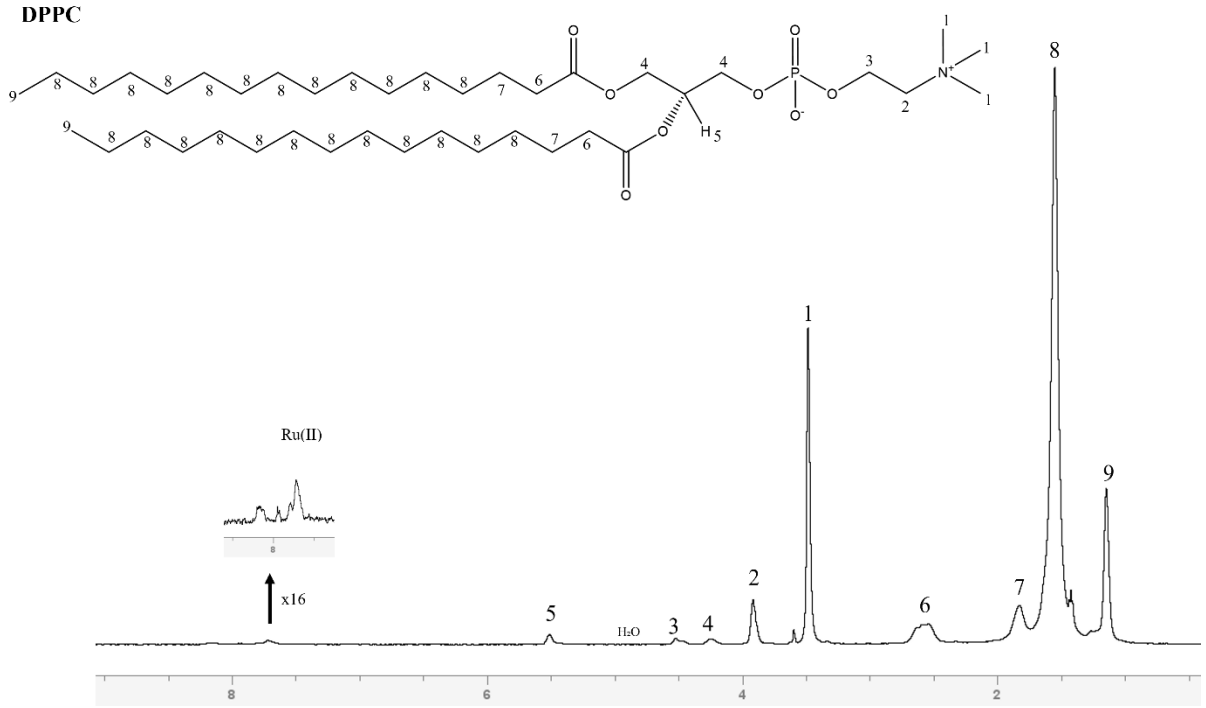

Figure S2.12: Superimposed ^{1}H HR-MAS NMR spectrum of DPPC:Ru1 MLVs. Acquisition parameters: pulse program noesypr1d (Bruker library), 32767 TD data points, 32 scans, 7002.801 Hz spectral width, acquisition time 2.34 s, relaxation delay 4 s.

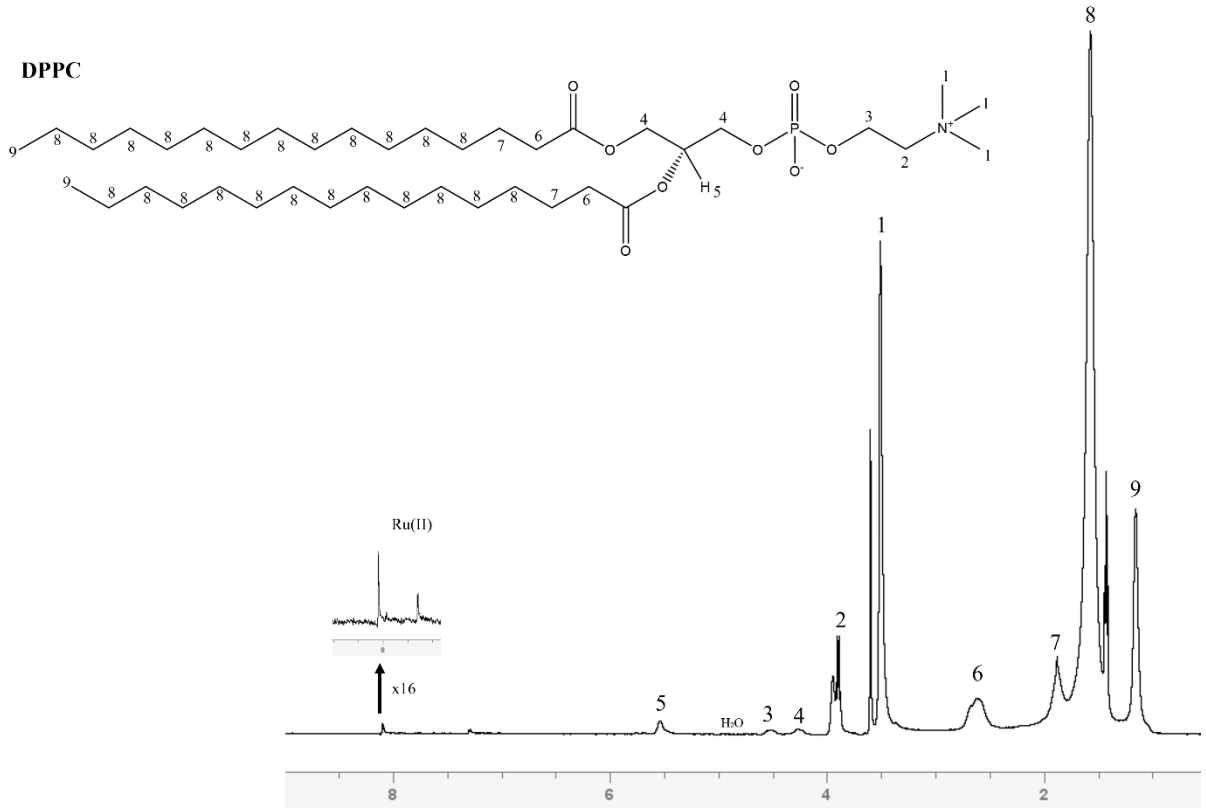

Figure S2.13: Superimposed ^{1}H HR-MAS NMR spectrum of DPPC:R2 MLVs. Acquisition parameters: pulse program noesypr1d (Bruker library), 32767 TD data points, 32 scans, 7002.801 Hz spectral width, acquisition time 2.34 s, relaxation delay 4 s.

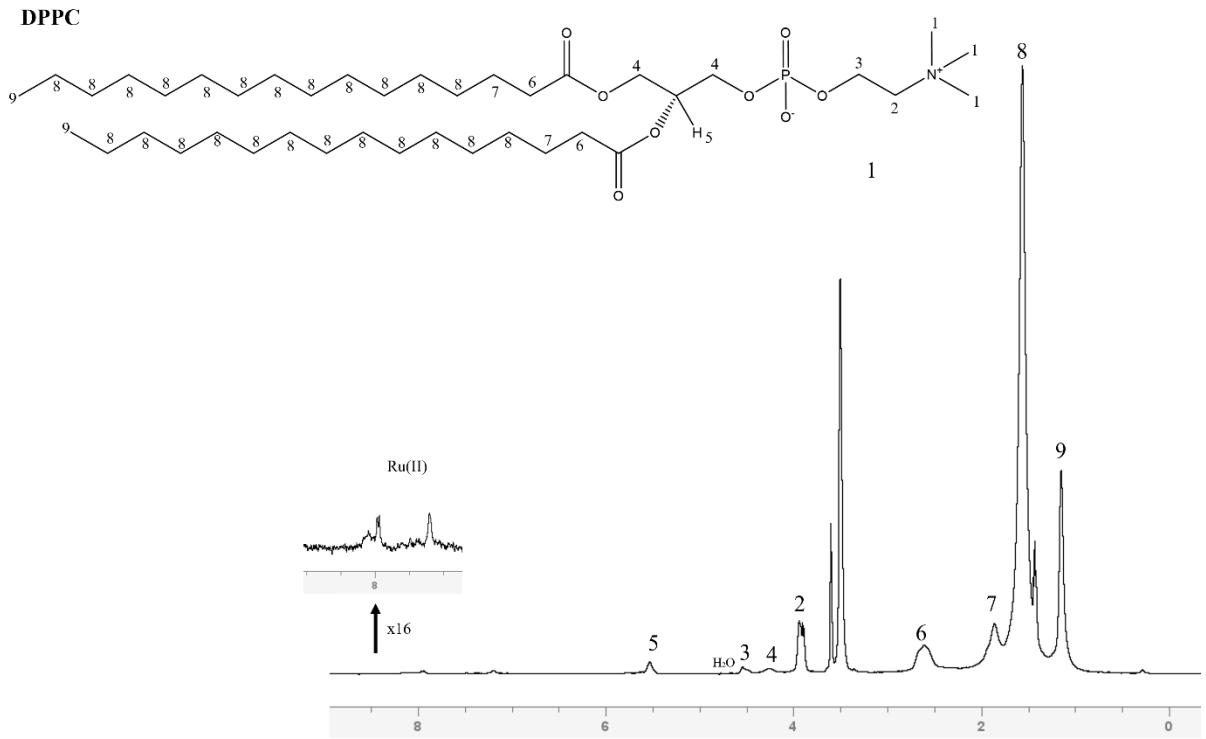

Figure S2.14: Superimposed ^{1}H HR-MAS NMR spectrum of DPPC:Ru3 MLVs. Acquisition parameters: pulse program noesypr1d (Bruker library), 32767 TD data points, 32 scans, 7002.801 Hz spectral width, acquisition time 2.34 s, relaxation delay 4 s.

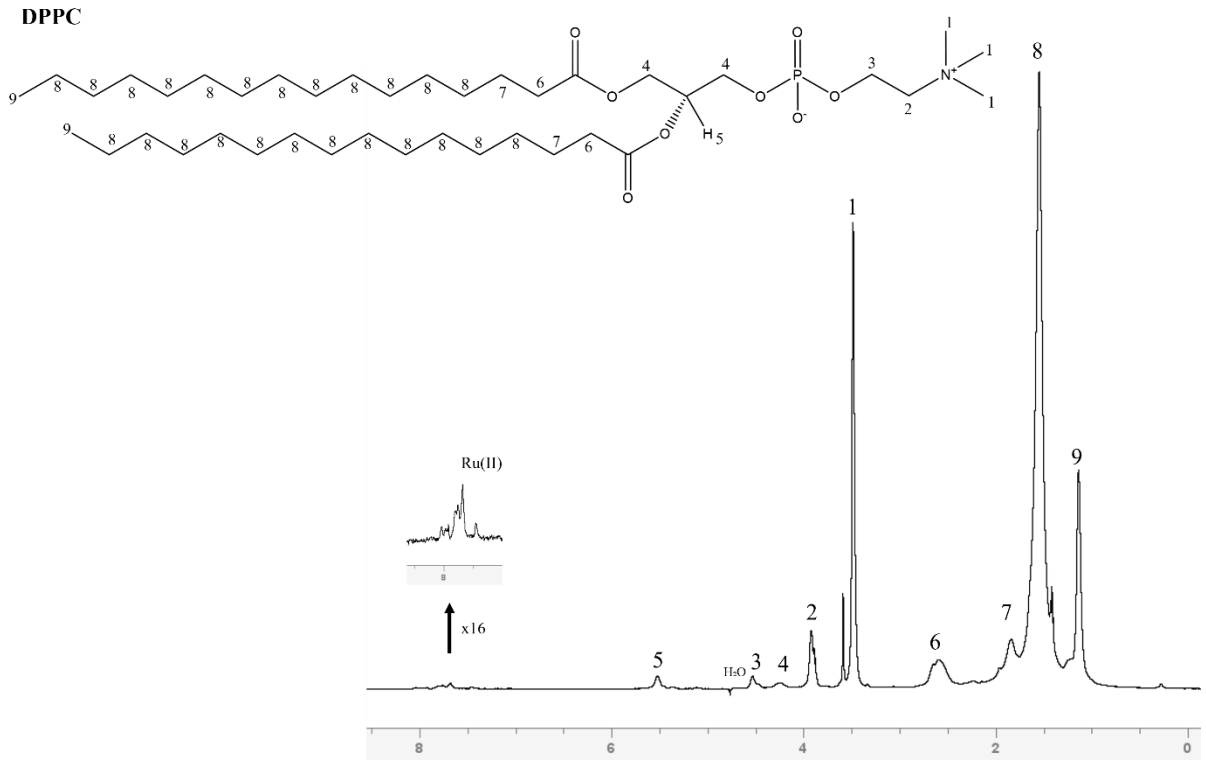

Figure S2.15: Superimposed ^{1}H HR-MAS NMR spectrum of DPPC:Ru4 MLVs. Acquisition parameters: pulse program noesypr1d (Bruker library), 32767 TD data points, 32 scans, 7002.801 Hz spectral width, acquisition time 2.34 s, relaxation delay 4 s.

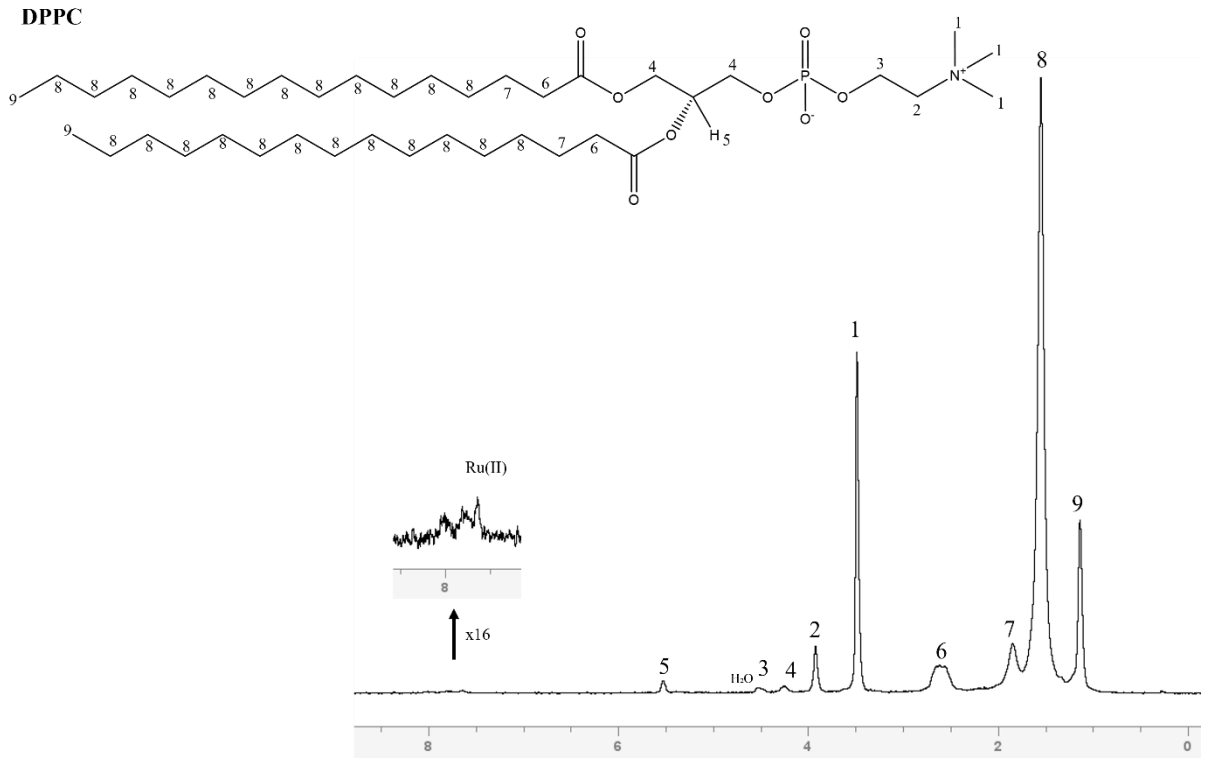

Figure S2.16: Superimposed ^{1}H HR-MAS NMR spectrum of DPPC:Ru5 MLVs. Acquisition parameters: pulse program noesypr1d (Bruker library), 32767 TD data points, 32 scans, 7002.801 Hz spectral width, acquisition time 2.34 s, relaxation delay 4 s.

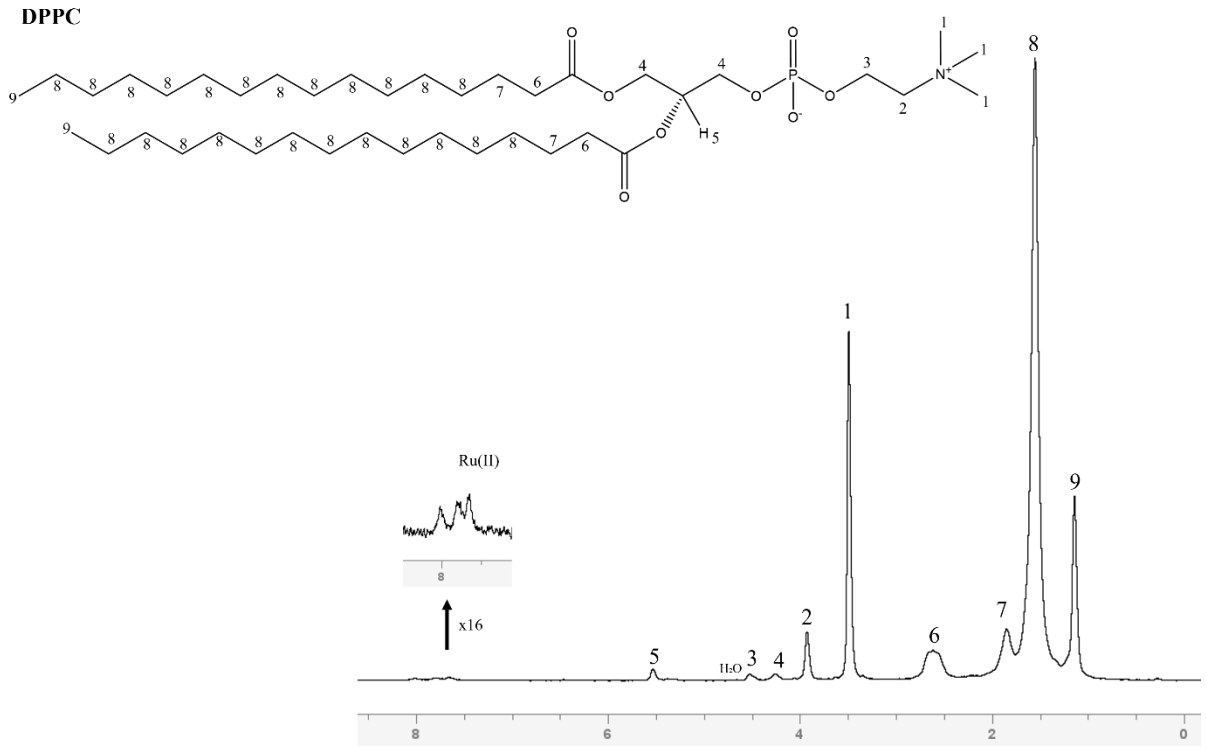

Figure S2.17: Superimposed ^{1}H HR-MAS NMR spectrum of DPPC:Ru6 MLVs. Acquisition parameters: pulse program noesypr1d (Bruker library), 32767 TD data points, 32 scans, 7002.801 Hz spectral width, acquisition time 2.34 s, relaxation delay 4 s.

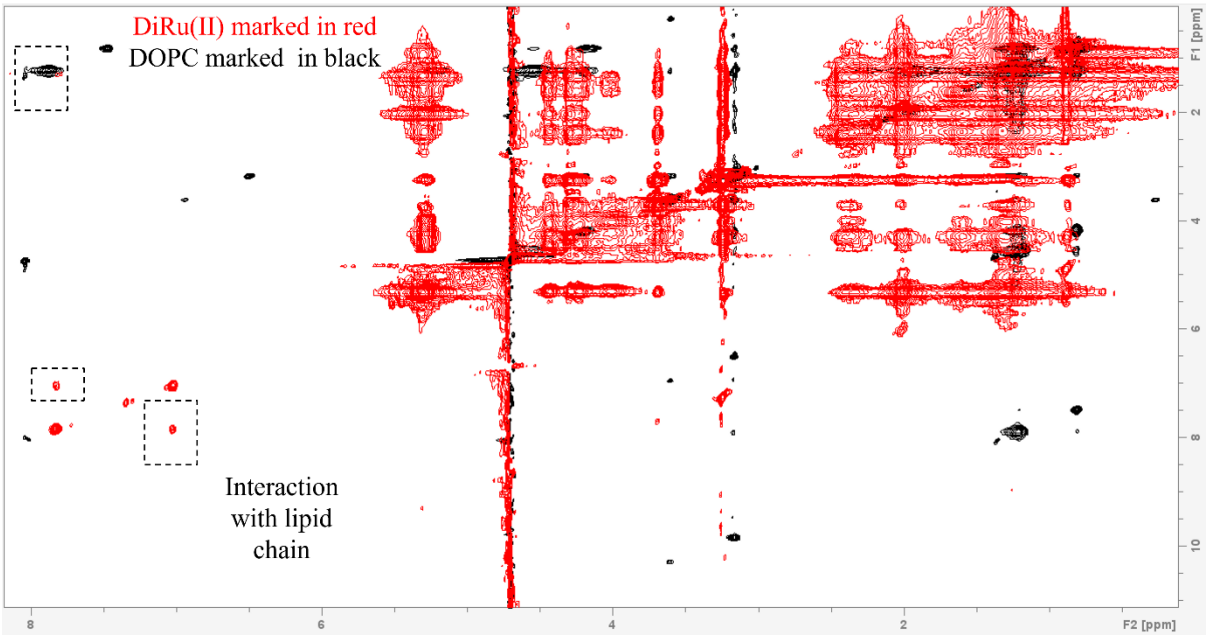

Figure S2.18: 2D NOESY NMR spectra of DOPC:Ru2 MLVs. Acquisition parameters: pulse program noesyph (Bruker library), 16 scans, relaxation delay 2 s, mixing time 100 ms.

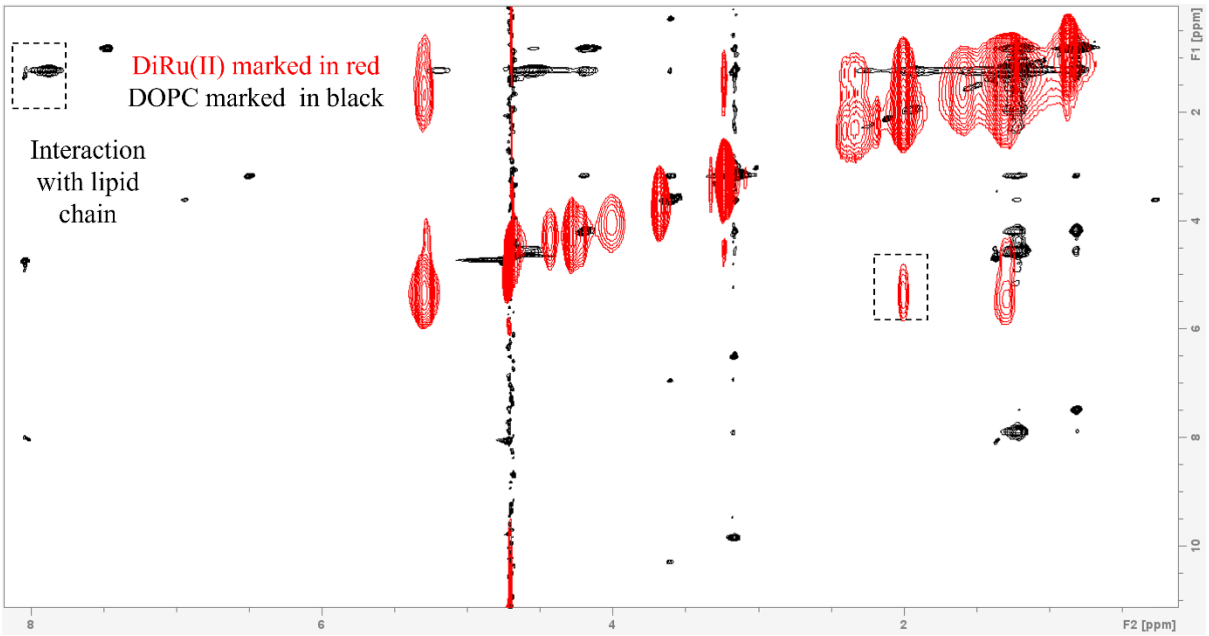

Figure S2.19: 2D NOESY NMR spectra of DOPC:Ru3 MLVs. Acquisition parameters: pulse program noesyph (Bruker library), 16 scans, relaxation delay 2 s, mixing time 100 ms.

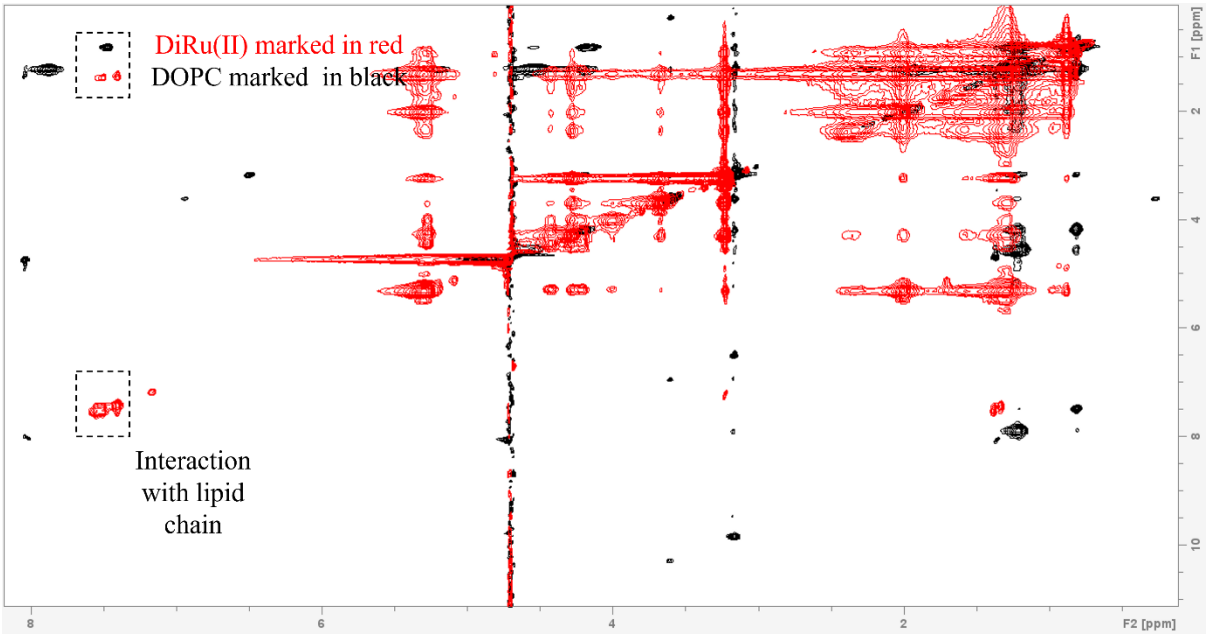

Figure S2.20: 2D NOESY NMR spectra of DOPC:Ru4 MLVs. Acquisition parameters: pulse program noesyph (Bruker library), 16 scans, relaxation delay 2 s, mixing time 100 ms.

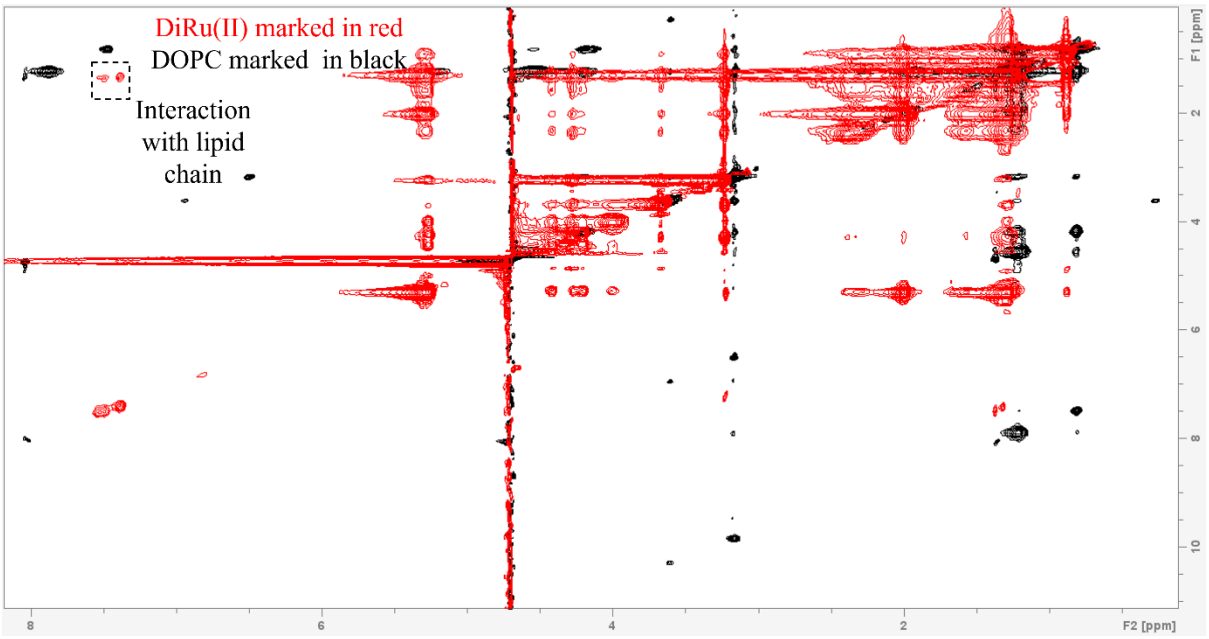

Figure S2.21: 2D NOESY NMR spectra of DOPC:Ru5 MLVs. Acquisition parameters: pulse program noesyph (Bruker library), 16 scans, relaxation delay 2 s, mixing time 100 ms.

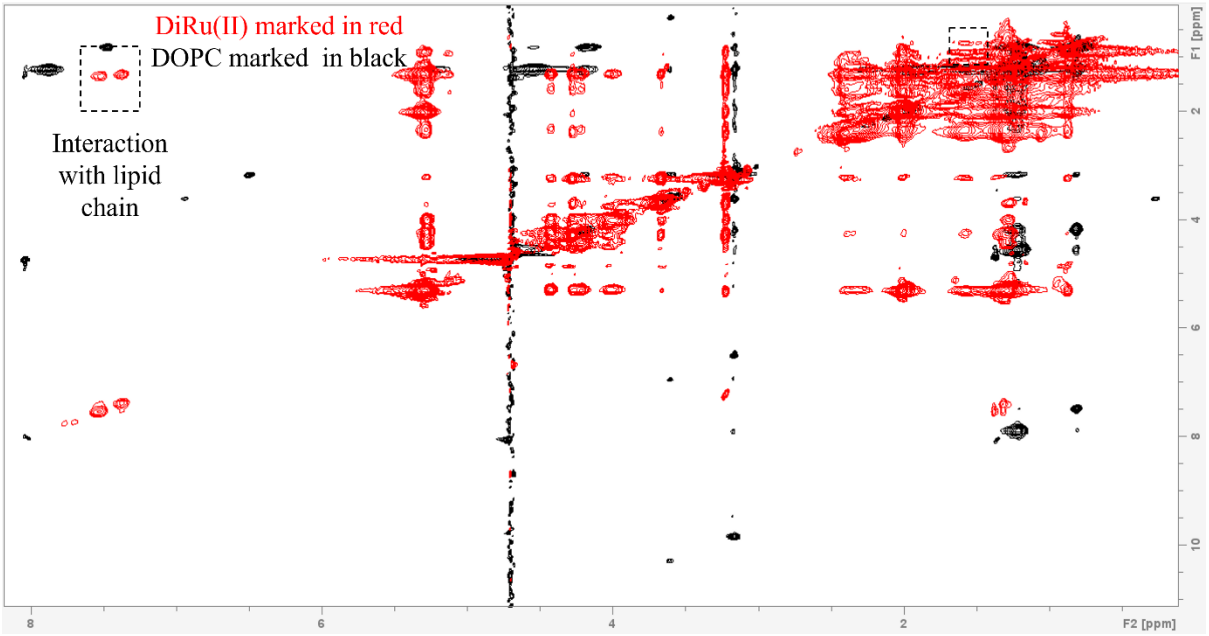

Figure S2.22: 2D NOESY NMR spectra of DOPC:Ru6 MLVs. Acquisition parameters: pulse program noesyph (Bruker library), 16 scans, relaxation delay 2 s, mixing time 100 ms.

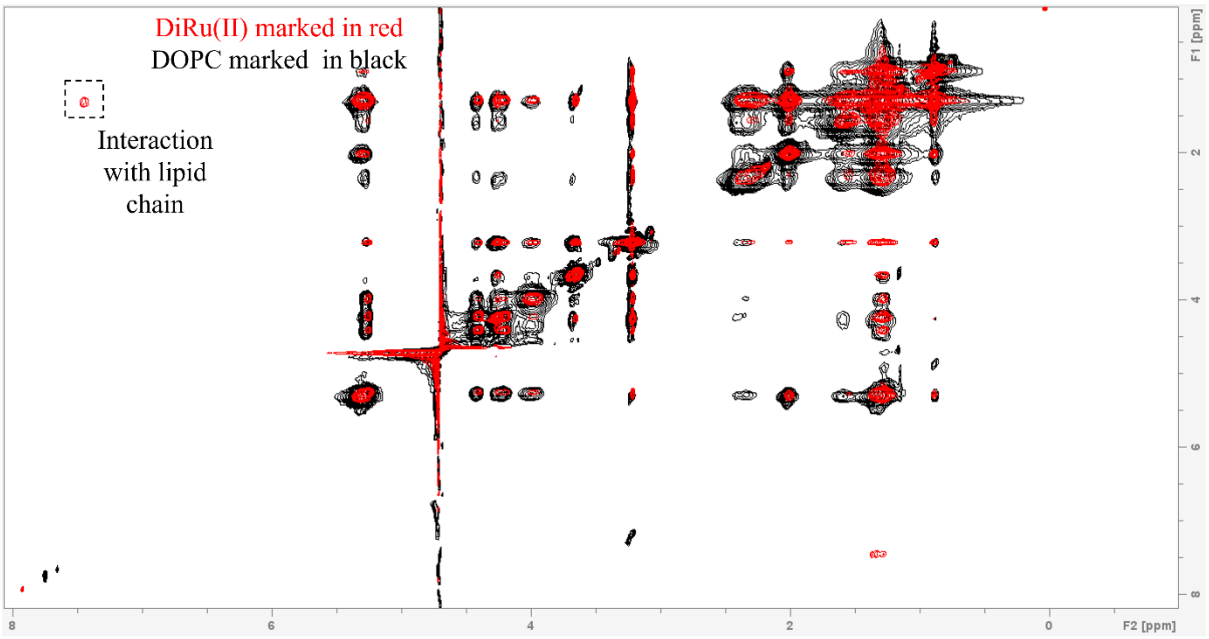

Figure S2.23: 2D NOESY NMR spectra of POPC:Ru1 MLVs. Acquisition parameters: pulse program noesyph (Bruker library), 16 scans, relaxation delay 2 s, mixing time 100 ms.

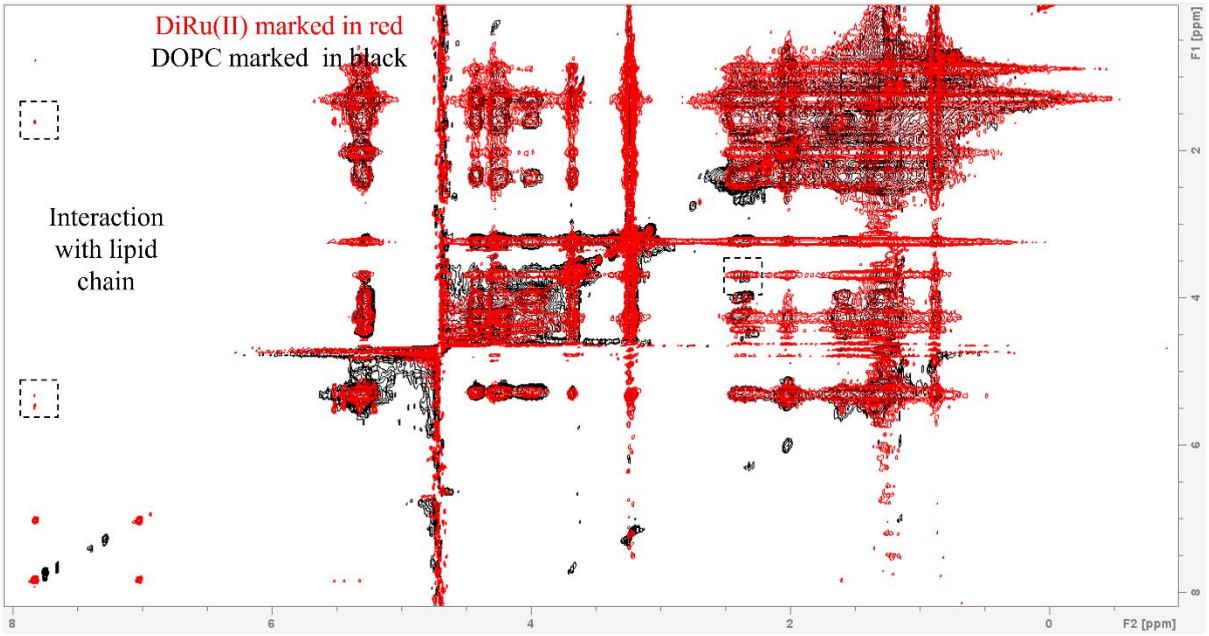

Figure S2.24: 2D NOESY NMR spectra of POPC:Ru2 MLVs. Acquisition parameters: pulse program noesyph (Bruker library), 16 scans, relaxation delay 2 s, mixing time 100 ms.

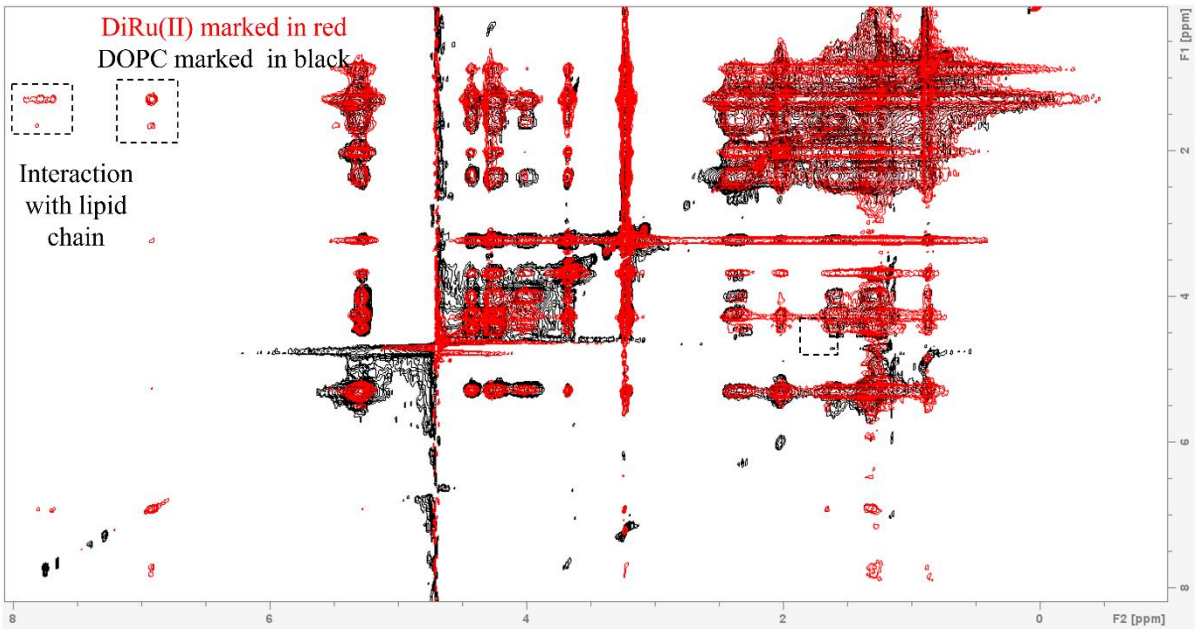

Figure S2.25: 2D NOESY NMR spectra of POPC:Ru3 MLVs. Acquisition parameters: pulse program noesyph (Bruker library), 16 scans, relaxation delay 2 s, mixing time 100 ms.

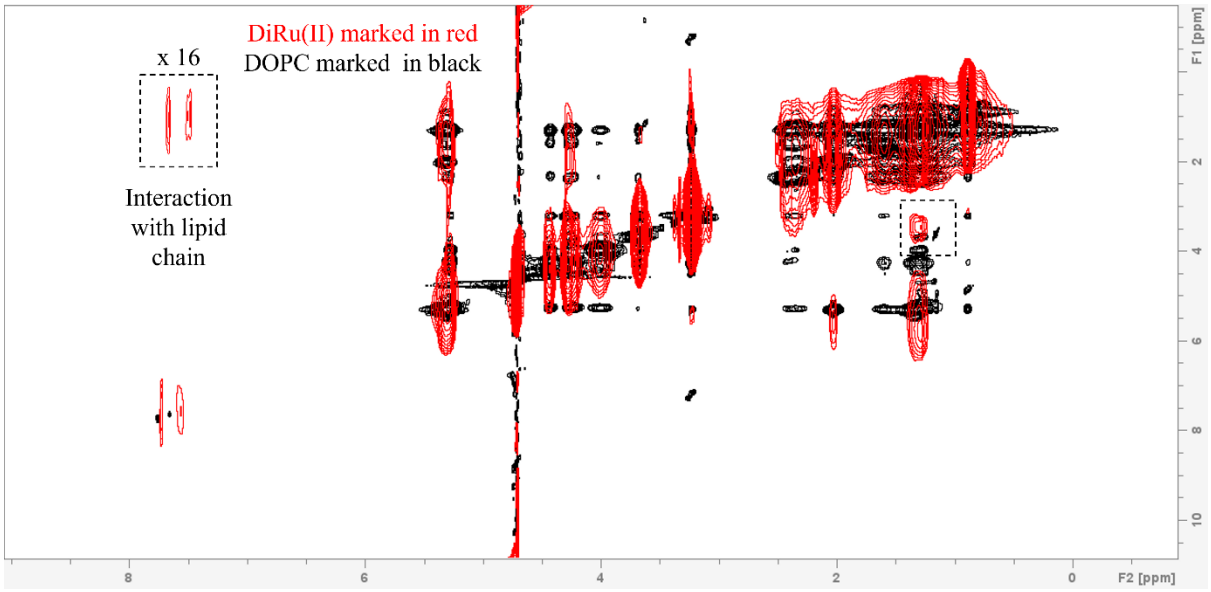

Figure S2.26: 2D NOESY NMR spectra of POPC:Ru4 MLVs. Acquisition parameters: pulse program noesyph (Bruker library), 16 scans, relaxation delay 2 s, mixing time 100 ms.

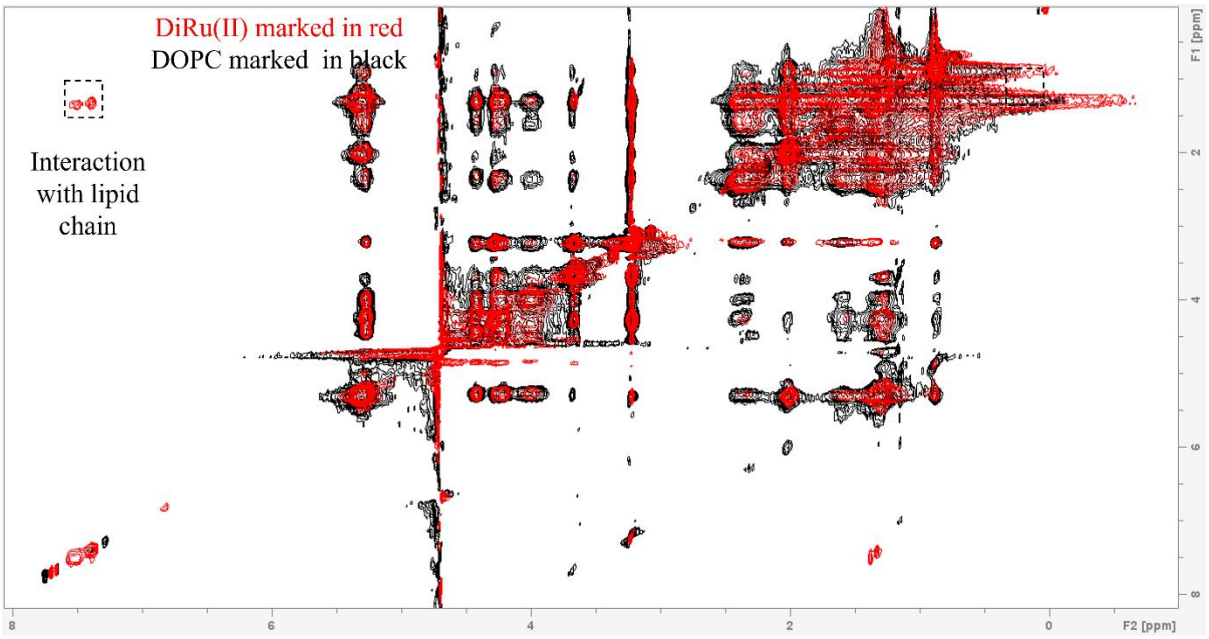

Figure S2.27: 2D NOESY NMR spectra of POPC:Ru5 MLVs. Acquisition parameters: pulse program noesyph (Bruker library), 16 scans, relaxation delay 2 s, mixing time 100 ms.

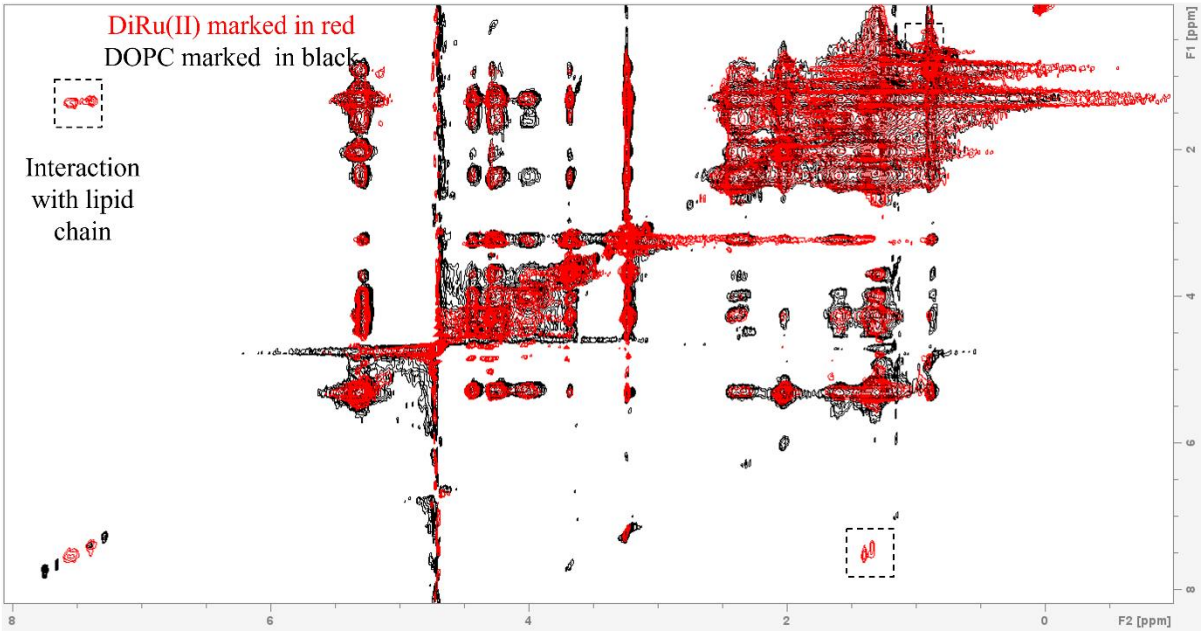

Figure S2.28: 2D NOESY NMR spectra of POPC:Ru6 MLVs. Acquisition parameters: pulse program noesyph (Bruker library), 16 scans, relaxation delay 2 s, mixing time 100 ms.

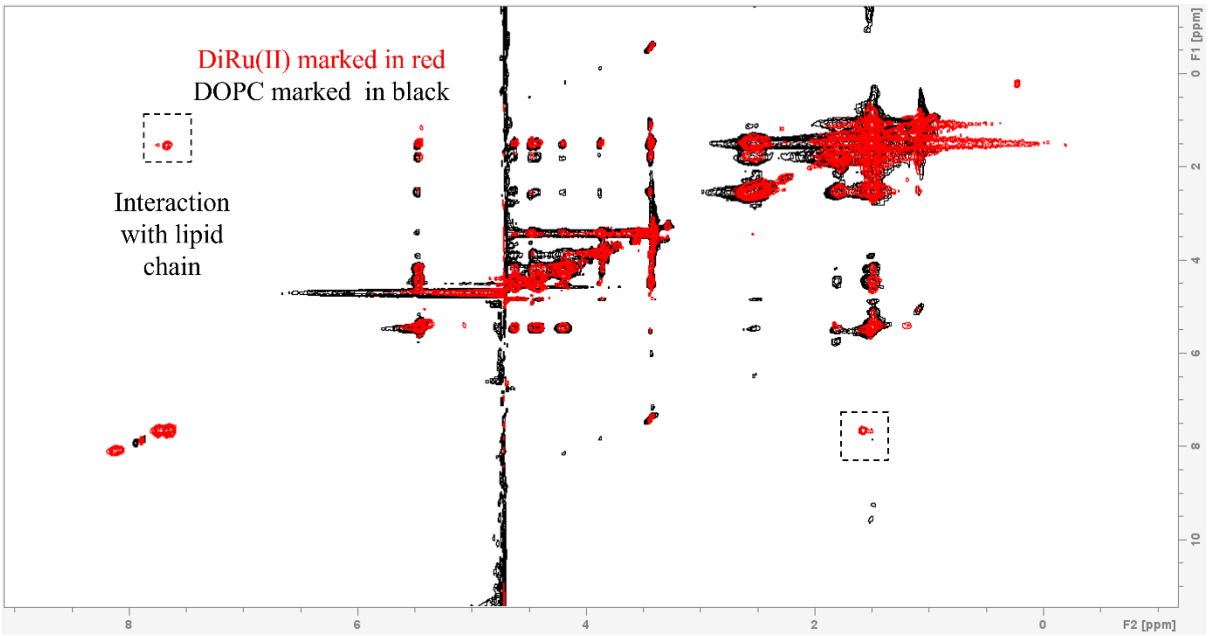

Figure S2.29: 2D NOESY NMR spectra of DPPC:Ru1 MLVs. Acquisition parameters: pulse program noesyph (Bruker library), 16 scans, relaxation delay 2 s, mixing time 100 ms.

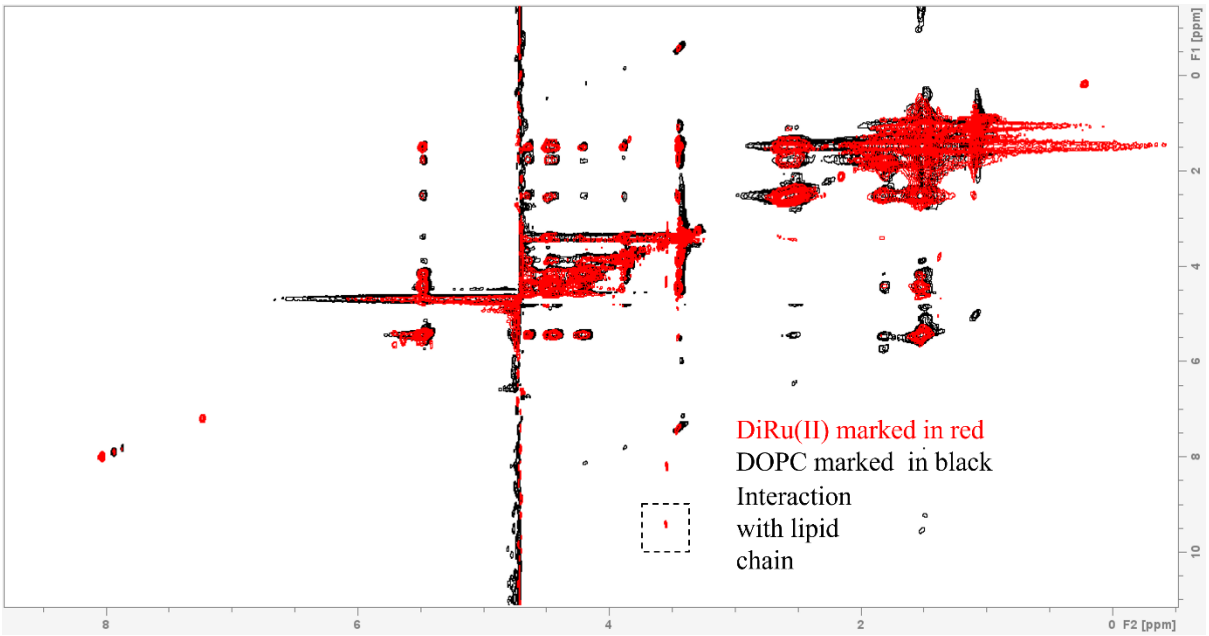

Figure S2.30: 2D NOESY NMR spectra of DPPC:Ru2 MLVs. Acquisition parameters: pulse program noesyph (Bruker library), 16 scans, relaxation delay 2 s, mixing time 100 ms.

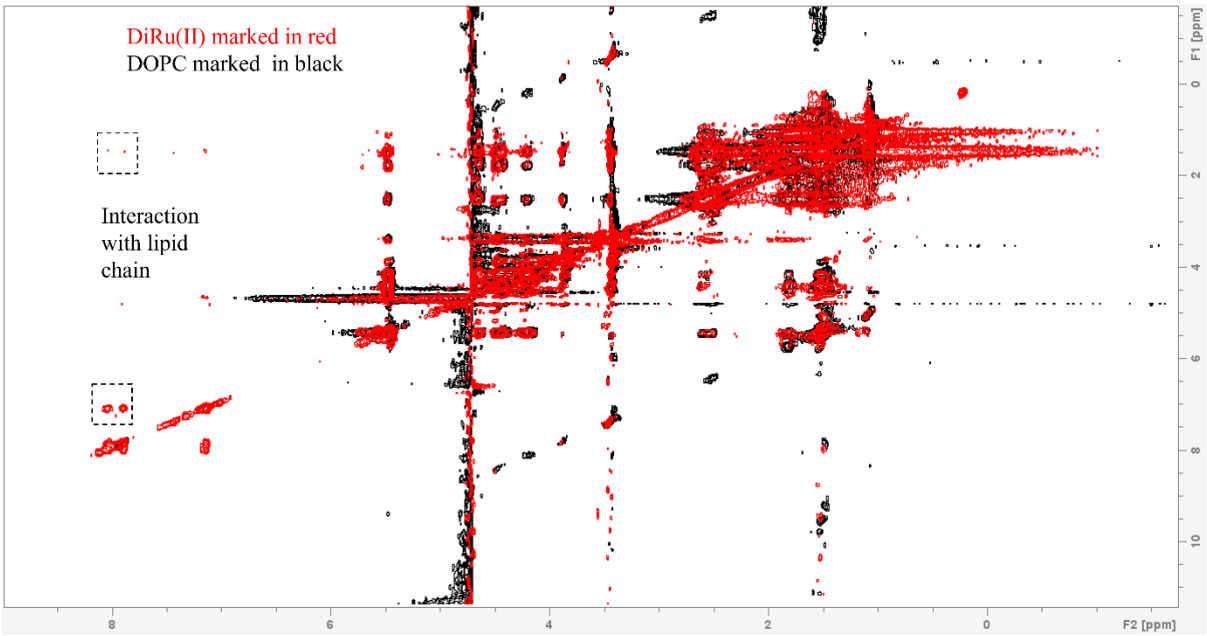

Figure S2.31: 2D NOESY NMR spectra of DPPC:Ru3 MLVs. Acquisition parameters: pulse program noesyph (Bruker library), 16 scans, relaxation delay 2 s, mixing time 100 ms.

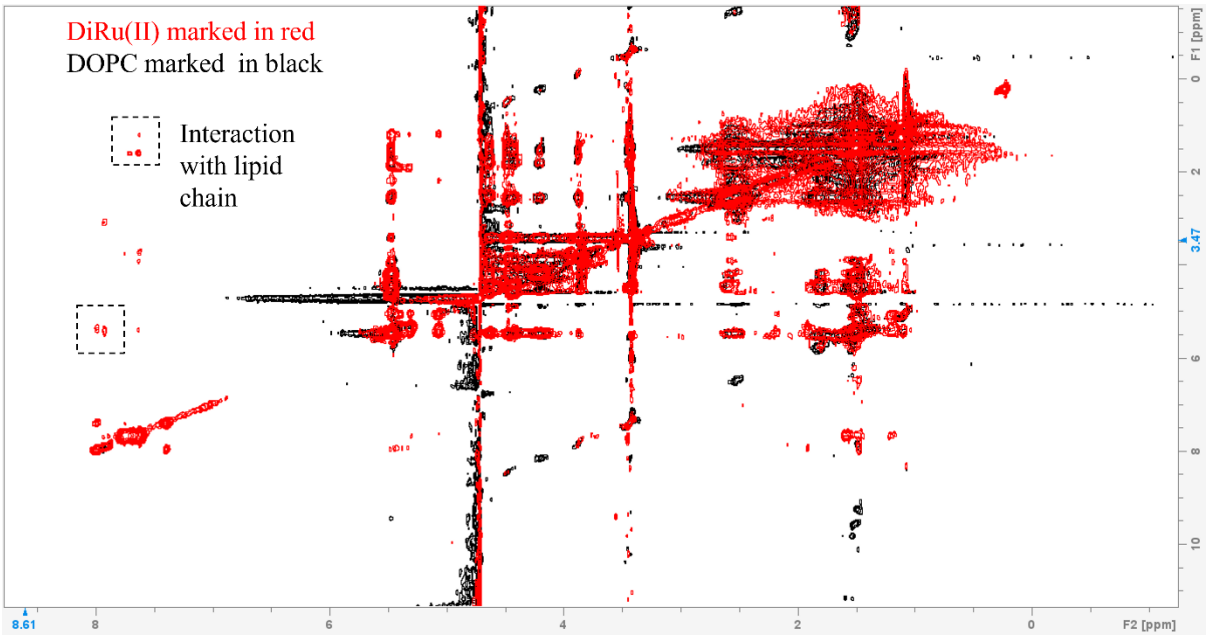

Figure S2.32: 2D NOESY NMR spectra of DPPC:Ru4 MLVs. Acquisition parameters: pulse program noesyph (Bruker library), 16 scans, relaxation delay 2 s, mixing time 100 ms.

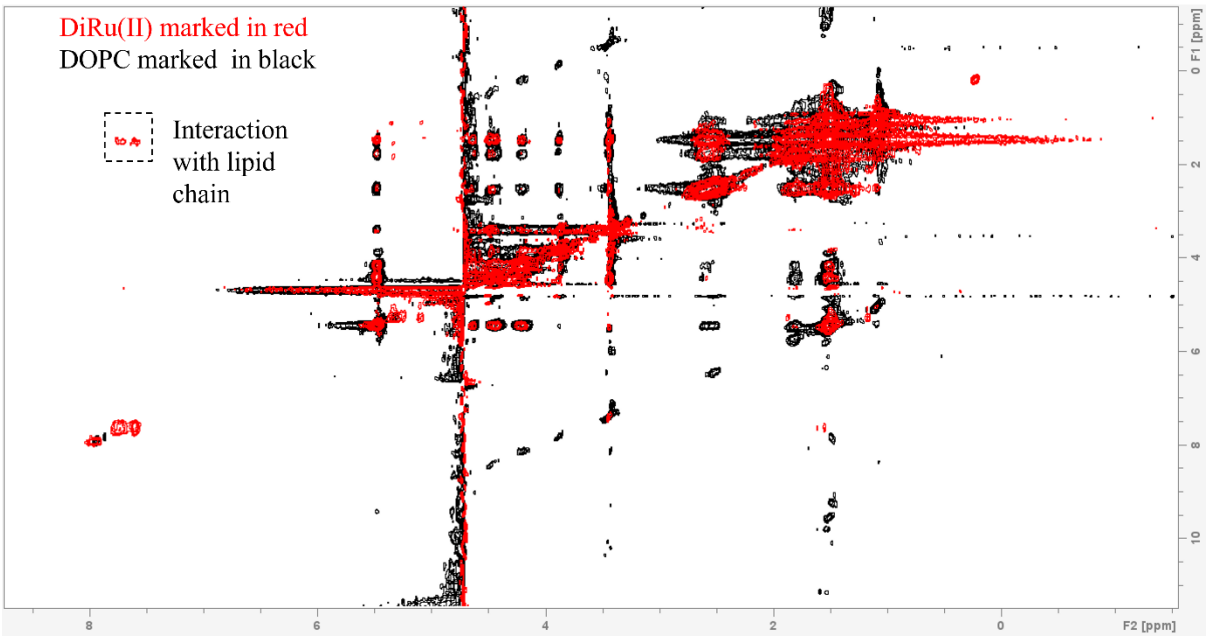

Figure S2.33: 2D NOESY NMR spectra of DPPC:Ru5 MLVs. Acquisition parameters: pulse program noesyph (Bruker library), 16 scans, relaxation delay 2 s, mixing time 100 ms.

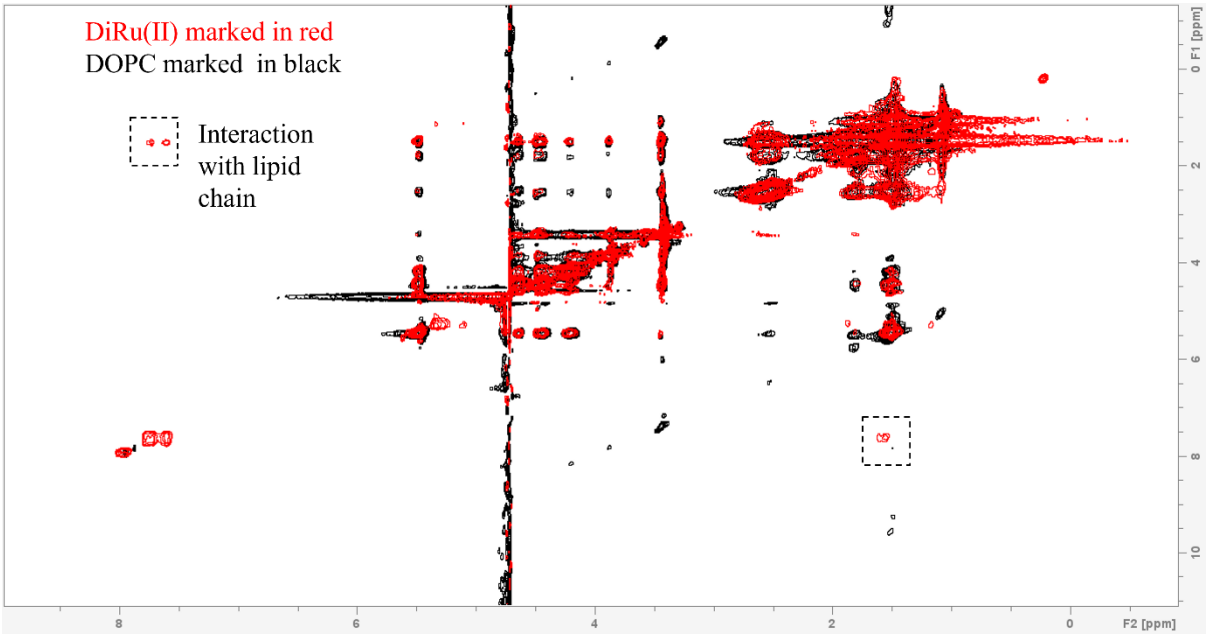

Figure S2.34: 2D NOESY NMR spectra of DPPC:Ru6 MLVs. Acquisition parameters: pulse program noesyph (Bruker library), 16 scans, relaxation delay 2 s, mixing time 100 ms.

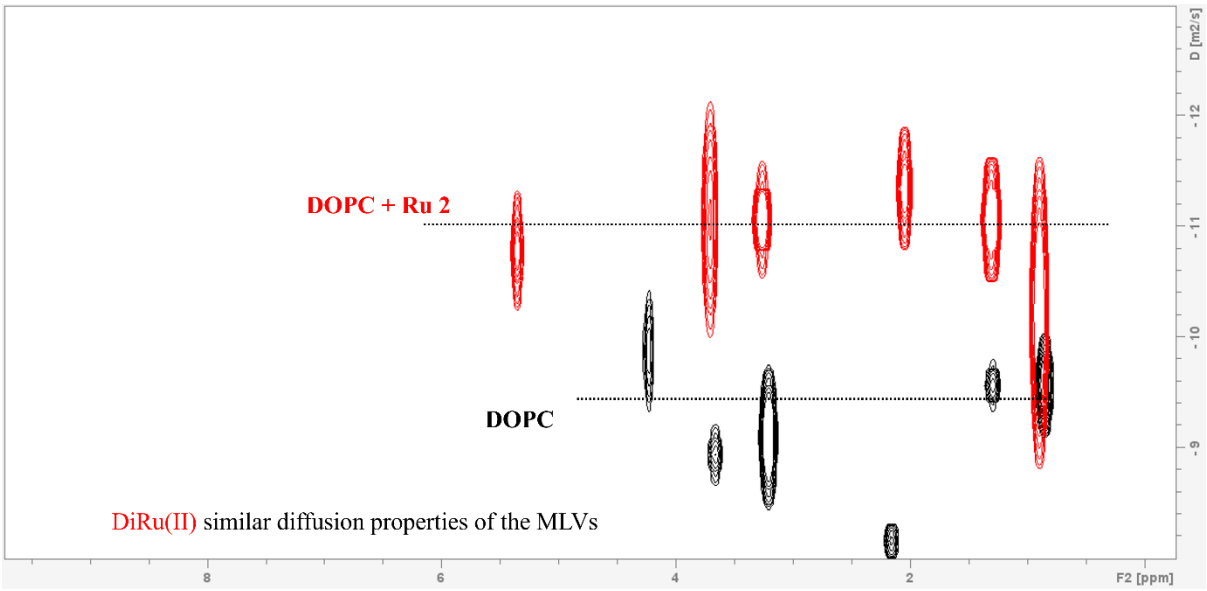

Figure S2.35: Overlay of ^{1}H DOSY HR-MAS NMR spectra of DOPC and DOPC:Ru2 MLVs. Acquisition parameters: pulse program ledbpcpgp2scprol.bi (Bruker library), 16 scans, relaxation delay 2 s.

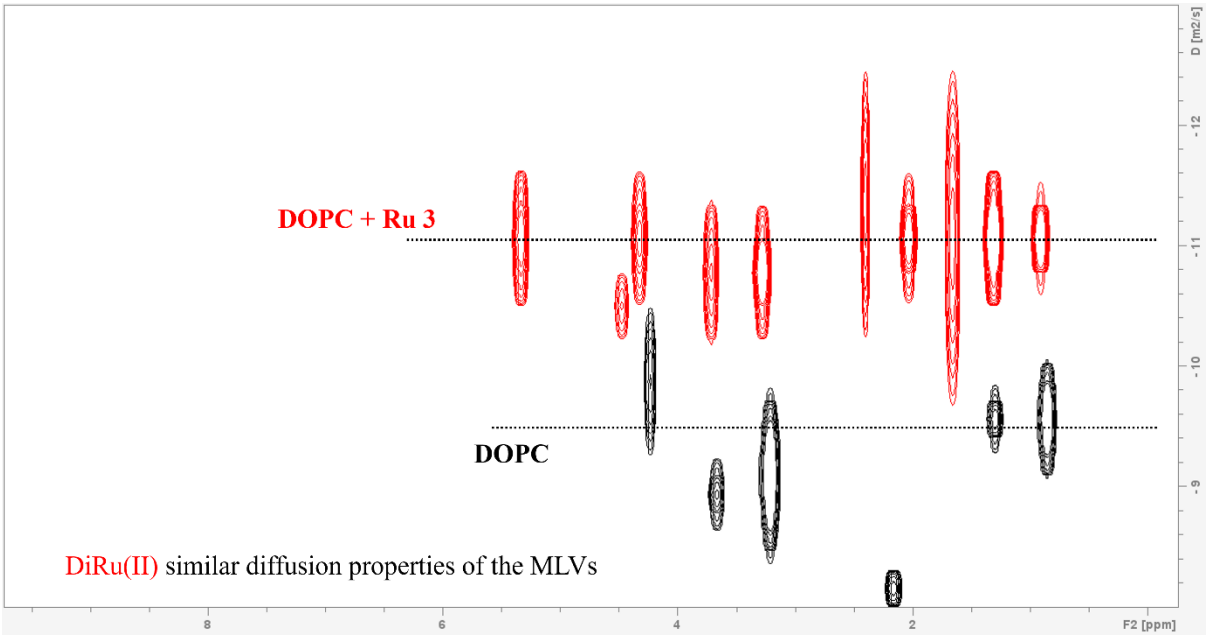

Figure S2.36: Overlay of ^{1}H DOSY HR-MAS NMR spectra of DOPC and DOPC:Ru3 MLVs. Acquisition parameters: pulse program ledbpcpgp2scprol.bi (Bruker library), 16 scans, relaxation delay 2 s.

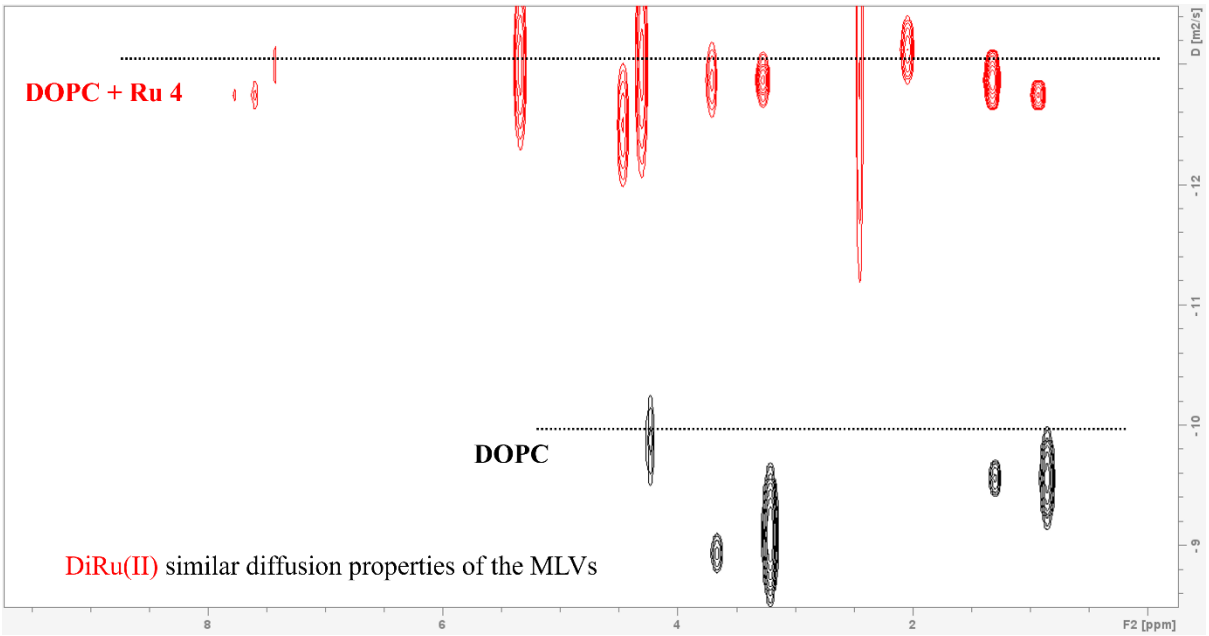

Figure S2.37: Overlay of ^{1}H DOSY HR-MAS NMR spectra of DOPC and DOPC:Ru4 MLVs. Acquisition parameters: pulse program ledbpcpgp2scprol.bi (Bruker library), 16 scans, relaxation delay 2 s.

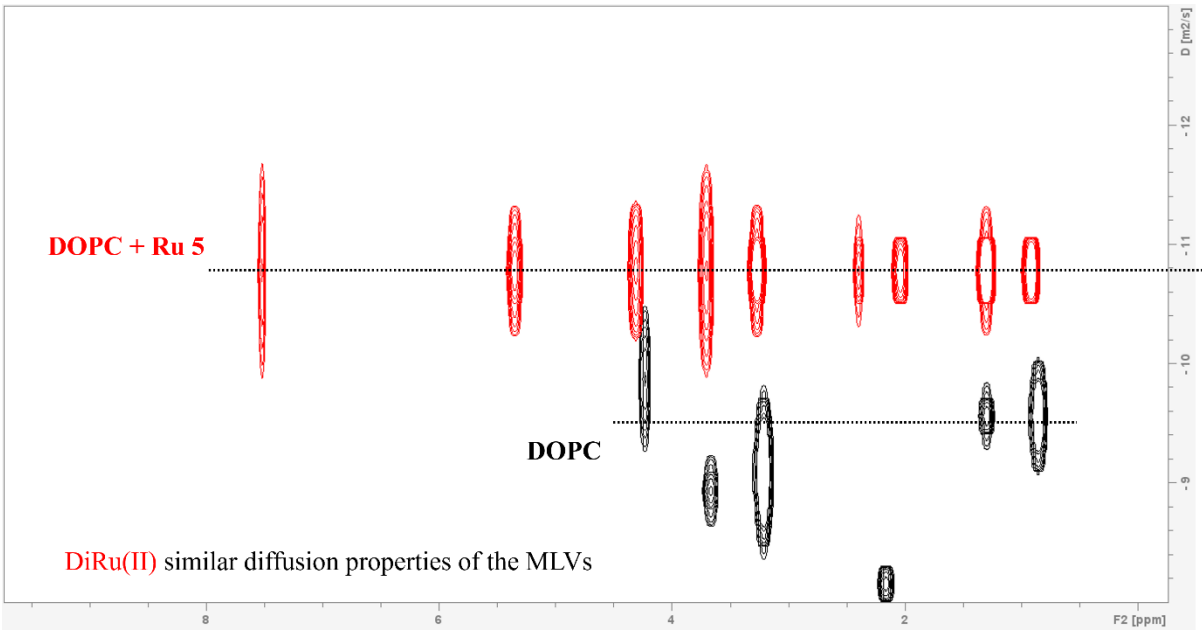

Figure S2.38: Overlay of ^{1}H DOSY HR-MAS NMR spectra of DOPC and DOPC:Ru5 MLVs. Acquisition parameters: pulse program ledbpcpgp2scprol.bi (Bruker library), 16 scans, relaxation delay 2 s.

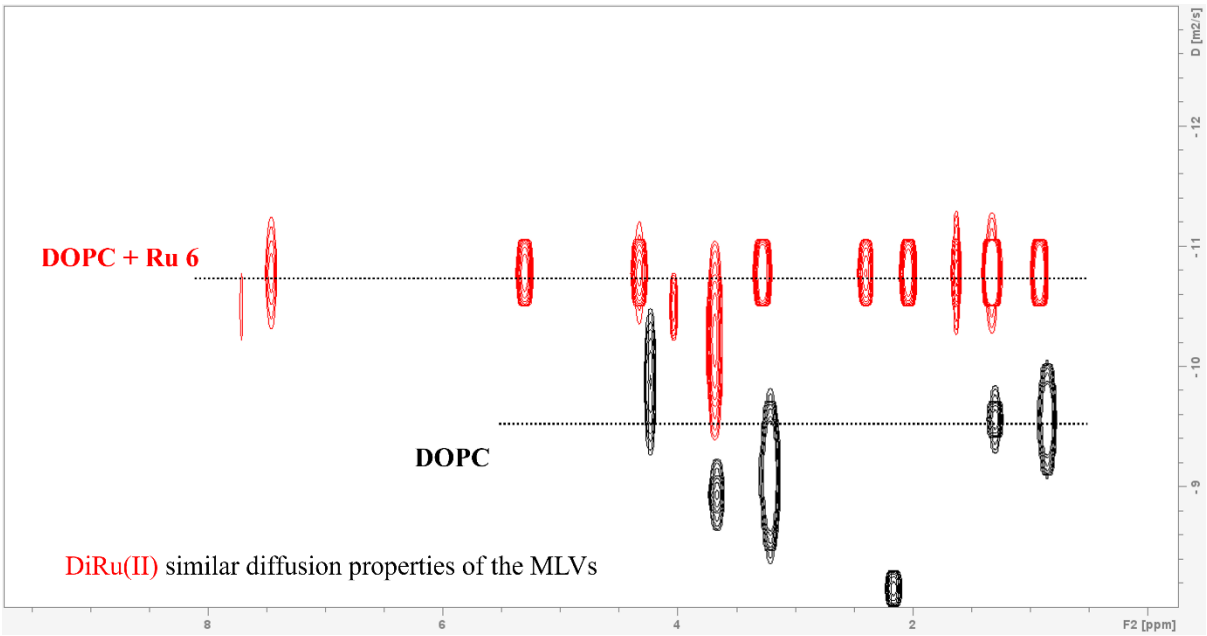

Figure S2.39: Overlay of ^{1}H DOSY HR-MAS NMR spectra of DOPC and DOPC:Ru6 MLVs. Acquisition parameters: pulse program ledbpcpgp2scprol.bi (Bruker library), 16 scans, relaxation delay 2 s.

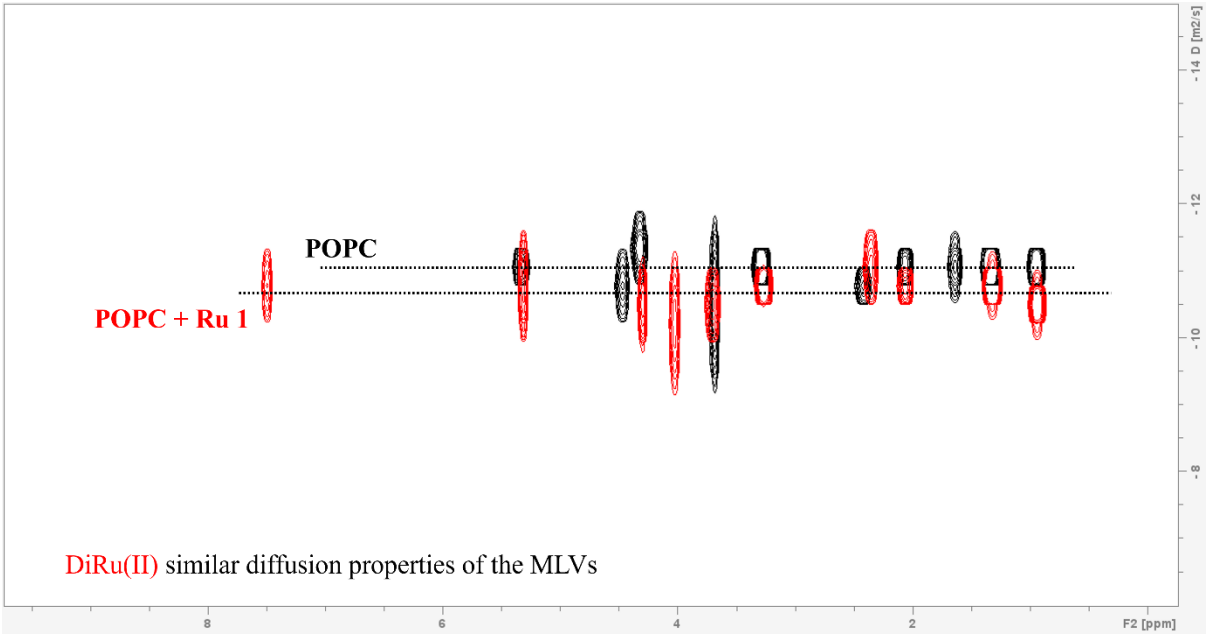

Figure S2.40: Overlay of ^{1}H DOSY HR-MAS NMR spectra of POPC and POPC:Ru1 MLVs. Acquisition parameters: pulse program ledbpcpgp2scprol.bi (Bruker library), 16 scans, relaxation delay 2 s.

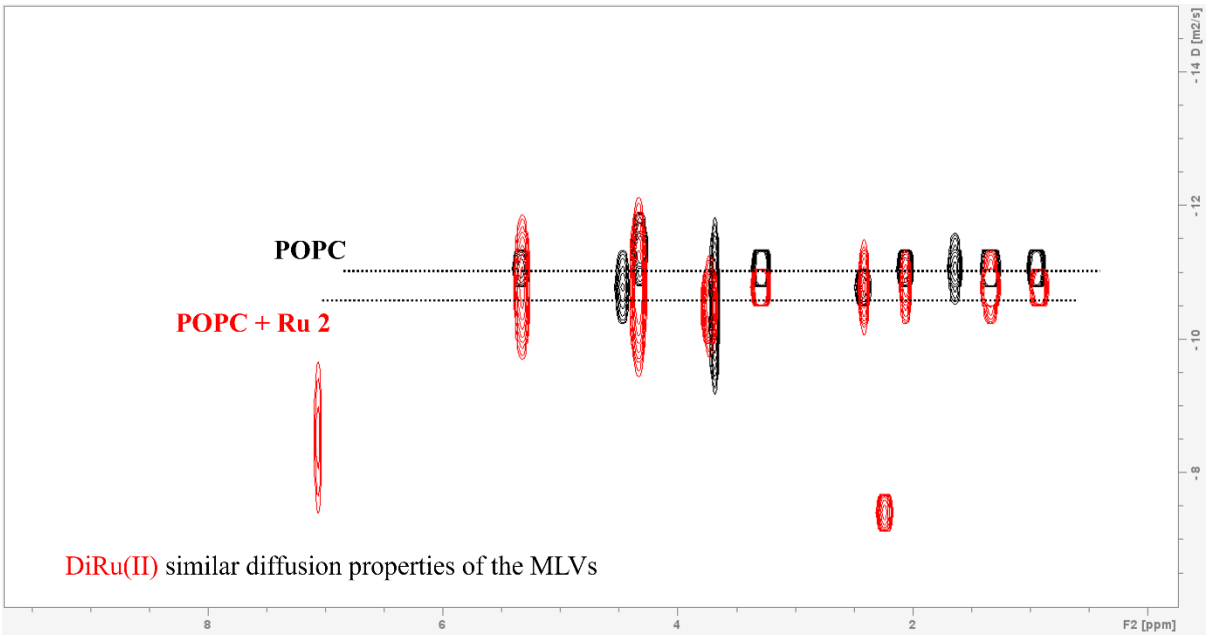

Figure S2.41: Overlay of ^{1}H DOSY HR-MAS NMR spectra of POPC and POPC:Ru2 MLVs. Acquisition parameters: pulse program ledbpcpgp2scprol.bi (Bruker library), 16 scans, relaxation delay 2 s.

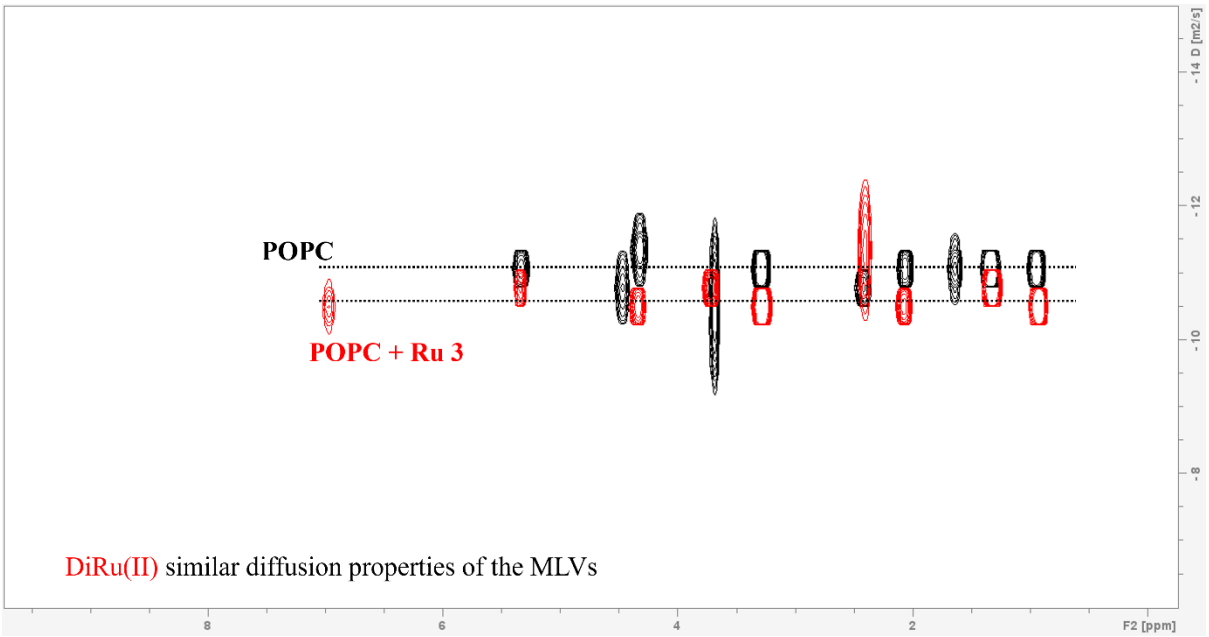

Figure S2.42: Overlay of ^{1}H DOSY HR-MAS NMR spectra of POPC and POPC:Ru3 MLVs. Acquisition parameters: pulse program ledbpcpgp2scprol.bi (Bruker library), 16 scans, relaxation delay 2 s.

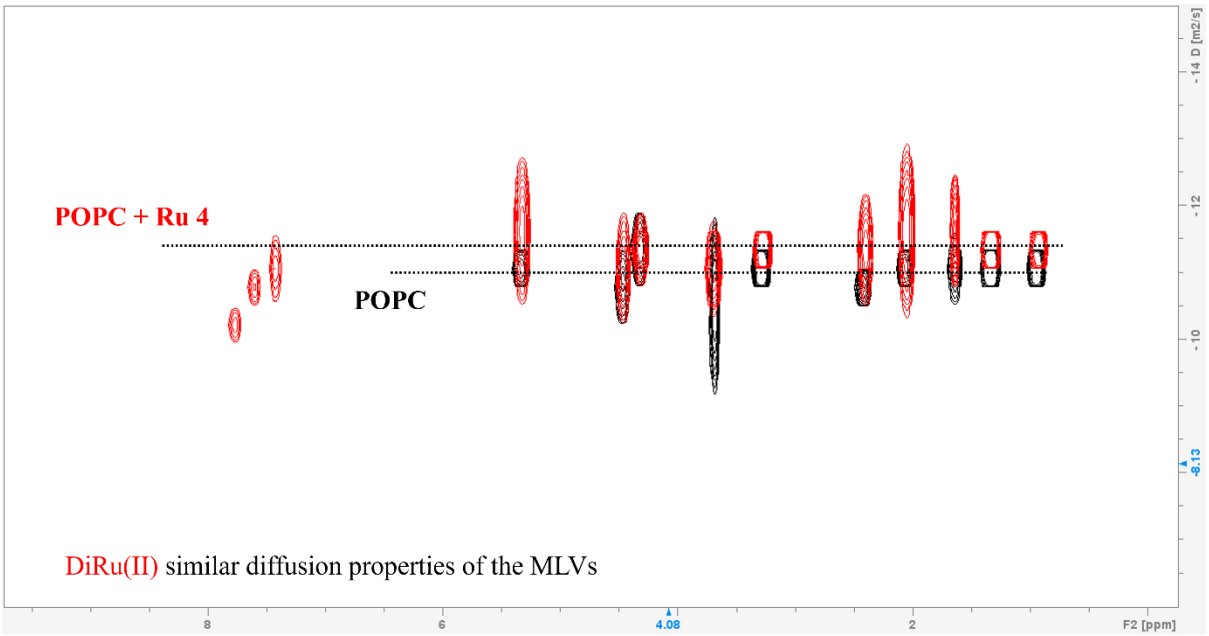

Figure S2.43: Overlay of ^{1}H DOSY HR-MAS NMR spectra of POPC and POPC:Ru4 MLVs. Acquisition parameters: pulse program ledbpcpgp2scprol.bi (Bruker library), 16 scans, relaxation delay 2 s.

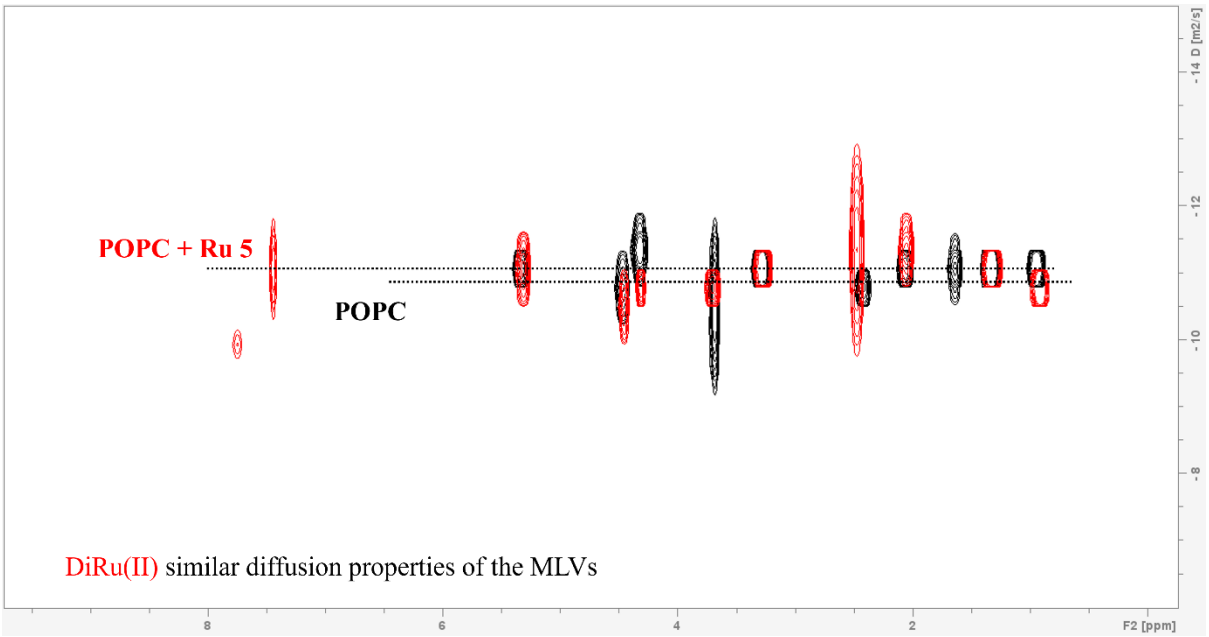

Figure S2.44: Overlay of ^{1}H DOSY HR-MAS NMR spectra of POPC and POPC:Ru5 MLVs. Acquisition parameters: pulse program ledbpcpgp2scprol.bi (Bruker library), 16 scans, relaxation delay 2 s.

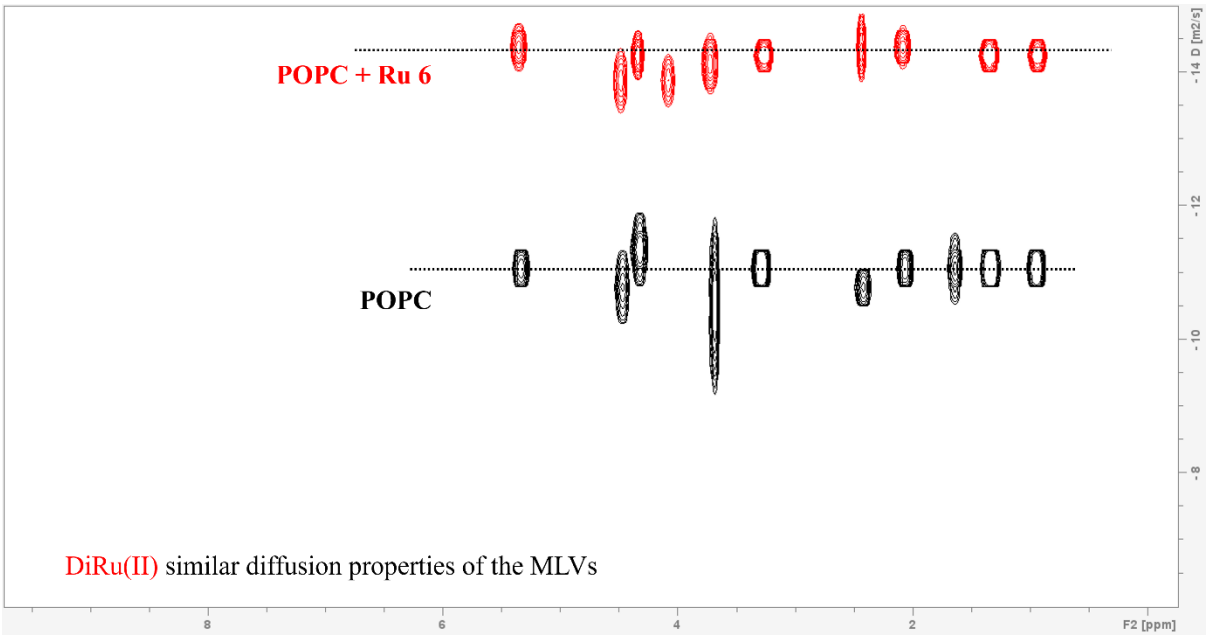

Figure S2.45: Overlay of ^{1}H DOSY HR-MAS NMR spectra of POPC and POPC:Ru6 MLVs. Acquisition parameters: pulse program ledbpcpgp2scprol.bi (Bruker library), 16 scans, relaxation delay 2 s.

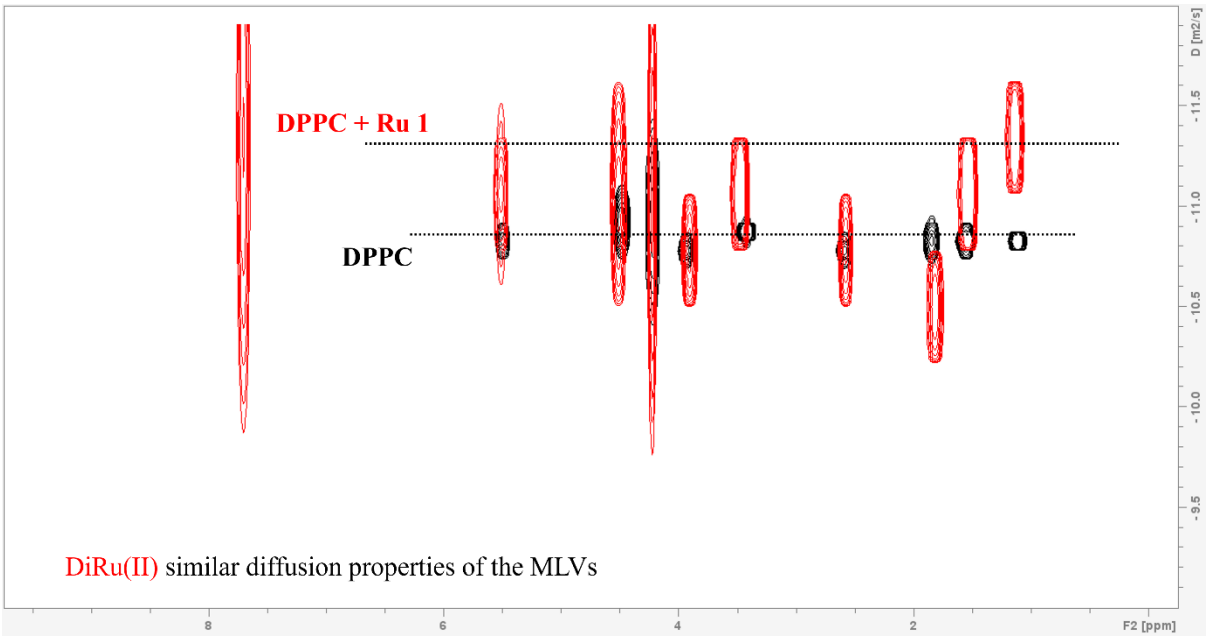

Figure S2.46: Overlay of ^{1}H DOSY NMR spectra of DPPC and DPPC:Ru1 MLVs. Acquisition parameters: pulse program ledbpcpgp2scprol.bi (Bruker library), 16 scans, relaxation delay 2 s.

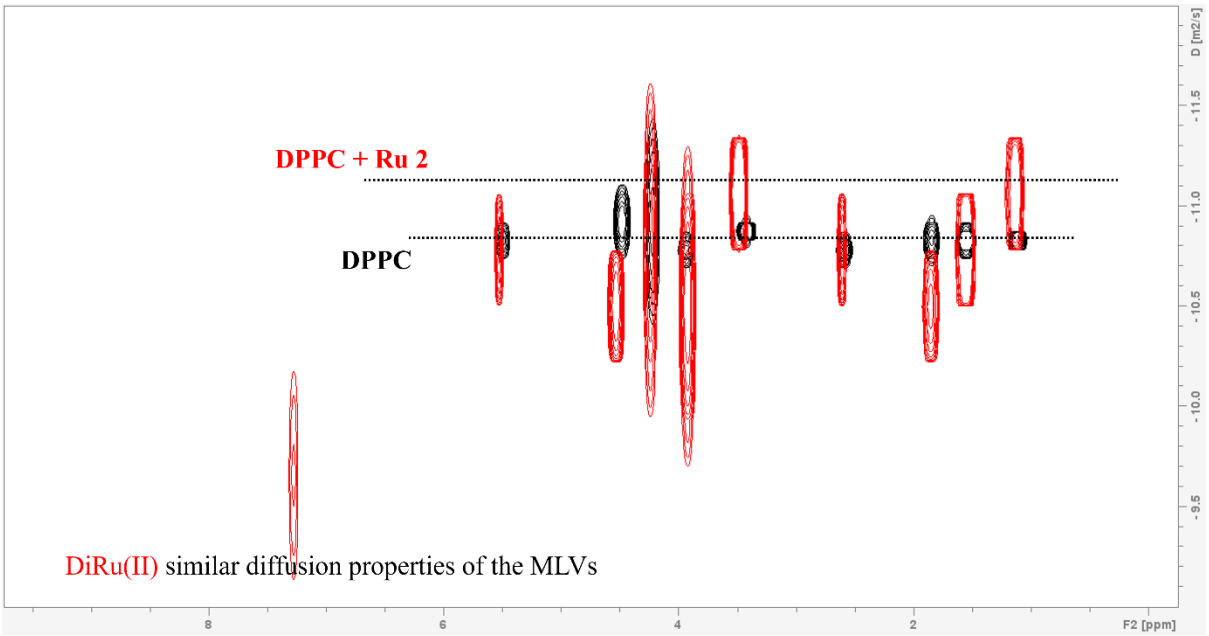

Figure S2.47: Overlay of ^{1}H DOSY NMR spectra of DPPC and DPPC:Ru2 MLVs. Acquisition parameters: pulse program ledbpcpgp2scprol.bi (Bruker library), 16 scans, relaxation delay 2 s.

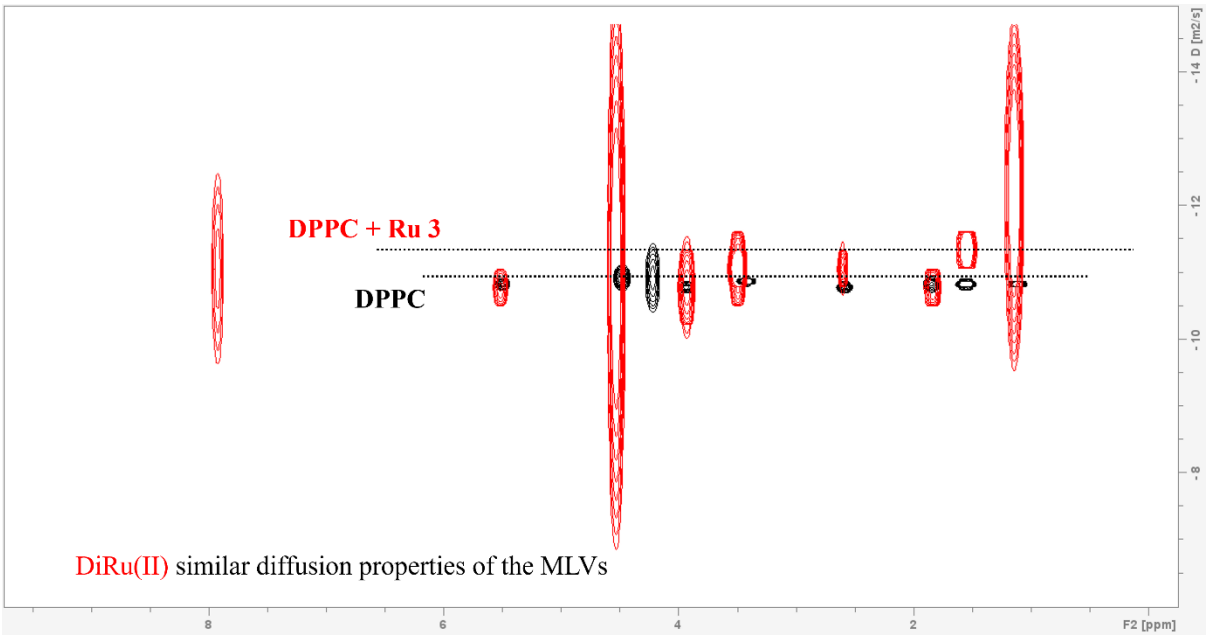

Figure S2.48: Overlay of ^{1}H DOSY NMR spectra of DPPC and DPPC:Ru3 MLVs. Acquisition parameters: pulse program ledbpcpgp2scprol.bi (Bruker library), 16 scans, relaxation delay 2 s.

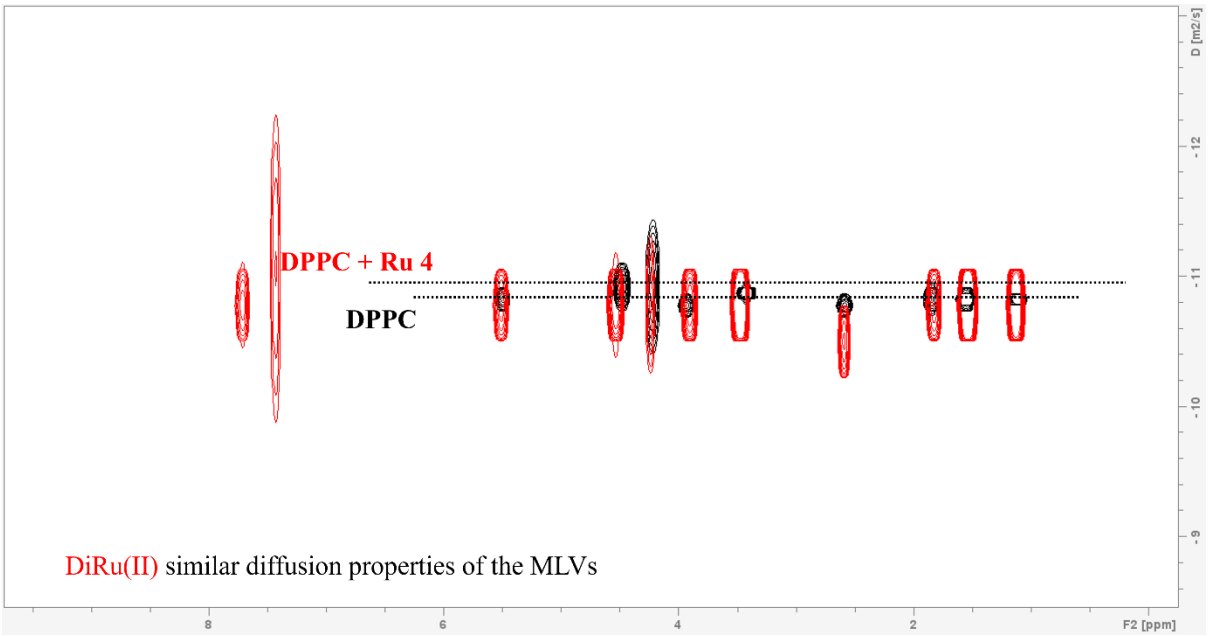

Figure S2.49: Overlay of ^{1}H DOSY NMR spectra of DPPC and DPPC:Ru4 MLVs. Acquisition parameters: pulse program ledbpcpgp2scprol.bi (Bruker library), 16 scans, relaxation delay 2 s.

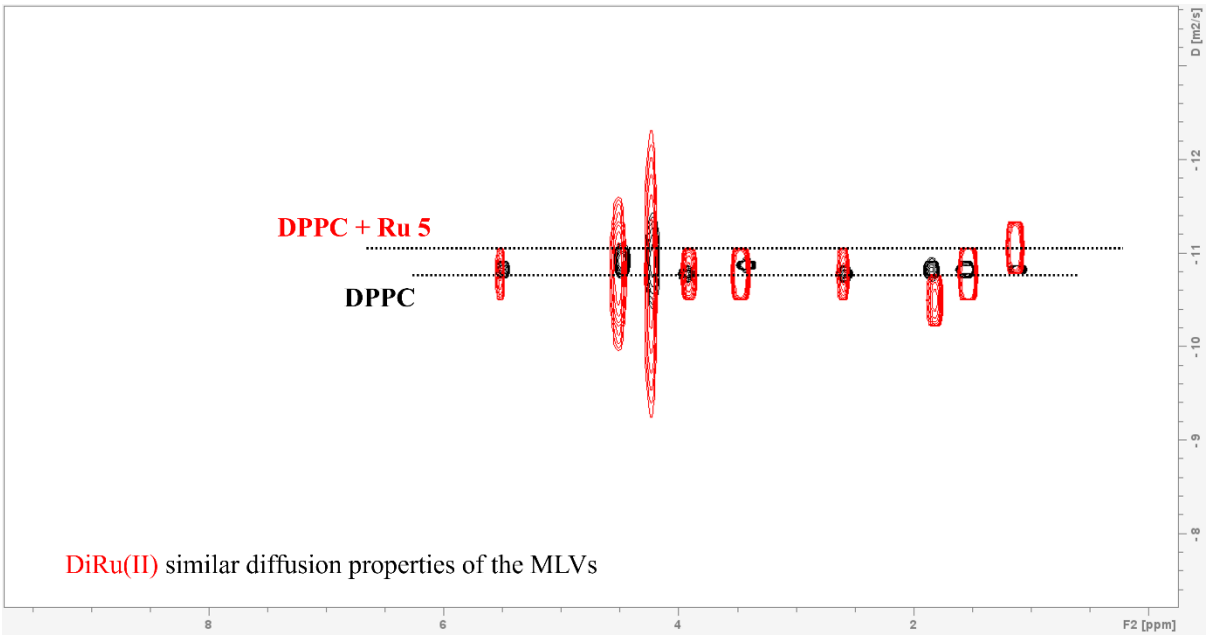

Figure S2.50: Overlay of ^{1}H DOSY NMR spectra of DPPC and DPPC:Ru5 MLVs. Acquisition parameters: pulse program ledbpcpgp2scprol.bi (Bruker library), 16 scans, relaxation delay 2 s.

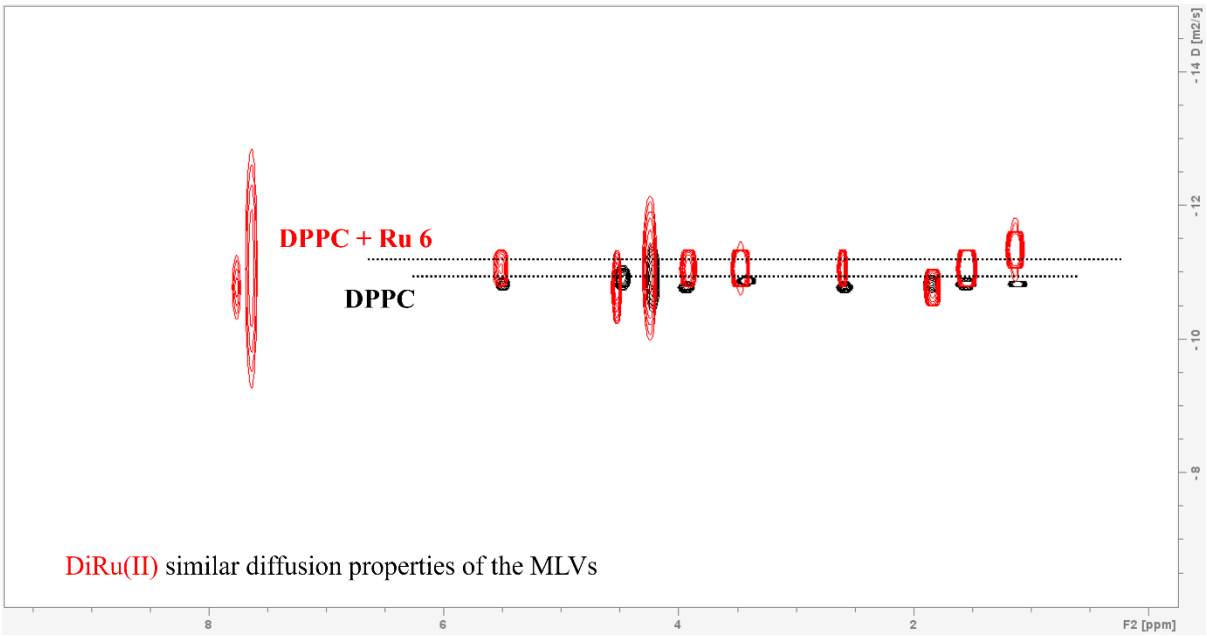

Figure S2.51: Overlay of ^{1}H DOSY NMR spectra of DPPC and DPPC:Ru6 MLVs. Acquisition parameters: pulse program ledbpcpgp2scprol.bi (Bruker library), 16 scans, relaxation delay 2 s.

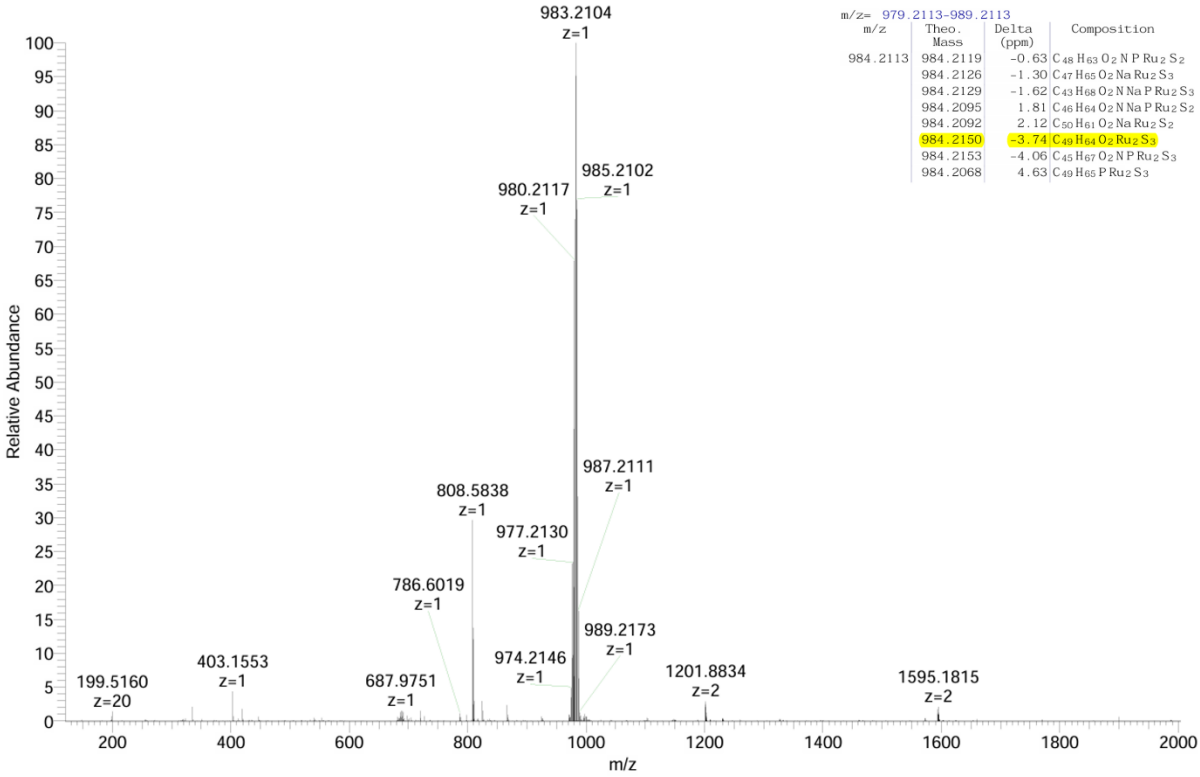

m/z= 979.2113-989.2113

m/z	Theo. Mass	Delta (ppm)	Composition
984.2113	984.2119	-0.63	$C_{48}H_{63}O_2NPRu_2S_2$
	984.2126	-1.30	$C_{47}H_{65}O_2NaRu_2S_3$
	984.2129	-1.62	$C_{43}H_{68}O_2NNaPRu_2S_3$
	984.2095	1.81	$C_{46}H_{64}O_2NNaPRu_2S_2$
	984.2092	2.12	$C_{50}H_{61}O_2NaRu_2S_2$
	984.2150	-3.74	$C_{49}H_{64}O_2Ru_2S_3$
	984.2153	-4.06	$C_{45}H_{67}O_2NPRu_2S_3$
	984.2068	4.63	$C_{49}H_{65}PRu_2S_3$

Figure S 2.52: ESI-MS in ACN/MeOH of DOPC with Ru1 in PBS.

List of Abbreviations and Acronyms for Part One

AD	alzheimer's disease
ADHD	attention deficit hyperactivity disorder
Ag	silver
ASD	autism spectrum disorder
ALA	alpha-lipoic acid
ALS	amyotrophic lateral sclerosis
As	arsenic
$AlCl_3$	aluminum (III) chloride
Au	gold
BAL	british antidot-lewsite
BAX	bcl-2-associated X protein
BBB	blood brain barrier
Bcl-2	B cell lymphoma-2
$C_{16}H_{18}ClN_3S \cdot 0.5\ ZnCl_2 \cdot x\ H_2O$	methylene blue zinc chloride double salt
Ca	calcium
Casp3	caspase 3
$CaCl_2 \cdot 2H_2O$	calcium chloride dihydrate
$CaNa_2EDTA$	edetate calcium disodium
Cd	cadmium
$CdCl_2$	cadmium chloride
$CH_3CH_2Hg^+$	ethyl mercury
CH_3Hg	methy lmercury
Co	cobalt
CoO	ubiquinol
COOH	carboxylic acid
CNS	central nervous system
Cu	copper
Cys	cystein
DD	developmental defect
D_2O	deuterated water
DHLA	dihydrolipoic acid
DMPS	dimercaptopropansulfonic acid
DMSA	dimercaptosuccinic acid
DMSO	dimethyl sulfoxide
EtOH	ethanol
Fe	iron
GAPDH	glyceraldehyde-3-phosphate dehydrogenase
GSH	glutathione
H_2O_2	hydrogen peroxide
H_2S	hydrogen sulfide
HOCl	hydrochlorous acid
Hb	hemoglobin

Hg	mercury
Hg^0	elemental mercury
Hg^{2+}	mercury (II) ion
$HgCl_2$	mercury (II) chloride
HgS	cinnabar
HgSe	tiemannite
Hpt	hours post-treatment
HSAB	hard-soft acid-base
K_1	stability constant stoichiometric
KCL	potassium chlorid
K_{eff}	effective stability constant
L	ligand
L_t	tissue concentration of the metal chelator
Li^+	lithium ion
M	solvated metal ion
M_t	tissue concentration of solvated metal ion
Mg^{2+}	magnesium (II) ion
$MgSO_4 \cdot 7H2O$	magnesium sulphate heptahydrate
ML	chelatable metal fraction
Mn	manganese
Mo	molybdenum
MS	multiple sclerosis
NaCl	sodium chloride
NiCd	nickel cadmium
NH_2	amino acid
NMR	nuclear magnetic resonance
NS	number of scans
Nrf2	nuclear factor erythroid 2-related factor 2
O_3	ozone
ONOO	peroxynitrite
Pb	lead
PbCl2	lead chloride
$PbCO_3$	cerussite
PbS	galena
$PbSO_4$	anglesite
PD	parkinson’s disease
pK_a	acid dissociation constant
Po^{2+}	polonium (II) ion
Pt^{2+}	platinum (II) ion
RLA	(R)- (+) lipoic acid
ROS	reactive oxygen species
Se	selenium
SH	thiol

SLA	(S)- (-) lipoic acid
Sn	tin
SO_3H	sulfonic acid
Sod 1	superoxide dismutase 1
TCI	tokyo chemical industry
TEL	tetraethyl lead
Zn	zinc
Zns	sphalerite

List of Abbreviations and Acronyms for Part Two

A2780cisR	cisplatin-resistant variant of human ovarian cancer cell line
ACN	acetonitrile
AFM	atomic force Microscopy
AziRu	azide (N_3^-) ruthenium
BCR-ABL	break point cluster- Abelson tyrosine kinase
C-C bond	carbon-carbon bond
C-H bond	carbon-hydrogen bond
CAR	chimeric antigen receptor
CDDP	cis-diamminedichloroplatinum
$CH2Cl_2$	dichloromethane
$CHCl_3$	chloroform
CML	chronic myeloid leukemia
cryo-EM	cryo-transmission electron microscopy
CT	computer tomography
ctDNA	circulating tumor DNA
Cu	copper
DACH	1,2- diaminocyclohexane
DDS	drug delivery systems
DLS	dynamic light scattering
DMPC	dimyristoyl phosphatidylcholine
DMPG	dimyristoyl phosphatidylglycerol
DNA	deoxyribonucleic acid
DOPC	dipalmitoylphosphatidylcholine
DOSY	diffusion ordered spectroscopy
DPPC	dioleoylphosphatidylcholine
e-/Å²	electrons through square angstrom
EPR	enhanced permeability and retention
EtOH	ethanol
ESI-MS	electrospray ionization mass spectrometry
FDA	food and drug administration
GUVs	giant unilamellar vesicles
HDAC	histone deacetylase
HPLC	**h**igh-performance liquid chromatography
HPV	human papillomavirus
HR-MAS	high-resolution magic angle spinning**.**
Hz	hertz
IMRT	intensity-modulated radiation therapy
Ir	iridium
K	kelvin
KP 1019	keppler 1019
KP 418	keppler 418
KH_2PO_4	potassium dihydrogen phosphate
kV	kilovolt
LUVs	large unilamellar vesicles
mA	milliampere
MCF -7	Michigan Cancer Foundation – 7
MeOH	methanol
MeOH-d_4	deuterated methanol

MLVs	multilamellar vesicles
MRI	magnetic resonance imaging
MVVs	multivesicular vesicles
Na_2HPO_4	disodium hydrogen phosphate
NaCl	sodium chloride
NAMI- A	new anti-tumor metallodrug-Italy A
NDDP	nano encapsulated diethylenetriaminepentaacetic acid-platinum
NGS	next-generation sequencing
NKP- 1339	NiKPoly 1339
NOESY	nuclear Overhauser effect spectroscopy
NTA	nanoparticle tracking analysis
OLVs	oligo lamellar vesicles
PBS	phosphate-buffered saline
Pd	palladium
PDI	polydispersity index
PET	positron emission tomography
POPC	palmitoyloleoylphosphatidylcholine
Pt	platinum
PTA	1,3,5-triaza-7-phosphoadamantane
RAPTA-C	ruthenium(II)-arene PTA Complex- Cymene
Rh	rhodium
RM175	ruthenium metal-based compound 175
RNA	ribonucleic acid
Ru	ruthenium
SEM	scanning electron microscopy
SUVs	small unilamellar vesicles
TEM	transmission electron microscopy

Declaration of Consent

Declaration of consent

on the basis of Article 18 of the PromR Phil.-nat. 19

Name/First Name:	Chakif Dib
Registration Number:	20-132-544
Study program:	PhD Chemistry and Molecular Sciences

Bachelor ☐ Master ☐ Dissertation ☑

Title of the thesis:	Comparative Study of Chelating Agents in the Treatment of Heavy Metal Poisoning on Early Zebrafish Embryo Development Followed by quantitative-PCR Studies
Supervisor:	Prof. Dr. Julien Furrer

I declare herewith that this thesis is my own work and that I have not used any sources other than those stated. I have indicated the adoption of quotations as well as thoughts taken from other authors as such in the thesis. I am aware that the Senate pursuant to Article 36 paragraph 1 litera r of the University Act of September 5th, 1996 and Article 69 of the University Statute of June 7th, 2011 is authorized to revoke the doctoral degree awarded on the basis of this thesis.
For the purposes of evaluation and verification of compliance with the declaration of originality and the regulations governing plagiarism, I hereby grant the University of Bern the right to process my personal data and to perform the acts of use this requires, in particular, to reproduce the written thesis and to store it permanently in a database, and to use said database, or to make said database available, to enable comparison with theses submitted by others.

Bern 15.01.2025

Place/Date

Signature

List of Conferences and Publications

Conferences

24 – 25 Aug 2023	*Poster* – **Structural investigation of chelating agents and their mercury, lead, and cadmium (II) complexes**, Swiss Chemical Society (SCS) – Fall Meeting 2023, Bern, Switzerland.
16 Jan 2024	*Poster* – **A Versatile Broadband Attached Proton Test Experiment for Routine ^{13}C Nuclear Magnetic Resonance Spectroscopy**, XXV Swiss NMR Symposium, Basel, Switzerland.
08 – 10 Jul 2024	*Flash Talk* – **Interactions of Cationic Dinuclear Trithiolato-bridged Arene Ruthenium (II) Complexes with Phospholipids Studied by HR-MAS NMR Spectroscopy** 5th International Symposium on Lipid Oxidation and Antioxidant (5th ISLOA), Bologna, Italy.
25 – 29 Aug 2024	*Oral Presentation* – **3D Printed µBeads as Drug Delivery Systems for Dinuclear Trithiolato-Bridged Arene Ruthenium (II) Complexes**, 17th European Biological Inorganic Chemistry (17th EuroBIC), Münster, Germany.
05 Sep 2024	*Oral Presentation* – **Comparative Study of Chelating Agents in the Treatment of Heavy Metal Poisoning on Early Zebrafish Embryo Developmentfollowed by q-PCR Studies**, Swiss Chemical Society – Fall Meeting 2024, Fribourg, Switzerland.

Paper 1 (Published)	P. Bigler, I. Gjuroski, **D. Chakif**, and J. Furrer, **'A Versatile Broadband Attached Proton Test Experiment for Routine 13C Nuclear Magnetic Resonance Spectroscopy'**, *Molecules*, vol. 29, no. 4, p. 809, Feb. 2024, doi: 10.3390/molecules29040809.